

30731



National Library of Canada

Bibliothèque nationale du Canada

CANADIAN THESES ON MICROFICHE

THÈSES CANADIENNES SUR MICROFICHE

NAME OF AUTHOR/NOM DE L'AUTEUR HING-LAN LAM

TITLE OF THESIS/TITRE DE LA THÈSE GENERATION MECHANISMS FOR THE TRANSIENT ULTRA LOW FREQUENCY OSCILLATIONS OF THE EARTH'S MAGNETIC FIELD (1-16 MHz) IN THE MORNING SECTOR

UNIVERSITY/UNIVERSITÉ U. OF ALBERTA

DEGREE FOR WHICH THESIS WAS PRESENTED/ GRADE POUR LEQUEL CETTE THÈSE FUT PRÉSENTÉE PH. D.

YEAR THIS DEGREE CONFERRED/ANNÉE D'OBTENTION DE CE GRADE 1976

NAME OF SUPERVISOR/NOM DU DIRECTEUR DE THÈSE DR. GORDON ROSTOKER

Permission is hereby granted to the NATIONAL LIBRARY OF CANADA to microfilm this thesis and to lend or sell copies of the film.

L'autorisation est, par la présente, accordée à la BIBLIOTHÈQUE NATIONALE DU CANADA de microfilmer cette thèse et de prêter ou de vendre des exemplaires du film.

The author reserves other publication rights, and neither the thesis nor extensive extracts from it may be printed or otherwise reproduced without the author's written permission.

L'auteur se réserve les autres droits de publication; ni la thèse ni de longs extraits de celle-ci ne doivent être imprimés ou autrement reproduits sans l'autorisation écrite de l'auteur.

DATED/DATE Oct. 22, 1976 SIGNED/SIGNÉ Hing-Lan Lam

PERMANENT ADDRESS/RÉSIDENCE FIXE P.O. BOX 137  
YUEN LONG  
N.T. HONG KONG

INFORMATION TO USERS

THIS DISSERTATION HAS BEEN  
MICROFILMED EXACTLY AS RECEIVED

This copy was produced from a microfiche copy of the original document. The quality of the copy is heavily dependent upon the quality of the original thesis submitted for microfilming. Every effort has been made to ensure the highest quality of reproduction possible.

PLEASE NOTE: Some pages may have indistinct print. Filmed as received.

Canadian Theses Division  
Cataloguing Branch  
National Library of Canada  
Ottawa, Canada K1A 0N4

AVIS AUX USAGERS

LA THÈSE A ÉTÉ MICROFILMÉE  
TELLE QUE NOUS L'AVONS RECUE

Cette copie a été faite à partir d'une microfiche du document original. La qualité de la copie dépend grandement de la qualité de la thèse soumise pour le microfilmage. Nous avons tout fait pour assurer une qualité supérieure de reproduction.

NOTA BENE: La qualité d'impression de certaines pages peut laisser à désirer. Microfilmée telle que nous l'avons reçue.

Division des thèses canadiennes  
Direction du catalogage  
Bibliothèque nationale du Canada  
Ottawa, Canada K1A 0N4

THE UNIVERSITY OF ALBERTA

GENERATION MECHANISMS FOR THE TRANSIENT ULTRA LOW  
FREQUENCY OSCILLATIONS (1 - 16 mHz) OF THE EARTH'S  
MAGNETIC FIELD IN THE MORNING SECTOR

by



HING-LAN LAM

A THESIS

SUBMITTED TO THE FACULTY OF GRADUATE STUDIES AND RESEARCH  
IN PARTIAL FULFILMENT OF THE REQUIREMENTS FOR THE DEGREE  
OF DOCTOR OF PHILOSOPHY

IN

GEOPHYSICS

DEPARTMENT OF PHYSICS

EDMONTON, ALBERTA

FALL, 1976

THE UNIVERSITY OF ALBERTA

FACULTY OF GRADUATE STUDIES AND RESEARCH

The undersigned certify that they have read, and recommend to the Faculty of Graduate Studies and Research, for acceptance, a thesis entitled GENERATION MECHANISMS FOR THE TRANSIENT ULTRA LOW FREQUENCY OSCILLATIONS (1 - 16 mHz) OF THE EARTH'S MAGNETIC FIELD IN THE MORNING SECTOR submitted by HING-LAN LAM in partial fulfilment of the requirements for the degree of Doctor of Philosophy in Geophysics.

..... *Robert Ratchko* .....  
Supervisor

..... *Shaulin* .....

..... *C.P.P. Casper* .....

..... *Donald R. Anderson* .....

..... *L.J. Holt* .....  
External Examiner

Date .. October 12, 1976 .....

## ABSTRACT

Data from a line of magnetometers stretching along a corrected geomagnetic meridian  $\sim 302^\circ\text{E}$  through western Canada are used to study the relationship between the convection westward electrojet and Pc 5 micropulsations in the morning sector. It was found that the dominant spectral bands in Pc 5 range occur within the same latitudinal range occupied by the electrojet. The intensity contours and the character of the polarization parameters clearly show that the pulsational activity follows the westward electrojet. Evidence of spatial oscillations of the borders of the electrojet at dominant Pc 5 frequencies is presented. The response of the Pc 5 micropulsations to rapid reconfigurations of the electrojet and the impulsive nature of the Pc 5 wave trains suggest that these micropulsations represent a transient response to changes in the three dimensional magnetosphere-ionosphere current system associated with large scale convection within the magnetosphere. The displacement current in the F-region and induction in the earth are suggested to have an important effect in the determination of the polarization of Pc 5 micropulsations.

In addition, an analysis and interpretation of data for a few rare 'Pc 4' giant micropulsations in the morning sector recorded during 1971 and 1974 (when three of

the stations were distributed along the same latitude line) indicate that these pulsations are highly localized both in latitudinal and longitudinal extent and occur during periods of extremely low activity in the magnetosphere. The 'Pc 4' activity appears to be influenced by the initiation of substorm activity; however, the region of pulsation disturbance is found to lie outside of the electrojet regions. It is suggested that the 'Pc 4' giant pulsations may be due to field line resonances.

## ACKNOWLEDGEMENTS

I am grateful to Dr. G. Rostoker, my thesis supervisor, for his guidance and discussions throughout the course of this research. I also wish to thank Dr. J. C. Samson, Dr. J. L. Kisabeth and Mr. R. G. Wiens for allowing me to use and modify some of their computer programmes. I would like to thank Professor R. Boström of the Royal Institute of Technology, Stockholm, for discussions on the interpretation of the polarization ellipse and the generation mechanism of Pc 5. Thanks are also due to Dr. J. V. Olson and Dr. B. V. Paranjape for discussions on some of the existing theoretical concepts on micropulsations and Dr. D. D. Wallis for allowing me to use his computer programme to determine baseline values for the magnetometer data.

The Department of Energy, Mines and Resources (Earth Physics Branch) aided the project by supplying two of the fluxgate magnetometers and by granting permission for the installation of recording systems at the Meenook and Resolute Magnetic Observatories. Thanks are also due to Environment Canada (Atmospheric Environment Service), Pacific Western Airlines and Transport Canada for permission to set up observatories at many of their installations in western Canada. The standard magnetograms utilized in this

study were supplied by the Department of Energy, Mines and Resources (Earth Physics Branch) and World Data Center A, Boulder, Colorado. The interplanetary magnetic field data used in this study were supplied by the National Space Science Data Center, NASA, Goddard Space Flight Center, Greenbelt, Maryland.

I wish to express my appreciation to Mrs. E. Tooley for doing an excellent job on the diagrams and Mrs. L. Cech for her excellent work in the arrangement and typing of this thesis.

Throughout this project I have received financial assistance in the form of a postgraduate scholarship from the National Research Council of Canada and in the form of a graduate teaching assistantship from the University of Alberta.



## TABLE OF CONTENTS

	Page
CHAPTER I INTRODUCTION	1
1.1 Definition and Classification of Micropulsations	1
1.2 The Magnetosphere	4
1.3 The Morphology of Pc 5 and 'Pc 4'	16
1.4 Purpose of this Thesis	32
CHAPTER II EXISTING THEORETICAL CONCEPTS	33
2.1 Hydromagnetic Waves	33
2.2 Poloidal and Toroidal Oscillations	39
2.3 Excitation Mechanisms	47
2.4 Wave Coupling	55
2.5 Summary	64
CHAPTER III EXPERIMENTAL DETAIL AND DATA PROCESSING	73
CHAPTER IV Pc 5 ACTIVITY IN THE MORNING SECTOR	81
4.1 The Relationship of Pc 5 Activity in the Morning Sector to the Auroral Westward Electrojet	81
4.2 Evidence for the Spatial Oscillations of the Electrojet	135
4.3 Generation Mechanism of Pc 5 Micropulsations	144

	Page
CHAPTER V 'Pc 4' ACTIVITY IN THE MORNING SECTOR	171
5.1 Observations	171
5.2 Generation Mechanism for 'Pc 4'	196
CHAPTER VI SUMMARY OF RESULTS AND CONCLUSIONS	203
6.1 Pc 5 Micropulsations	203
6.2 'Pc 4' Micropulsations	205
6.3 Conclusions	206
REFERENCES	208
APPENDIX A INSTRUMENTATION	221
APPENDIX B DETERMINATION OF POLARIZATION PARAMETERS AND PHASES FROM 3-DIMENSIONAL VECTOR TIME SERIES	229
APPENDIX C INFERENCE OF ELECTRIC CURRENTS FROM GROUND MAGNETIC DATA	239

## LIST OF TABLES

TABLE		PAGE
1	Micro-pulsation Classifications	3
2	Code names and locations of the magnetometer stations in operation during late 1971 and early 1972.	75
3	Code names and locations of the magnetometer stations in operation during the summer of 1974.	76
4	Magnitudes of the peak powers for different spectral components for the intervals of interest.	103
5	Interplanetary magnetic field values and Kp indices for the events selected for analysis.	130
6	List of values of the circuit elements of the equivalent circuit.	154
7	Eigenperiods and eigenfrequencies of the first harmonic toroidal and poloidal and the second harmonic toroidal oscillations for different number densities in the equatorial plane.	199

## LIST OF ILLUSTRATIONS

FIGURE		PAGE
1	Three dimensional representation of the configuration of the magnetosphere [after Heikkila, 1973]. The diagram has been modified by Rostoker [1976] to show the plasma mantle particle distribution.	5
2	Schematic diagram of the magnetosphere projected on the noon-midnight meridian plane illustrating the Birkeland current flow in the evening sector [after Rostoker and Boström, 1976]. The diagram has been modified to show the locations of the auroral oval.	11
3	An artist's conception of the auroral oval.	12
4	Electric field configuration in the magnetotail projected on the cross-sectional area of the tail [after Rostoker and Boström, 1976].	13
5	Direction of ionospheric currents (Hall current $I_H$ and Pedersen current $I_p$ ) and Birkeland current flow and the orientation of the ionospheric electric field in the polar ionosphere [after Rostoker and Boström, 1976]. The diagram has been modified to show the flow of currents in the dayside and the net downward field-aligned currents in the morning sector and the net upward field-aligned currents in the pre-midnight quadrant.	15
6	An example of Pc 5 micropulsations recorded at the station of Fort Reliance (70.3°N geomagnetic). The disturbance is recorded in the local magnetic coordinate system (H, D, Z). H points towards the local magnetic north, D east and Z downward. Local time is approximately UT less seven hours.	17

FIGURE

PAGE

7. Polar plots of the auroral oval (between dotted lines), the intensity maxima of Pc 5's (between solid lines), and the plasmapause (dashed lines) in corrected geomagnetic coordinates [after Samson, 1972]. 19
8. The diurnal and latitudinal variations of the sense of polarization for Pc 5 pulsations of  $\sim 5$  MHz in the horizontal plane [after Samson et al., 1971]. 23
9. Average sense of polarization in the horizontal plane of micropulsations in the spectral range 3.3 - 100 MHz. The shaded regions marked C have predominantly clockwise polarization and those marked CC have predominantly counter clockwise polarization. The unshaded regions have no predominant sense of polarization [after Rankin and Kurtz, 1970]. 24
10. An example of 'Pc 4' giant pulsations recorded at station of Fort McMurray (64.2°N geomagnetic). 29
11. Polar plots of the velocity vectors for the three waves which can be excited in a highly conducting compressible hydro-magnetic medium [after Ferraro and Plumpton, 1966]. 37
12. Schematic diagram of equatorial plane of the magnetosphere showing the senses of polarization induced by a Kelvin-Helmholtz instability at the magnetopause [after Orr, 1973]. 49
13. Projection of the particle trajectory showing the diffusions of protons due to waves with a magnetic field component in the direction of the principal normal to the dipole field lines [after Dungey, 1965]. 52
14. Schematic representation of the variation of amplitude and polarization as a function of L for unstable surface waves on the magnetopause coupled to a resonant field line [after Chen and Hasegawa, 1974a]. 61

FIGURE		PAGE
15	Latitude-dependence of magnetic variations during four time periods when sinusoidal oscillations were observed at the lowest latitude. All three stations are located at the same magnetic longitude [after Lanzerotti et al., 1973].	65
16	The local time distribution of the detached plasma regions, [after Chappell, 1974].	71
17	Locations of the magnetometer stations in corrected geomagnetic coordinates. The data recorded by stations indicated by squares were used in this thesis. Data from the stations indicated by solid circles were used to determine the region over which the micropulsation disturbance extended. Only standard magnetograms were available from the stations indicated by solid circles.	74
18	Magnetograms from the University of Alberta magnetometer stations for the event occurring on Day 235, 1971. The time scale is marked in hours of Universal Time. The station code names and coordinates are listed in Table 2.	83
19	1-20 MHz bandpass filtered micropulsation data for the Day 235, 1971 event. The original data are shown in Figure 18.	84
20	1-20 MHz bandpass filtered micropulsation data for the Day 235, 1971 event.	85
21	Magnetogram for the Day 16, 1972 event.	86
22	1-20 MHz bandpass filtered micropulsation data for the Day 16, 1972 event.	87
23	Magnetograms for the Day 17, 1972 event.	88
24	1-20 MHz bandpass filtered micropulsation data for the Day 17, 1972 event.	89

## FIGURE

## PAGE

- 25 Latitude profiles showing the magnetic perturbation pattern along the Alberta meridian line. The data are presented in geomagnetic dipole coordinates with X positive northwards, Y positive eastwards and Z positive downwards. The arrowheads at the bottom of each frame delineate the borders of the convection westward electrojet. The Universal Time at which the profile is taken is given at the top of the frame. 91
- 26 Plots of contours of equal relative intensity of micropulsations in the 1.3-2.5 MHz spectral band (upper panel). The location of the electrojet (indicated by solid lines) is superposed on the intensity maximum indicated by the dark band (lower panel) for the Day 16, 1972 event. The locations of our stations are indicated by the stars on the ordinate axis. 93
- 27 Same as Figure 26 except for the Day 235, 1971 event. 95
- 28 Same as Figure 26 except for the Day 17, 1972 event. 96
- 29 Power spectra of the three magnetic components (H,D,Z) at the University of Alberta magnetometer stations. The top panel shows the power spectra at our most northern station, with the lowest panel showing the spectra at our most southern station. The spectra were calculated in the interval indicated at the top of the Figure. The records were filtered with a 1-20 MHz bandpass filter. The stations that were within the confines of the westward electrojet during most of the time interval are indicated by the term WJ. These power spectra are for the Day 17, 1972 (1100-1200 UT) event. 97

FIGURE		PAGE
30	Same as Figure 29 except for the Day 17, 1972 (1200-1300 UT) event.	99
31	Same as Figure 29 except for the Day 16, 1972 (1700-1800 UT) event.	100
32	Same as Figure 29 except for the Day 17, 1972 (1700-1800 UT) event.	101
33	Latitude profiles of the powers in three components in different spectral bands. The borders of the westward electrojet are indicated by the dashed lines. This latitude profile is for the Day 16, 1972 (1500-1600 UT) event.	104
34	Same as Figure 33 except for the Day 17, 1972 (1500-1600 UT) event.	105
35	Same as Figure 33 except for the Day 17, 1972 (1700-1800 UT) event.	106
36	Polarization ellipses in the H-D plane. The centres of the ellipses are at the latitudes of the stations which are indicated by the stars on the ordinate axis. The sizes of the ellipses are not scaled to the average intensities and all the major axes have the same length. Ellipses that are shaded depict clockwise (CW) polarization while the ellipses that are not shaded depict counter-clockwise (CC) polarization. The location of the convection westward electrojet indicated by solid lines is superposed in the background. The plot is for the Day 16, 1972 event.	108
37	Same as Figure 36 except that the polarization ellipses are in the H-Z plane for the Day 16, 1972 event.	109
38	Same as Figure 36 except that the polarization ellipses are in the D-Z plane for the Day 16, 1972 event.	110
39	Same as Figure 36 except for the Day 235, 1971 event.	111



FIGURE		PAGE
40	Same as Figure 37 except for the Day 235, 1971 event.	112
41	Same as Figure 38 except for the Day 235, 1971 event.	113
42	Same as Figure 36 except for the Day 17, 1972 event.	114
43	Same as Figure 37 except for the Day 17, 1972 event.	115
44	Same as Figure 38 except for the Day 17, 1972 event.	116
45	Variation in the sense of polarization in H-D plane as a function of invariant latitude and Universal Time. The location of the electrojet is superposed in the background. The locations of our stations are indicated by the stars on the ordinate axis. CW refers to clockwise polarization. This plot is for the Day 17, 1972 event.	120
46	Same as Figure 45 except for polarization in the H-Z plane.	121
47	Same as Figure 45 except for polarization in the D-Z plane.	123
48	Latitude profile of powers and relative phase changes for the Day 17, 1972 (1500-1600 UT) event at 4.0 mHz. The locations of our stations are indicated at the top. INLAT stands for invariant latitude. The borders of the convection westward electrojet are indicated by the dashed lines.	124
49	Same as Figure 48 except for the Day 16, 1972 (1700-1800 UT) event at 2.2 mHz.	125

## FIGURE

## PAGE

- 50 Plot of demarcation lines (dotted lines) in the H-D plane and the line of intensity maximum (dashed line) as a function of invariant latitude and Universal Time. The location of the convection westward electrojet is superposed in the background. This plot is for the Day 235, 1971 event in the 2-3 MHz band. 127
- 51 Same as Figure 50 except for the Day 16, 1972 event in the 1.3-2.5 MHz band. 128
- 52 Same as Figure 50 except for the Day 17, 1972 event in the 3.3-5.1 MHz band. 129
- 53 Plots of intensity contours and the convection westward electrojet. The relative intensity at each station was determined with respect to the maximum intensity for the entire interval. These plots are for the Day 235, 1971 event in the 2.0-3.0 MHz band. 132
- 54 Same as Figure 53 except for the Day 16, 1972 event in the 1.3-2.5 MHz band. 133
- 55 Same as Figure 53 except for the Day 16, 1972 event in the 4.1-5.3 MHz band. 134
- 56 Same as Figure 53 except for the Day 17, 1972 event in the 1.5-2.8 MHz band. 136
- 57 Same as Figure 53 except for the Day 17, 1972 event in the 3.3-5.1 MHz band. 137
- 58 Location of the convection westward electrojet and the filtered magnetograms for CONT and FTCH in the Z-component. The borders of the electrojet were determined at intervals of 23 sec. For display purposes the magnetograms are placed between the electrojet borders. This plot is for the Day 17, 1972 (1300-1400 UT) event. 139
- 59 Same as Figure 58 except that the poleward border is not shown and the magnetograms are for MCMU and MENK in the H-component. The plot is for the Day 17, 1972 (1200-1400 UT) event. 140

FIGURE		PAGE
60	Same as Figure 58 except that the magnetograms are for CONT and RELI in the H-component. The plot is for the Day 17, 1972 (1700-1800 UT) event.	141
61	Plot showing the oscillations of the equatorward border of the convection westward electrojet and the magnetogram for SMIT for the Day 17, 1972 (1500-1800 UT) event. The lower panel shows the variation in magnitude of the negative $\Delta X$ peak in the latitude profiles of magnetic perturbations. The units for HMAX are $\gamma$ .	143
62	An equivalent LCR circuit for the proposed model three-dimensional current system. $\epsilon$ is the energy source associated with extraction of energy from convecting plasma. $L_M$ is the inductance associated with the magnetic energy in the generator region. $C_M$ is the capacitance associated with the kinetic energy of the convecting plasma in the generator region. $C_I$ is the capacitance associated with the F-region of the ionosphere. $R_I$ is the resistance associated with the E-region of the ionosphere.	146
63	The diurnal variation of the ionospheric electric field in the region of the auroral oval [after Mozer and Lucht, 1974].	149
64	Field lines from rings of constant latitude as viewed from above and projected into the equatorial plane. Lines are shown for every 2 hours of local time [after Mead and Fairfield, 1975].	150
65	A simplified version of the circuit shown in Figure 62. $C'_M = C_M + C_I$ . This circuit determines the frequency of the LC-oscillations thought to represent the Pc 5 micropulsations.	156

## FIGURE

## PAGE

- 66 Latitude profiles of magnetic perturbations in geomagnetic coordinates. Each successive profile is separated by  $\sim 2$  minutes. The profiles in the left column (i.e., profiles A, C and E) show that the  $\Delta Y$  step occurred at low latitude while the profiles in the right column (i.e., profiles B, D and F) show that the  $\Delta Y$  step occurred at higher latitudes. The borders of the westward electrojet are indicated by arrow heads at the bottom of each frame. Note the motion of the equatorward border. 160
- 67 A theoretical latitude profile along a meridian  $4^\circ$  to the west of the central meridian of the ionospheric portion of the model current system. The model three-dimensional current system involves both the westward Hall current, southward Pedersen current and Birkeland sheet currents. The current system has a latitudinal extent of  $4^\circ$  and longitudinal extent of  $16^\circ$ . A current of  $10^5$  A was used in the calculation. 162
- 68 A differential profile for one quarter cycle of the oscillation in borders and intensity of the current system shown in Figure 67. 164
- 69 Two differential profiles one quarter of a cycle apart. The data were bandpass filtered (100 MHz). The perturbation pattern was associated with micropulsations at  $\sim 6$  mHz. 165
- 70 Magnetograms for the Day 347, 1971 event. 172
- 71 1-20 MHz bandpass filtered magnetograms for the Day 347, 1971 event. 173
- 72 Magnetograms for the Day 253, 1974 event. 174
- 73 1-20 MHz bandpass filtered magnetograms for the Day 253, 1974 event. 175
- 74 Magnetograms for the Day 254, 1974 event. 176

FIGURE		PAGE
75	1-20 MHz bandpass filtered magnetograms for the Day 254, 1974 event.	177
76	Magnetograms for the Day 255, 1974 event.	178
77	1-20 MHz bandpass filtered magnetograms for the Day 255, 1974 event.	179
78	Raw power spectra for the three components (H, D, Z) for the Day 347, 1971 (1745-1845 UT) event. The data were filtered with a 1-20 MHz bandpass filter.	182
79	The locations of the convection westward electrojet plotted as a function of invariant latitude and Universal Time for the Day 347, 1971 event.	184
80	Same as Figure 78 except for the Day 253, 1974 (1330-1430 UT) event.	185
81	Same as Figure 78 except for the Day 254, 1974 (0945-1045 UT) event.	186
82	Same as Figure 78 except for the Day 255, 1974 (1000-1100 UT) event.	188
83	Latitude profiles of power and relative phase along with the polarization ellipses for the Day 347, 1971 (1745-1845 UT) event at 11.2 MHz. The locations of the stations are indicated at the top of the figure. The ellipses that are shaded indicate CW polarization and those that are not shaded indicate CC polarization.	189
84	Longitude profile showing variations of power, relative phase and polarization. The longitude is measured in the geomagnetic coordinate system. MCMU is $\sim 3^\circ$ equatorward of the three other stations (which lie approximately along the same latitude line) and is due south of URAN. The plot is for the Day 253, 1974 (1330-1430 UT) event at 12.5 MHz.	191

FIGURE		PAGE
85	Same as Figure 84 except for the Day 254, 1974 (0945-1045 UT) event at 11.7 mHz.	192
86	Same as Figure 84 except for the Day 255, 1974 (1000-1100 UT) event at 11.7 mHz.	193
A1	Block diagram of the basic magnetic recording system at each station.	222
A2	Gain curve of the magnetometer.	224
A3	Theoretical frequency response curve for the magnetometer.	225
A4	Block diagram of the digital recording system.	227
B1	The spectral window for smoothing the periodograms.	237
B2	Variation of the confidence interval and bandwidth.	238
C1	A latitude profile for an E-W current system with 20° E-W extent [after Kisabeth, 1972].	241
C2	Latitude profiles associated with current systems having various latitudinal current distributions [after Kisabeth, 1972].	243
C3	A latitude profile for a N-S current system with 4° E-W extent [after Kisabeth, 1972].	245
C4	A latitude profile for a N-S current system with 4° E-W extent [after Kisabeth, 1972].	246

## CHAPTER I

### INTRODUCTION

#### 1.1 Definition and Classification of Micropulsations

The earth's magnetic field is not constant but fluctuates with time with periods ranging from small fractions of a second to more than 30 millions of years. While the longer period changes are of internal origin, variations with periods less than a few days are of external origin. That part of the geomagnetic spectrum which covers a frequency range of 1.7 to 5000 mHz with the corresponding period range of 0.2 seconds to 10 minutes is generally referred to as geomagnetic micropulsations. Their amplitudes can vary from a fraction of a gamma to hundreds of gammas (1 gamma = 1 nT =  $10^{-5}$  gauss). This thesis deals with micropulsations in the 1 to 16 mHz frequency range.

The history of micropulsations stretches back over more than a century. In 1861, Stewart, while studying a great magnetic storm recorded at Kew Observatory, noted: "The exertion of the disturbing force was of a throbbing or pulsatory character. The interval of time between two of these minute pulsations may be said to have varied from half a minute, or the smallest observable portion of time, up to four or five minutes." [Stewart, 1861]. Since then, a great diversity of papers has appeared in the literature dealing

with the topic of micropulsations. The largest increase in the output of papers came about in the late 1950's after the I.G.Y. More recent advances in the study of pulsations have stemmed from the improvement of instrumentation, viz. the development of induction magnetometers, establishment of magnetic tape recording systems, etc.

Studies of the characteristics of micropulsations have led to the separation of this activity into various groups and many authors have devised their own classification systems. In order to avoid confusion and to standardize the nomenclature used, a classification system was approved at the thirteenth General Assembly of the IUGG in Berkeley, California [Jacobs et al., 1964]. In this classification system, micropulsations were divided into two main groupings: those of regular and continuous appearance called Pc, and those with an irregular form called Pi. The Pc group was further divided into five subgroups and the Pi group into two subgroups. The classification is shown in Table 1. It should be emphasized that the properties of different classes may overlap and that there may be different source mechanisms producing pulsations within the same class. Until a better classification system is devised based on the correlative and genetic properties of micropulsations, the above classification based on morphological properties will continue to be useful. This thesis is concerned with the regular and continuous pulsations in the spectral range 1 - 16 mHz in the



Table 1 Micropulsation Classifications

Pc	Frequency (mHz)	Period (sec)	Pi	Frequency (mHz)	Period (sec)
Pc 1	200-5000	0.2-5	Pi 1	25-1000	1-40
Pc 2	100-200	5-10	Pi 2	6.7-25	40-150
Pc 3	22.2-100	10-45			
Pc 4	6.7-22.2	45-150			
Pc 5	1.7-6.7	150-600			

morning sector. Thus, the pulsations discussed in this thesis belong to the groups Pc 4 and Pc 5.

### 1.2 The Magnetosphere

Since micropulsations are of external origin, a brief description of the earth's magnetic field and plasma environment is warranted here.

The earth is enclosed in a cavity, called the magnetosphere, which is carved out of the solar wind by the earth's magnetic field. The basic configuration of the magnetosphere is shown in Figure 1.

The idea that a stream of particles flows outward from the sun into interplanetary space originated as long as 300 years ago with the work of Halley. Near the beginning of this century, Störmer [1906] and Birkeland [1908, 1913] introduced the concept that charged particles of solar origin might be responsible for the production of geomagnetic storms and auroras. Chapman and Ferraro [1931] described the solar plasma from the hydromagnetic point of view in the early thirties. Their model suggested that discrete clouds of plasma were emitted from the sun during solar flares. Guided by the observation that the type I tails emitted by comets (tails of ionized material which scatter sunlight) always point away from the sun regardless of the position of the comet on its trajectory, Biermann [1951] developed a more realistic picture which featured continual flow of plasma away

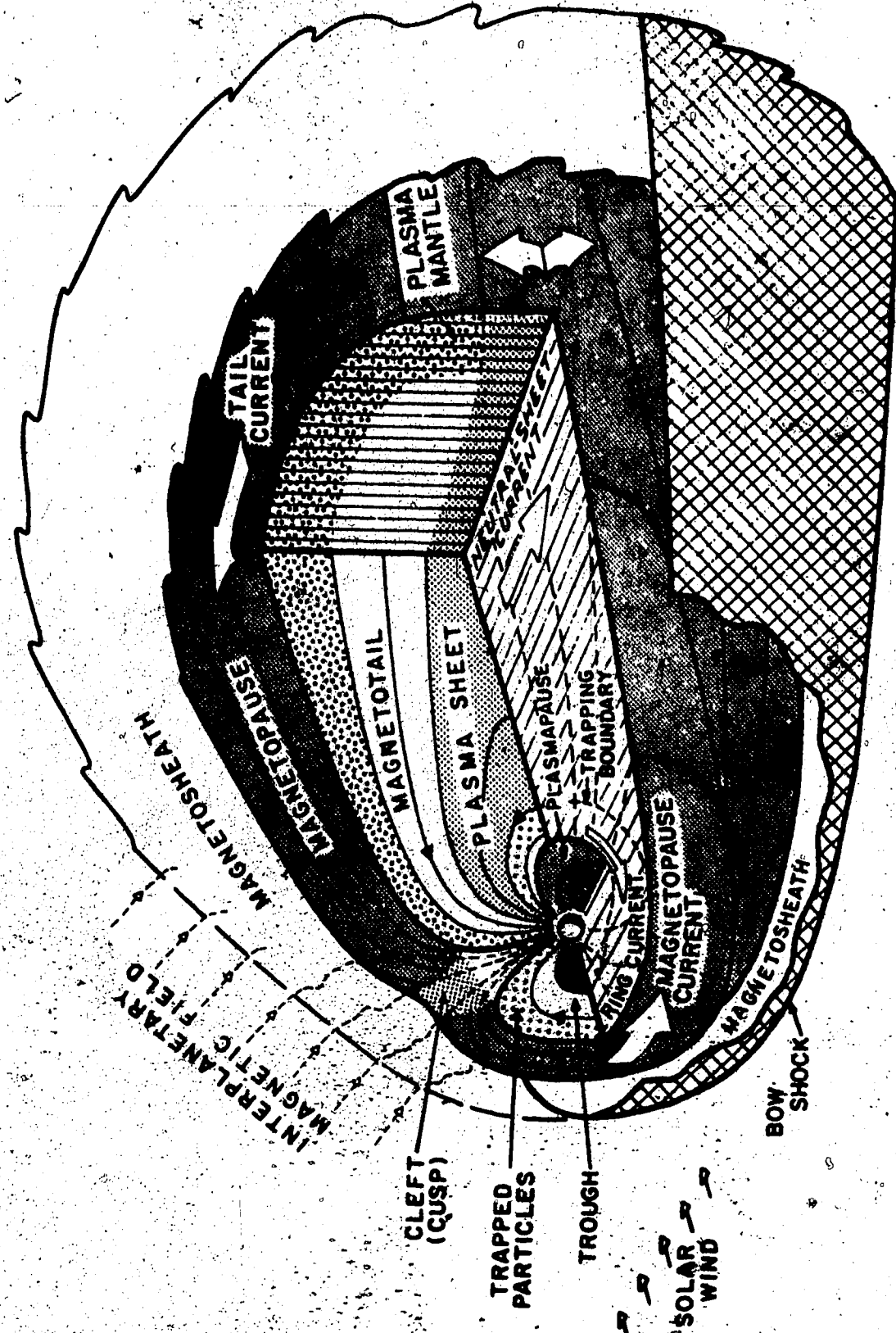


Figure 1

from the sun (which is now known as the solar wind). After Biermann's contribution, Chapman [1959] in the late fifties, developed a model for the solar atmosphere in static equilibrium and predicted that a finite pressure must be exerted inward on the solar atmosphere at great distances. Parker [1960] pointed out this error of finite pressure at infinity in Chapman's theory. In a series of papers beginning in 1957 on the investigation of the expansion of the solar corona into interplanetary space, Parker developed a general theory of steady, radial and spherically symmetric flow of plasma from the sun. [See Parker, 1963].

The investigation of interplanetary space by artificial satellites and space probes has confirmed the model of the solar wind as developed by Parker. It is now established that the solar wind is a completely ionized medium composed primarily of hydrogen (protons and electrons) with about 5% of ionized He streaming continually from the sun. The solar wind carries with it the coronal magnetic field from the sun which is termed the interplanetary magnetic field (IMF). Approximately 80% of the IMF is confined to the ecliptic plane with a small component perpendicular to the ecliptic plane. This normal component of the IMF seems to play a major role in the initiation of magnetospheric storm and substorm activity [Dungey, 1953, 1961; Fairfield and Cahill, 1966; Rostoker and Fälthammer, 1967]. Substorm activity tends to be enhanced less than an hour after the normal component of the IMF has

turned southward (i.e., pointing below the ecliptic plane) [Arnoldy, 1971; Rostoker et al., 1972; Meng et al., 1973].

Typical values for the solar wind parameters at the orbit of the earth are: bulk velocity  $\sim 300-500$  km/sec, number density  $\sim 5-10/\text{cm}^3$ , IMF  $\sim 5-10\gamma$  (the field strength increases with high solar activity), temperature  $\sim 5 \times 10^4$  °K (It can vary between  $10^4$  °K and  $10^6$  °K. The temperature tends to be higher when the sun is active.), Alfvén velocity  $\sim 50-100$  km/sec and velocity of sound in the solar wind  $\sim 100-200$  km/sec.

Since the solar wind is both supersonic and super-Alfvénic, a standing magnetohydrodynamic shock wave is set up approximately  $14 R_E$  in front of the earth. Downstream from the standing shock, the bulk flow becomes subsonic (the Mach number being  $\sim 0.2$ ) and the solar wind plasma is thermalized. This region of shocked plasma is called the magnetosheath. The position at which the dynamic pressure of the shocked solar wind plasma is balanced by the outward pressure of earth's magnetic field marks the boundary of the magnetosphere, called the magnetopause (which is about 100 km thick). On the dayside, the magnetospheric magnetic field lines are more or less dipolar and have a magnitude of  $\sim 50\gamma$  just inside the magnetopause. However, under the sweeping action of the solar wind, the magnetic field lines are greatly distended on the night side forming a magnetotail which reaches beyond the orbit of the moon at  $\sim 60 R_E$ . The center of the tail is

dominated by a region of energetic plasma (number density  $\sim 0.1-30/\text{cm}^3$ ) known as the plasma sheet. The plasma sheet thickness increases from about  $5 R_E$  near the center of the tail to about  $10 R_E$  near the flanks. Its width is about  $20 R_E$ . The center of the plasma sheet marks a region of magnetic field reversal known as the neutral sheet (which is about 600 km thick). On either side of the plasma sheet are regions of low plasma density ( $\leq 0.01/\text{cm}^3$ ) and enhanced magnetic field termed the tail lobes. Typical magnetic field strengths in the near earth plasma sheet are  $\sim 10\gamma$  while the tail lobe at similar distances from the earth has field strength of 15-20 $\gamma$ .

The magnetosphere is populated by 'cold' plasma, 'hot' plasma and energetic electrons and protons. The 'cold' or thermal plasma refers to particles with energies in the range of a few eV to a few tens of eV. They form a region of dense plasma surrounding the earth called the plasmasphere. This volume of cold plasma has a toroidal shape with cross section resembling the dipole field. The plasmasphere has a field aligned boundary called the plasmopause. The plasmopause separates the region of high thermal plasma density, the plasmasphere ( $\sim 100$  electrons/ $\text{cm}^3$  in the equatorial plane) from a region of low plasma density, the plasma trough ( $\sim 1$  electron/ $\text{cm}^3$  in the equatorial plane). The mean equatorial radius of the plasmopause is typically about  $4 R_E$ , but may

vary from about  $7 R_E$  during extreme quiet periods to  $2-3 R_E$  during disturbed times. Outside the plasmopause, the thermal plasma density decreases approximately as  $R^{-4}$ . Inside the plasmopause, the density distribution along field lines is more or less in agreement with a diffusive equilibrium model which gives a much less rapid decrease than the  $R^{-4}$  model.

The 'hot' plasma refers to particles whose energies range from several tens of eV to several tens of keV. This plasma population, though less dense than the thermal plasma, carries the largest share of the particle energy density. The energetic particles are particles with energies that range from a few hundred keV to a few MeV (for electrons) and a few hundred MeV (for protons). They are the least numerous group of particles and constitute the so-called trapped Van Allen radiation belts.

It is now well known that energy from the solar wind penetrates to the interior of the magnetosphere and is transferred from one place to another within the magnetosphere through the convective motion of the flux tubes (and their frozen-in plasma)  $[\vec{V}_E = \frac{\vec{E} \times \vec{B}}{B^2}]^1$  as well as the gradient drift  $[\vec{V}_G = \frac{W_{\perp}}{eB} \hat{B} \times \nabla B]^2$  and curvature drift

<sup>1</sup> MKS units are used.  $\vec{E}$  is the electric field and  $\vec{B}$  the magnetic field.

<sup>2</sup>  $W_{\perp} = \frac{1}{2} m v_{\perp}^2$  is the K.E. of the particle associated with the gyration around field lines.  $e$  is the charge of the particle.  $\hat{B}$  is a unit vector parallel to  $\vec{B}$ .

$[\vec{V}_C = (\frac{2W_{\parallel}}{eB^2})\hat{B} \times (\hat{B} \cdot \nabla)\hat{B}]^3$  of the energetic particles.

Recent studies by Rosenbauer et al. [1975] suggest that solar wind plasma gains entry to the magnetosphere through the polar cleft and becomes part of the plasma mantle streaming downtail away from the earth. It is thought that the plasma mantle particles eventually populate the plasma sheet and acquire a drift velocity and field-aligned streaming velocity toward the earth [Rostoker, 1976].

Insofar as the motion of the plasma sheet particles close to the earth is concerned, curvature and gradient drift become significant causing electrons to drift eastward and protons westward. The drifting particles have a component of their population which precipitates into the upper atmosphere both exciting and ionizing the constituent atmospheric particles. It is now understood that the plasma sheet of the magnetotail maps into a region of enhanced auroral luminosity and electrical conductivity called the auroral oval [Frank, 1971; Lassen, 1974] (Figure 2). An artist's conception of the auroral oval is shown in Figure 3.

Rostoker and Boström [1976] have suggested that the electric field driving the ionospheric current originates in the magnetosphere as shown in Figure 4. Since the plasma in the magnetotail is collisionless, one may consider the conductivity along the magnetic field lines to be nearly

---


$$^3 W_{\parallel} = \frac{1}{2} m v_{\parallel}^2$$



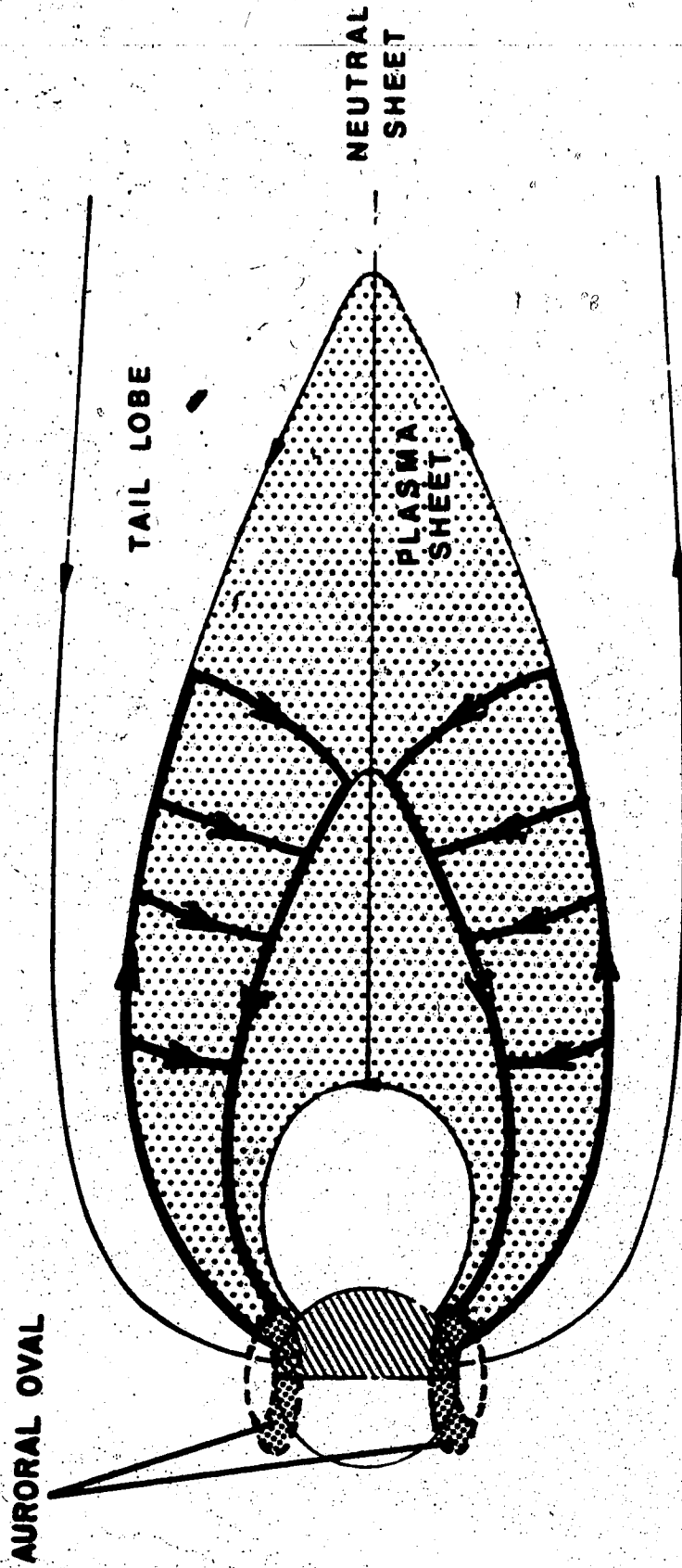


Figure 2

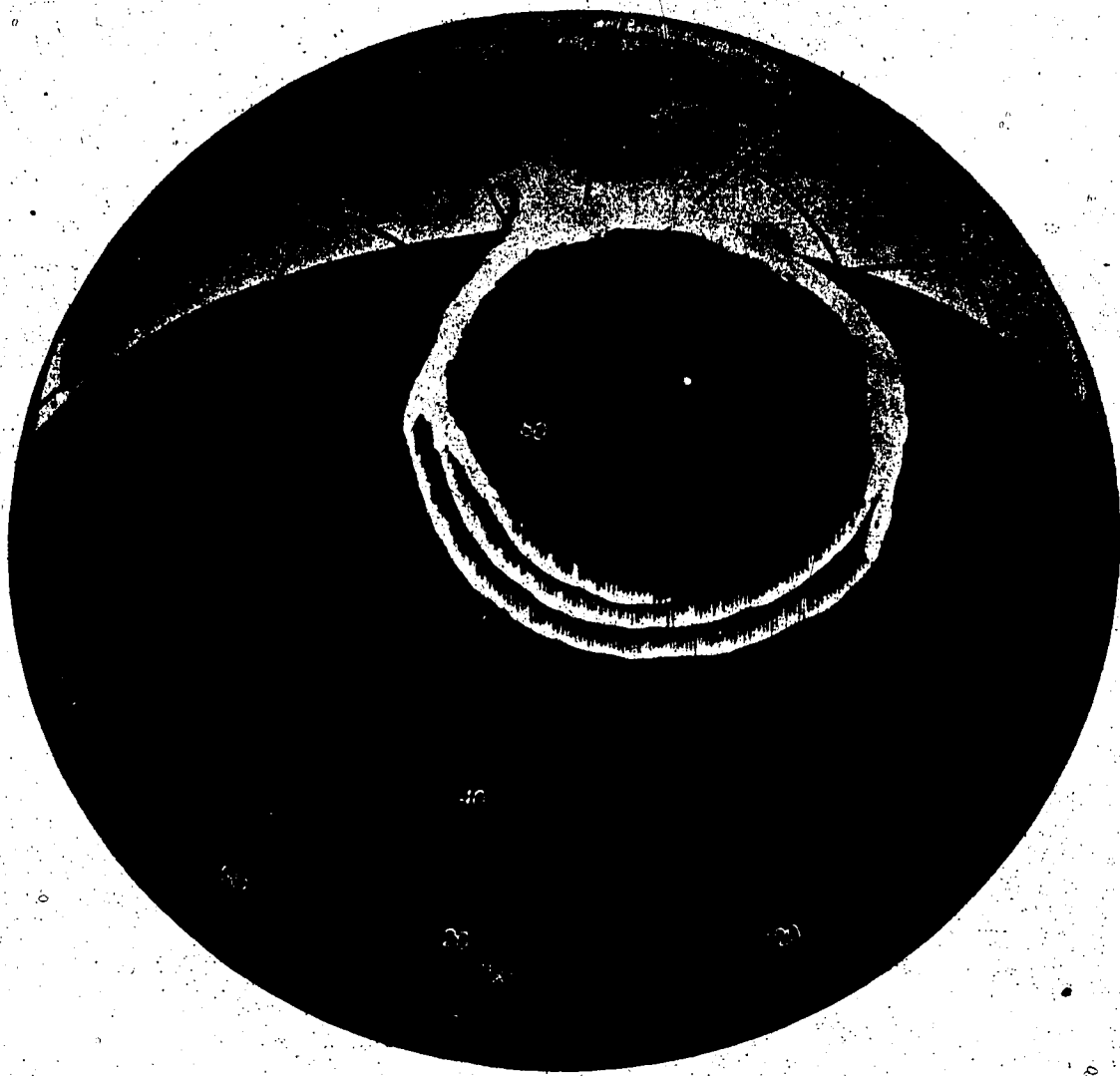


Figure 3

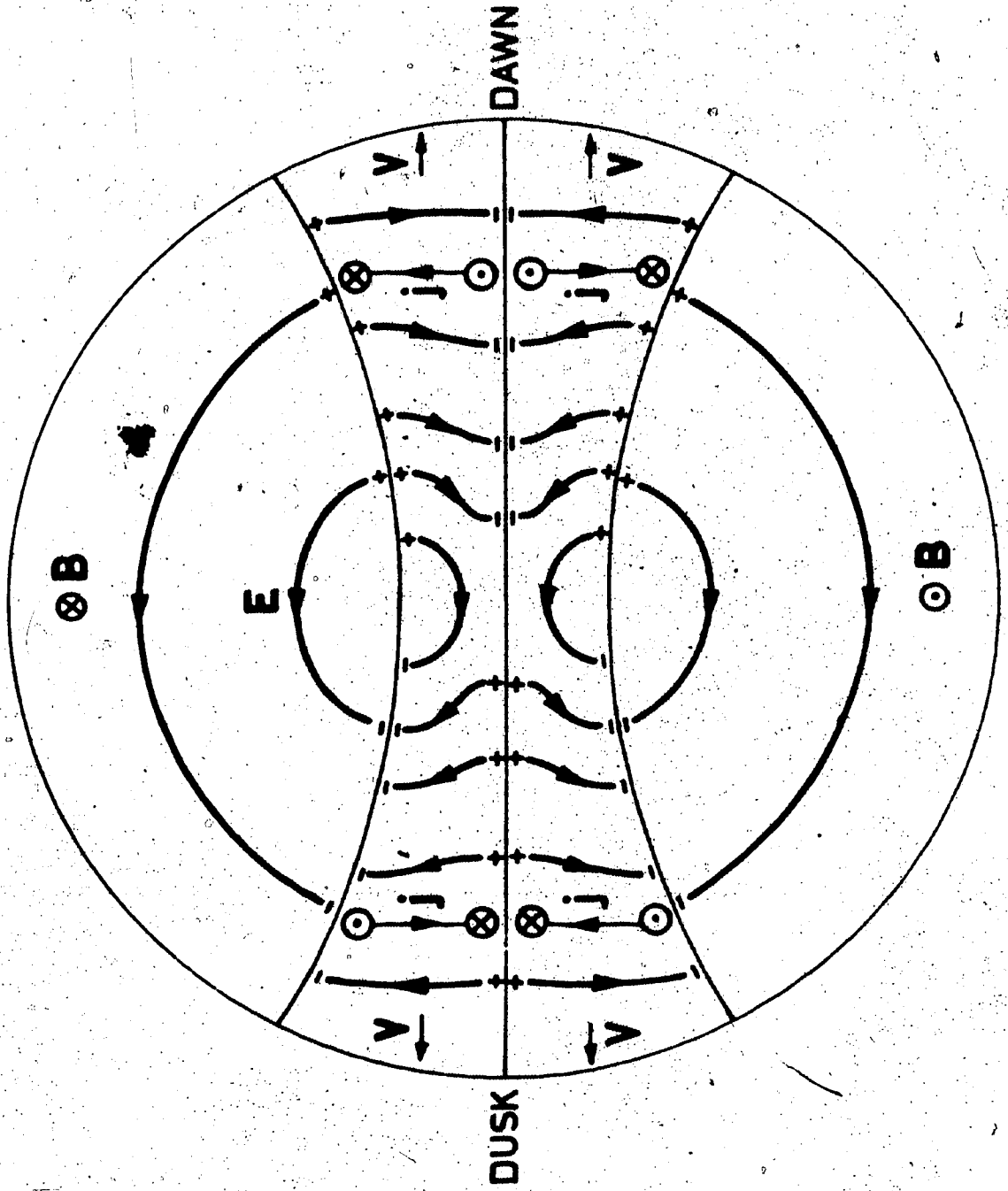


Figure 4

infinite, in which case the magnetic field lines may be considered as equipotentials. Thus any electric field normal to the magnetic field in the magnetosphere will map along magnetic lines of force into the ionosphere. The magnetospheric electric field when mapped into the ionosphere is shown in Figure 5. As mentioned earlier, the auroral oval is a region of enhanced conductivity due to energetic particle precipitation. Thus, the existence of electric fields in a region of high conductivity results in electric current flow.

In Figure 5, it can be seen that the Hall currents (current flow whose direction is perpendicular to both the electric field and magnetic field) are driven in the auroral oval such that the flow is eastward in the evening sector (the eastward electrojet) and westward in the morning sector (the westward electrojet). Based on the electric field data of Heppner [1972] and Mozer and Lucht [1974], it is considered that the above mentioned electrojets are Hall currents flowing in the E-region of the ionosphere ( $\sim 100$  km above the surface of the earth). In addition to the Hall currents, direct (Pedersen) currents flow in the direction of the N-S electric field. The conductivity discontinuities at the edges of the auroral oval cause the ionospheric current to diverge and flow along the magnetic lines of force. These field-aligned currents (the Birkeland currents) flow into and out of the tail region and couple the magnetosphere to the ionosphere.

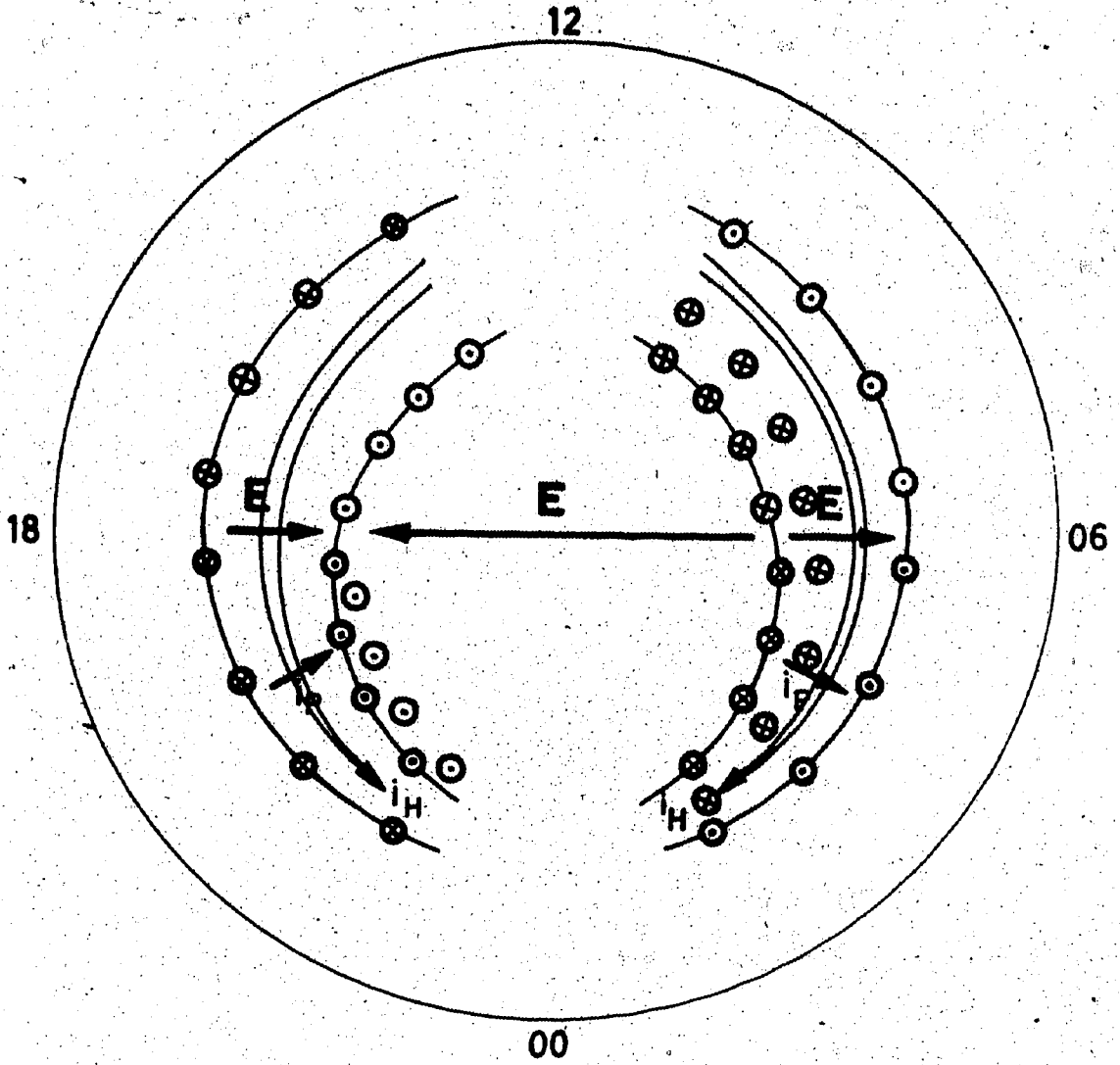


Figure 5

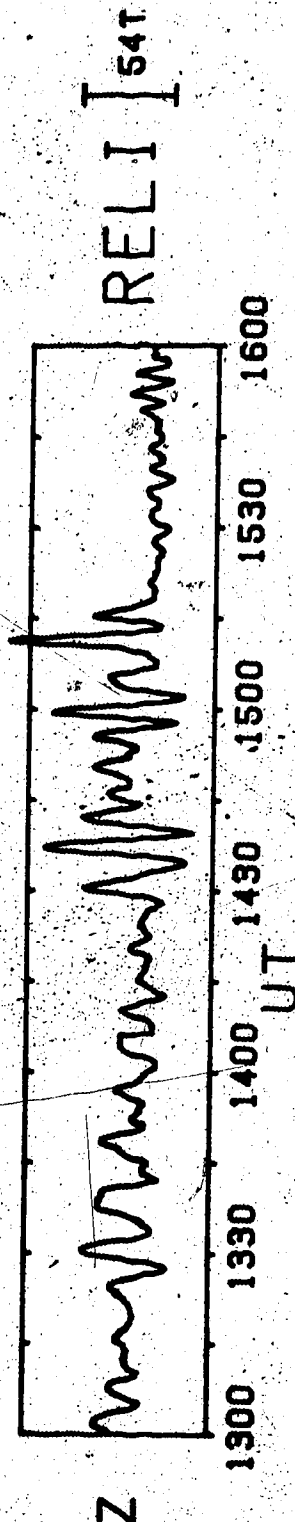
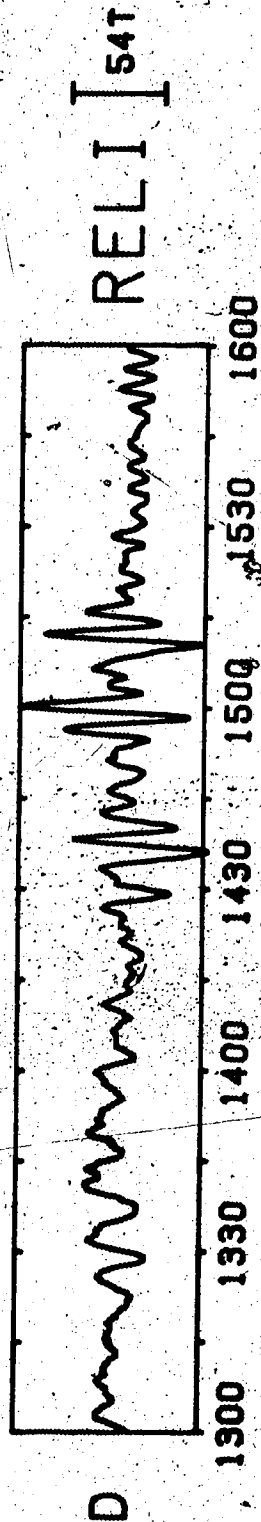
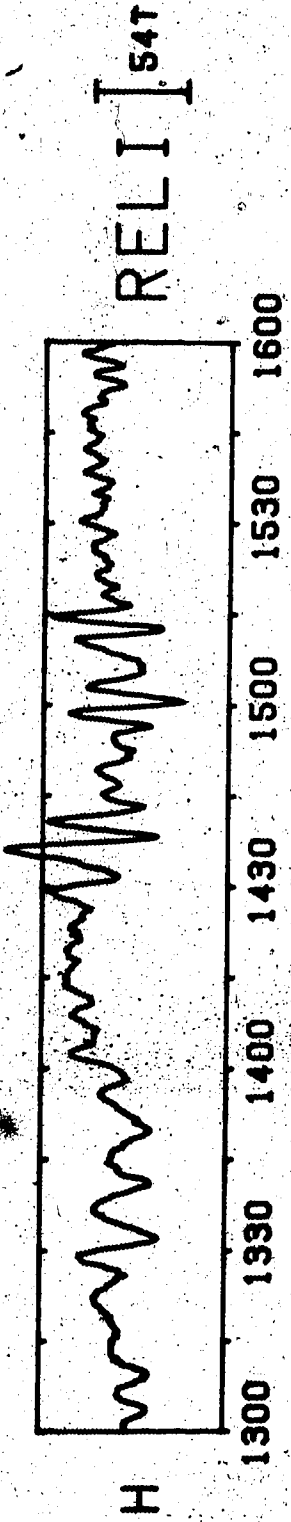
They have been observed using magnetometers aboard polar orbiting satellites [Zmuda and Armstrong, 1974] and are thought to be driven by MHD generation processes in the magnetotail [Rostoker and Boström, 1976]. The flow pattern of these currents is already shown in Figure 2. Finally, we note that there tends to be net downward current flow in the morning sector and net upward flow in the evening sector [Yasuhara et al., 1975]. As we shall demonstrate later in this thesis, Pc 5 micropulsations in the morning sector which have peak amplitudes in the auroral oval are generated by a combination of spatial and temporal oscillations of the current systems described above.

### 1.3 The Morphology of Pc 5 and 'Pc 4'

#### (a) Pc 5

This class of pulsations with the longest period has amplitudes of a few gammas to several hundred gammas. The oscillations are rather regular, with a wave train consisting of a series of damped type variations lasting about an hour or more. An example of Pc 5 recorded at high latitudes is shown in Figure 6. The duration and amplitude of the wave trains in the morning hours are generally longer and greater respectively than those in the afternoon. The oscillations are most sinusoidal in the morning and early afternoon [Jacobs and Wright, 1965]. The Z-component (the vertical component) of such pulsations can reach appreciable amplitude in the auroral

DAY 45 1972



zone [Eleman, 1966] or at the latitude of maximum intensity of the horizontal components [Samson, 1972]. A given Pc 5 event has the same frequency at all latitudes [Ellis, 1960; Obertz and Raspopov, 1968; Samson and Rostoker, 1972]. There are only a few exceptional cases in which the H-component varies with latitude [Siebert, 1964; Voelker, 1968; Rostoker and Samson, 1972]. Oscillations similar in amplitude and period often appear simultaneously at conjugate stations [Nagata et al., 1963; Jacobs and Wright, 1965].

It is now well established that the occurrence frequencies and amplitudes of Pc 5 maximize in the auroral zone ( $65^{\circ}$  -  $70^{\circ}$  geomagnetic latitude) [Jacobs and Sinno, 1960; Kato and Saito, 1962; OI', 1963; Kokubun and Nagata, 1965; Obertz and Raspopov, 1968; Hirasawa, 1970; Gupta, 1973, 1974]. Samson [1972] found that the intensity maximum of Pc 5 follows the statistical auroral oval as illustrated in Figure 7.

Gupta [1973] carried out a statistical study of the occurrence frequencies of Pc 5 using seven Canadian stations covering a latitudinal range ( $83.1^{\circ}$ N -  $54.3^{\circ}$ N) and a longitudinal range ( $287.7^{\circ}$ E -  $347.2^{\circ}$ E). He found that the diurnal variation in occurrence frequencies of Pc 5 shows a peak in the morning and a peak in the evening hours for all stations. The evening peak is more dominant in the polar zone. In the auroral zone, the morning peak is more dominant in agreement



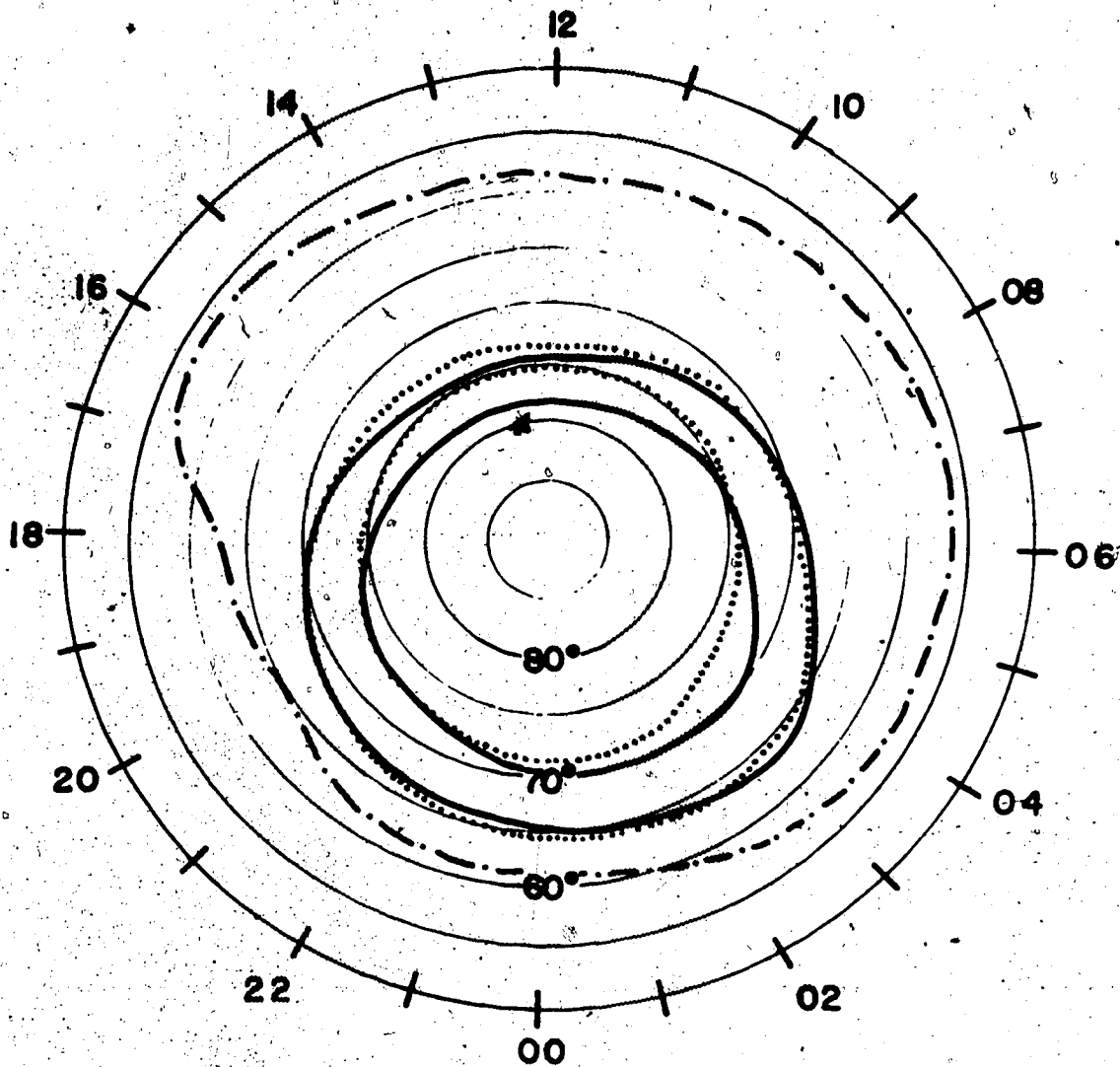


Figure 7

with the results of Saito [1964] and Hirasawa [1970] who noticed that the occurrence frequency peak in the morning is sharply defined and centered near 0400-1000 LMT. Gupta also noted a midnight peak in the auroral zone. In the sub-auroral zone, the evening peak is more pronounced. Saito [1964] noted that Pc 5 are observed with equal probability over most of the day in mid latitudes. The basic diurnal variation pattern of the occurrence frequency of Pc 5 is unchanged for different seasons and different levels of magnetic activity [Gupta, 1973]. While simultaneous occurrences of Pc 5 rarely were noted at the seven Canadian stations (about 2% of the events), Gupta found simultaneous occurrence in the auroral zone stations covering an area of  $10^\circ$  latitude and  $20^\circ$  in longitude in more than half of the events he studied. Obertz and Raspopov [1968] observed that the characteristic longitudinal extent of Pc 5 is  $60^\circ$ . The following results of Gupta [1973] should be noted in passing: 27 day recurrence tendency is weak; correlation between occurrence and Kp is good up to  $Kp = 5^\circ$  and  $\Sigma Kp = 37$ ; correlation between occurrence and daily and monthly mean relative sunspot numbers is poor; there is greater occurrence of Pc 5 in summer than in winter.

The diurnal variation in amplitude of Pc 5 shows a peak in the early morning and another in the evening [Jacobs and Sinno, 1960; Kato and Sato, 1962; Kokubun and Nagata, 1965] with the morning peak dominating the evening one.

Gupta [1974] noticed that, in the auroral zone, the diurnal amplitude maximizes in the morning and this peak tends to move northward reaching the polar station of Resolute Bay around noon. Saito [1964] also observed a single maximum in the diurnal variation of amplitude at the high latitude stations of Fort Churchill and Point Barrow. Only occasionally did Gupta find a maximum of amplitude during prenoon and post noon hours for the seven Canadian stations. He also reported a midnight peak for all the auroral zone stations and that the diurnal variation pattern of Pc 5 amplitude showed no clear relationship with seasons or with magnetic activity. The amplitudes of Pc 5 do not show 27 day recurrence tendency but seem to have a linear relationship with Kp up to a level of 6- .

The polarization of Pc 5 in the horizontal plane exhibits both latitudinal and diurnal variations. Kaneda et al. [1964] and Obertz and Raspopov [1968] showed that Pc 5 exhibit pronounced latitudinal change in the sense of polarization. They reported that Pc 5 at Barrow ( $68.6^\circ$ ) had cw polarization (clockwise polarization looking along the direction of the magnetic field) and Pc 5 at College ( $64.7^\circ$ ) and Sitka ( $60^\circ$ ) had cc (counter-clockwise) polarization when the center of activity was between College and Barrow. An appreciable latitudinal phase shift in the H-component accompanied the polarization reversal. Samson et al. [1971]

also found that Pc 5 observed at stations south of Fort Smith ( $67.3^\circ$ ) had a sense of polarization opposite to that at Cambridge Bay ( $76.8^\circ$ ). In addition, Samson et al. [1971] noted that the line of intensity maximum of Pc 5 coincided with the demarcation line separating the regions of opposite polarization.

Earlier, before the discovery of the demarcation line, studies of the diurnal variation of Pc 5 polarization in the northern auroral zone region by Nagata et al. [1963], Kato and Utsumi [1964] and Kokubun and Nagata [1965] indicated that the sense of polarization in the horizontal plane was predominantly cc in the morning and cw in the evening. Samson et al. [1971] also observed the above polarization patterns equatorward of the demarcation line. A summary of both the latitudinal and diurnal variations of the H-D polarization of Pc 5 is shown in Figure 8.

The polarization characteristics of a broad band of micropulsations have been investigated statistically by Rankin and Kurtz [1970]. They have analysed the magnetic data recorded at 14 stations distributed in central and southwest Alberta from  $49^\circ 51'N$  geographic to  $54^\circ 26'N$  and  $112^\circ 17'W$  geographic to  $117^\circ 50'W$ . The average senses of polarization in the horizontal plane of micropulsations in the spectral range 3.3 - 100 mHz are shown in Figure 9. This spectral range covers the higher frequency bands of Pc 5, and the complete Pc 4 and Pc 3 bands. It can be seen from Figure 9

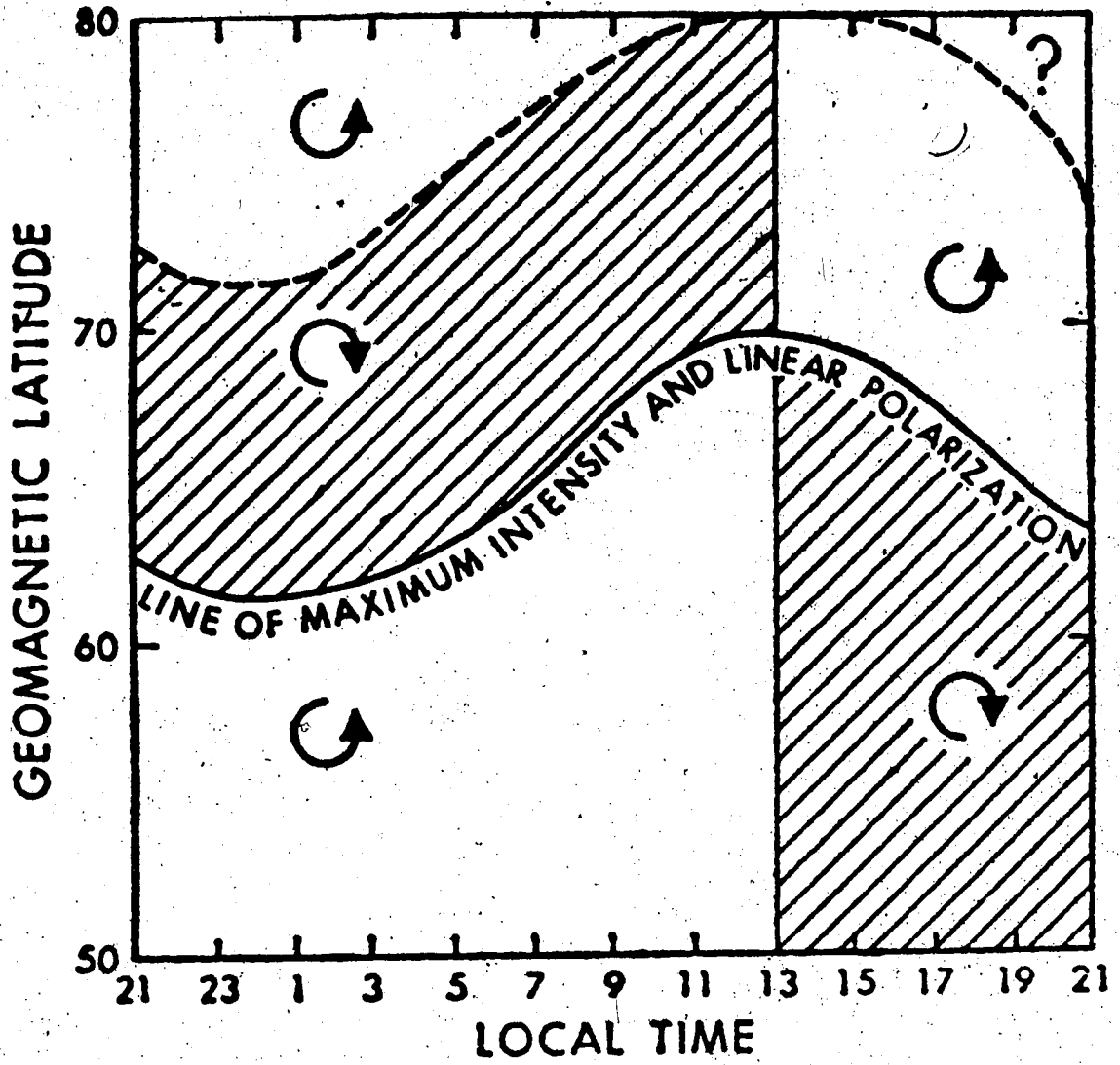


Figure 8

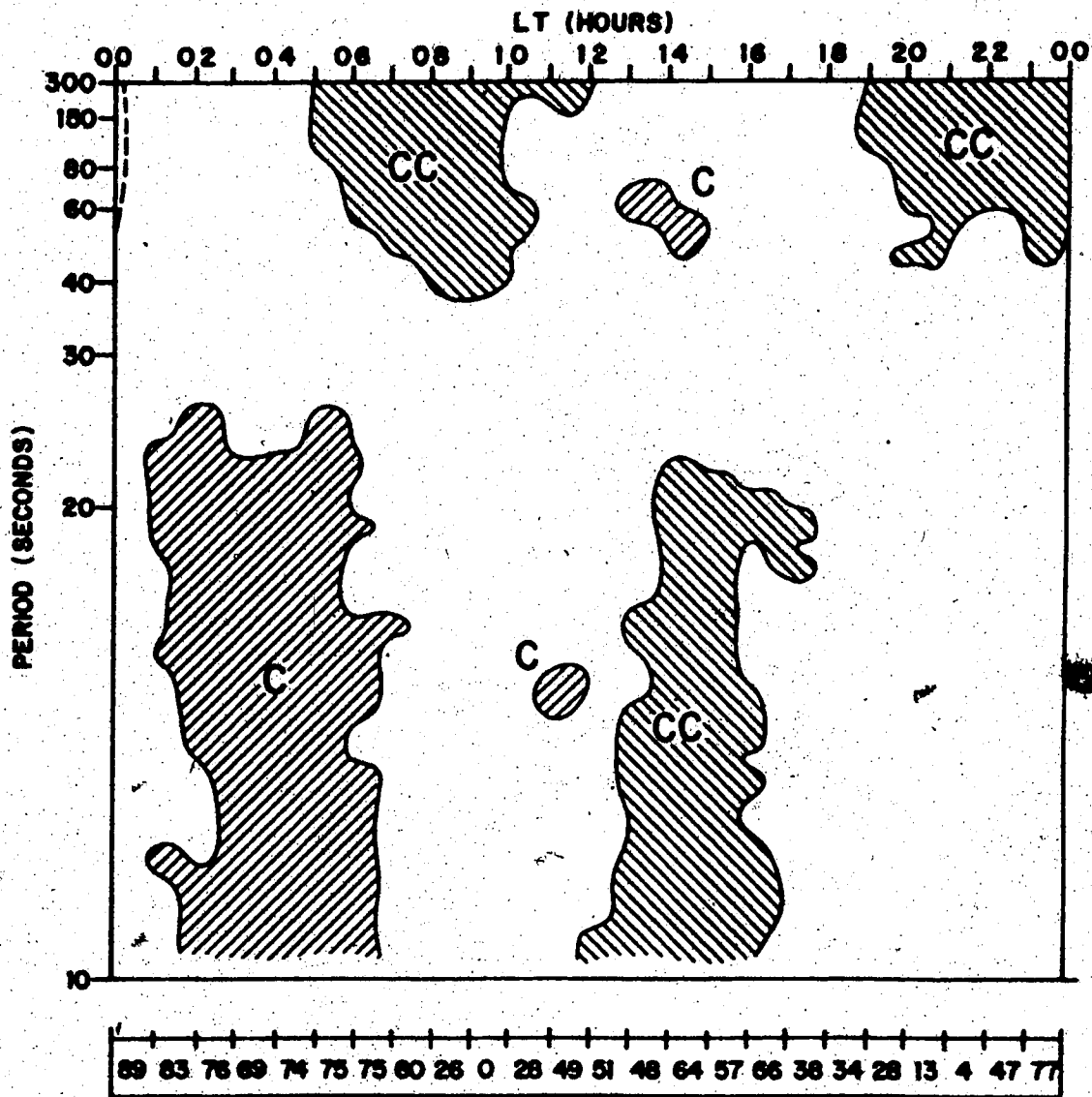


Figure 9

that the diurnal polarization pattern of high latitude Pc 4 and Pc 5 pulsations are similar, while the sense of polarization of Pc 3's (22.2 - 100 mHz corresponding a period range of 10-45 seconds) is opposite to that of Pc 4, 5's with cw polarization in the morning and cc polarization in the afternoon.

The cc polarization in the morning and cw polarization in the evening are valid not only for the statistical case but also for simultaneous observations on both morning and evening sides of the earth [Troitskaya, 1967]. This characteristic in polarization has led Nagata et al. [1963] and Kokubun and Nagata [1965] to suggest that Pc 5 pulsations are due to transverse hydromagnetic waves on magnetic field lines near the magnetopause excited by a hydromagnetic interaction of the solar wind and the geomagnetic field. Atkinson and Watanabe [1966] subsequently suggested that the transverse hydromagnetic waves are a result of a surface wave motion at the magnetopause and the surface wave is generated through the development of Kelvin-Helmholtz instability as first suggested by Dungey [1954]. Based on this distinct diurnal variation pattern of polarization in H-D plane, Samson et al. [1971] also tended to favour the idea that Pc 5 pulsations are generated through the development of Kelvin-Helmholtz instabilities at the magnetopause. A more detailed discussion on the theory of micropulsations will be given in the next chapter.

The diurnal variation of the sense of polarization is reversed in the southern auroral zone compared to the northern auroral zone [Nagata et al., 1963]. This is to be expected since the senses of polarization are conserved along field lines [Nagata et al., 1963; Jacobs and Wright, 1965]. In mid latitudes the diurnal polarization characteristics are more complicated with four sectors alternating from cw to cc [Saito, 1964].

With regard to the polarization ellipses in the H-D plane, Samson [1972] observed that the morning sector has consistently elliptical cc polarization and that the afternoon sector has a mixture of senses of polarization and a predominance of almost linear polarization in H. The ellipses at the high latitude stations ( $58.4^\circ - 76.8^\circ$ ) are predominantly polarized in the H direction.

There have been only a few studies on the polarization characteristics in the vertical planes for a few events [Paulson et al., 1965; Wilson, 1966; Annexstad and Wilson, 1968]. Samson [1972] carried out a statistical study on the polarization characteristics in the H-Z and D-Z planes. Most of the stations show cw polarization in the H-Z plane over the entire day. The ellipses are predominantly polarized in the H direction. From the analysis of the polarization characteristics in the H-Z plane, Samson concluded that the perturbation magnetic field of Pc 5 is definitely not polarized transverse to the main geomagnetic field. The senses of polariza-



tion in the D-Z plane at Cambridge Bay (76.8°) and Fort Smith (67.3°) are cc in the morning and slightly cw in the afternoon and evening with the reverse being true at the southern stations. The major axes at most stations seem to favour the D direction in the interval (5 - 9 LT) in the D-Z plane. At other times, the polarizations are more confused.

This thesis is concerned with the Pc 5 pulsations in the morning sector which have 'cleaner' wave forms and 'clearer' polarization characteristics than pulsations occurring at other times of day. The Pc 5 pulsations which occur during the main phase of geomagnetic storms and are confined to the afternoon sector [Barfield et al., 1972; Lanzerotti et al., 1975] and the midnight Pc-5 noted by Gupta [1973, 1974] will not be dealt with in this thesis since these pulsations, though in the Pc 5 range, are probably due to different origins.

(b) 'Pc 4'

Pc 4 is described as a regular and continuous pulsation with period between 45 and 150 sec. This existing classification fails to describe the unique features of the kind of pulsations reported by Rolf [1931], Harang [1932, 1936, 1939, 1940-1944], Sucksdorff [1939], Veldkamp [1960] and Annexstad and Wilson [1968]. They referred to that particular pulsation within a narrow band in the Pc 4 range as giant pulsations or Pg's. However these are not giant pulsations in the literal sense because their maximum ampli-

tudes only reach 30 gammas or so which is comparatively much less than those of Pc 5 which reach hundreds of gammas. We will refer to this unique pulsation as 'Pc 4' to be distinguished from other Pc 4's such as those associated with the plasmopause studied by Lanzerotti et al. [1974].

A typical example of 'Pc 4' recorded at our stations is shown in Figure 10. It can be seen that the waveform is highly sinusoidal and well modulated. The average period of 'Pc 4' is 87 sec and its duration varies between 10 minutes and several hours [Sucksdorff, 1939].

The occurrence of 'Pc 4' is rare. Rolf [1931] reported 28 occurrences from almost 9 years of data from the auroral zone station of Abisko. Sucksdorff [1939] observed 150 events over 25 years (1914-1938) of data at Sodankylä with an average of 6 'Pc 4' events per year. Korobkova et al. [1959] found not one single case in the 20 years of data at Tikhaya Bay ( $71.1^\circ$ ) and none were observed at the Soviet polar stations during I.G.Y. Rolf [1931], Harang [1932, 1940-1944] and Sucksdorff [1939] noted that 'Pc 4' occurs most frequently during early morning hours (2-7 LT), around equinoxes and in years of minimum solar activity. The 'Pc 4' pulsations also tend to recur for successive days at intervals of about 24 hours [Sucksdorff, 1939].

The 'Pc 4' pulsations are extremely localized in latitude. This feature is well illustrated by an event on

DAY254 1974

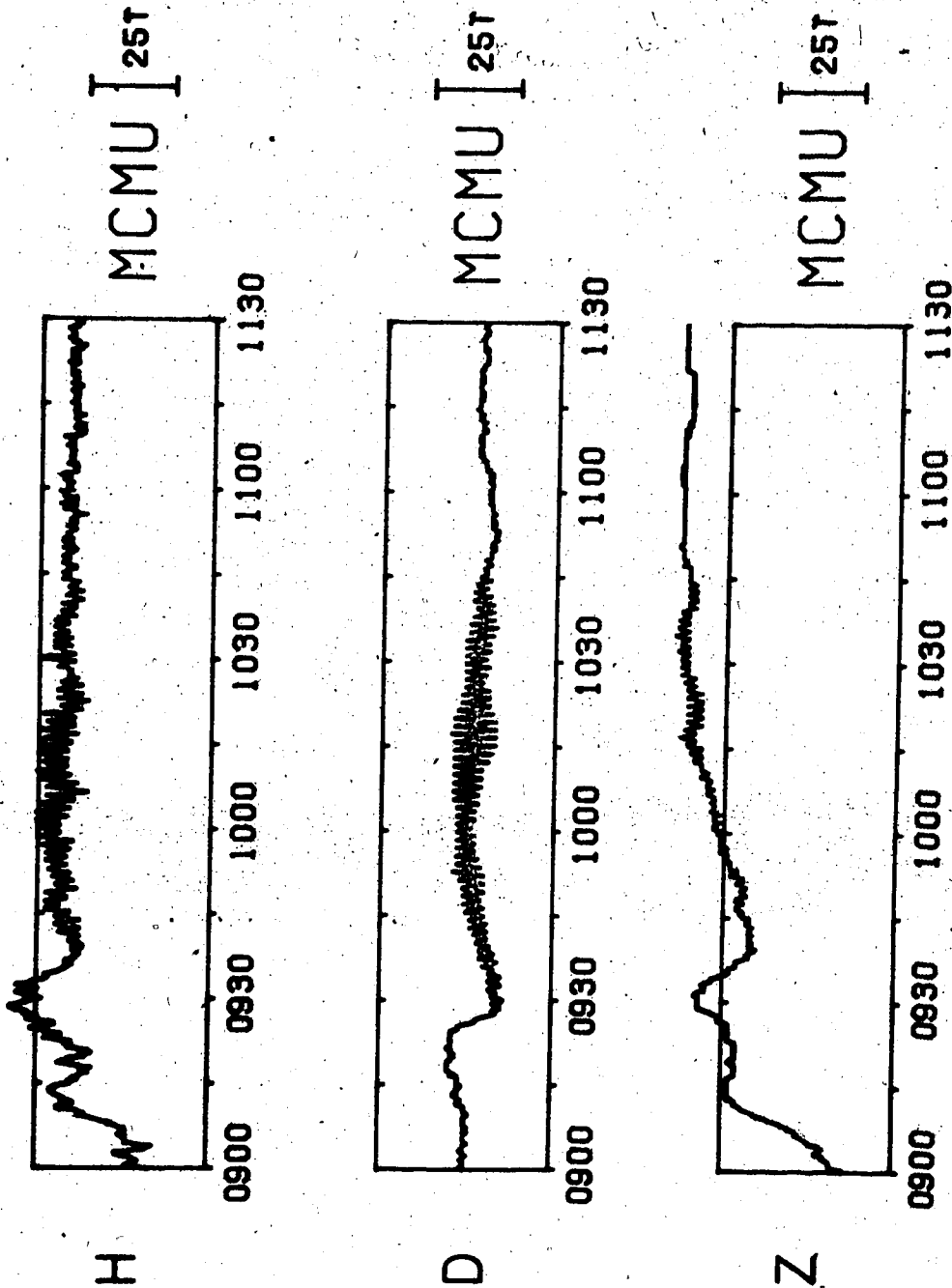


Figure 10

July 17, 1958 studied by Veldkamp [1960] using a large number of stations in Europe. The latitudinal distribution of amplitude of that particular event maximized at  $\sim 57^\circ\text{N}$  geomagnetic and the amplitude dropped to the noise level about  $5^\circ$  north and  $5^\circ$  south of the latitude of maximum intensity. The pulsations occurred in a strip confined within  $50^\circ$  to  $60^\circ$  (The overall spatial distribution of the pulsations was confined to a small area about 1000 km by 1000 km.). The times of beginning and ending of the pulsations were different for different stations and almost simultaneous occurrence was restricted to adjacent stations which were less than 500 km apart. Most stations registered cc polarization in the horizontal plane. Veldkamp contended that the observed period of 105 sec fits well with eigen oscillations of period  $\sim 100$  sec predicted by Obayashi and Jacobs [1958] for field lines emanating from  $57^\circ$  geomagnetic latitude.

Annexstad and Wilson [1968] analysed 20 'Pc 4' events recorded at College and its conjugate, Macquarie Island during years of minimum solar activity. None of the 20 events was seen at polar and mid latitude stations. 75% of the events at College were polarized in cc sense on horizontal plane while 67% of the events at Macquarie Island were polarized in cw sense. Therefore, continuity of the sense of polarization was preserved along the magnetic field lines. 70% of the ellipses in the horizontal plane had their major axis aligned within

$\pm 45^\circ$  of E-W. This means that 'Pc 4' has a larger D-component than the H-component. The polarization ellipses in the H-D plane for the two stations were mirror images of each other across an E-W line. Annexstad and Wilson contended that the 'Pc 4' is a result of the  $n = 2$  (first even mode) mode of a transverse hydromagnetic wave propagating along field lines to conjugate points.

It should be noted that Harang [1939] noticed simultaneous occurrence of pulsations on magnetic records and in the scattering region of radio waves at heights of 650-800 km. He used a powerful transmitter at a frequency greater than the penetration frequency  $f_o F_2$  (i.e., the minimum frequency at which the O wave can penetrate the F layer) and obtained pulsating echoes above the F layer. These pulsating echoes coincided both in duration and period with 'Pc 4' pulsations.

We were fortunate to observe a few occurrences of these rare 'Pc 4' pulsating in our data and they are documented in this thesis.

A more complete review on micropulsations can be found in the following reviews: Jacobs and Westphal [1964], Hultqvist [1966], Troitskaya [1967], Campbell [1967], Saito [1969], Jacobs [1970] and Orr [1973].

#### 1.4 Purpose of This Thesis

A total of nine magnetic stations were in operation in 1971 and early 1972 in Western Canada, arranged approximately along a corrected geomagnetic meridian, and providing very good spatial coverage for high latitude micropulsation events. In particular, the close spacing of stations in the auroral zone provides reliable information on the motion of the convection auroral electrojet.

It is the object of this thesis to present the relationship between the Pc 5 micropulsations and the convection westward electrojet and to demonstrate that the generation mechanism for Pc 5 is due to the oscillation of the three dimensional current system associated with the convection westward electrojet.

In addition, an analysis and interpretation of the rare 'Pc 4' micropulsations recorded during 1971 and 1974 (when three of the stations were distributed along the same latitude line) will be presented, and we shall show that these events may well represent the pure resonance effects which have been proposed by several authors as a source for long period micropulsation activity.

## CHAPTER II

### EXISTING THEORETICAL CONCEPTS

Most of the attempts to explain pulsations in the earth's magnetic field are based on the concept of hydromagnetic waves which were proposed by Alfvén in 1942 [Alfvén, 1942]. This chapter begins with a brief review of the modes of propagation of hydromagnetic waves in a perfectly conducting fluid permeated by a uniform magnetic field. This is then followed by a discussion of the modes of hydromagnetic oscillations of the medium in the presence of a non-uniform magnetic field such as a dipole field. The excitation mechanisms are discussed next, and the theories of the coupling of energy from an external source to a local field line are reviewed. The chapter is concluded by comments on the existing theoretical concepts as related to experimental observations.

#### 2.1 Hydromagnetic Waves

A qualitative review of the subject of hydromagnetic waves is presented in this section. Much more comprehensive treatments can be found in any standard text on plasma physics [e.g., Alfvén and Fälthammar, 1963].

The crudest approximation to plasma behaviour is to regard the plasma as a perfectly conducting fluid. In addi-

tion to the hydrodynamic properties, the fluid possesses equally important electromagnetic properties. In order that strong interaction between electromagnetic and hydrodynamic phenomena exist, the inequality

$$L \gg \sqrt{\frac{\rho}{\mu_0}} \frac{1}{B\sigma}$$

must be satisfied, where  $L$  is the linear dimension of the conducting medium of density  $\rho$ , permeability  $\mu_0$  and conductivity  $\sigma$  in the presence of a magnetic field  $B$  [Lundquist, 1952]. Under normal laboratory conditions this criterion is not satisfied, but the situation is very different in the magnetosphere where the linear dimension is quite large.

Let us consider a nonviscous and compressible fluid of infinite conductivity permeated by a uniform magnetic field  $\vec{B}_0$ . Let us assume that  $\vec{B}_0$  is curl free (i.e.,  $\nabla \times \vec{B}_0 = 0$ ), the magnitudes of the perturbed quantities are small compared with those in the unperturbed state and the displacement current is negligible compared to the conduction current. Then, combining Maxwell's equations and the basic equations of hydrodynamics, one can deduce that three distinctly different waves can be excited in the hydro-magnetic medium. They are the Alfvén waves (also known as the shear Alfvén waves or anisotropic Alfvén wave when propagating along field lines), the slow magneto-sonic wave



(or slow magneto-acoustic wave) and the fast magneto-sonic wave (also known as fast magneto-acoustic waves and, when propagating across field lines, modified Alfvén wave, compressional Alfvén wave or isotropic Alfvén wave). The wave frequency must be low compared to the ion cyclotron frequency otherwise the ions will not partake fully in the wave motion. If the angle between the propagation direction and the field  $\vec{B}_0$  is  $\theta$ , then the phase velocity of the Alfvén wave is equal to  $V_A \cos \theta$  and the phase velocities of the magneto-sonic waves are given by the two real and non-negative roots of the quadratic equation for the phase velocities  $v^2$

$$v^4 - v^2(V_A^2 + V_S^2) + V_A^2 V_S^2 \cos^2 \theta = 0$$

which yields

$$v^2 = \frac{1}{2}(V_A^2 + V_S^2) \pm (V_A^4 + V_S^4 - 4V_S^2 V_A^2 \cos^2 \theta)^{1/2}$$

where  $V_A = \frac{B_0}{(\mu_0 \rho)^{1/2}}$  is the Alfvén velocity,  $V_S = \sqrt{\frac{dp}{d\rho}}$  is the velocity of an ordinary sound wave,  $P$  is the plasma pressure and  $\rho$  is the mass density.

The phase velocity  $V_A \cos \theta$  of the Alfvén wave is equivalent to motion of the phase fronts in the direction  $\vec{B}_0$  with speed  $V_A$ . The Alfvén wave is thus a transverse wave. The slow magneto-sonic wave propagates with a speed which is smaller than the lesser of  $V_S$  and  $V_A$ . The fast magneto-sonic

wave propagates with a speed which exceeds the greater of  $V_S$  and  $V_A$ . The two magneto-sonic waves are neither longitudinal nor transverse except when propagating along field lines or perpendicular to the field lines.

These waves are most conveniently discussed by means of polar plots of the velocity vectors of the three waves as shown in Figure 11. The vector  $\overrightarrow{OV}$  drawn from the origin  $O$  to a point  $V$  on any one curve represents the velocity of a wave and also the direction of the wave normal. Let us consider the special cases of propagation along field lines and across field lines.

It is found that a pure Alfvén wave with speed  $V_A$  and a pure sound wave (ion acoustic wave) with speed  $V_S$  propagate in the direction of the magnetic field (i.e.,  $\theta = 0$ ). A simple physical picture can be obtained for the pure Alfvén wave as follows. Because of the infinite conductivity assumption, one can picture the magnetic lines of force 'materialized' into elastic strings to which the conducting fluid particles have been 'glued'. Thus, the magnetic lines of force possess inertia (provided by the ions) and a tension  $\frac{B_0^2}{\mu_0}$ . When the fluid of density  $\rho$  is disturbed from rest, the lines of force will perform transverse oscillations (i.e., the direction of particle motion is perpendicular to the direction of propagation parallel to the undisturbed magnetic field  $\vec{B}_0$ ; the magnetic perturbation  $\vec{b}$  is perpendicular to  $\vec{B}_0$ ).

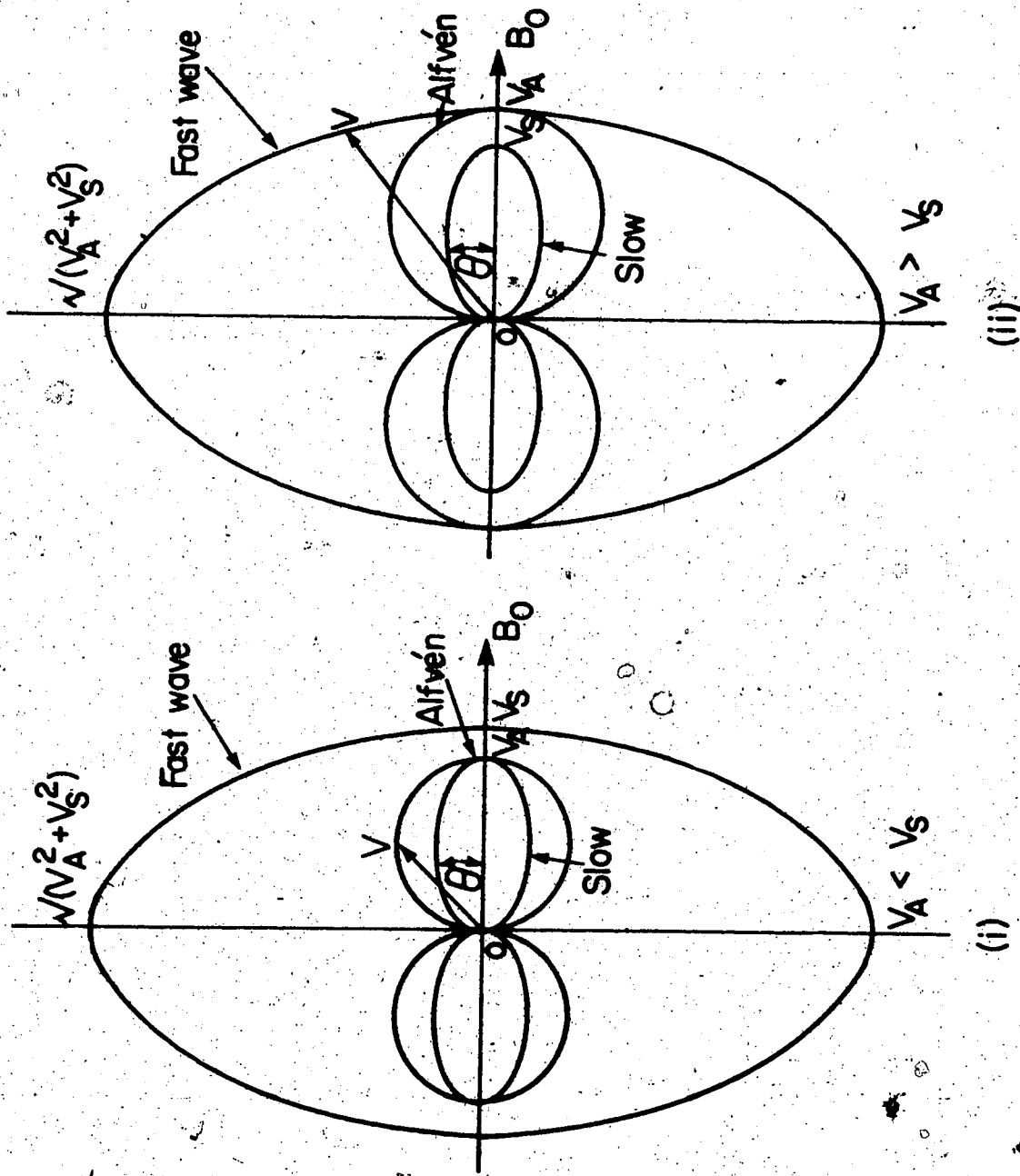


Figure 11

The phase velocity of the wave is equal to  $\sqrt{\frac{\text{tension}}{\text{density}}}$  (i.e.,  $V_A = \frac{B_0}{(\mu_0 \rho)^{1/2}}$ ) in analogy to the definitions of the velocity of the transverse wave propagating along a stretched string. The transverse nature of this mode implies field line guidance of energy. The Alfvén waves cause no density perturbation of the medium and would have been excited had the medium been incompressible. This concept of transverse oscillations of magnetic lines of force was used by Obayashi and Jacobs [1958] to compute the plasma density distribution of the 'outer atmosphere' making use of the observed period of micropulsations. The stretched string analogy enabled them to postulate that the characteristic period of oscillating lines of force is given by  $T = 2 \int \frac{dS}{V_A}$ , the integration being over the length of the magnetic line of force.

The sound wave that also propagates parallel to  $\vec{B}_0$  involves no electromagnetic effects (in contrast to the Alfvén wave which is a purely hydromagnetic phenomenon) and is a longitudinal wave (i.e., particle motion is parallel to the direction of propagation which is parallel to  $\vec{B}_0$ ). This mode can be thought of as a sound wave travelling in a pipe, the rigidity of the pipe corresponding to the stiffness of the magnetic field.

There is only one mode that propagates perpendicular to the field lines (i.e.,  $\theta = 90^\circ$ ). This is the fast magneto-sonic wave moving across the field with a speed given by

$\sqrt{v_S^2 + v_A^2}$  and causing compressions and rarefactions in the lines of force without changing their direction. This wave is essentially a longitudinal sound wave (i.e., direction of particle motion is parallel to the direction of propagation which is perpendicular to  $\vec{B}_0$ ;  $\vec{b}$  is parallel to  $\vec{B}_0$ ) modified by the presence of the magnetic field.

## 2.2 Poloidal and Toroidal Oscillations

Let us consider a hydromagnetic medium of infinite conductivity permeated by a nonuniform magnetic field  $\vec{B}_0$  such as a dipole field. It is assumed that the medium is incompressible so that the acoustic mode waves in the plasma density are suppressed. Consider a thin shell surrounding the surface of revolution of a line of force. Then, upon being perturbed, the thin shell may experience two modes of oscillations of the medium; namely poloidal oscillations and toroidal oscillations. Poloidal oscillations can be visualized as compressions and expansions of the magnetic shells. The toroidal oscillations can be pictured as azimuthal twistings of the magnetic shells. Because of the nonuniformity of the magnetic field  $\vec{B}_0$ , extra terms involving the spatial derivatives of  $\vec{B}_0$  are introduced into the governing equations. As a result, the poloidal and toroidal modes are coupled together.

Dungey [1954] was the first to attempt to explain micropulsations in terms of poloidal and toroidal oscilla-

tions of the earth's magnetic field. Using Maxwell's equations and the fundamental equation of hydrodynamics, he was able to derive two coupled partial differential equations describing poloidal and toroidal oscillations. Since Dungey's work has had tremendous impact on the field of micropulsations, it is worthwhile to see how the coupled partial differential equations are derived.

Neglecting all external forces of non-electromagnetic origin such as those due to viscosity, gravity and pressure gradients and assuming the plasma velocity  $\vec{V}$  to be small so that inertial terms can be neglected, the basic equation of hydrodynamics can be written in the form<sup>1</sup>

$$\rho \frac{\partial \vec{V}}{\partial t} = \vec{J} \times \vec{B} \quad (1)$$

where  $\rho$  is the mass density of the plasma and  $\vec{J} \times \vec{B}$  is the mechanical force exerted by the magnetic field  $\vec{B}$  on a volume element carrying the current density  $\vec{J}$ . The displacement current is negligible compared to the conduction current.

Considering  $\vec{B}$  as the sum of a constant dipole field  $\vec{B}_0$  and a small disturbance  $\vec{b}$  ( $|\vec{B}_0| \gg |\vec{b}|$ ), assuming  $\vec{B}_0$  to be curl free (i.e.,  $\nabla \times \vec{B}_0 = 0$ ) and using Maxwell's equation  $\nabla \times \vec{B} = \mu_0 \vec{J}$ , equation (1) becomes

$$\rho \frac{\partial \vec{V}}{\partial t} = \frac{1}{\mu_0} (\nabla \times \vec{b}) \times \vec{B}_0 \quad (2)$$

<sup>1</sup> MKS units are used.

Taking the vector product of the time derivative of equation (2) with  $\vec{B}_0$  and making use of Ohm's Law  $\vec{E} = -\vec{V} \times \vec{B}_0$  for a medium of infinite conductivity, equation (2) becomes

$$\mu_0 \rho \frac{\partial^2 \vec{E}}{\partial t^2} = \vec{B}_0 \times \vec{B}_0 \times (\nabla \times \nabla \times \vec{E}) \quad (3)$$

Then, using the definition for Alfvén velocity  $\vec{V}_A = \frac{\vec{B}_0}{(\mu_0 \rho)^{1/2}}$  equation (3) becomes

$$\frac{\partial^2 \vec{E}}{\partial t^2} = \vec{V}_A \times \vec{V}_A \times (\nabla \times \nabla \times \vec{E}) \quad (4)$$

Analogous wave equations for  $\vec{V}$  and  $\vec{b}$  may be similarly derived.

The above equation is the linearized hydromagnetic wave equation for an infinitely conducting fluid without plasma pressure gradients. It is the first stepping stone for many authors who have attempted to develop a theory for micropulsations [eg. Westphal and Jacobs, 1962; Orr and Mathew, 1971; among others].

Expressing equation (3) in spherical polar coordinates  $(r, \theta, \phi)$  and using  $\vec{B}_0 = (B_r, B_\theta, 0)$ , Dungey [1954] obtained the following two equations relating the azimuthal component of the electric field of the disturbance  $E_\phi$  to the azimuthal component of the fluid particle velocity  $V_\phi$ :

$$\left\{ -\frac{\rho}{B_0^2} \frac{\partial^2}{\partial t^2} + \frac{\partial^2}{\partial r^2} + \frac{\sin \theta}{r^2} \frac{\partial}{\partial \theta} \frac{1}{\sin \theta} \frac{\partial}{\partial \theta} \right\} r \sin \theta E_\phi$$

$$= \sin \theta \left\{ B_r \frac{\partial}{\partial \theta} - B_\theta \frac{\partial}{\partial r} \right\} \frac{1}{r \sin \theta} \frac{\partial V_\phi}{\partial \phi} \quad (5)$$

$$\left\{ \mu_0 \rho \frac{\partial^2}{\partial t^2} - \frac{1}{(r \sin \theta)^2} [(\vec{B}_0 \cdot \nabla)(r \sin \theta)^2 (\vec{B}_0 \cdot \nabla) + B_0^2 \frac{\partial^2}{\partial \phi^2}] \right\} \frac{V_\phi}{r \sin \theta}$$

$$= \frac{\mu_0}{(r \sin \theta)^3} \left[ B_r \frac{\partial}{\partial \theta} - B_\theta \frac{\partial}{\partial r} \right] r \sin \theta \frac{\partial E_\phi}{\partial \phi} \quad (6)$$

Equation (5) is the equation for poloidal oscillations ( $E_\phi$ ) which is coupled to toroidal oscillations ( $V_\phi$ ) by the term on the right hand side of equation (5). Equation (6) is the equation for toroidal oscillations which is again coupled to poloidal oscillations by the term on the right hand side of equation (6).

The above equations are too complicated to be of much use and they still have not been solved analytically. Dungey [1954] decoupled the two modes by assuming axial symmetry (i.e.,  $\frac{\partial}{\partial \phi} = 0$  which implies that the phenomenon is longitude independent and the disturbance may be considered to occur in phase over the whole earth).

As a result of this decoupling procedure, the equation for poloidal oscillations becomes



$$\left\{ \frac{\rho}{B_0^2} \frac{\partial^2}{\partial t^2} - \frac{\partial^2}{\partial r^2} - \frac{\sin \theta}{r^2} \frac{\partial}{\partial \theta} \frac{1}{\sin \theta} \frac{\partial}{\partial \theta} \right\} r \sin \theta E_\phi = 0 \quad (7)$$

and that of toroidal oscillations becomes

$$\left\{ \mu_0 \rho \frac{\partial^2}{\partial t^2} - \frac{1}{(r \sin \theta)^2} [(\vec{B}_0 \cdot \nabla)(r \sin \theta)^2 (\vec{B}_0 \cdot \nabla)] \right\} \frac{V_\phi}{r \sin \theta} = 0 \quad (8)$$

It can be shown from Ohm's Law and Faraday's Law and the axial symmetry consideration that the poloidal oscillations governed by equation (7) involve the following set of quantities

$$[0 \ 0 \ E_\phi]; [b_r \ b_\theta \ 0]; [V_r \ V_\theta \ 0]$$

and the toroidal oscillations involves the remaining set

$$[E_r \ E_\theta \ 0]; [0 \ 0 \ b_\phi]; [0 \ 0 \ V_\phi]$$

From the above sets of relationships, it can be seen that the plasma motion and the perturbation magnetic field lie in the meridian plane for the poloidal mode. The Poynting vector points across the field lines and the hydro-magnetic energy spreads to fill the volume. As a result, the whole cavity resonates and the period of oscillations for the poloidal mode will not be latitude-dependent.

For the toroidal mode, the motion of plasma is in the azimuthal direction and the perturbation magnetic field

is polarized in the east-west direction. The Poynting vector is directed along the field lines and the hydromagnetic energy is guided along them. Since equation (8) involves operator  $(\mathbf{E}_0 \cdot \nabla)$ , the poloidal mode may be understood in terms of oscillations along magnetic lines of force where the period of oscillation will be latitude-dependent.

In principle, the eigenperiods of the fundamental and higher modes of hydromagnetic oscillations may be computed from equations (7) and (8). The first attempt to explain Pc's (under the old classification) in terms of poloidal oscillations was made by Kato and Akasofu [1955] who did not take into consideration the dipole character of the earth's magnetic field. This approach was further developed by Kato and Watanabe [1957] and Watanabe [1959]. These early analyses attempted to force the poloidal equation into a simply separable and soluble form through convenient assumptions concerning the plasma density and field dependence. The eigenperiods of oscillations depend upon the spherical shell bounded by the earth's surface and the outer boundary of the 'outer atmosphere'. A fundamental period of oscillation of about 180 seconds was estimated. The poloidal mode was also discussed later by other researchers such as Jacobs and Westphal [1964] and Carovillano et al. [1966]. The fundamental period of poloidal oscillations is equal to four times the travel time for a hydromagnetic wave from the ionosphere

to the boundary such as the magnetopause in the equatorial plane [Dungey and Southwood, 1970].

The fundamental period of the toroidal oscillation was computed by Dungey [1954] making use of equation (8). Using a constant plasma density distribution ( $\rho = 10^{-18}$  kg/cm<sup>3</sup>), and assuming perfect reflection at the earth's surface, he obtained the following relation for the fundamental periods

$$T_0 = \frac{0.6}{\cos^8 \lambda}$$

where  $\lambda$  is the geomagnetic latitude.  $T_0$  for  $\lambda = 65^\circ$  is 11 minutes. Westphal and Jacobs [1962] derived similar equations for small amplitude hydromagnetic oscillations in cylindrical coordinates. Since the equations in this system are somewhat simpler than in the spherical coordinate system, they were able to compute the eigenperiods of toroidal oscillations for compressed dipole fields using a variable density distribution. If  $\rho$  varies as  $R^{-6}$  where  $R$  is the radial distance from the center of the earth,  $V_A$  is constant and the eigenperiod of toroidal oscillation is equal to twice the travel time for a hydromagnetic wave moving along a field line between conjugate points (as in the 'stretched string' model of Obayashi and Jacobs [1958]). For other forms of plasma density distribution, the validity of this 'time of flight' method in determining the fundamental period is reduced [Radoski, 1966].

If the disturbance has a longitudinal dependence, it can be represented in the form  $e^{im\phi}$  where  $m$  is an integer.  $m = 0$  corresponds to the symmetric modes described by the decoupled equations (7) and (8) presented earlier. Large  $m$  would correspond, of course, to the asymmetric modes which are associated with disturbances highly localized and varying rapidly in longitude. Dungey [1954] and Radoski [1967] have discussed the asymmetric poloidal mode. Since the perturbation magnetic field is transversely polarized radially in the meridian plane for this mode and its energy guided along field lines, it is referred to as the guided poloidal mode. The equations governing the guided poloidal mode and the toroidal mode are very similar. Radoski [1972] has considered the asymmetric toroidal mode and found that the periods of symmetric and asymmetric modes have a similar spatial dependence and are almost linearly related. Orr and Mathew [1971] have computed the eigenperiods for the symmetric toroidal and the asymmetric guided poloidal mode for dipole field lines. They found that the first harmonic period for the guided poloidal mode is approximately 20% longer than that for the toroidal mode and that higher harmonics have almost identical periods for the two modes.

The effects of weak coupling between the symmetric modes through the inclusion of the Hall current in the generalized Ohm's Law and the use of a simplified field configuration (a hydromagnetic wedge model) have been con-

sidered by McClay [1970]. He found that the toroidal mode resonance is spatially localized but the poloidal mode is also evident outside the resonance region. Because of coupling, a large portion of the cavity should oscillate with the same frequency. The poloidal mode exhibits close spaced eigenfrequencies. The sense of polarization of the perturbations changes across the region of the toroidal resonance. Later, he studied the normal modes of oscillations in a loaded concentric cylinder model [McClay, 1973]. In this model, the medium oscillates in its entirety without regard to local conditions and the eigenfrequencies depend on the arbitrary cavity size. Radoski [1974] has studied the asymptotic temporal behaviour of the asymmetric coupled modes in a cylindrical model. He found that as the system evolves toward the steady state, the energy is preferentially transferred to the toroidal mode with the poloidal mode decaying away.

### 2.3 Excitation Mechanisms

In the previous section, we discussed the normal modes of oscillations in a hydromagnetic medium permeated by a non-uniform magnetic field when the system is perturbed. No mention was made of the sources of energy involved in the perturbation of the system. A discussion is therefore presented here on the excitation mechanisms of long period micropulsations.

The most popular excitation mechanism is undoubtedly the so-called Kelvin-Helmholtz instability, supposedly generated at the magnetopause due to interaction of the solar wind with the magnetosphere. The Kelvin-Helmholtz instability arises by the distortion of the interface between two fluids in relative motion. The first reference to the instability was made by Helmholtz [1868] with reference to hydrodynamic processes. Helmholtz's discussion was largely qualitative. The problem was treated analytically by Lord Kelvin in later years [Kelvin, 1910]. A simple hydrodynamic example of the instability is the phenomenon of wind over water. When the wind speed exceeds a critical limit (660 cm/sec according to Lord Kelvin), the instability will manifest itself as surface waves. Dungey [1954] was the first to suggest that the flow of the solar plasma along the boundary of the magnetosphere would generate waves in the same way that wind generates waves on water. The evidence from ground observations of micropulsations which suggest the Kelvin-Helmholtz instability as a source is the diurnal variation pattern for polarization in the horizontal plane (cc in the morning and cw in the evening). If surface waves are generated at the magnetopause through the development of the Kelvin-Helmholtz instability as the solar wind flows around the magnetosphere (to the west on the morning side and to the east on the evening side as shown in Figure 12), then the plasma will have an

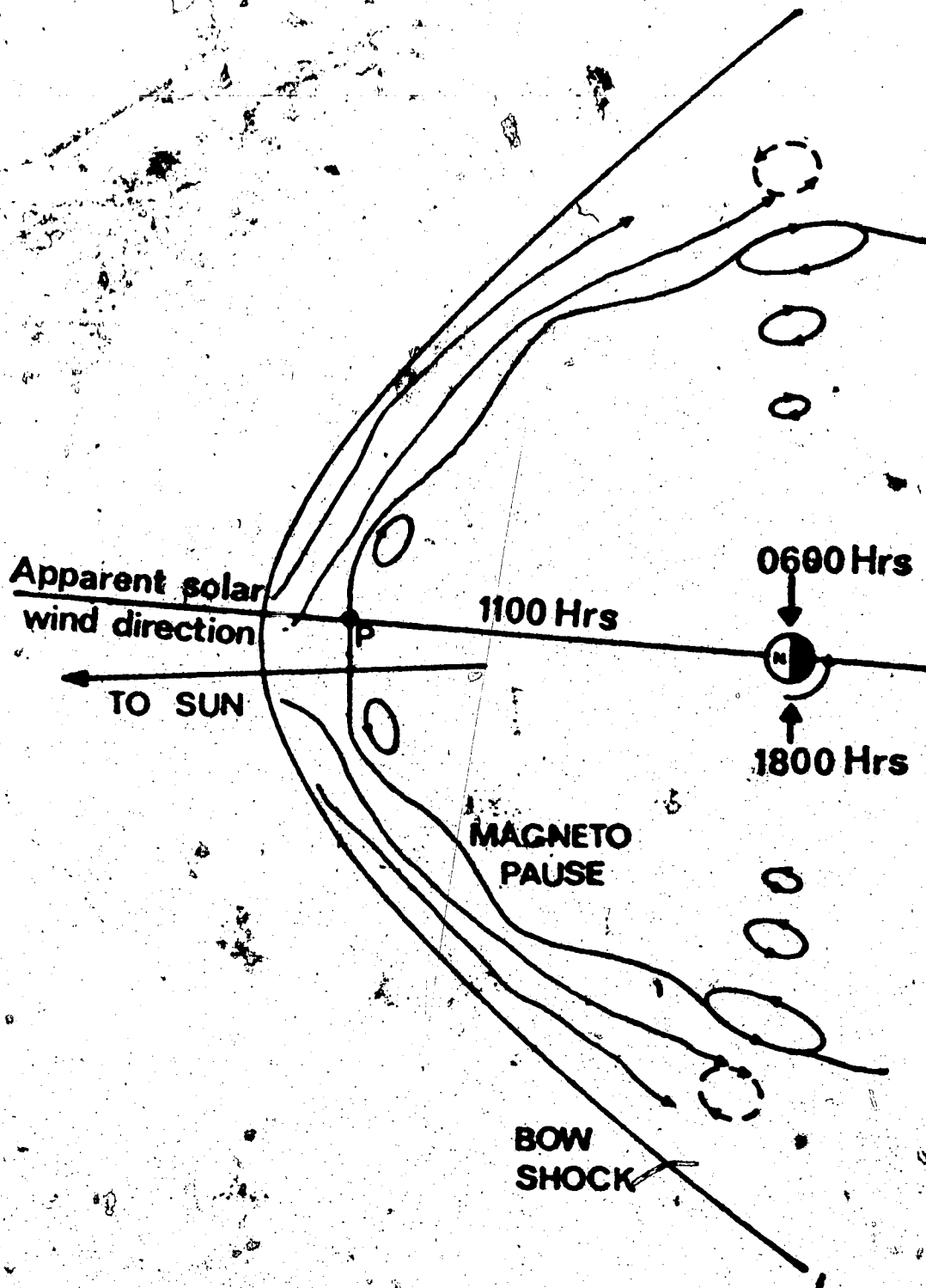


Figure 12

approximately elliptical motion, the rotation being in the opposite sense along the dawn and dusk meridian. Since the magnetic field lines are 'frozen' into the plasma, the field lines near the surface of the magnetosphere will rotate with the plasma particles, thus generating elliptically polarized hydromagnetic waves which then propagate to the earth along the magnetic field lines [Atkinson and Watanabe, 1966]. The waves (looking along the direction of the field) will be polarized in the cc direction on the dawn side and cw on the evening side. This seems to explain the ground observations of diurnal variation of polarization in the horizontal plane, and the satellite observations made by Dungey and Southwood [1970], although there is some controversy on the stability of the magnetopause due to Kelvin-Helmholtz type [Sen, 1965; Dessler and Fejer, 1968; Fejer, 1964; Southwood, 1968].

Swift [1967] has suggested that electrostatic oscillations may be responsible for long period micropulsations. The electrostatic field couples to magnetic variations by inducing currents in the conducting ionosphere. The oscillation essentially occurs in a field-aligned column of enhanced (or depleted) ionization stretching between conjugate hemispheres. The energy comes from the free energy associated with gradients in particle density.



The interaction that occurs between hydromagnetic waves and energetic protons bouncing between hemispheres may lead to wave amplification [Dungey, 1968; Southwood et al., 1969; Dungey and Southwood, 1970]. Quasitransverse modes of large azimuthal wave number  $m$  may be excited by taking energy from energetic particles through the bounce resonance instability. The change in energy  $W$  which results in wave growth is proportional to a change in the  $L$  shell parameter and is independent of the energy or pitch angle of the particle. The energy exchange is a consequence of diffusion processes in  $(W, L)$  space. The most effective diffusion mechanism for the particles in  $L$  is the tilting of field lines in the meridian plane caused by the component of the wave field which is along the principal normal of the geomagnetic field (e.g. the field of the guided poloidal wave). The mean velocity vector of the particle is also tilted. If the perturbation magnetic field reverses sign when the particle bounces, the particle zigzags across  $L$  as shown in Figure 13.

Kimura and Matsumoto [1968] suggested that Pc 5 pulsations are a result of the oscillations of the field lines due to a hydromagnetic instability which is excited by an electron or ion beam (such as precipitating auroral particles) passing through some part of the magnetospheric plasma. The excited wave has a frequency proportional to the

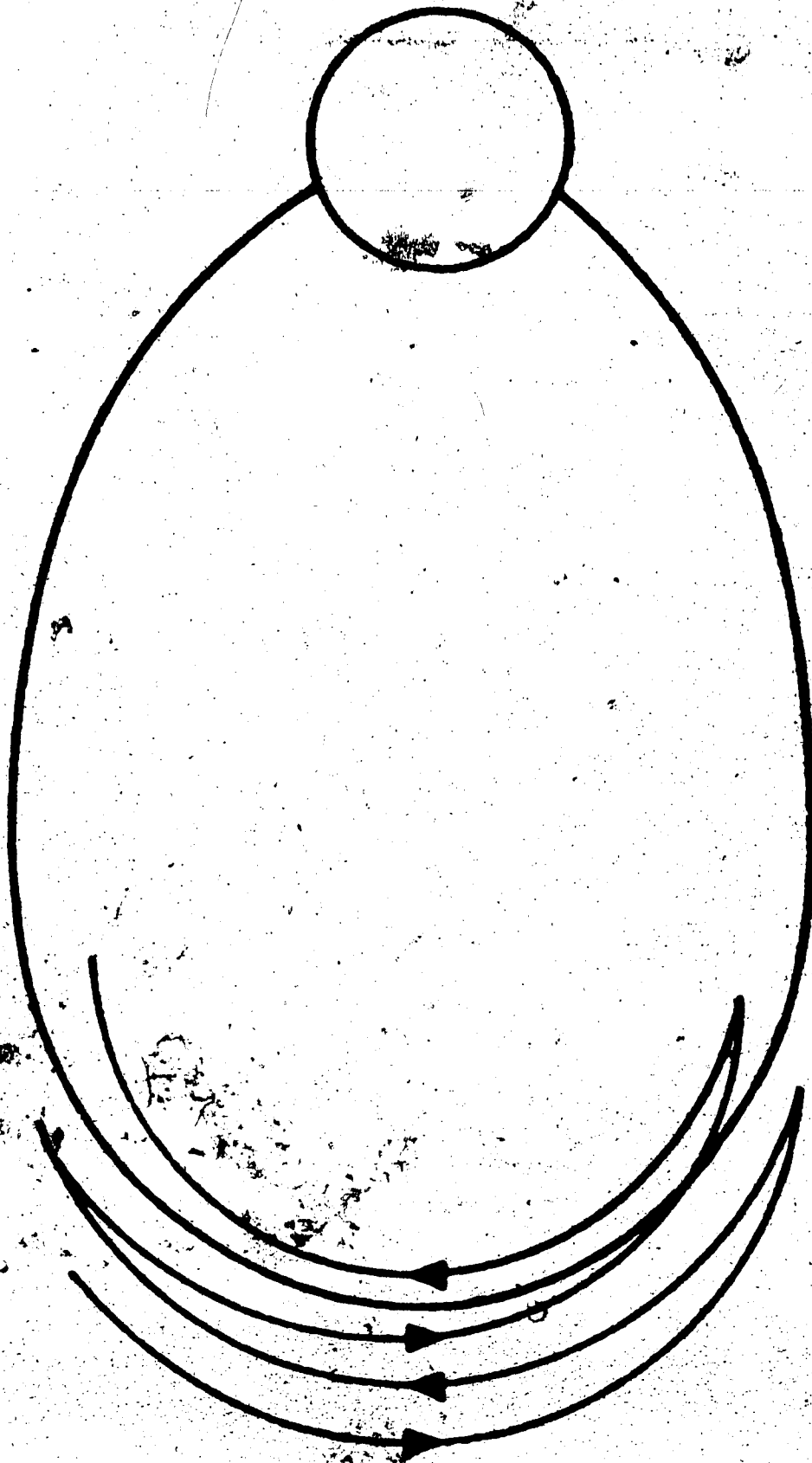


Figure 13

excess charge density, while the polarization of the excited wave depends largely on the sign of the excess charge. An electron rich beam causes instability in the Alfvén mode which is polarized in the cc direction looking in the direction of the magnetic field while a proton rich beam causes instability in the modified Alfvén mode which is polarized in the cw direction. However, there is a threshold beam velocity below which the instability can be suppressed. Kimura and Matsumoto claimed that the diurnal variation in the sense of polarization in the horizontal plane (i.e., cc in the morning and cw in the evening) can be interpreted in terms of these instabilities, although a mechanism in which different signs of excess charge will arise in the morning and evening was not discussed in detail by the authors.

By extending the theory of the mirror instability [Chandrasekhar et al., 1958] to consider gradients in both the magnetic field  $B$  and the hot plasma density  $n$ , a co-existing cold plasma, and the effect of finite cyclotron radius, Hasegawa [1969] has suggested that the particle and field phenomena seen by Explorer 26 at  $L = 5$  on April 18, 1965 geomagnetic storm in the afternoon sector [Brown et al., 1968] after the first large proton enhancements can be explained by the occurrence of a mirror instability in the magnetosphere. He has called this instability the drift mirror instability because of the coupling with the drift

waves produced by  $\nabla B$  and  $\nabla n$ . For the onset of the instability, it is necessary for the proton fluxes to have strongly anisotropic pitch-angle distributions and an enhanced energy density. When the perpendicular plasma pressure exceeds a critical value, the plasma tries to expel the magnetic field by its diamagnetic effect. As a consequence, the plasma compensates for the decrease in the magnetic field pressure and the parallel component of the local magnetic field is decreased. The instability has been called the mirror instability because a loss cone distribution inherently creates such an anisotropic pressure. Since the mode causing the mirror instability is non-oscillatory, the oscillations are produced by coupling with the drift wave created by the ion drift perpendicular to the magnetic field. Thus, the drift mirror instability developed by Hasegawa explains the sudden inflection in the increase (decrease) of the proton fluxes (magnetic field intensity) and the subsequent out-of-phase oscillations of the field and fluxes in the Pc 5 frequency range as observed by Explorer 26.

Cladis [1971] has used a simplified model, based on a two-dimensional solution of Maxwell's equations, to demonstrate the possible occurrence of a resonance phenomenon in the magnetosphere. He has suggested that this resonance was responsible for certain correlated pulsations of the magnetic field and of the trapped particles observed in the outer magne-

tosphere (such as the one observed by Explorer 26 mentioned in the last paragraph). The resonance is excited by the VB drift of energetic trapped particles that have an inhomogeneous distribution in the direction of the drift motion. The field lines oscillate as standing waves in the meridional plane and form a wave pattern in the azimuthal direction that moves with a phase velocity equal to the mean azimuthal drift velocity of the particles. Particles with drift velocities near the velocity of this travelling wave become bunched in the potential wells of the wave. Particles with higher or lower drift velocities, and particles that drift in the opposite direction, alternately lose and gain energy as they drift 'over' the wave. Consequently, these particles drift periodically across L shells, tending to follow the oscillating field lines. Thus, the event observed by Explorer 26 mentioned in the last paragraph can be explained within the context of Cladis' theory. The field line oscillations were initiated by the westward drift of the sharp proton front. The bunching of the low-energy protons accounts for the oscillations of the local field. The out-of-phase relationship of the proton flux and the magnetic field results from the diamagnetic effect of the bunched protons.

#### 2.4. Wave Coupling

In section 2.2, we have discussed one group of theories of pulsations which deals with the resonance process and in section 2.3 we have discussed the other group of

theories of pulsations which concerns the excitation mechanism. A natural step to take is therefore to combine the active and passive aspects of the theories and treat the problem of coupling between the active and passive modes. Coupling between these modes has been studied in detail by Chen and Hasegawa [1974a,b], Hasegawa and Chen [1974], and Southwood [1974a,b].

Before we start discussing the coupling, some comments about the terminology of poloidal and toroidal modes are in order. Experimental evidence indicates that the assumption of axisymmetry which is used in many theoretical treatments is incorrect. For example, the assumption of axisymmetry is incapable of explaining the diurnal variation of polarization in the horizontal plane, the elliptical polarization and the spatially localized nature of the pulsations. Therefore, rather than assuming axisymmetry, the condition of  $|k_{\perp}| \gg |k_{\parallel}|$  would be much more reasonable where  $k_{\perp}$  and  $k_{\parallel}$  are the wave numbers in the directions perpendicular and parallel to the magnetic field. For this condition, as pointed out by Lanzerotti and Fukunishi [1974], the distinction between the terms poloidal and toroidal becomes meaningless because of the coupling of the compressional and shear Alfvén modes. It would therefore be better for discussions if the terms toroidal and poloidal were not used.

The equation of motion of a fluid element is

$$\rho \frac{\partial \vec{v}}{\partial t} = \vec{J} \times \vec{B} - \nabla P \quad (9)$$

where  $\rho$  is the mass density,  $\vec{V}$  the perturbed fluid velocity,  $\vec{J}$  the current density,  $\vec{B}$  the magnetic flux density and  $P$  the plasma pressure. Assuming small perturbations, using Maxwell's equations  $\nabla \times \vec{B} = \mu_0 \vec{J}$  and substituting the displacement vector  $\vec{\xi}$  (defined by  $\frac{\partial \vec{\xi}}{\partial t} = \vec{V}$ ) for  $\vec{V}$ , equation (9) becomes

$$\rho \frac{\partial^2 \vec{\xi}}{\partial t^2} = \frac{1}{\mu_0} (\nabla \times \vec{b}) \times \vec{B}_0 + \frac{1}{\mu_0} (\nabla \times \vec{B}_0) \times \vec{b} - \nabla p \quad (10)$$

where  $\vec{b}$  is the perturbation magnetic flux density,  $\vec{B}_0$  the unperturbed magnetic flux density and  $p$  the perturbation plasma pressure.

Using  $\vec{b} = \nabla \times (\vec{\xi} \times \vec{B}_0)$  and after some algebraic manipulations, equation (10) becomes

$$\mu_0 \rho \frac{\partial^2 \vec{\xi}}{\partial t^2} - (\vec{B}_0 \cdot \nabla)^2 \vec{\xi} = -\mu_0 \nabla \left[ p + \frac{\vec{B}_0 \cdot \vec{b}}{\mu_0} \right] + \vec{C} \quad (11)$$

where

$$\vec{C} = (\vec{b} \cdot \nabla) \vec{B} - (\vec{B} \cdot \nabla) [(\vec{\xi} \cdot \nabla) \vec{B} + \vec{B}(\nabla \cdot \vec{\xi})]$$

Equation (11) indicates a coupling between a shear Alfvén wave (the right hand side is equal to zero) and a surface wave whose dispersion relation is given by  $\nabla^2 \left( p + \frac{\vec{b} \cdot \vec{B}}{\mu_0} \right) = 0$ . The strength of the coupling is decided by the vector  $\vec{C}$  which appears as a consequence of the non-uniform magnetic field. Chen and Hasegawa [1974a] then solved the coupled equation in dipole coordinates while Hasegawa and Chen [1974] solved the

problem in Cartesian coordinates using straight magnetic field lines and obtained the essential feature of the results.

In the simplified model of Hasegawa and Chen [1974], equation (11) becomes

$$\mu_0 \rho \frac{\partial^2 \xi}{\partial t^2} - (\vec{B}_0 \cdot \nabla)^2 \xi = -\mu_0 \left( p + \frac{\vec{b} \cdot \vec{B}_0}{\mu_0} \right) - \vec{b} (\vec{B}_0 \cdot \nabla) (\nabla \cdot \xi) \quad (12)$$

After relating the perturbations  $p$  and  $\xi$  through the adiabatic equation of state for a compressible fluid and the continuity equation, using  $\vec{b} = \nabla \times (\xi \times \vec{B}_0)$ , taking the Laplace time and Fourier space transformations of the displacement vector  $\xi$  and assuming a field line resonance relatively localized in the east-west direction such that the azimuthal wavelength is much smaller than the length of the field line (i.e.,  $k_{\perp} \gg k_{\parallel}$ ), equation (12) further reduces to

$$\frac{d^2 \xi_y}{dy^2} + \frac{d \ln \epsilon}{dy} \frac{d \xi_y}{dy} - k_{\perp}^2 \xi_y = 0 \quad (13)$$

Here the nonuniformity is taken in the  $y$  direction which corresponds to the radial direction directed toward the earth, the magnetic field is assumed to be parallel to the  $z$ -direction and  $\epsilon = \omega^2 \mu_0 \rho(y) - k_{\parallel}^2 B^2(y)$ .

Equation (13) describes surface waves ( $\nabla^2 \xi_y = 0$ ) away from the resonant field line. Around the resonant field



line, where  $\epsilon \rightarrow 0$ , the second term in equation (13) dominates over the third term and a strong coupling between the surface wave and the resonant shear Alfvén wave occurs.

Introducing a small positive imaginary part of  $\omega$  in  $\epsilon$  such that  $\epsilon = \epsilon_r + i\epsilon_i$ , to take into account the ionospheric dissipation physically and to remove the singularity mathematically, [see also Southwood, 1974a] and expanding the equation around  $\epsilon_r(y_0) = 0$ , equation (13) becomes

$$\frac{d^2 \epsilon_y}{dy^2} + \frac{1}{y - y_0 + i\gamma^1} \frac{d\epsilon_y}{dy} - k_{\perp}^2 \epsilon_y = 0 \quad (14)$$

where  $\gamma^1 = \frac{\epsilon_i}{\partial \epsilon_r / \partial y}$  (Southwood [1974a] has obtained a similar equation for the perturbation electric field).

The general solution of equation (14) can be expressed in terms of the modified Bessel function of the second kind. The corresponding eigenmode is shown to be continuous unless a monochromatic frequency source is assumed. An expression for  $\epsilon_x$  can be obtained near the resonant point by using the incompressible and transverse nature of the shear Alfvén wave. The expressions for the horizontal components of the perturbation magnetic field  $\vec{b}$  (which is related to  $\vec{E}$  by  $\vec{b} = \nabla \times (\vec{E} \times \vec{B}_0)$ ) can thus be derived and detailed predictions can be made concerning the sense of polarization and the orientation angle of the major axis of the polarization ellipse with respect to the point of resonance and azimuthal direction of wave propagation.

For negative azimuthal wave number ( $k_{\perp} < 0$ ) which corresponds to azimuthal propagation of the wave towards west from noon in the morning sector, the major axis lies in the second quadrant of the H-D plane if the Alfvén speed is decreasing toward the earth at the resonant field line. This tilt is predicted to switch across noon as the azimuthal propagation is towards the east from noon in the afternoon sector.

The theories of Chen and Hasegawa [1974a] and Southwood [1974a] predict a reversal of sense of polarization in the H-D plane across the position of resonant field line and across noon as observed by Samson et al. [1971] (see Figure 8).

Chen and Hasegawa [1974a] summarized the wave amplitude, the ellipticity and sense of polarization as a function of radial position in the equatorial plane in a schematic diagram shown in Figure 14. A similar sketch was also derived by Southwood [1974a]. The diagram illustrates the essence of the theory of Chen and Hasegawa [1974a] and Southwood [1974a]: Surface waves (generated at the magnetopause presumably by the Kelvin-Helmholtz instability) evanescent towards the earth are coupled to the shear Alfvén wave representing the oscillation of the resonant field line where the wave amplitude peaks sharply and across which the sense of polarization reverses. Hasegawa and Chen [1974]

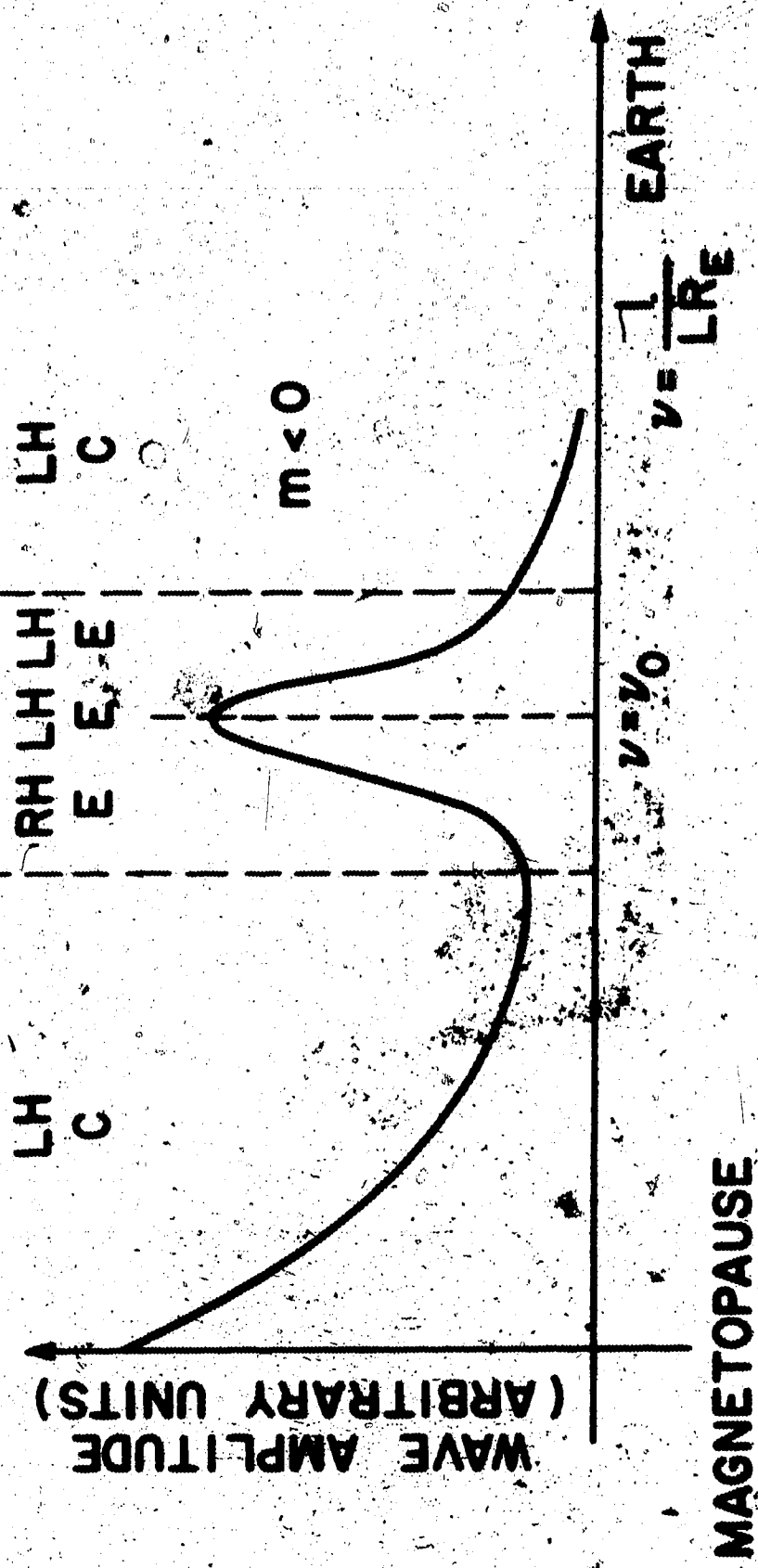


Figure 14

62

have used the "guitar string" analogy to emphasize the monochromatic character of the surface wave. Picking one string of an infinite number of coupled strings with a gradual change in lengths produces a wide band sound which corresponds to all the resonant frequencies of the strings. The sound decays as the inverse power of time due to phase mixing among oscillations of different strings. Hence, to excite a local field line, an excitor with a monochromatic frequency which corresponds to the resonant frequency of the particular field line is needed.

However, a nonharmonic broad band source such as an impulse can excite sharply localized shear Alfvén waves at sharp discontinuities in the plasma parameters (such as number density). This aspect of the theory for pulsations has been considered by Chen and Hasegawa [1974b] and Hasegawa and Chen [1974]. An initial value approach was applied. They added a source term  $S$ , which corresponds to the initial conditions on the right hand side of equation (13) which now becomes

$$\frac{d^2 \xi_y}{dy^2} + \frac{d \ln \epsilon}{dy} \frac{d \xi_y}{dy} - k_{\perp}^2 \xi_y = S(\omega, y) \quad (15)$$

Chen and Hasegawa [1974b] noted that, as Uberoi [1972] had already pointed out, equation (15) has an exact analogy with the wave equation describing an electrostatic oscillation in a nonuniform cold plasma, which has been studied extensively by Barston [1964] and Sedláček [1971a,b].

Using the analogy, Chen and Hasegawa [1974b] proposed the existence of a continuous frequency spectrum (non-collective mode) and a discrete frequency spectrum (collective mode).

The non-collective mode corresponds to oscillations with position-dependent frequencies and damping proportional to the inverse power of time. If the driving source has a continuous spectrum, oscillations with a frequency which varies continuously with latitude will be excited at all latitudes. Hence, to excite localized waves with a particular latitude-dependent frequency, a driving source composed of monochromatic waves is needed as mentioned earlier for the steady state.

The collective mode corresponds to the eigenmode of a surface wave excited at sharp gradients in the plasma distribution by an impulse which has a frequency spectrum that contains the eigenfrequency. The excited wave damps exponentially. The damping rate becomes smaller as the plasma discontinuity becomes sharper. As is expected from a surface wave, the collective mode has a peak in amplitude at the density gradient and decays away exponentially. As the profile becomes smoother and smoother, the mode is damped more and more until one is left eventually with a continuous spectrum. In the absence of a discontinuity, the eigenmode in the magnetosphere is simply a diffused damped mode corresponding to the non-collective oscillation and a mono-

chromatic oscillation is excited only by a monochromatic source.

Chen and Hasegawa [1974b] have used the above theoretical approach to explain the observations of plasmopause-associated micropulsations observed by Lanzerotti et al. [1973] as shown in Figure 15. The damped oscillations observed at  $L = 3.2$  are assumed to be the excitation of weakly damped surface eigenmodes which exist at the sharp density gradient of the plasmopause. At  $L = 4.0$  away from the plasmopause, only modes corresponding to the continuous spectrum were excited and, consequently, damped due to spatial phase mixing. Finally, it should be noted that damped Alfvén waves attributed to surface eigenmodes have also been observed in laboratory theta pinch experiments [Grossman and Tataronis, 1973].

## 2.5 Summary

In this section, we shall evaluate the theories presented earlier in the light of relevant observational data.

Since the time varying non-uniform magnetosphere is clearly not symmetric, the uncoupled symmetric poloidal and toroidal modes are not good approximations to actual conditions. As mentioned in the previous section, experimental evidence exists which demonstrates that the assumption of axisymmetry which is used in many theoretical treatments is

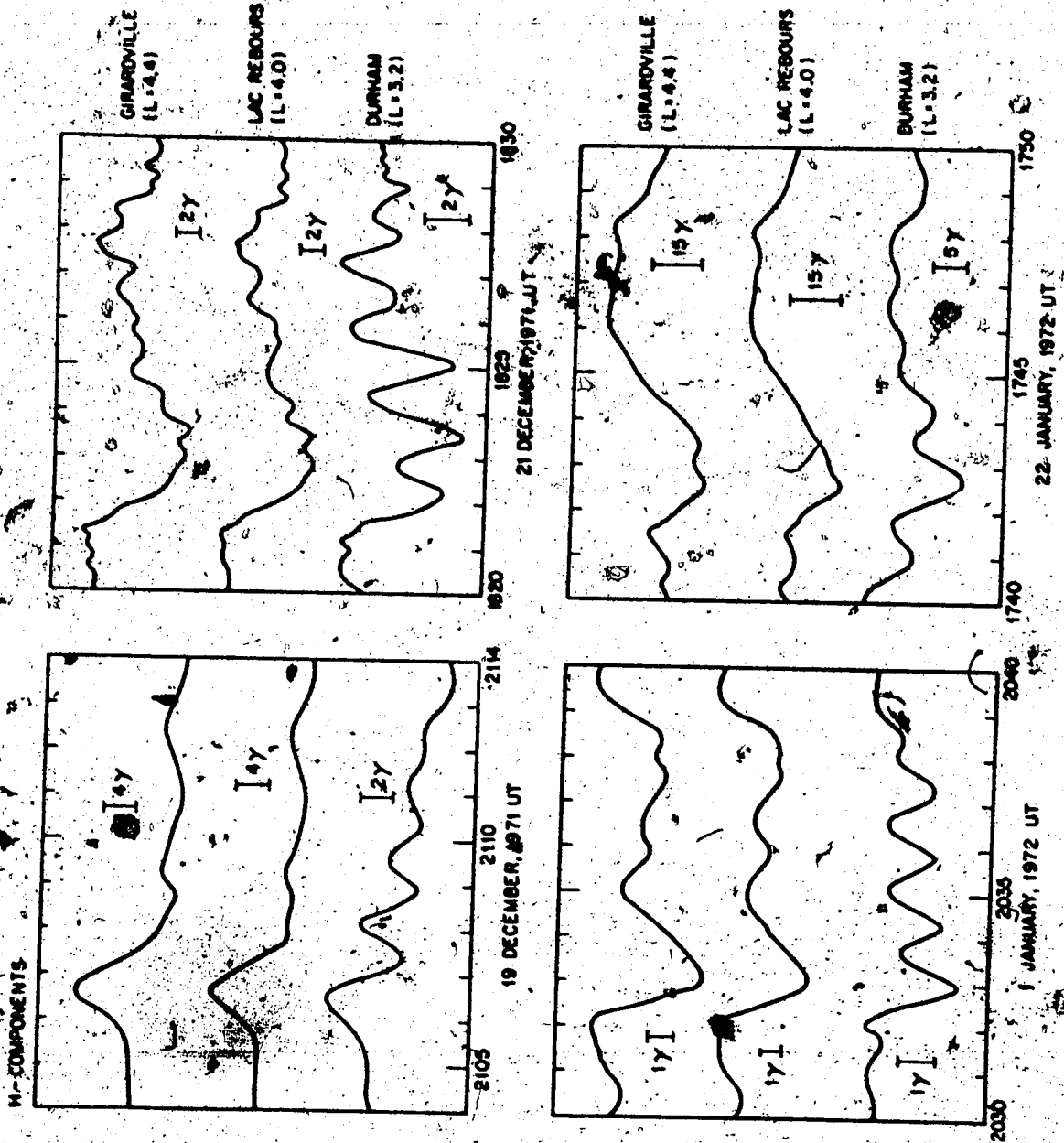


Figure 15

incorrect. The symmetric modes are unable to explain the local time dependence of the observed pulsations, localization in latitude and longitude of the pulsations, the diurnal variation in the sense of polarization, the elliptical polarization, the phase differences between stations, etc. As for the asymmetric modes, in order to maintain a mathematically tractable form models chosen for the study may not be particularly realistic.

Although the ground observations of the sense of polarization in the horizontal plane in the morning sector and afternoon sector [e.g. Samson et al., 1971], the satellite observations of the local time dependence for the polarization near the magnetopause [Dungey and Southwood, 1970] and the semiannual variation of geomagnetic activity [Boller and Stolov, 1970] seem to favour the Kelvin-Helmholtz instability, there is observational evidence against this mechanism as a source for micropulsations. Green [1976], using three stations at geomagnetic latitude  $\sim 54^\circ$  in the British Isles, found that the large majority of the Pc 3 and Pc 4 pulsation events have the western stations leading in phase (independent of LT) which for a propagating disturbance implies eastward phase motion from the dawn side towards dusk. Such a direction of wave motion is contrary to that of a surface wave generated by Kelvin-Helmholtz instability in the morning sector (i.e., westward propagation from noon towards dawn). Lanzarotti et al.



[1972] observed that three-quarters of the events detected at conjugate points near  $L = 4$  during the winter solstice were cc polarized and that no significant switch in polarization was observed around local noon. These observations argued against Kelvin-Helmholtz instability as a source although it has been pointed out by Chen and Hasegawa [1974a] that the tilt of the major axis of the ellipse rather than the sense of rotation is a more critical parameter in finding the direction of azimuthal wave propagation at low latitude. Orr [1973] has also presented arguments against the Kelvin-Helmholtz instability as a cause for the dominant peak in occurrence frequency in the morning at a latitude of  $70.9^\circ$  observed by O1' [1963]. He has used the findings of Frank [1971], McDiarmid et al. [1972], and Alekseev and Shabansky [1972] regarding the latitudes of the last closed field lines to suggest that the pulsations reported by O1' were generated within the magnetosphere and not near the boundary so that the idea that the pulsations are due to surface waves at the boundary as a result of Kelvin-Helmholtz instability must be regarded as dubious.

Swift [1967] explained the Pc 5 by an electrostatic drift wave instability. However, Hasegawa [1971] has pointed out that the electrostatic drift instability is rather unlikely to occur in the magnetosphere because of ion Landau damping in a high  $\beta$  plasma and the stabilizing effects of a

fractional mixture of cold electrons. In addition, the theory of Swift as it stands is developed purely for electrostatic perturbations. Hence, a coupling scheme to the electromagnetic mode must be worked out to allow the theory to be evaluated using the observations.

Green [1976] found that the longitudinal phase variation of Pc 3 and Pc 4 pulsations consists almost entirely of low  $m$  (azimuthal wave number) modes, which suggest that the bounce resonance mechanism [Southwood et al., 1969] is not a viable source.

Although the theory based on the non-neutral plasma distribution [Kimura and Matsumoto, 1968] can explain the cc (in the horizontal plane) polarization in the morning and cw polarization in the afternoon, it is not apparent why different signs of excess charge should arise in the morning and evening.

The local drift mirror instability [Hasegawa, 1969] may explain the storm time Pc 5 observed by satellites near the equatorial plane in the afternoon sector where the storm time partial ring current is enhanced and the plasma pressure at the equator in the magnetosphere is sufficiently high to excite some of the high  $\beta$  plasma instabilities. On the other hand, Cladis [1971] has offered another plausible interpretation of the data.

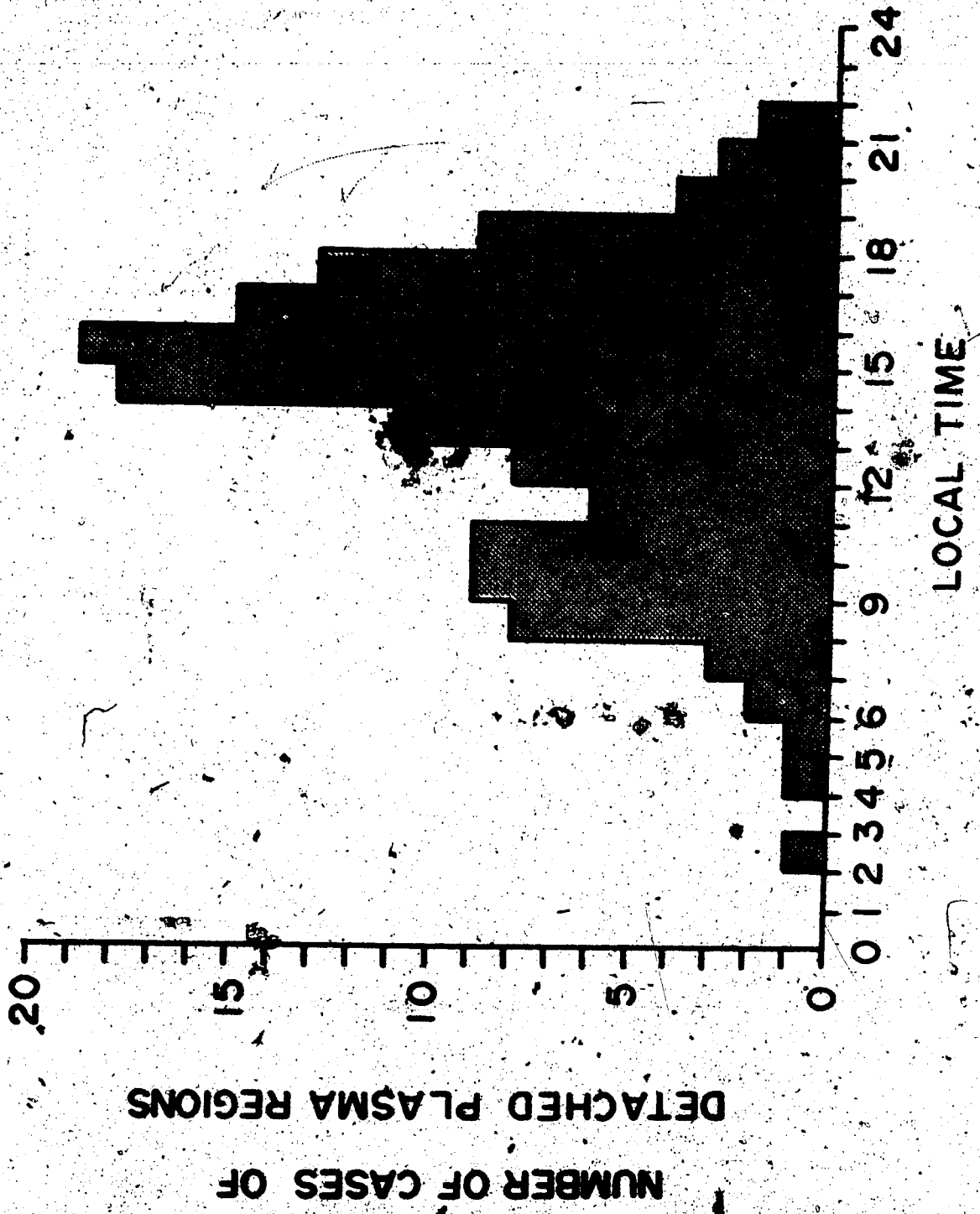
The steady state field line resonance model of Chen and Hasegawa [1974a] and Southwood [1974a] seems to explain the observations of Samson et al. [1971]. Figure 8 which shows the diurnal and latitudinal variation of the horizontal sense of polarization was compiled by Samson et al. [1971] using data from stations which were widely separated in the north. The two northern-most stations are separated by approximately  $10^\circ$  of latitude. This large separation between the two northern-most stations is crucial in determining the demarcation line and line of intensity maximum. Clearly, more stations are needed to fill in the gap in order to help distinguish among the many competing generation mechanisms for Pc 5 pulsations. Finally, it should be noted that Southwood [1975] has discussed the manner in which the field line resonance model may break down. He has pointed out the limitations of the linear theory which treats the continuously varying Alfvén speed across the field lines:

The generation of surface waves at a density gradient by an impulse [Chen and Hasegawa, 1974b] explains the weakly damped oscillations observed at  $L = 3.2$  by Lanzerotti et al. [1973] and the damped type pulsations associated with sudden commencements and sudden impulses; i.e., Pc 4 and Psc 5 [Saito and Matsushita, 1967]. Thermal plasma density gradients exist at the plasmopause and in regions of detached plasma outside the plasmopause [Chappell, 1974]. The local

time distribution of regions of detached plasma is shown in Figure 16. It can be seen that the afternoon sector has a large concentration of regions of detached plasma. Chappell [1974] pointed out that the smaller peak in the distribution of regions of detached plasma between 0800 and 1100 LT is not thought to be physically significant but probably represents an overlap in sampling in this local time sector. Therefore, the 'cleaner' pulsations observed in the morning sector are probably not related to the surface eigenmode theory of Chen and Hasegawa [1974b] which requires a density gradient.

Wilson [1966] has used a rotating line current as a model for the current systems driven in the ionosphere by hydromagnetic waves. However, it has been pointed out by Samson [1971] that this model does not explain the variation in the sense of polarization in the H-D plane with latitude and the large Z component at the latitude of the maximum in the intensity of the horizontal component.

Finally, it should be noted that Hughes [1974] has studied the screening effect of the ionosphere and atmosphere on long period micropulsations. Assuming the ionosphere to be horizontally uniform, the flat earth to be perfectly conducting and neglecting the inhomogeneities in the magnetosphere which cause coupling between the fast and the transverse mode, Hughes has obtained expressions relating the magnetic field of the hydromagnetic waves in the magneto-



sphere to that observed on the ground. He has found that any disturbance seen on the ground due to a localized hydromagnetic wave in the magnetosphere will have no vertical current associated with it. Consequently, the magnetic field due to transverse waves must be seen rotated through  $90^\circ$  when observed on earth, the rotation being caused by the effects of currents flowing in the ionosphere. If the horizontal scale length of variation is greater than the height of the ionosphere, the polarization ellipse in the H-D plane observed at the ground must be rotated through  $90^\circ$  to obtain those in the magnetosphere.

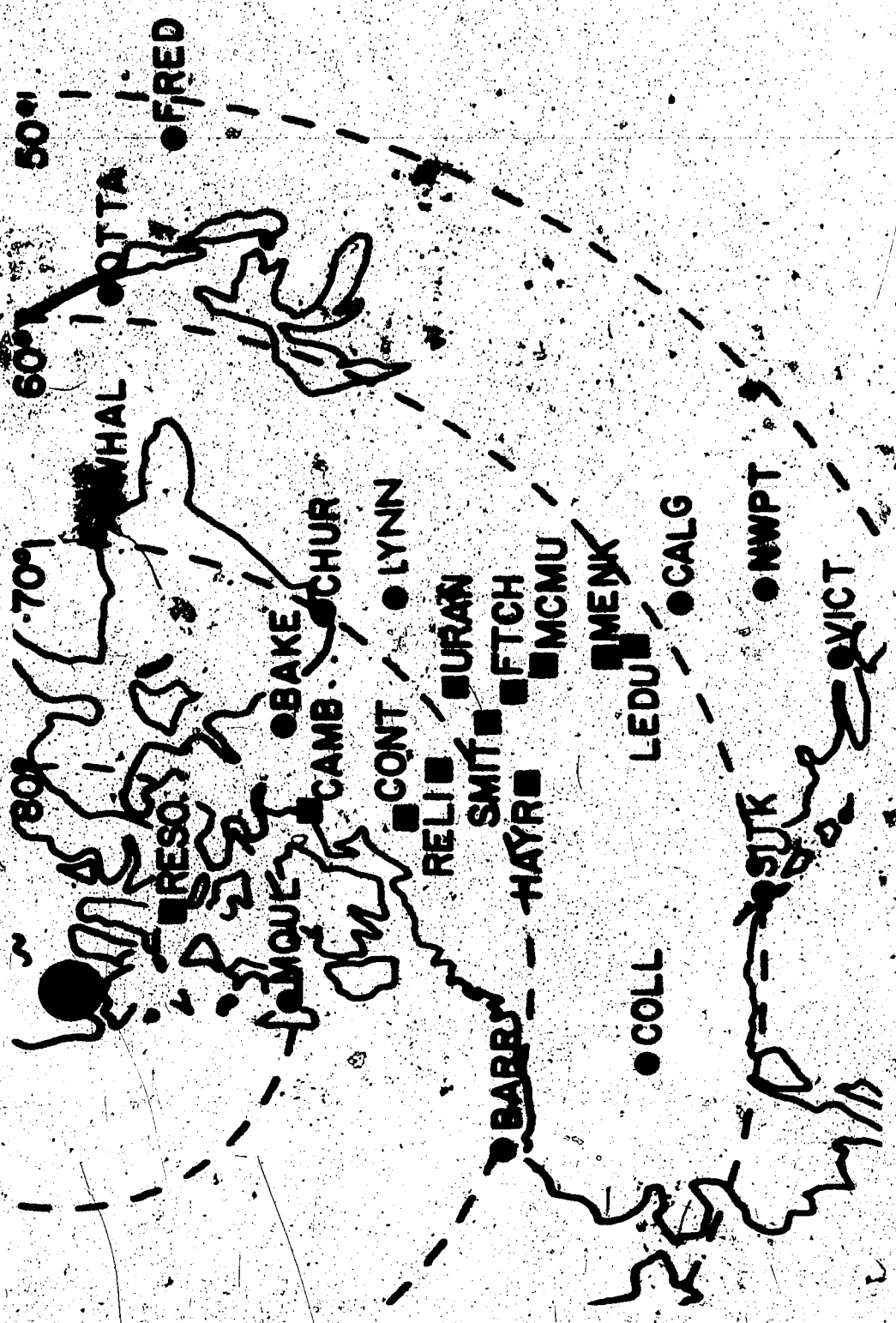
From the above considerations, it is not unreasonable to conclude that the theories for pulsations in the Pc 4 and Pc 5 range are far from being complete. In this thesis, a new theory based on the temporal and spatial variations of the three dimensional current system flowing along the auroral oval is proposed. It will also be pointed out, that the steady state field line resonance model might be operative for some special and rare events.

## CHAPTER III

### EXPERIMENTAL DETAIL AND DATA PROCESSING

The data to be presented in this thesis were obtained from magnetometers operated by the University of Alberta along a common geomagnetic meridian. A line of these stations started operating in Western Canada along the corrected geomagnetic meridian  $\sim 301^\circ\text{E}$  in the summer of 1969. The line was in full operation in late 1971 and early 1972 with nine closely spaced stations spanning the latitude range from  $\sim 60.6^\circ$  (geomagnetic) to  $83.1^\circ\text{N}$ . The coordinates and code names of the nine stations are given in Table 2. The meridian line of magnetometers discontinued operations in the spring of 1972. In the summer of 1974, four stations were set up in the region of the auroral oval; three of the stations were along a common geomagnetic latitude line. The coordinates and code names of the four stations in operation during the summer of 1974 are given in Table 3. The locations of the stations are shown in Figure 17.

Each station was equipped with a three-component fluxgate magnetometer, together with a WWVB time code receiver, analog-to-digital system, and digital tape recorder. The detector head at all the stations except Resolute Bay



**CORRECTED GEOMAGNETIC COORDINATES**

Figure 17



Table 2 Code Names and Locations of the Magnetometer Stations in Operation During Late 1971 and Early 1972.

Station	Code	Geographic		Corr. Geom.	
		°N	°E	°N	°E
Resolute Bay	RESO	74.7	265.1	84.3	306.0
Cambridge Bay	CAMB	69.1	255.0	77.7	301.0
Contwoyto Lake	CONT	65.5	249.7	74.2	297.0
Fort Reliance	RELI	62.7	251.0	71.4	300.0
Fort Smith	SMIT	60.0	248.0	68.1	300.8
Fort Chipewyan	FTCH	58.8	248.0	67.0	301.6
Fort McMurray	MCMU	56.7	248.8	65.0	302.7
Meanook	MENK	54.6	246.7	62.5	301.2
Leduc	LEDU	53.3	246.5	61.2	301.5

Station	Code	Centered Dipole		Inv. Lat.	L
		°N	°E		
Resolute Bay	RESO	83.0	289.4	83.2	71.4
Cambridge Bay	CAMB	76.8	296.6	76.9	19.5
Contwoyto Lake	CONT	72.6	295.8	72.7	11.3
Fort Reliance	RELI	70.3	300.1	70.5	8.9
Fort Smith	SMIT	67.3	300.0	67.5	6.8
Fort Chipewyan	FTCH	66.3	302.1	66.4	6.2
Fort McMurray	MCMU	64.2	303.5	64.5	5.4
Meanook	MENK	61.9	300.8	62.2	4.5
Leduc	LEDU	60.6	302.9	60.9	4.2

Table 3 Code Names and Locations of the Magnetometer Stations  
in Operation During the Summer of 1974

Station	Code	Geographic °N	Geographic °E	Corr. °N	Geom. °E	Centered °N
Hay River	HAYR	60.8	244.2	68.0	294.4	67.3
Fort Smith	SMIT	60.0	248.0	68.1	300.8	67.3
Uranium City	URAN	59.6	251.5	68.6	304.1	67.4
Fort McMurray	MCMU	56.7	248.8	65.0	302.7	64.2

was oriented in local magnetic (H,D,Z) coordinates. The detector head at Resolute Bay was oriented in the geographic (X,Y,Z) coordinates system. Data were recorded digitally on 7-track magnetic tape at a rate of  $\sim 1$  sample/component/2 sec. The timing was accurate to within  $\pm 0.1$  seconds. The dynamic range of the system was  $\pm 1000\gamma$  with a sensitivity of  $\pm 1\gamma$ . The records were timed by recording WWVB directly on tape every 7 hr 38 min. A more complete description of the instrumentation is given in Appendix A.

The data on the 7-track 'field tapes' were unpacked onto 9-track 'master tapes' for each station. Where the data blocks could not be timed accurately by the computer due to the occurrence of bad data blocks between successive WWVB blocks, the data were timed by correlating the micropulsations (in the D-component) occurring in this time interval with those recorded at adjacent stations. Much of the data recorded at Contwoyto Lake was timed manually in this manner with an accuracy of  $\sim \pm 1$  minute. This particular process of timing proved to be a long and tedious task and phase information at the station of Contwoyto Lake is, of course, less reliable.

After the data from all stations were transferred to 9-track 'master tapes', a series of 'event tapes' were created with each tape containing a series of files. In each file all available data from the line of stations for a

S



specified period of time (event) were written using the same format as was used for the 'master tapes'. This allowed the study of a specific event by only utilizing one file from an 'event tape' rather than nine 'master tapes'.

The data in the event tape were then ready to be processed. The characteristics of the micropulsations considered in this thesis were determined by using the cross-spectral matrix formalism. The basic concept of this approach was outlined by Born and Wolf [1959], and applied by Fowler et al. [1967], Rankin and Kurtz [1970], Samson et al. [1971], and Fukunishi et al. [1975] among others. In our analysis, the data were detrended with a 1-20 mHz zero-phase shift Butterworth digital bandpass filter [Alpaslan, 1968]. A data window of length 60 minutes was utilized, and cosine tapers at either end of the data window were used to eliminate any remaining traces of the transient response of the filter and to improve the shape of the smoothed spectral window. The autopower and crosspower spectral estimates were calculated using the Fast Fourier Transform algorithm [Gentleman and Sande, 1966]. To employ the algorithm, zeroes were added so that the number of data points could be factored into integral products of 2. Raw and smoothed power spectra were plotted to determine the spectral peaks using the autopower spectral estimates. From the cross-spectral matrices  $J_{ij}(r_m, r_m)$  (where  $J_{ij}$  is the smoothed cross spectral

estimate at a frequency of component  $i$  and component  $j$  at the same station), the polarization ratios, the ellipticities and polarization angles in the H-D, H-Z and D-Z planes were determined. From the station-to-station cross-spectral matrices  $J_{ij}(r_m, r_n)$  (where  $J_{ij}$  is the smoothed cross-spectral estimate for a frequency of component  $i$  at station  $r_m$  and component  $j$  at station  $r_n$ ), coherencies and phases were determined. A more detailed discussion of the determination of polarization and phase from a three-dimensional vector time series is given in Appendix B.

Since this thesis deals with the relationship between the micropulsation activity in the morning sector and the convection westward electrojet, information on the positions of the electrojet was necessary. To establish the latitudinal boundaries of the convection electrojet, the magnetic data were put in a latitude profile format. This presentation technique was used previously by Walker [1964], Bonnevier et al. [1970] and Kisabeth and Rostoker [1971]. A latitude profile shows the magnetic perturbations in three components plotted against latitude at a given instant of time. A quiet time baseline was chosen to determine the perturbation. The base line for each station was determined from the smoothed daily means of the magnetic variations which had excluded large magnetic perturbations. The latitude profiles are then interpreted using techniques developed

by Kisabeth [1972] to obtain information about the locations of the electrojet boundaries. A more detailed discussion of the inference of the distribution of electric currents in the ionosphere and magnetosphere from ground magnetic data is given in Appendix C.

Finally, we note that the data were analysed in the local magnetic coordinate system (H, D, Z) for the polarization characteristics of micropulsations and that the data were transformed to the centered dipole system (X, Y, Z) before being portrayed in the form of latitude profiles. Frequency bands which had distinct spectral peaks and high polarization ratios at most of the stations were selected for analysis. The intensity is the total power of the coherent signal (i.e., the sum of all three components H, D and Z). If  $I_m$  is the largest of the intensities at all the stations in a given interval, then the relative intensity at a station  $i$  is defined by  $I_i/I_m$ . Intensity contours can then be plotted as a function of invariant latitude and Universal Time. Universal Time is used throughout the text. An approximate conversion to local geomagnetic time at our stations can be made by subtracting  $8\frac{1}{2}$  hours from the given Universal Time while local time is approximately Universal Time less 7 hours. The date of an event is expressed in terms of number of days after the beginning of the year (January 1 is Day 1).

## CHAPTER IV

### Pc 5 ACTIVITY IN THE MORNING SECTOR

In this chapter, we first present observations that the micropulsation activity in the Pc 5 range in the morning sector is closely related to the convection westward electrojet. The evidence that the electrojet itself exhibits spatial oscillations are dealt with next. From the observational characteristics of Pc 5 micropulsation activity as related to the westward electrojet, a model regarding the generation mechanism of the Pc 5 activity is then presented.

#### 4.1 The Relationship of Pc 5 Activity in the Morning Sector to the Auroral Westward Electrojet

This section includes and extends the work of Lam and Rostoker [1975] reported earlier. The results of analysing three days' activities will be presented to illustrate the relationship of the Pc 5 activity in the morning sector to the auroral westward electrojet.

The events selected for analysis are chosen from three separate days. They are Day 253, 1971 and Days 16 and 17, 1972. All the events occurred in the morning sector, spanning the local time regime from pre-dawn to local magnetic noon. The magnetograms both unfiltered and filtered (with a 1-20 MHz digital filter) for the events are shown in

Figures 18, 19, 20 (Day 235, 1971), 21, 22 (Day 16, 1972), 23 and 24 (Day 17, 1972). A magnetogram is an amplitude-time plot of the magnetic perturbations in the H (the component pointing towards the local magnetic north), D (the component pointing eastward) and Z (the component pointing downward) coordinates recorded at our stations, the northern-most station being RESO (see Table 2 for the name of the station) and the most southern one being LEDU. The perturbations are plotted as a function of universal time (local time for our stations is approximately equal to universal time less seven hours). It is apparent from the magnetograms that the amplitudes of the oscillations are rather large (up to  $\sim 100\gamma$  peak to peak for Days 16 and 17). The pulsations seem to occur in bursts and over different latitudinal ranges at different intervals of time. For example, in Figure 24, one can see a northward shift of activity as a function of time. This trend will later be shown to be related to the locations of the convection westward electrojet.

The locations of the convection westward electrojet plotted as a function of invariant latitudes and universal time will be used as a frame of reference for the presentation of the pulsation data. Both the poleward border and the equatorward border of the electrojet were inferred from a series of successive latitude profiles of the magnetic perturbations (see Appendix C for more detail regarding the



DAY235 1971

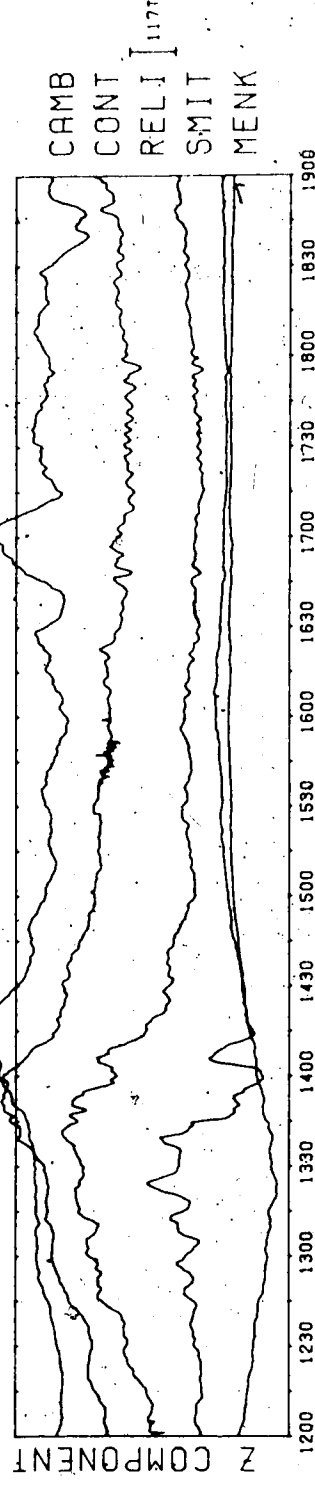
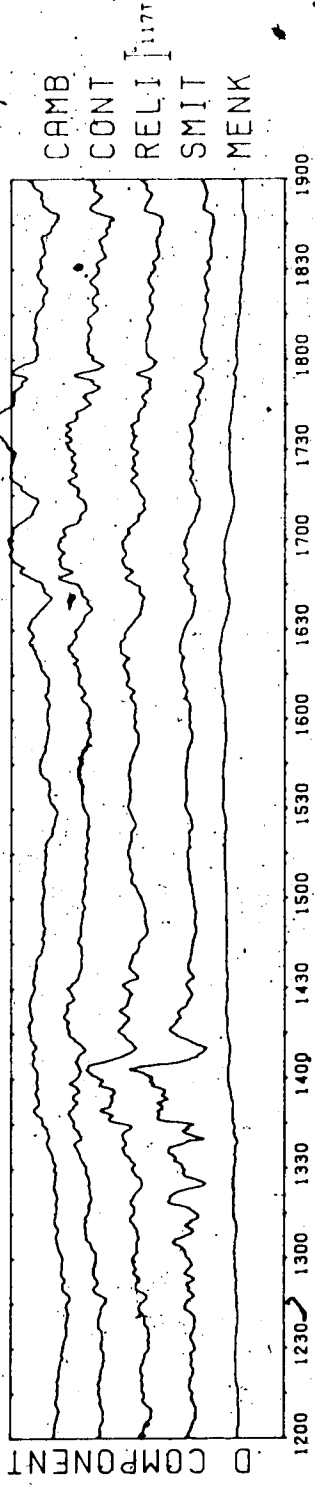
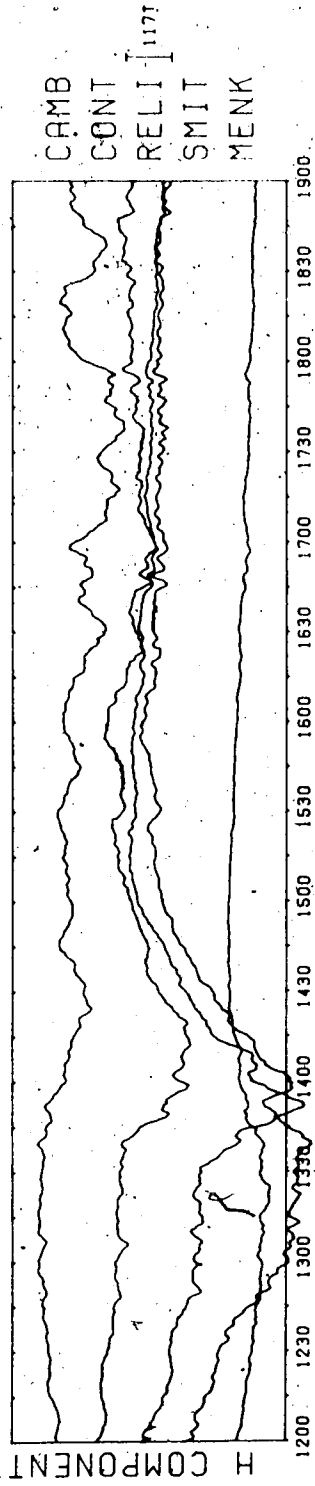


Figure 18

DAY 235, 1971

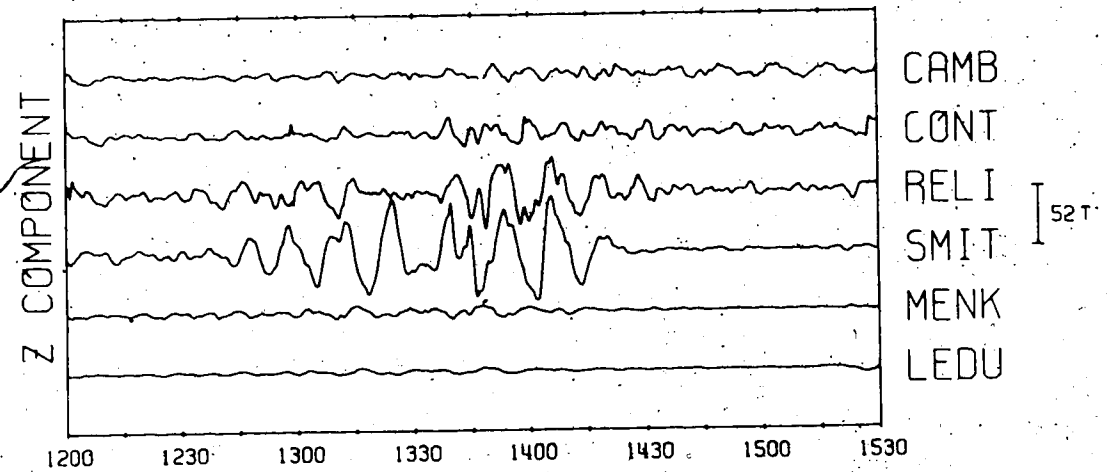
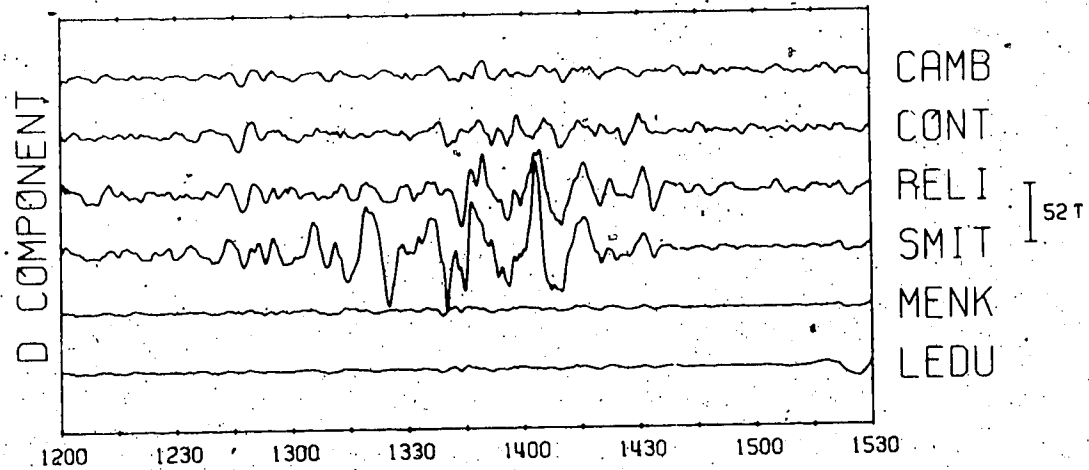
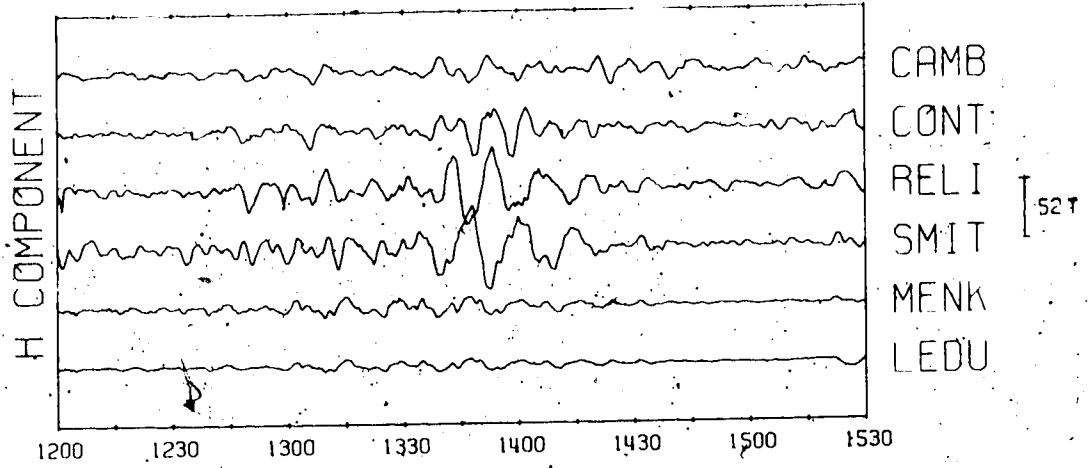


Figure 19

DAY 235, 1971

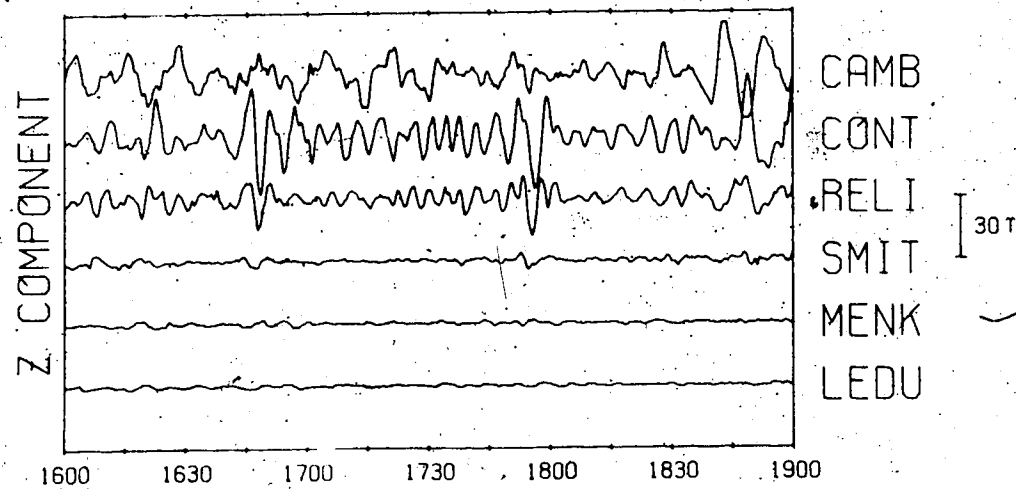
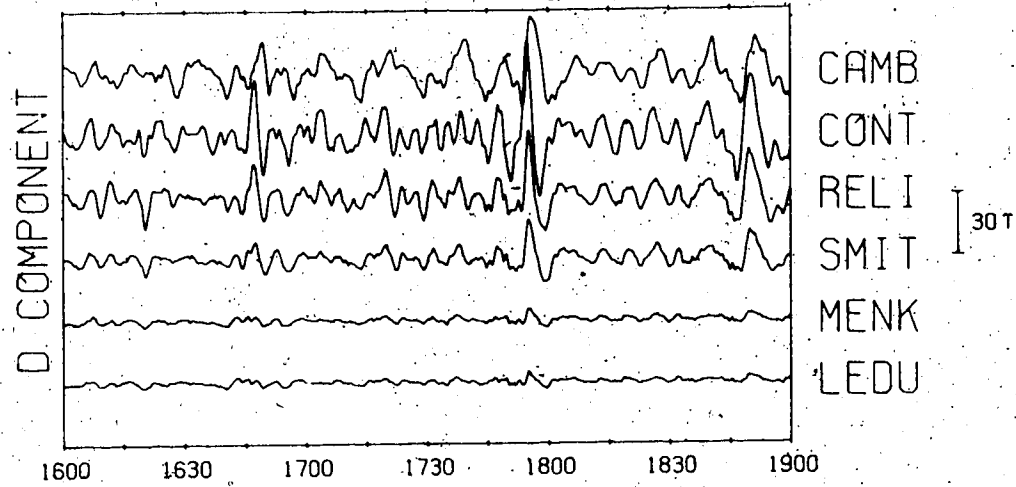
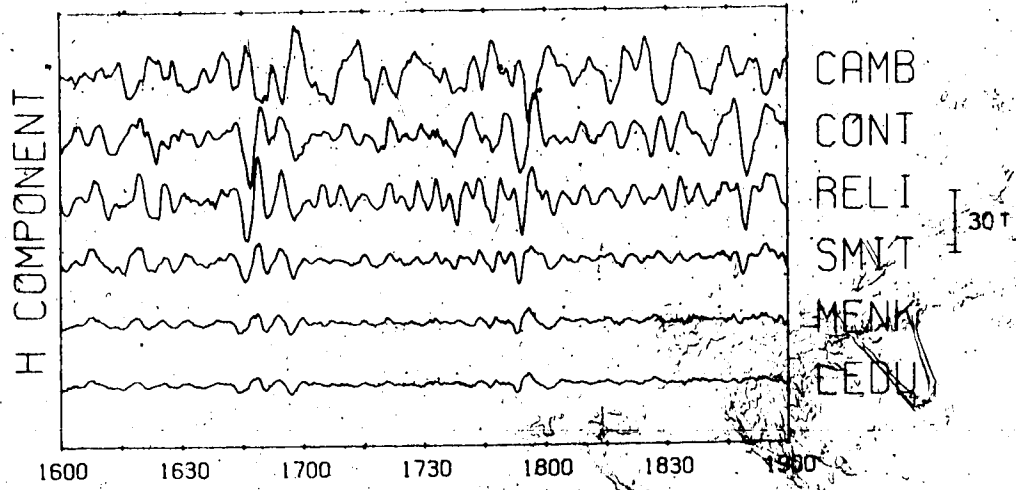


Figure 20

DAY 16 1972

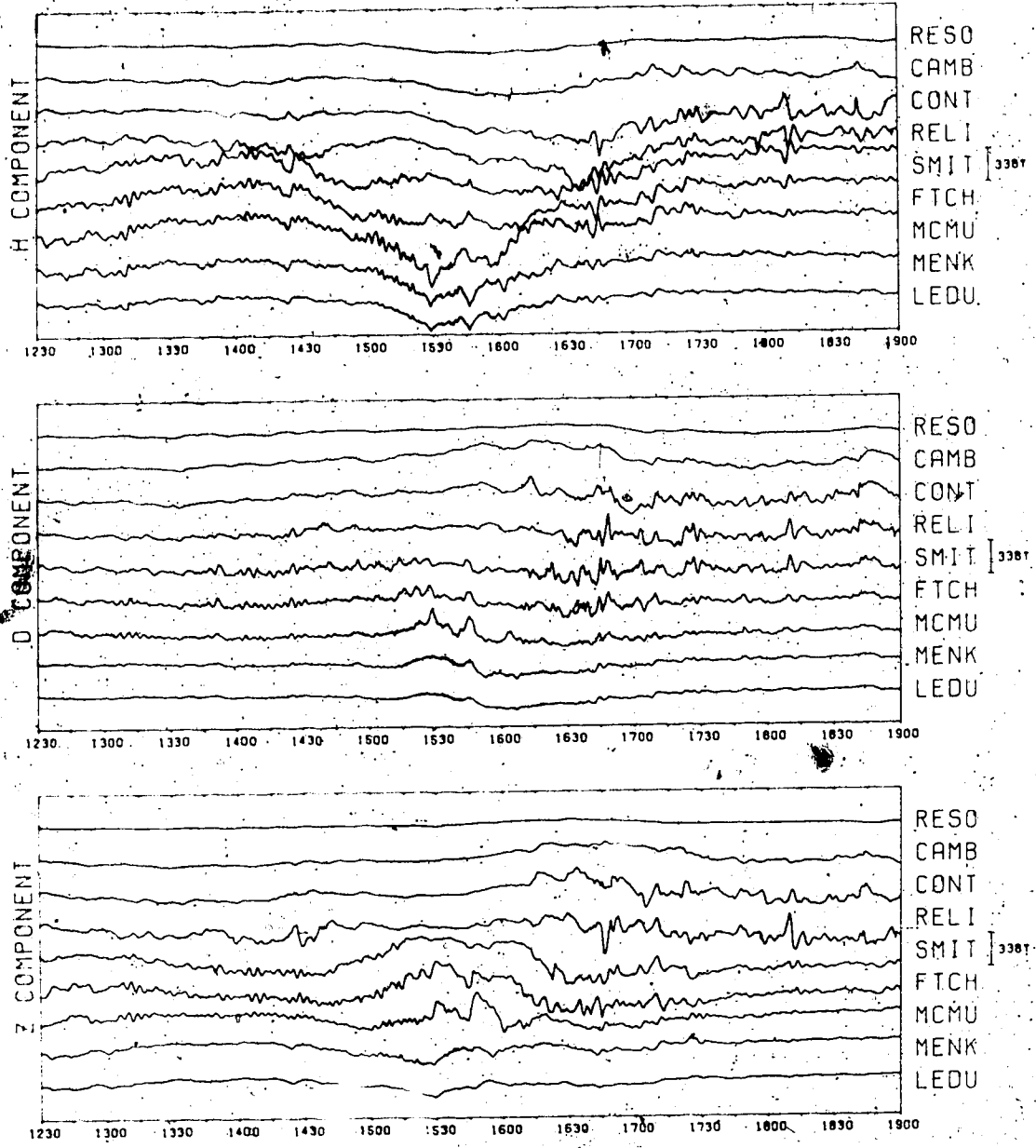


Figure 21

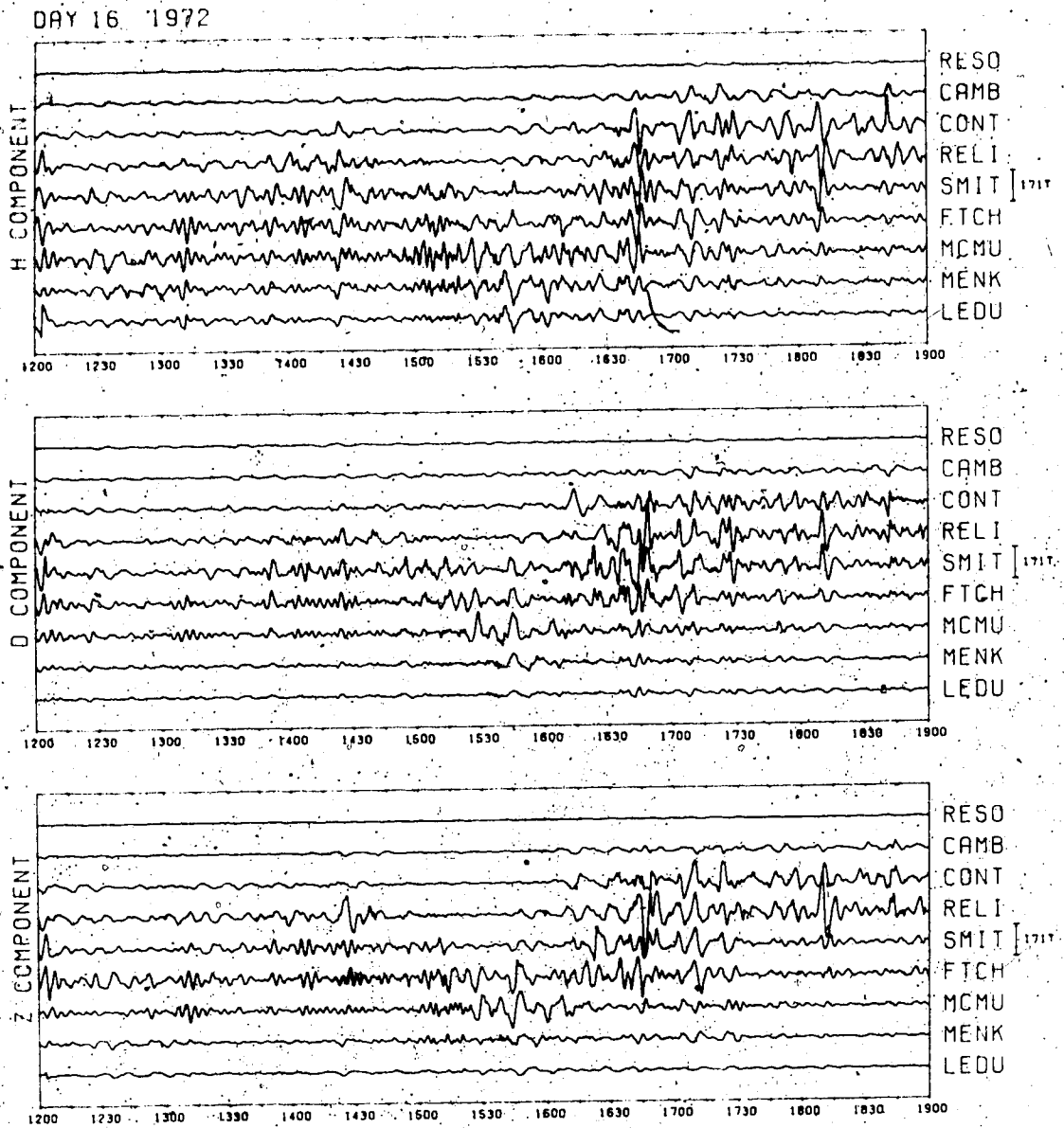


Figure 22

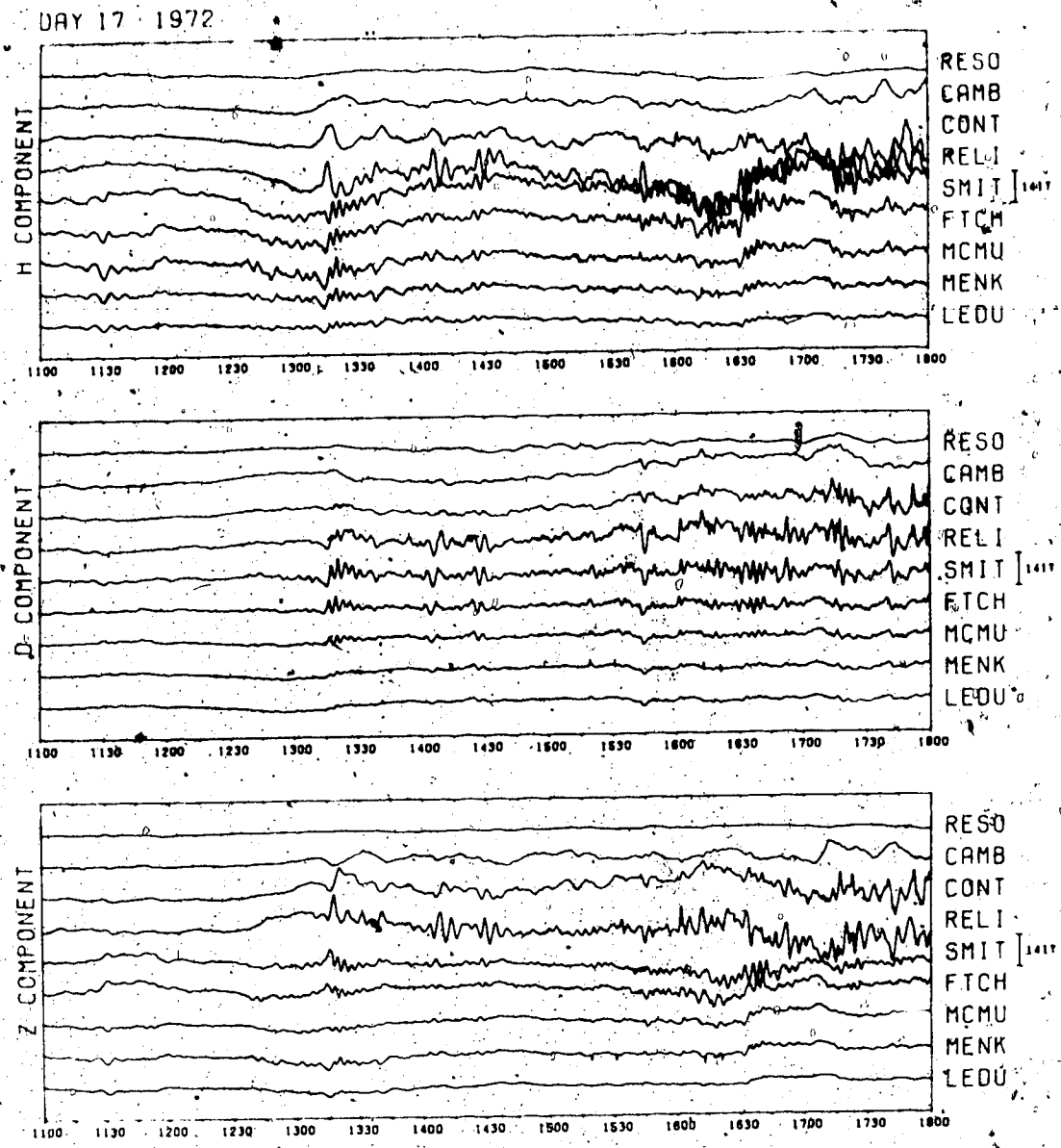


Figure 23

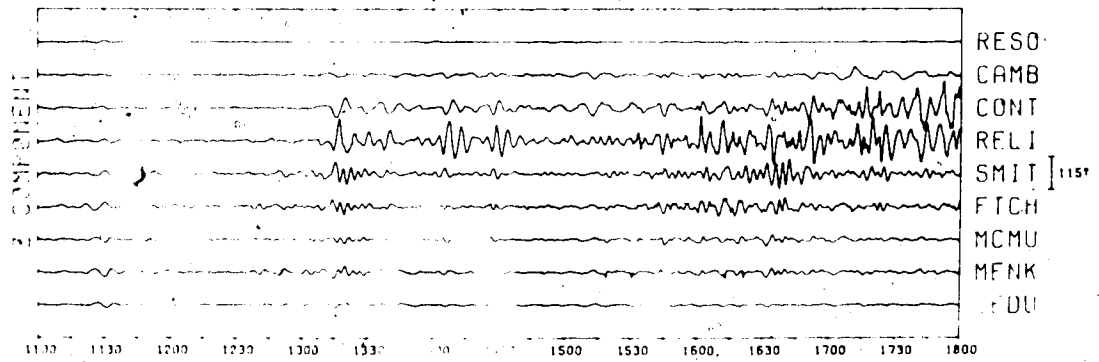
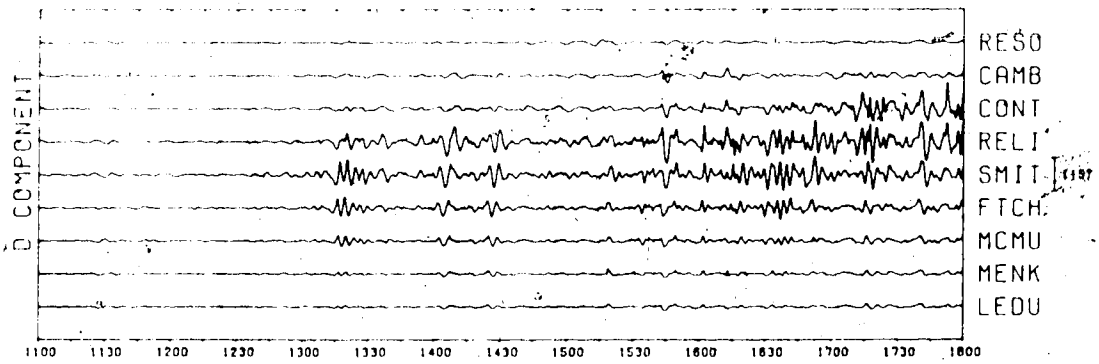
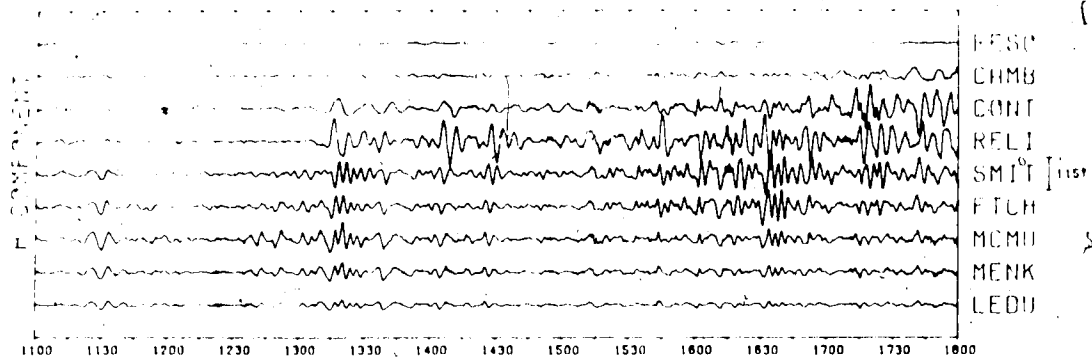


Figure 24

interpretations of the latitude profiles).

Some examples of the latitude profiles from which the borders of the electrojet were inferred are shown in Figure 25. The borders of the electrojet are indicated by arrowheads in Figure 25 and were inferred by assuming that there is a gaussian distribution current density across the electrojet. For each profile the horizontal components (H,D) were rotated to provide orthogonal horizontal components (X,Y) in the centered dipole system. For our stations dipole latitude is essentially the same as invariant latitude (invariant latitude was chosen because the project was initiated with a view of comparing ground pulsations data with satellite data).

Figure 25A shows that the convection westward electrojet was located near our southern stations around 1517 UT. About an hour later at 1631 UT this westward electrojet was located over our northern stations as shown in Figure 25B. Figure 25C and D illustrate the rapid poleward motion of the equatorward border of the westward electrojet within a short time. It can be seen that the equatorward border of the westward electrojet shifted northward substantially (about  $4^\circ$ ) in a few minutes. It is interesting to note that an eastward electrojet (Figure 25D) appeared in the latitudes where the lower portion of the westward electrojet was (Figure 25C). Finally it should be noted from these latitude profiles that the Y profiles which



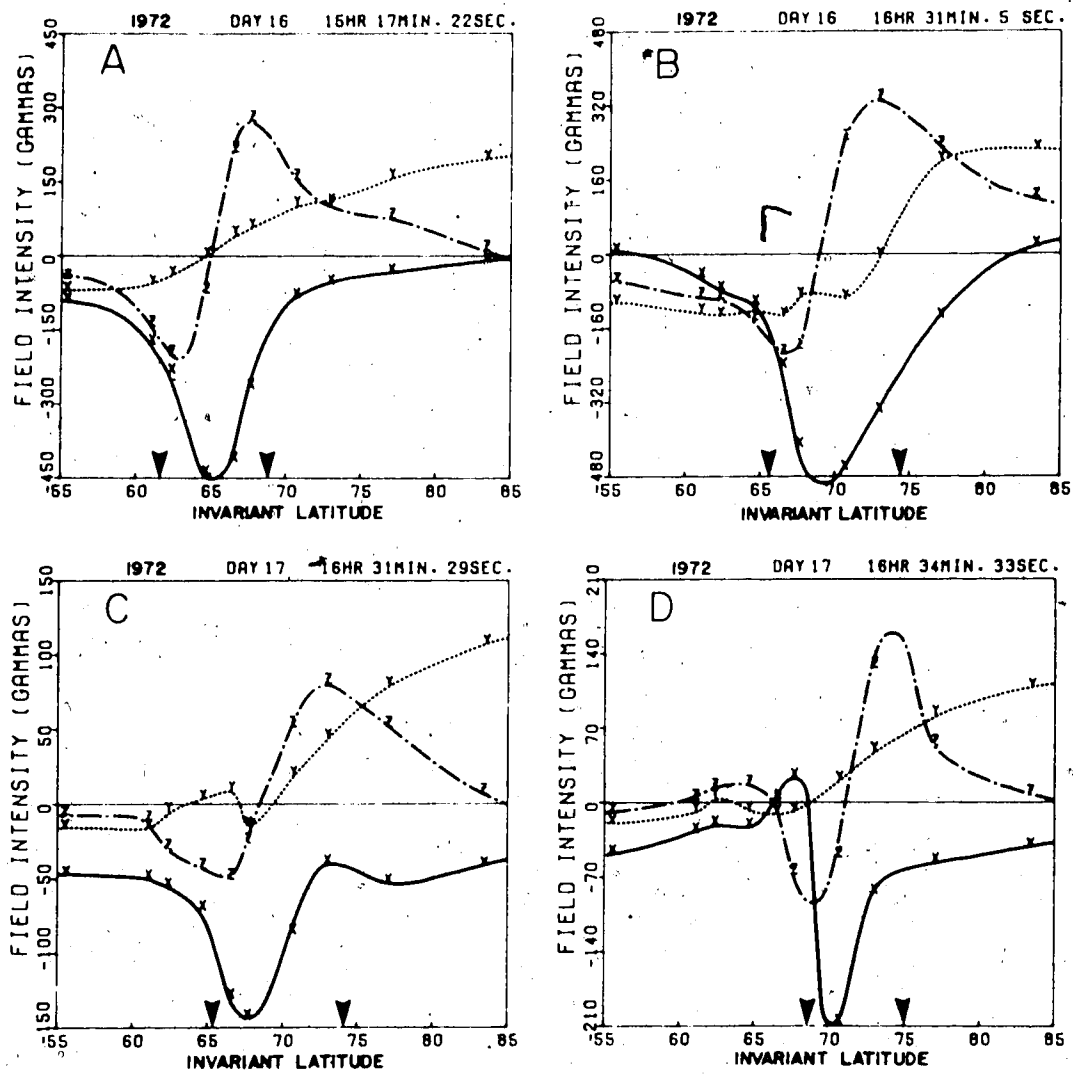


Figure 25

exhibit a more or less step-like function (Figure 25B shows the step clearly) are indicative of the net downward field-aligned current flowing into the latitudinal regime occupied by the westward electrojet. The tilting of the electrojet with respect to our line of stations probably prevents profiles in Figure 25A, C and D from showing a clear step-like function in Y.

To see how the Pc 5 activity is related to the location of the westward electrojet, intensity contours of a selected frequency band were plotted against the background of the electrojet as a function of invariant latitude and universal time as shown in the next few figures. Each figure consists of two portions. The upper portion is the intensity contours of the micropulsation activity plotted as a function of latitude and universal time. The stars on the ordinate indicate the locations of our stations in invariant latitude. Only the first and last letter of the code name of our stations are plotted. For example, R0 represents RESO (Resolute Bay). The lower portion of the figure consists of the poleward borders and equatorward borders represented by solid lines of the electrojet (which were inferred from a series of latitude profiles about 10 minutes apart) and the intensity maximum of the pulsation activity represented by the shaded area.

Figure 26 shows the intensity contours of the pulsational activity in the lower frequency band (1.3 - 2.5

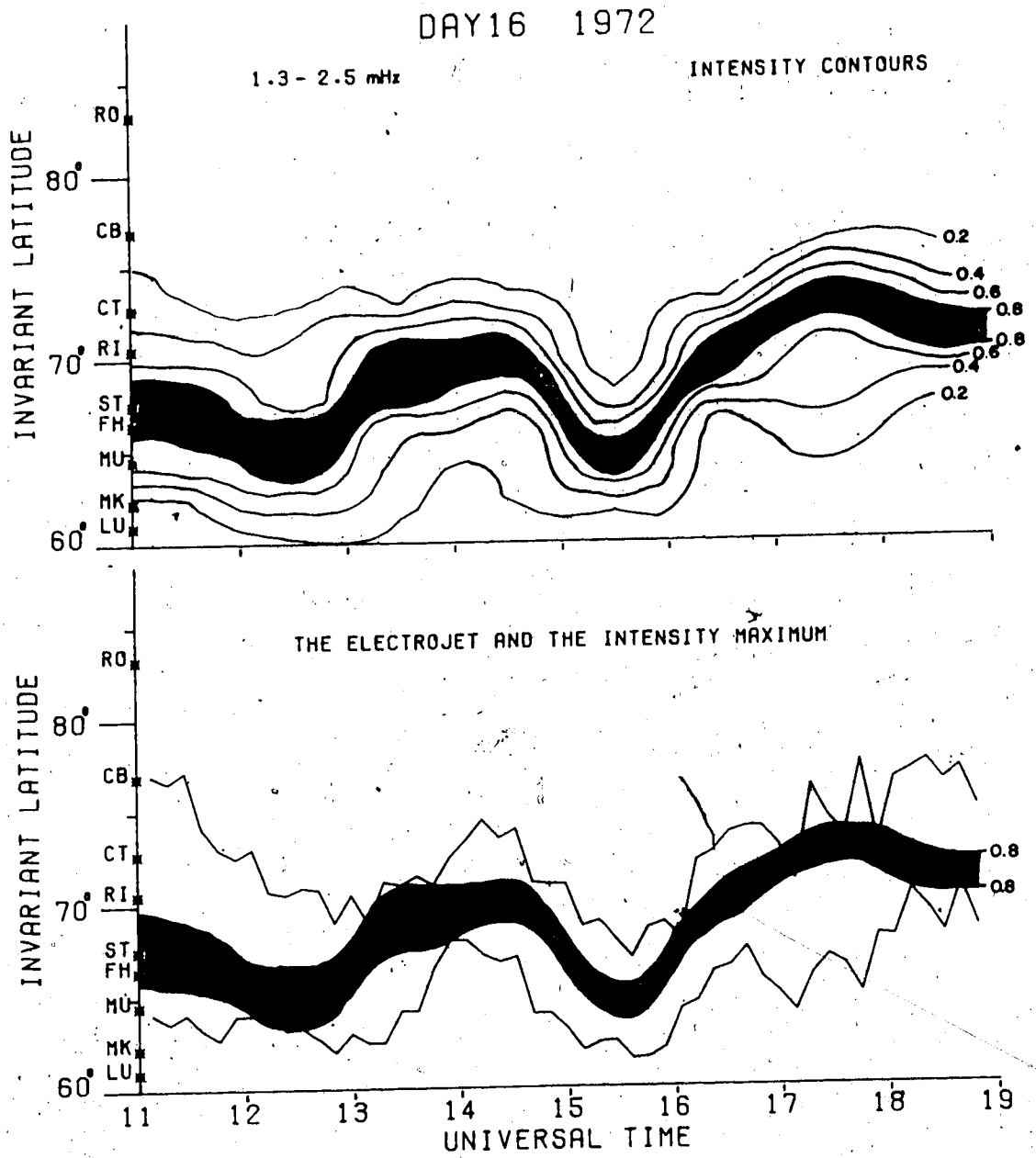


Figure 26

mHz) of the Pc 5 spectrum for Day 16, 1972. The 'meandering' of both the electrojet and the intensity maximum with time can clearly be seen. The next two diagrams, Figures 27 and 28, illustrate that the Pc 5 activity in the higher frequency bands of 2.0 - 3.0 mHz and 3.3 - 5.1 mHz for Day 235, 1971 and Day 17, 1971 respectively again 'follows' the electrojet very well. The proximities of the contour lines in the upper portion of the above figures and the locations of the intensity maximum with respect to the electrojet shown in the lower portion of the figures for different spectra bands in the Pc 5 range for three different events clearly illustrate that the region of Pc 5 oscillations is confined to the region of the auroral electrojet.

To demonstrate further that the micropulsation activity is intimately related to the westward electrojet, we present in the next few figures the power spectra corresponding to different locations of the westward electrojet. The powers in H, D and Z covering a frequency range of 1 to 16 mHz were plotted for all our stations, RESO being our most northern station and LEDU our most southern station. The power spectra are characterized by six degrees of freedom. The spectrum is truncated at  $0.4 \gamma^2/\text{mHz}$  power level because of possible quantizing errors at lower power levels. Figure 29 shows the power spectra for the interval 1100 - 1200 UT for Day 17, 1972. During

DAY 235 1971

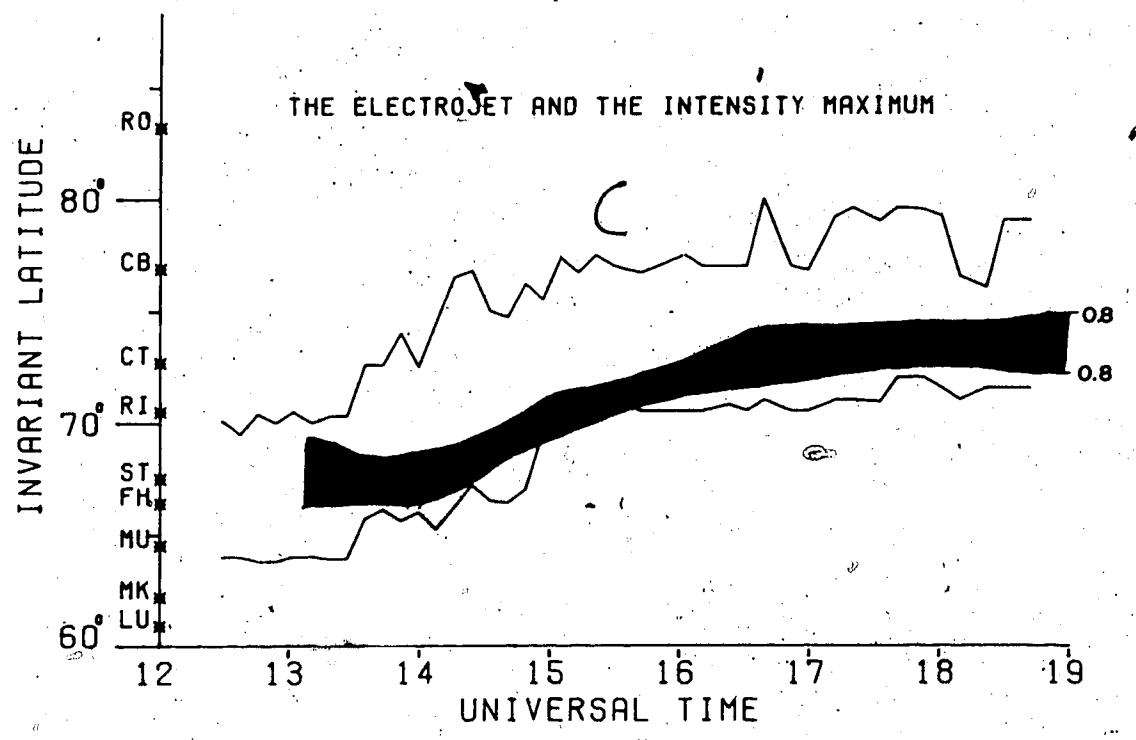
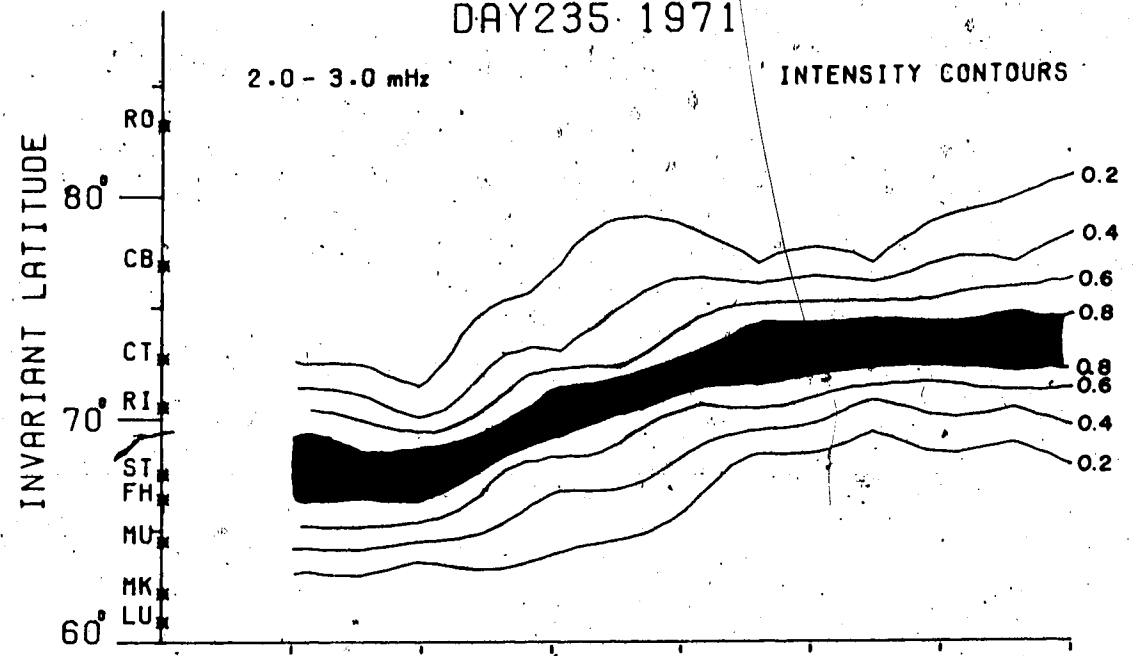


Figure 27

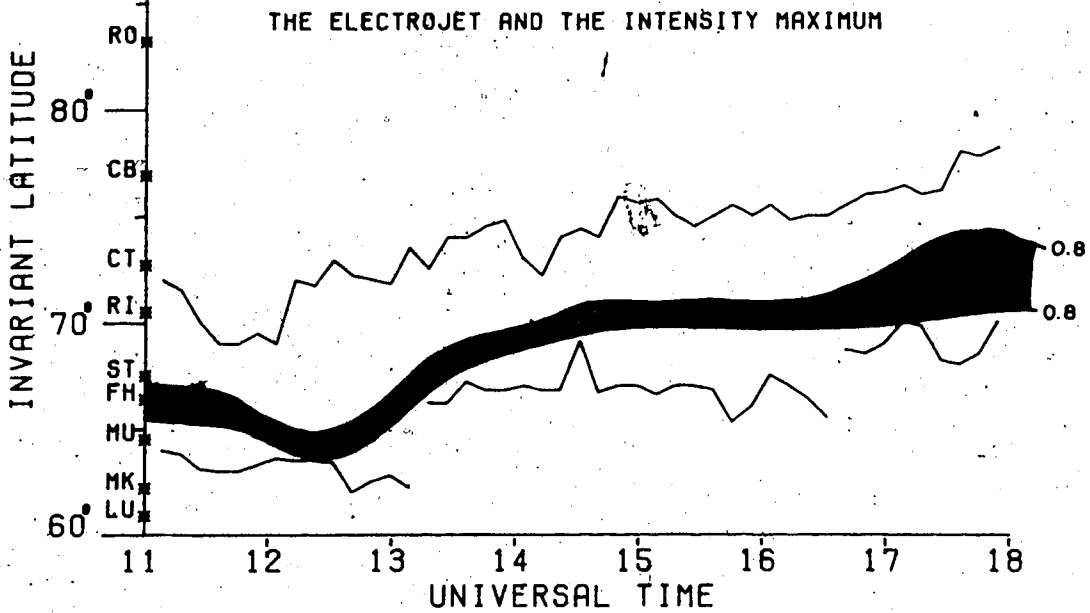
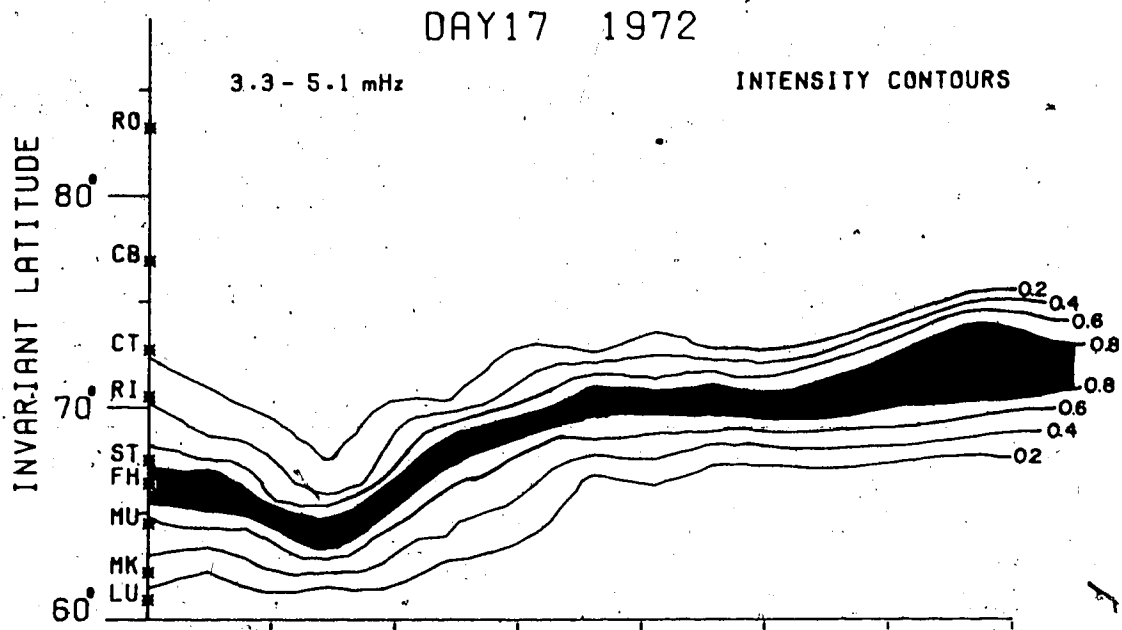


Figure 28

DAY 17 1972 (1100-1200)

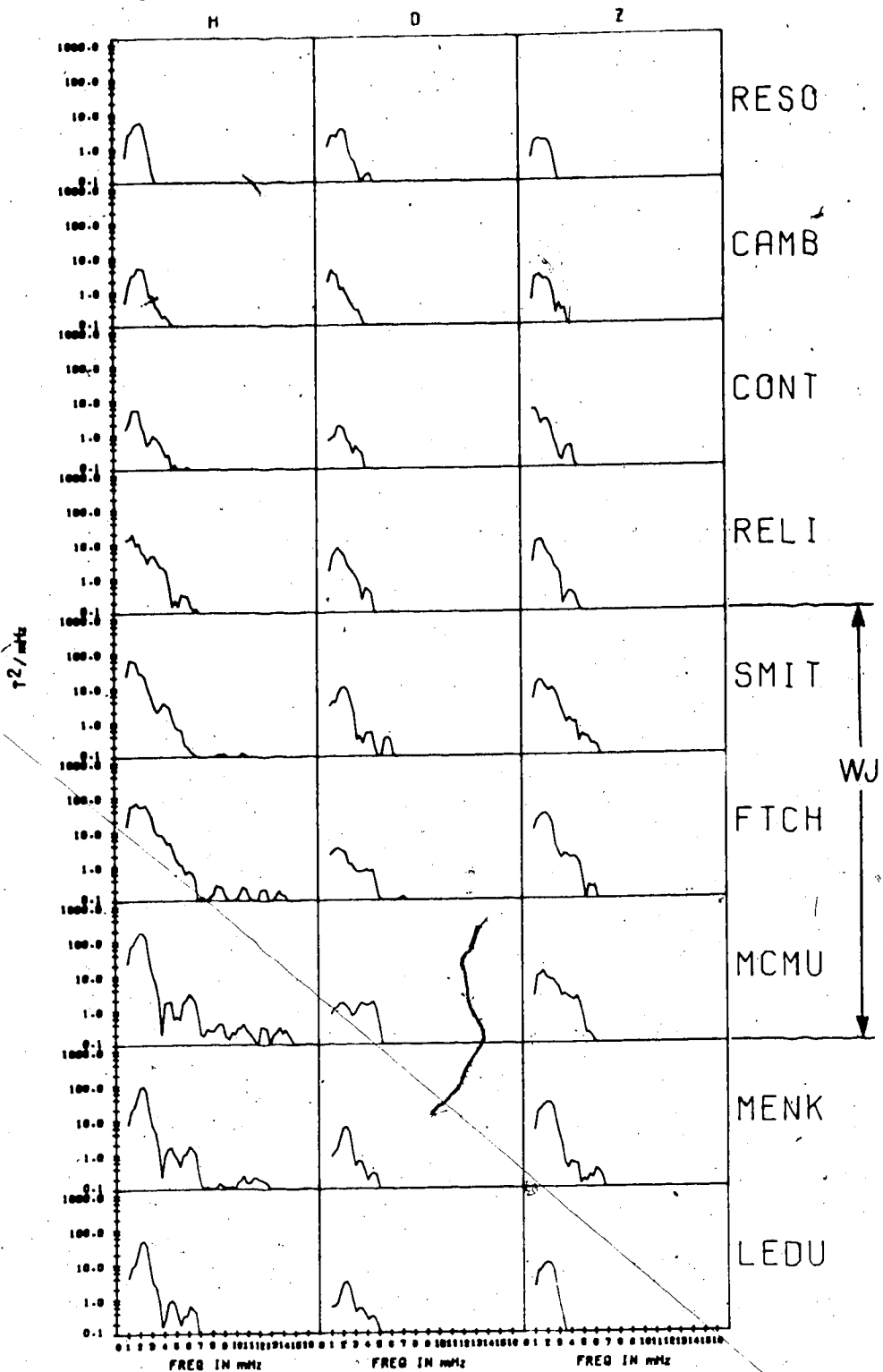


Figure 29

this interval, the westward electrojet was located near our southern stations. The stations that were within the electrojet most of the time are indicated in the figure. It can be seen that inside the electrojet and near the equatorward border the power level was much enhanced, particularly in the H component. The presence of high frequency peaks in the Pc 4 band in the stations inside the electrojet was evident. The stations poleward of the electrojet have very low power and show no high frequency peaks at all. However, as the electrojet shifted poleward, the enhanced power levels and the high frequency peaks also shifted northward as shown in Figures 30, 31 and 32. The contrast can clearly be seen in the power spectra for CONT for the four different time intervals.

To demonstrate further that the pulsational activity peaks in the same latitudinal range occupied by the westward electrojet and to show that all the spectral components in the Pc 5 band peak in the same latitudinal range, we present in the next three figures the latitude profiles of the powers of different frequencies for three time intervals corresponding to three different locations of the westward electrojet. The magnitudes of the powers are not shown in the diagrams because we are only interested in where the powers of a particular frequency band peak. Besides, the powers almost drop to noise levels outside the



DAY 17 1972 (1200-1300)

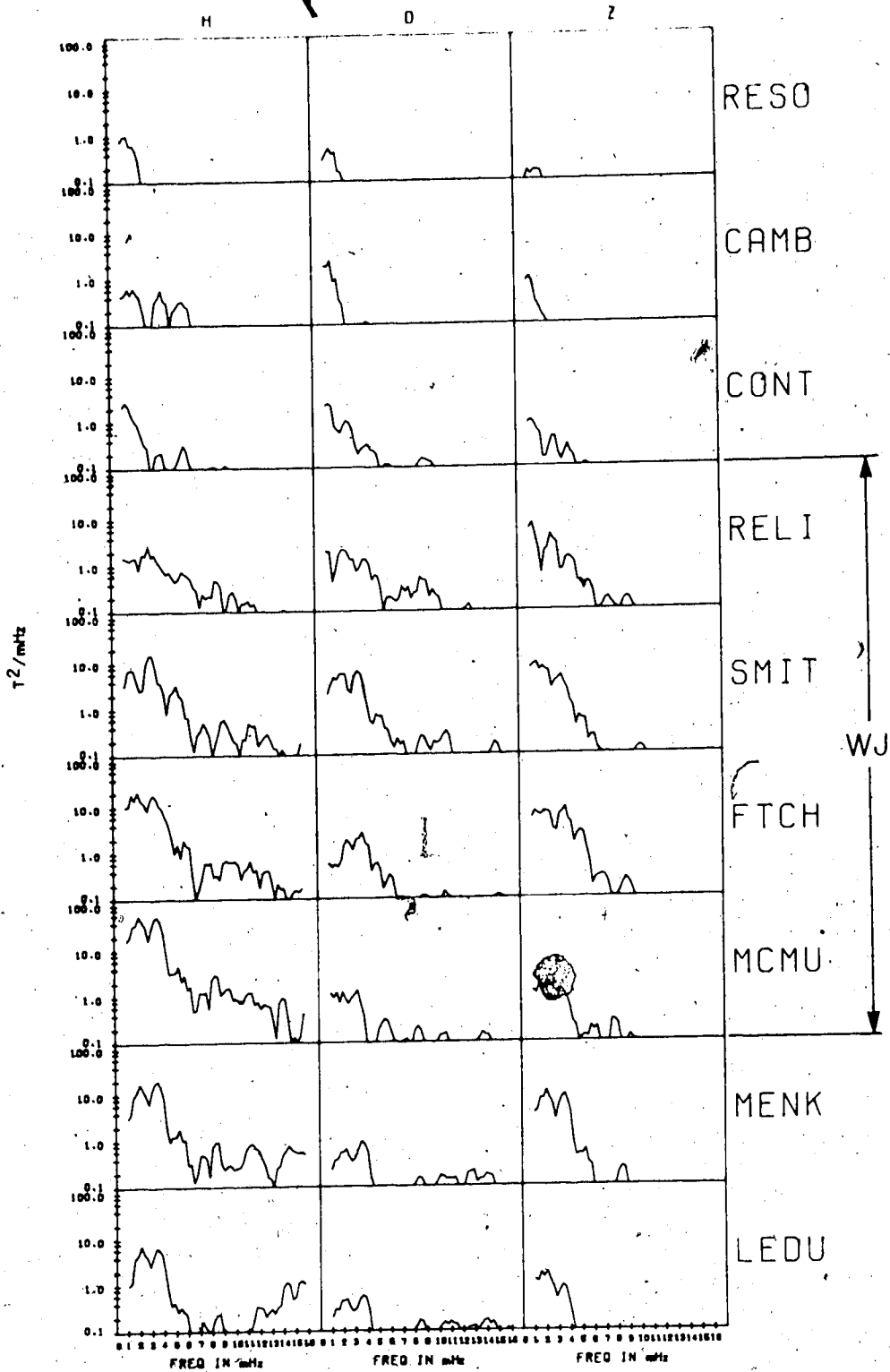


Figure 30

DAY 16 1972 (1700-1800)

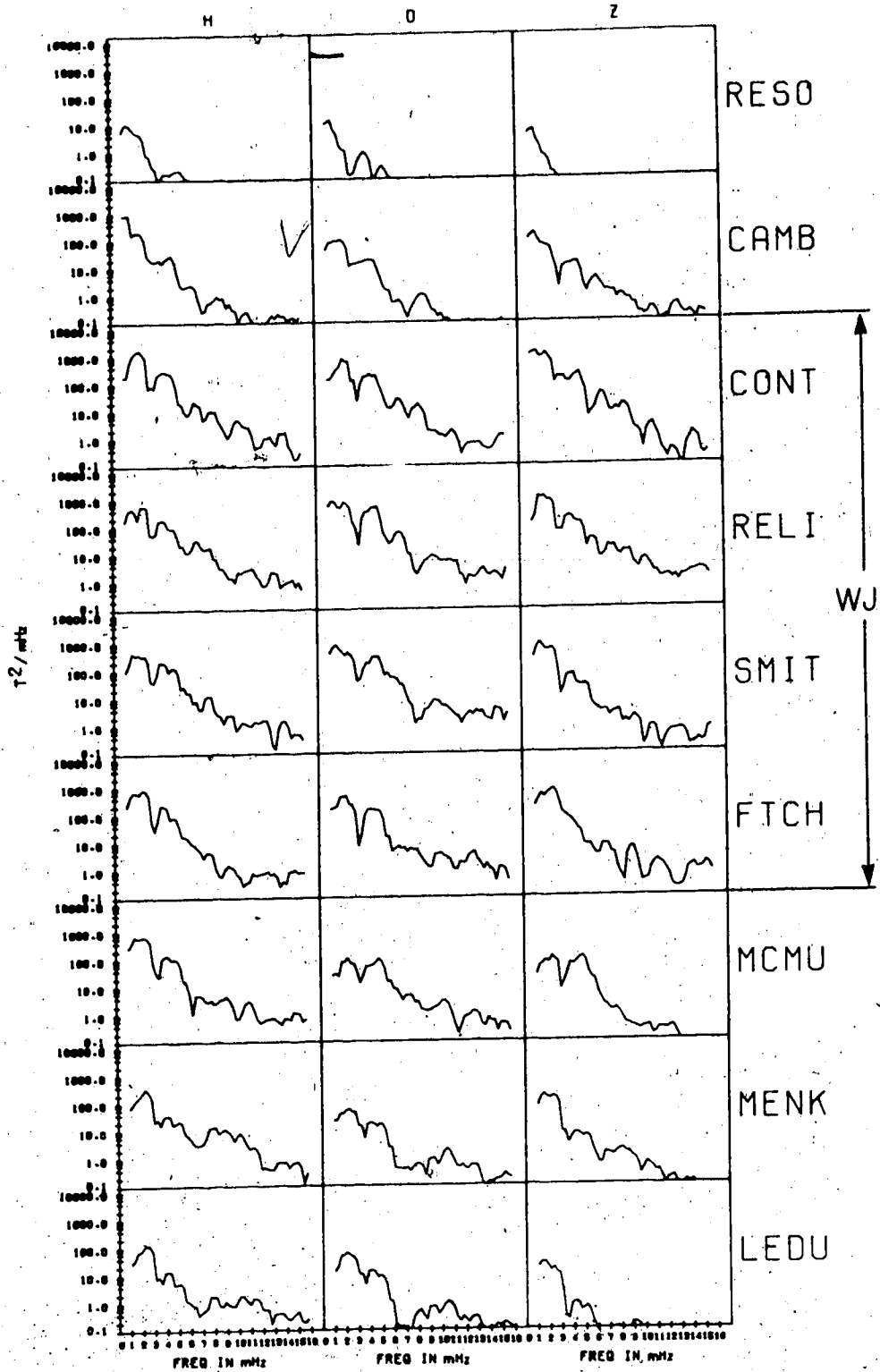


Figure 31

DAY 17 1972 (1700-1800)

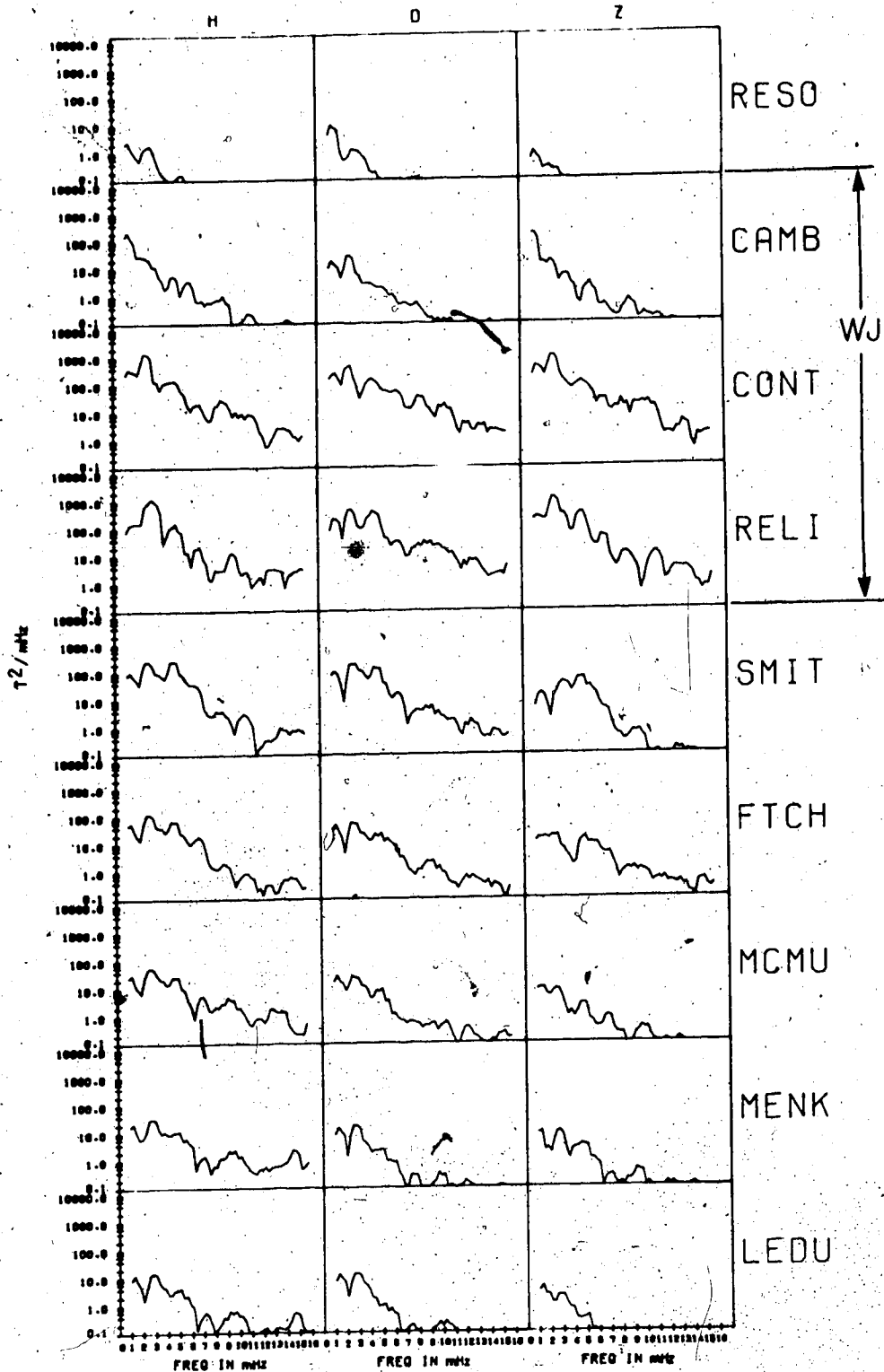


Figure 32

confines of the electrojet as is evident in the intensity contour plots (see for example Figure 28). Nonetheless, the magnitudes of the peak powers were compiled in Table 4 which gives an idea of the relative intensity of activity in the different frequencies and a comparison of the magnitude of powers in different components.

It can be seen in Figure 33 that when the westward electrojet was located at low latitudes (the dashed lines indicate the borders of the westward electrojet), all the spectral components (1.7 MHz, 5.0 MHz and 7.1 MHz) peak within the confines of the electrojet. As the electrojet shifted to higher latitudes as shown in Figures 34 and 35, the peaks of powers in different frequency bands also shifted. Again note the contrast in power level at CONT (the third dot from the right) for these three time intervals. These observations that the low frequency end of the Pc 5 spectrum maximizes at low latitudes ( $\sim 64^\circ$ ) as well as at high latitudes ( $\sim 73^\circ$ ) and that different spectral components all peak in the same latitudinal range occupied by the westward electrojet clearly suggests that the current system associated with the convection auroral electrojet dominates other sources (such as the resonant oscillations of field lines) in its contribution to the low frequency band of the micropulsation spectrum.

TABLE 4

Day 16, 1972 (1500-1600)

Frequency (mHz)	1.7	5.0	7.1
H peak power ( $\gamma^2$ /mHz)	1659.8(MCMU)	559.0(MCMU)	186.0(MCMU)
D peak power ( $\gamma^2$ /mHz)	969.8(MCMU)	61.0(SMIT)	23.5(SMIT)
Z peak power ( $\gamma^2$ /mHz)	1611.6(MCMU)	171.0(FTCH)	104.4(MCMU)

Day 17, 1972 (1500-1600)

Frequency (mHz)	1.5	4.0	6.1
H peak power ( $\gamma^2$ /mHz)	360.3(RELI)	235.0(RELI)	40.7(FTCH)
D peak power ( $\gamma^2$ /mHz)	116.0(RELI)	69.6(RELI)	34.4(SMIT)
Z peak power ( $\gamma^2$ /mHz)	164.1(CONT)	126.1(RELI)	15.9(SMIT)

Day 17, 1972 (1700-1800)

Frequency (mHz)	1.2	2.8	5.1	7.1
H peak power ( $\gamma^2$ /mHz)	379.9(CONT)	1384.4(CONT)	248.8(SMIT)	22.1(RELI)
D peak power ( $\gamma^2$ /mHz)	218.4(CONT)	500.9(CONT)	297.9(RELI)	35.1(CONT)
Z peak power ( $\gamma^2$ /mHz)	432.5(CONT)	1142.7(RELI)	334.6(RELI)	41.5(RELI)

DAY 16, 1972 (1500-1600)

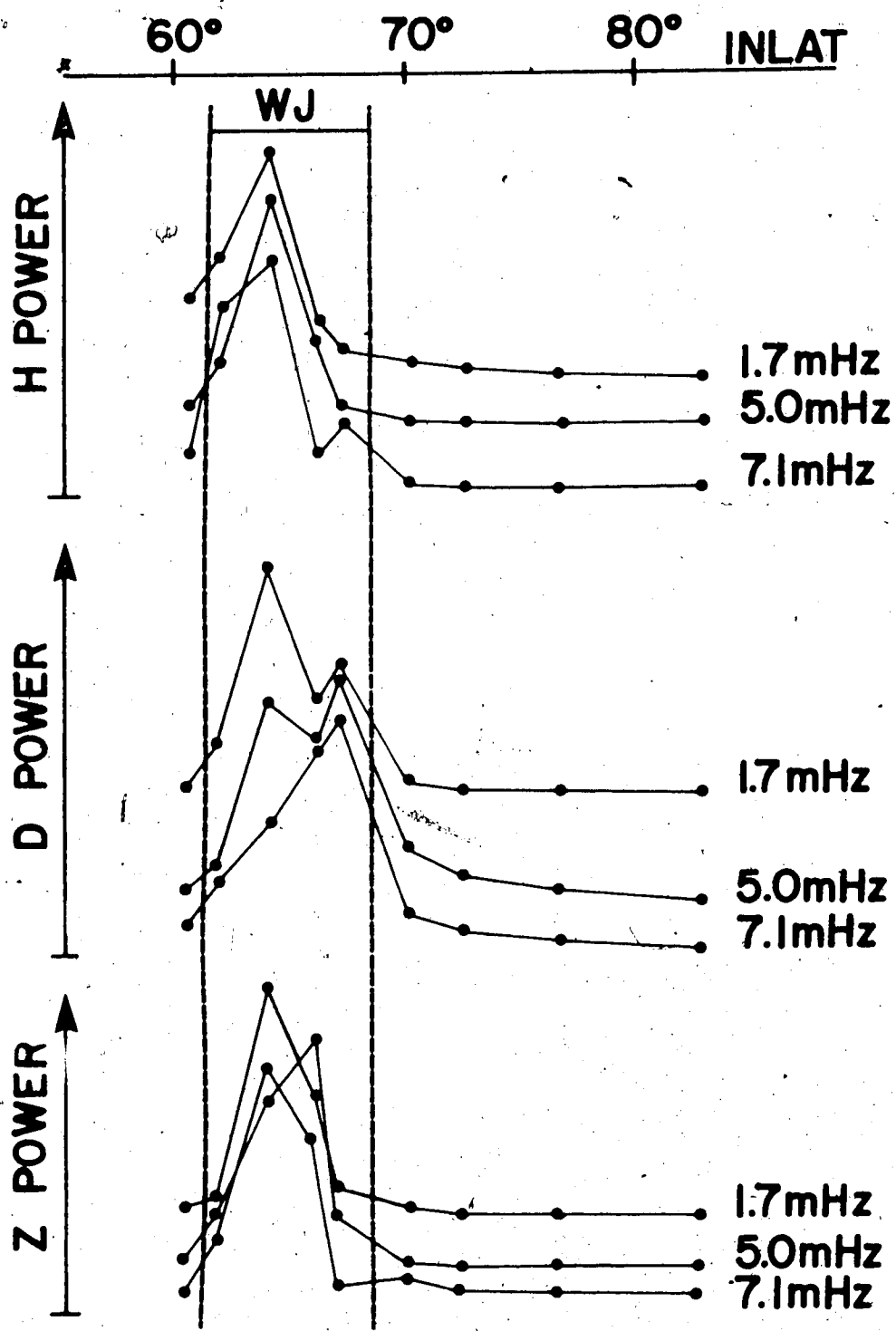


Figure 33

# DAY 17, 1972 (1500-1600)

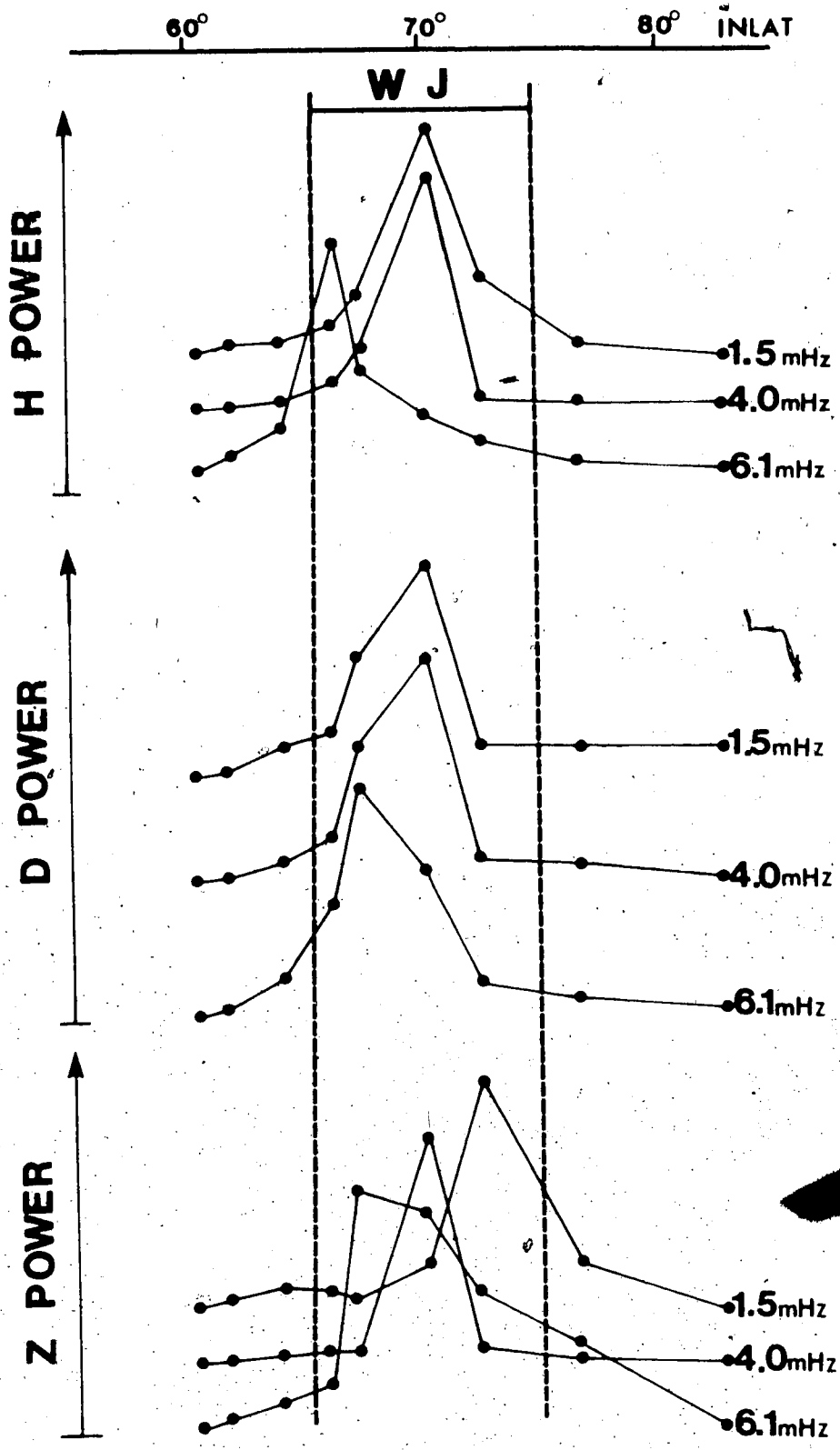


Figure 34

DAY 17, 1972 (1700-1800)

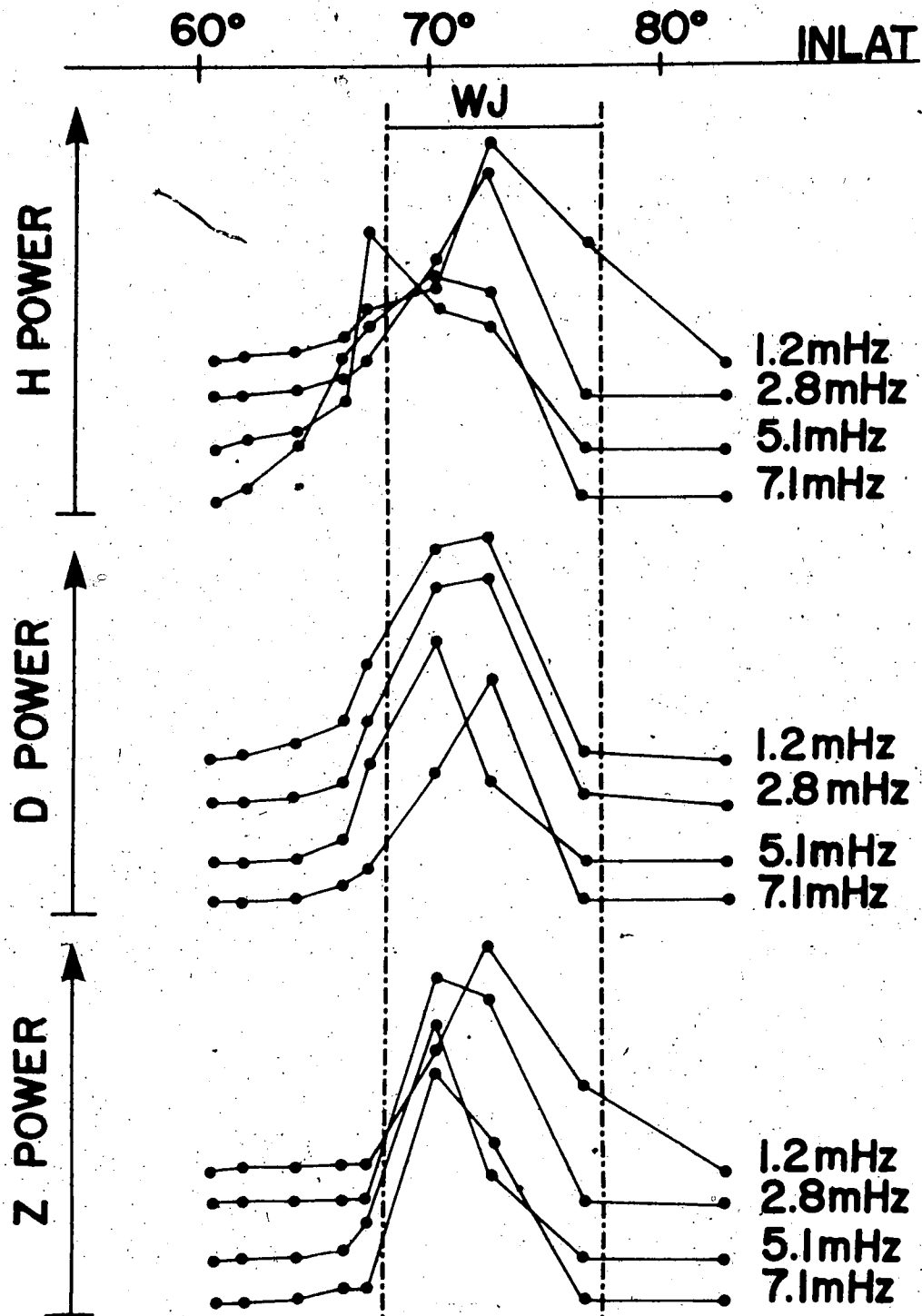


Figure 35



The close relationship between the Pc 5 activity and the convection westward electrojet can further be substantiated by the results of the polarization analysis which now follows. The shapes and tilts of the polarization ellipses as well as the sense of polarization (see Appendix B for more details regarding the determination of the polarization parameters from a three dimensional vector time series) were projected on to the three orthogonal planes. The plane is viewed from a direction in which the coordinates form a left handed system (e.g., downward on the horizontal H-D plane). The polarization ellipses in the H-D, H-Z and D-Z planes for the three different spectral bands chosen from the three events we presented were positioned as a function of latitude and universal time with the convection westward electrojet superimposed on the background as in Figures 36, 37, 38 (Day 16, 1972 in the 1.3-2.5 mHz band), 39, 40, 41 (Day 235, 1971 in the 2.0-3.0 mHz band), 42, 43 and 44 (Day 17, 1972 in the 3.3-5.1 mHz band). The ellipses that are shaded indicate polarization in the clockwise direction (CW) in the plane while those that are not shaded are polarized in the counter-clockwise (CC) direction.

An examination of the polarization ellipses in the H-D plane (Figures 36, 39, and 42) would indicate that the behaviour of the ellipses follows the electrojet. There appears to be a tendency for the ellipses to be tilted in the

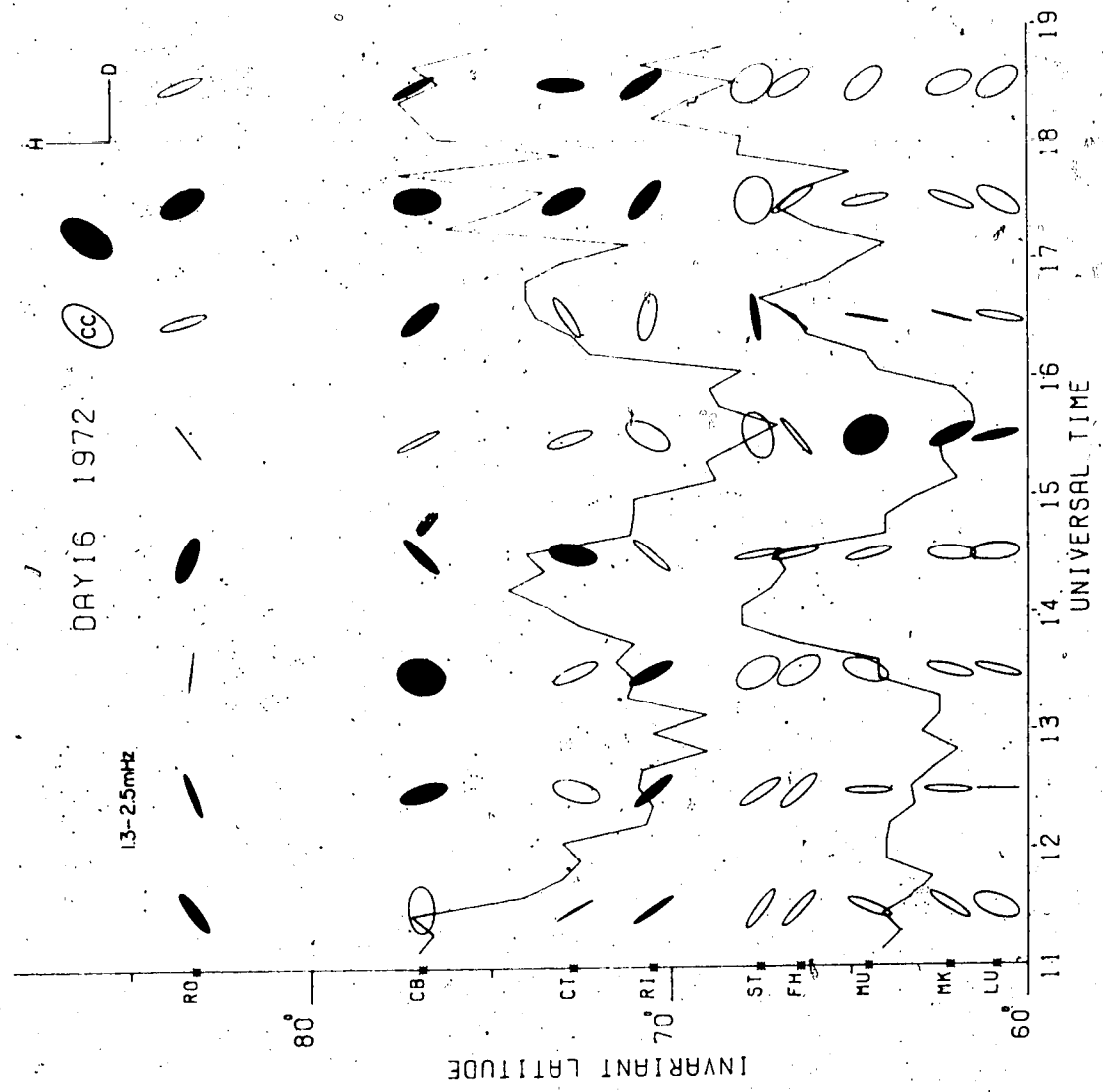


Figure 36

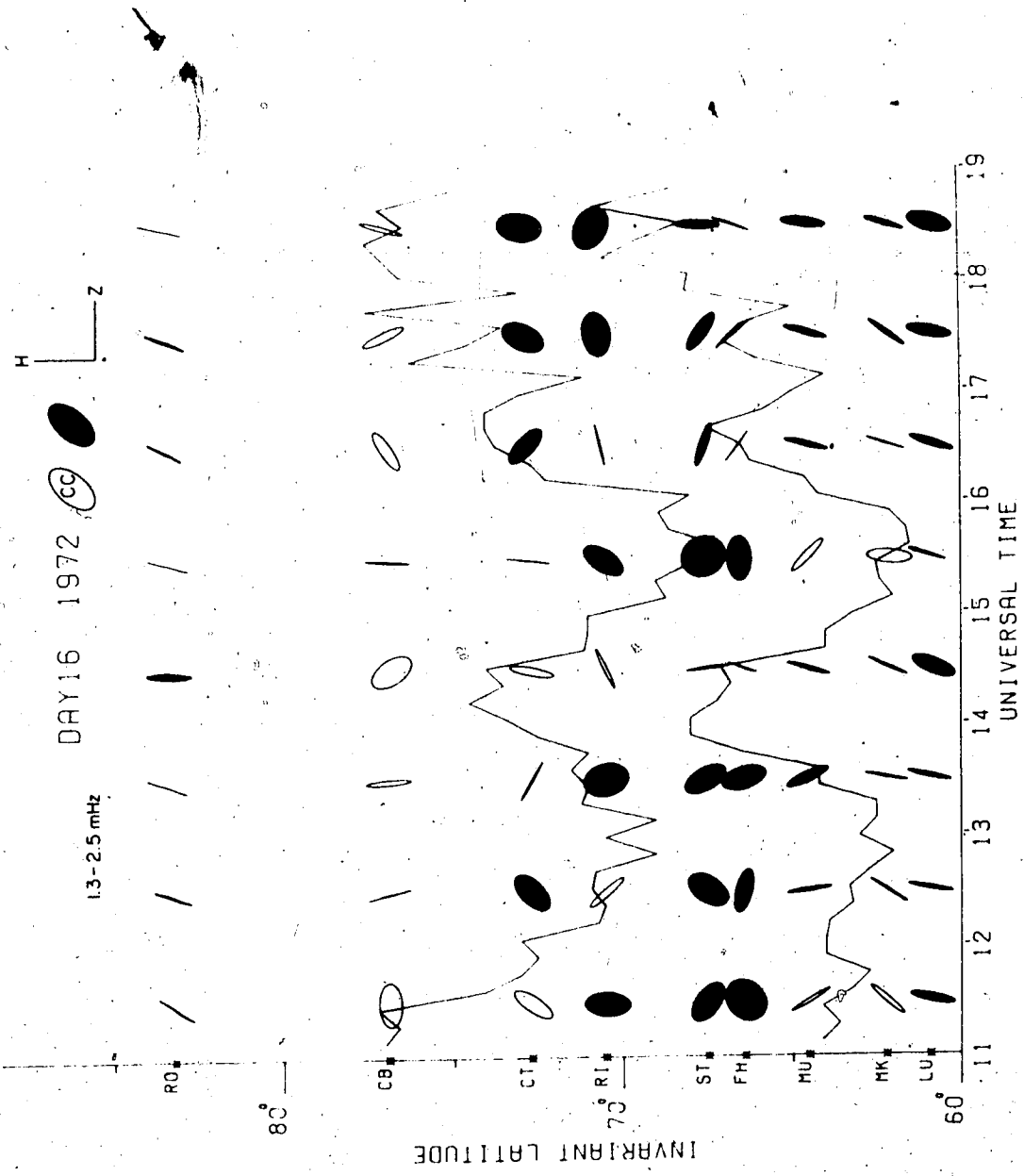


Figure 37

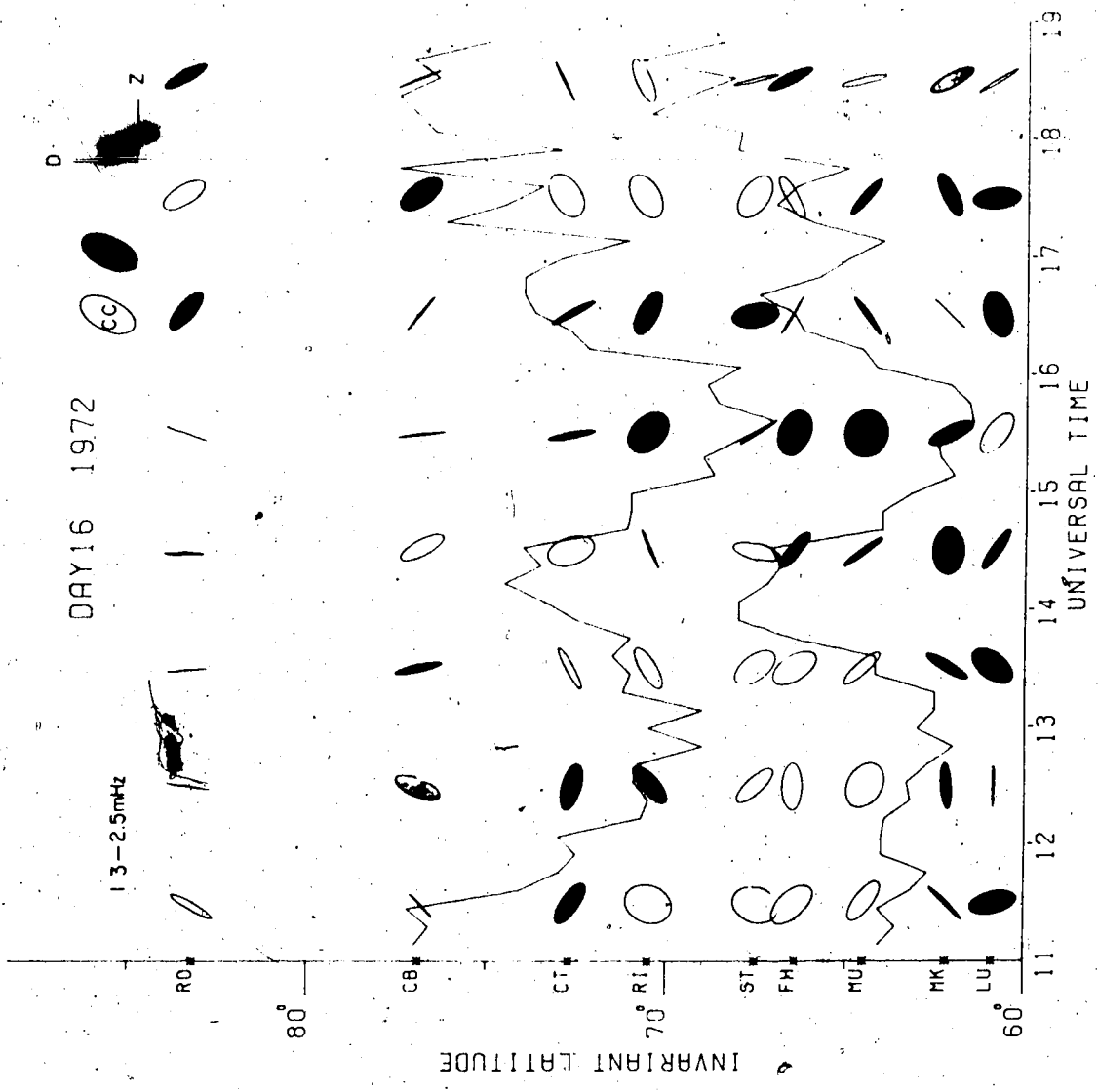


Figure 38

DAY 235 1971

2-3mhz

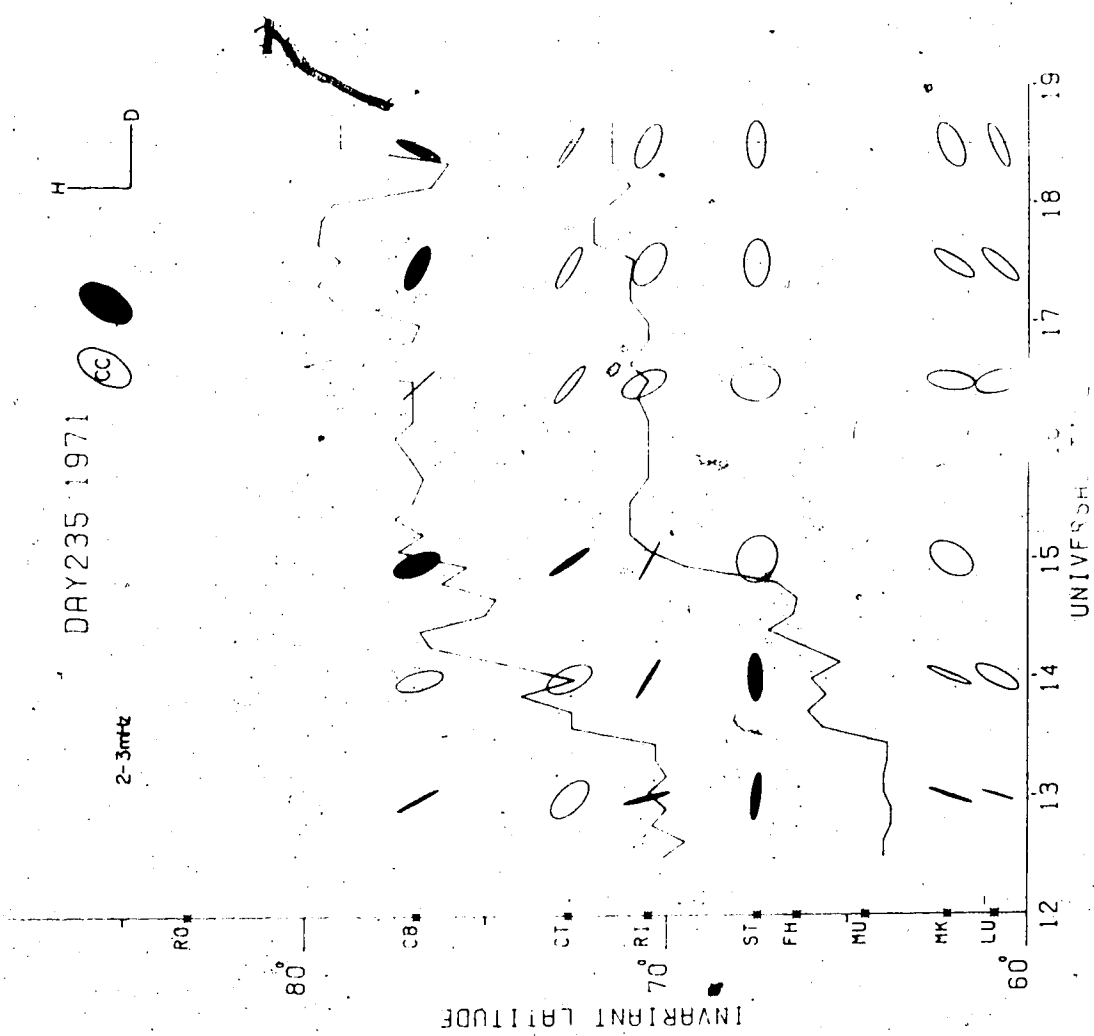


Figure 39

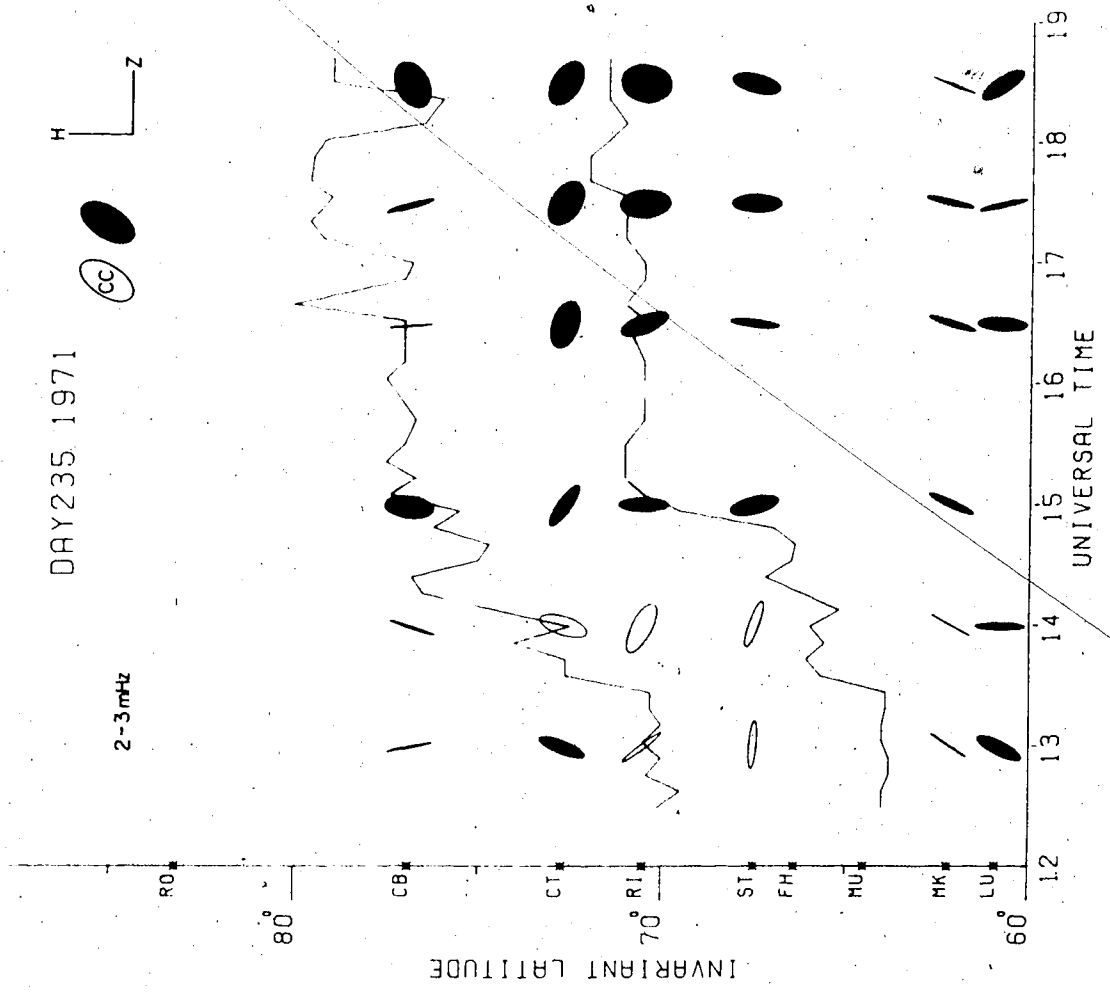



Figure 40

DAY 235 1971 (CC) 

2-3 mHz

RO\*

80°

INVARIANT LATITUDE

CB\*

CT\*

70° RI\*

ST\*

FH\*

MU\*

HK\*

LU\*

60°

UNIVERSAL TIME

12

13

14

15

16

17

18

19

Figure 41

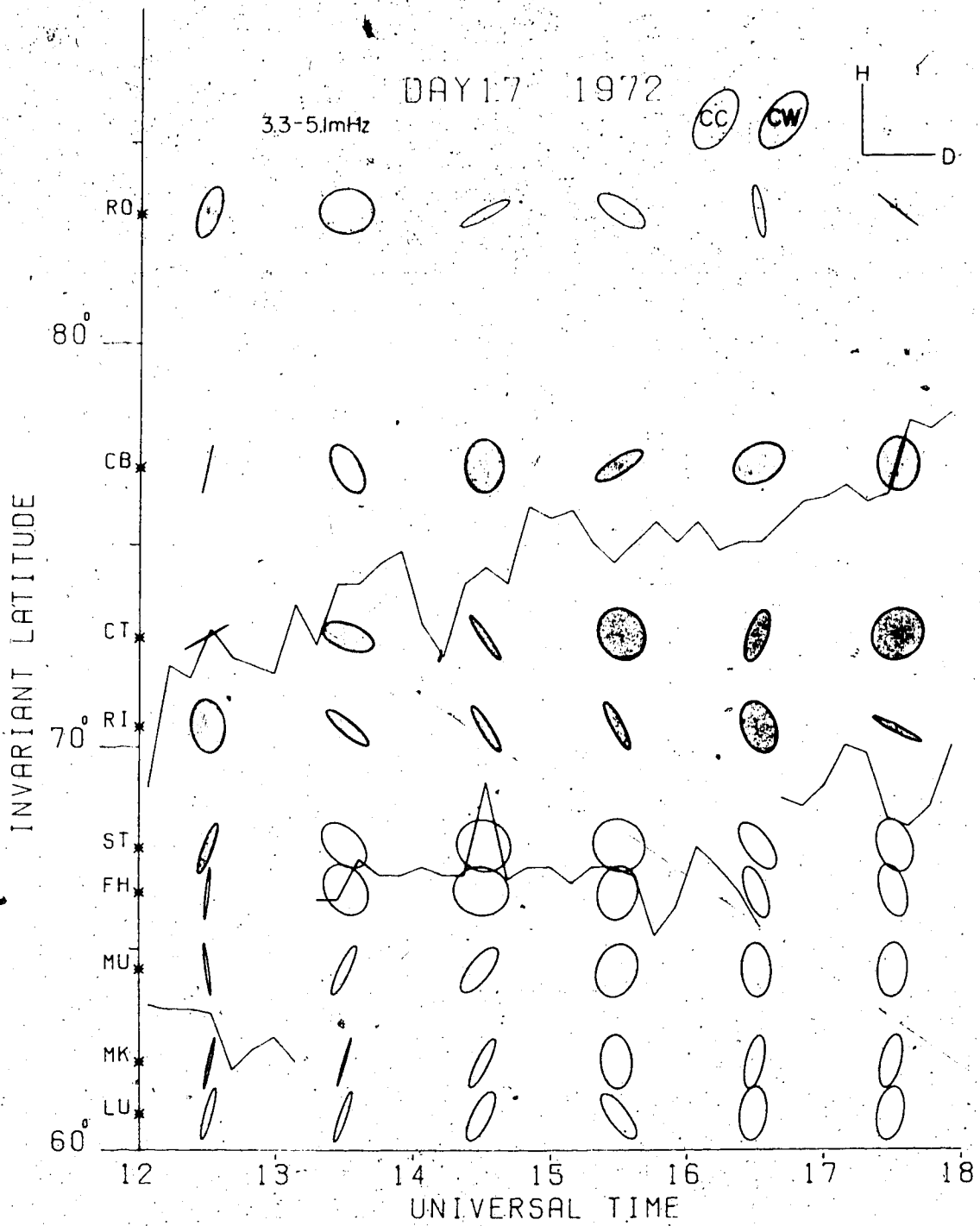


Figure 42



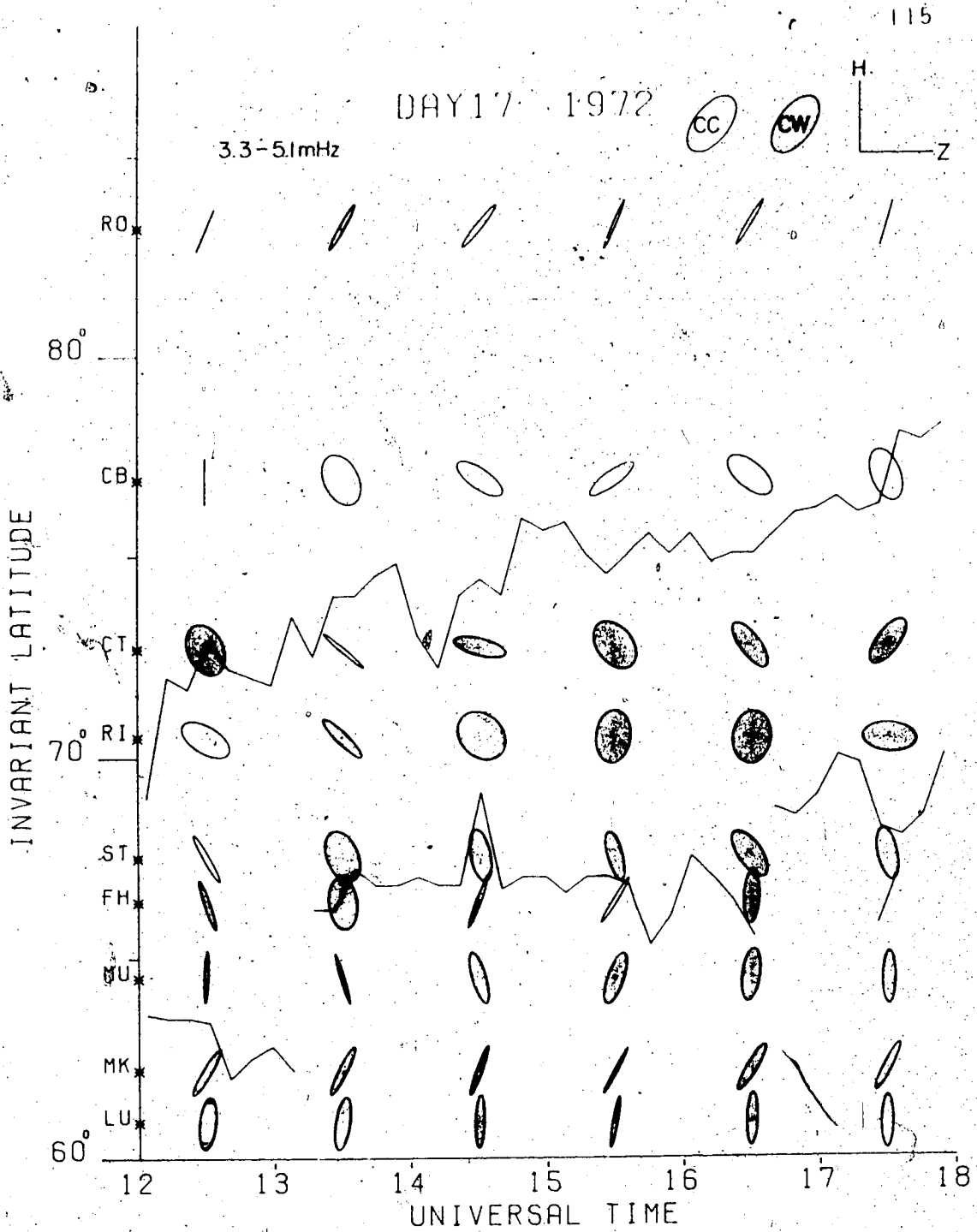


Figure 43

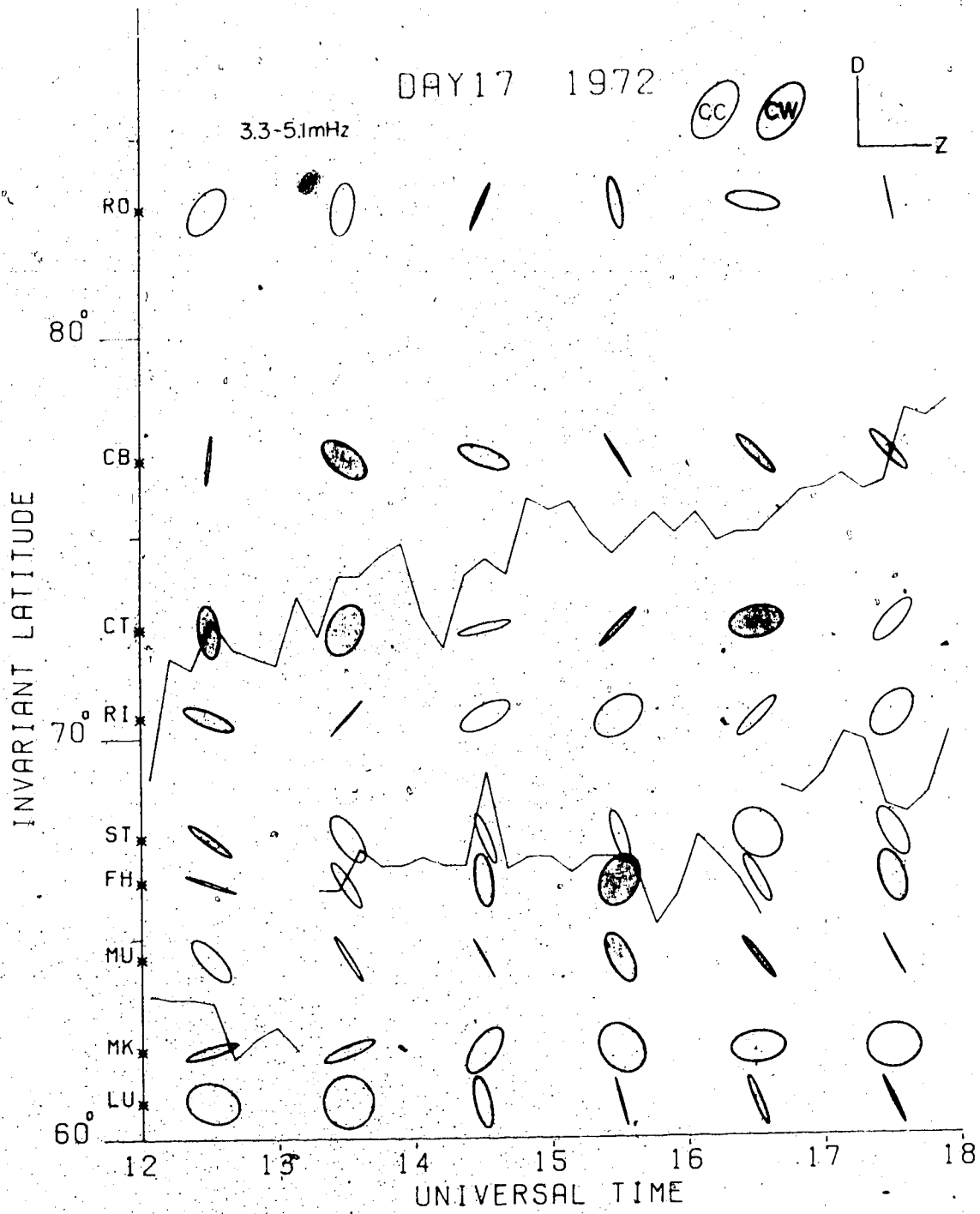


Figure 44

second quadrant of the H-D plane inside and in the vicinity of the westward electrojet, indicating that the phase difference between H and D at a particular location in or close to the electrojet is greater than  $90^\circ$ . Away from the electrojet in the south, the ellipses have a tendency to be tilted in the first quadrant of the H-D plane indicating that the phase difference between H and D is less than  $90^\circ$ . The ellipses are more inclined towards H than towards D implying that the perturbations in H are generally greater than those in D for the Pc 5 micropulsations. The sense of polarization for the stations in the south is generally CC (indicating that H lags D in phase) while the sense of polarization for the stations in the north is predominantly CW (indicating that H leads D in phase). This pattern agrees with the polarization analyses by previous workers (see Figure 8). However, with the locations of the convection westward electrojet as a frame of reference, our analyses indicate that the demarcation line (the line across which the sense of polarization reverses) follows the electrojet, shifting northward with the electrojet (Figures 39 and 42) or 'meandering' with the electrojet (Figure 36). Note that in Figure 36, for the UT interval 1500-1600, the polarization ellipses at the southern stations have CW sense of polarization while the sense of polarization at the northern stations is CC. This particular pattern appears to be opposite to the statistically determined

polarization pattern shown in Figure 8 for this particular local time. However, this happens at a time, when the westward electrojet has reached its furthest southward position. Based on previous results, one would anticipate the senses of polarization to switch to CC equatorward of LEDU so that the switch in sense of polarization in the H-D plane would occur at the equatorward border of the electrojet.

In the H-Z plane (Figures 37, 40, 43), the sense of polarization of the ellipses seems to be opposite to that in the H-D plane with predominantly CW polarization in the south and CC polarization in the north. Again, the demarcation line appears to follow the electrojet. The ellipses inside and in the vicinity of the electrojet are mostly tilted in the second quadrant indicating that the phase difference between H and Z at a station is greater than  $90^\circ$  while the ellipses far away from the electrojet are tilted predominantly in the first quadrant indicating that the phase difference between H and Z is less than  $90^\circ$ . The ellipses are inclined more towards H than towards Z implying that the H perturbations are greater than the Z perturbations. H lags Z in phase for the CC polarization ellipses and leads Z in phase for the CW polarization ellipses.

The polarization in the D-Z plane (Figures 38, 41, and 44) appears to be a little more complicated. Nevertheless, some information can be extracted from it. For example,

there appear to be two reversals in the sense of polarization, one associated with the poleward border of the electrojet and the other associated with the equatorward border. Going along our line of stations, one encounters CW ellipses (D leads Z in phase), then, CC ellipses (D lags Z in phase) and CW ellipses again. In general, the ellipses seem to be inclined at an angle of  $45^\circ$  towards the axes indicating that the magnitudes of perturbation in D are approximately equal to those in Z. It seems that the tilts of ellipses inside the electrojet are opposite to those outside of the electrojet (Figure 44 illustrates this statement best). The tilt in the first quadrant implies that the phase difference between D and Z at a particular station is less than  $90^\circ$  while the tilt in the second quadrant implies that the phase difference between the two components is greater than  $90^\circ$ .

We summarize the general senses of polarization schematically using the results of Day 17, 1972 in the following three diagrams.

Figure 45 shows the sense of polarization in the H-D plane. The point that this diagram is intended to illustrate is that the demarcation line follows the electrojet.

Figure 46 shows the sense of polarization in the H-Z plane and indicates that the sense of polarization in the H-Z plane seems to be opposite to that in the H-D plane.

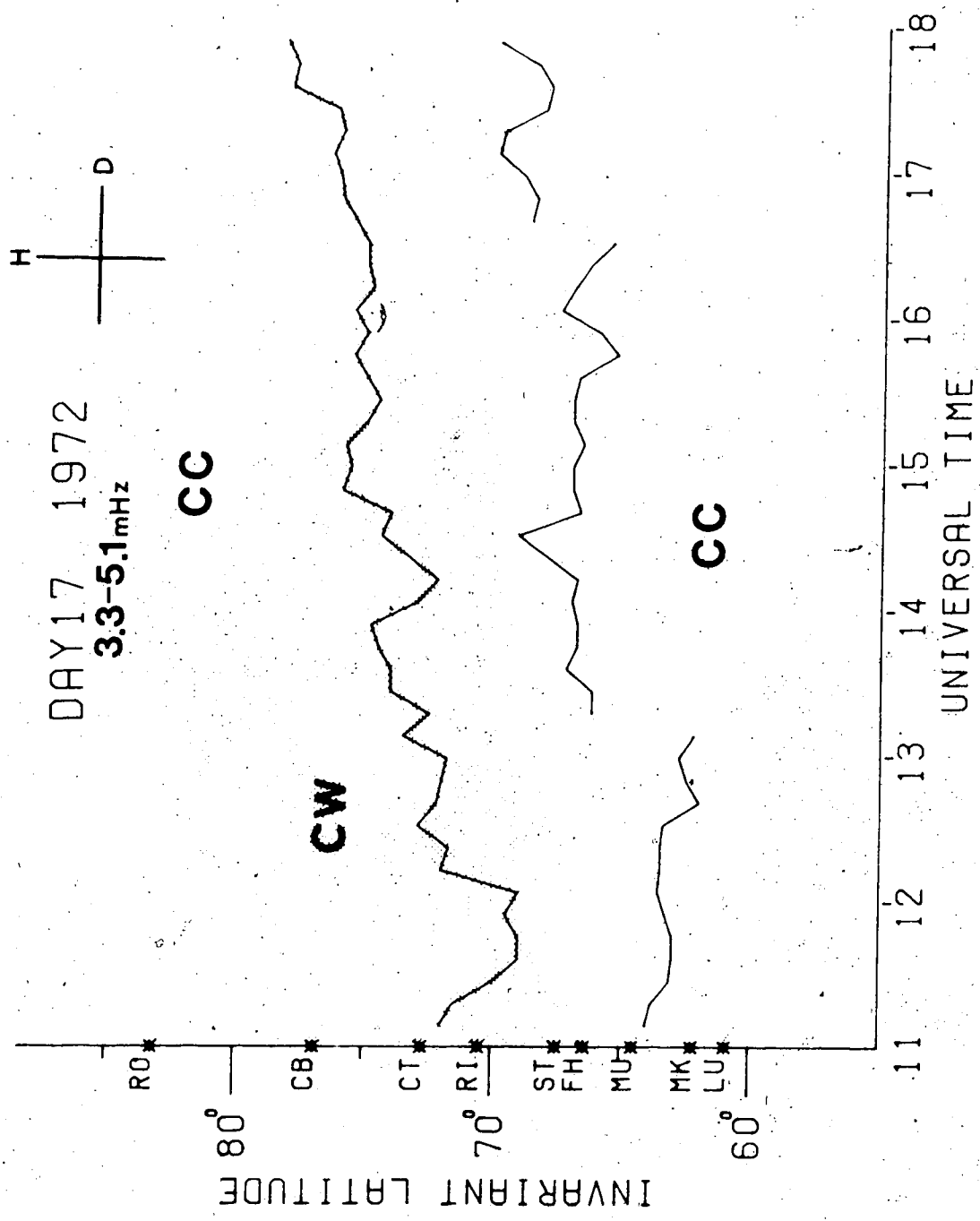


Figure 45

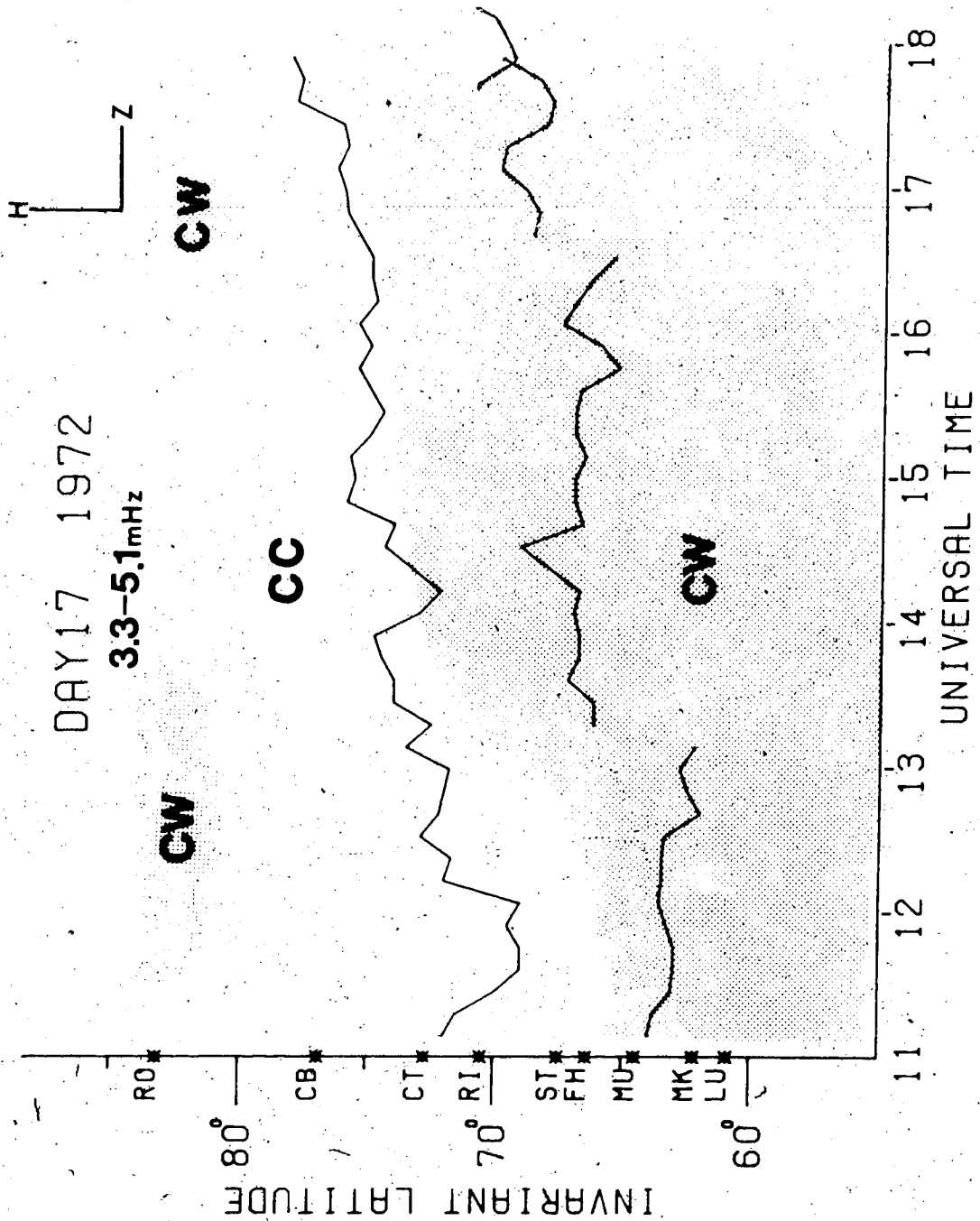


Figure 46

Figure 47 shows the sense of polarization in the D-Z plane. Except for the time intervals when the whole electrojet undergoes rapid variations in its position (for example the time interval of 1500-1700 on Day 16, 1972 shown in Figure 38), there are two reversals in the sense of polarization, one associated with the poleward border of the electrojet, the other with the equatorward border.

The senses of polarization discussed above can be understood in terms of the relative phase changes across the stations. Typical examples of the phase changes are shown in the next two diagrams. The top three panels in Figures 48 and 49 show that the powers in three components peak within the confines of the electrojet as mentioned earlier. The bottom three panels show the relative phase changes across the stations in three components. The phase difference between any two components at a given station is not shown, as information on this is implicit in the shapes, tilts and sense of polarization of the polarization ellipses shown earlier. The magnitude of the phase at a given station is not important because of its cyclic nature. It is the profile of the phase that is of interest. It can be seen from Figures 48 and 49 that there is one rapid phase change of about  $180^\circ$  in H across the region of maximum power; there is very little phase change in D; there are two rapid phase changes in Z. Thus, the reversal in the sense of polarization in the H-D



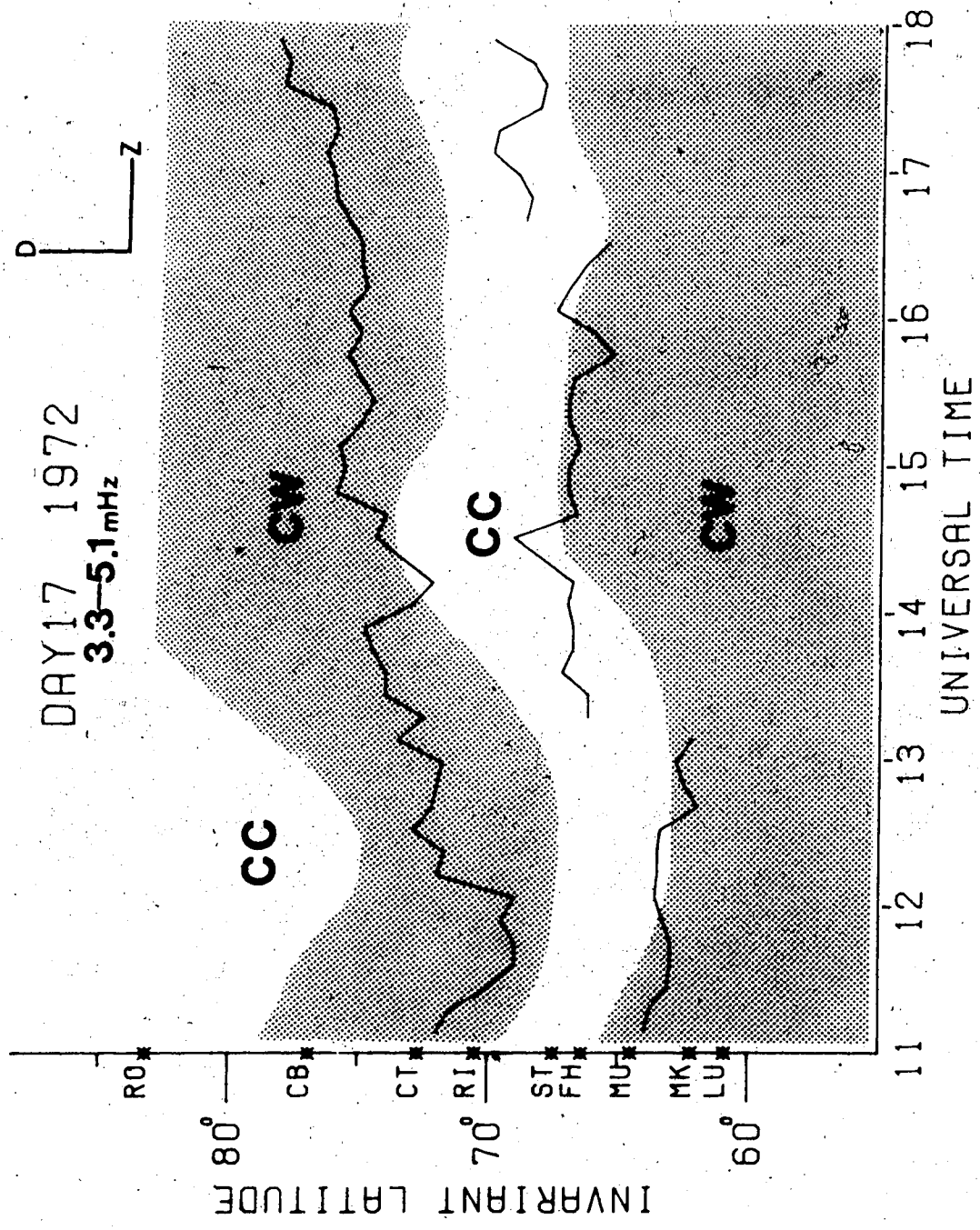


Figure 47

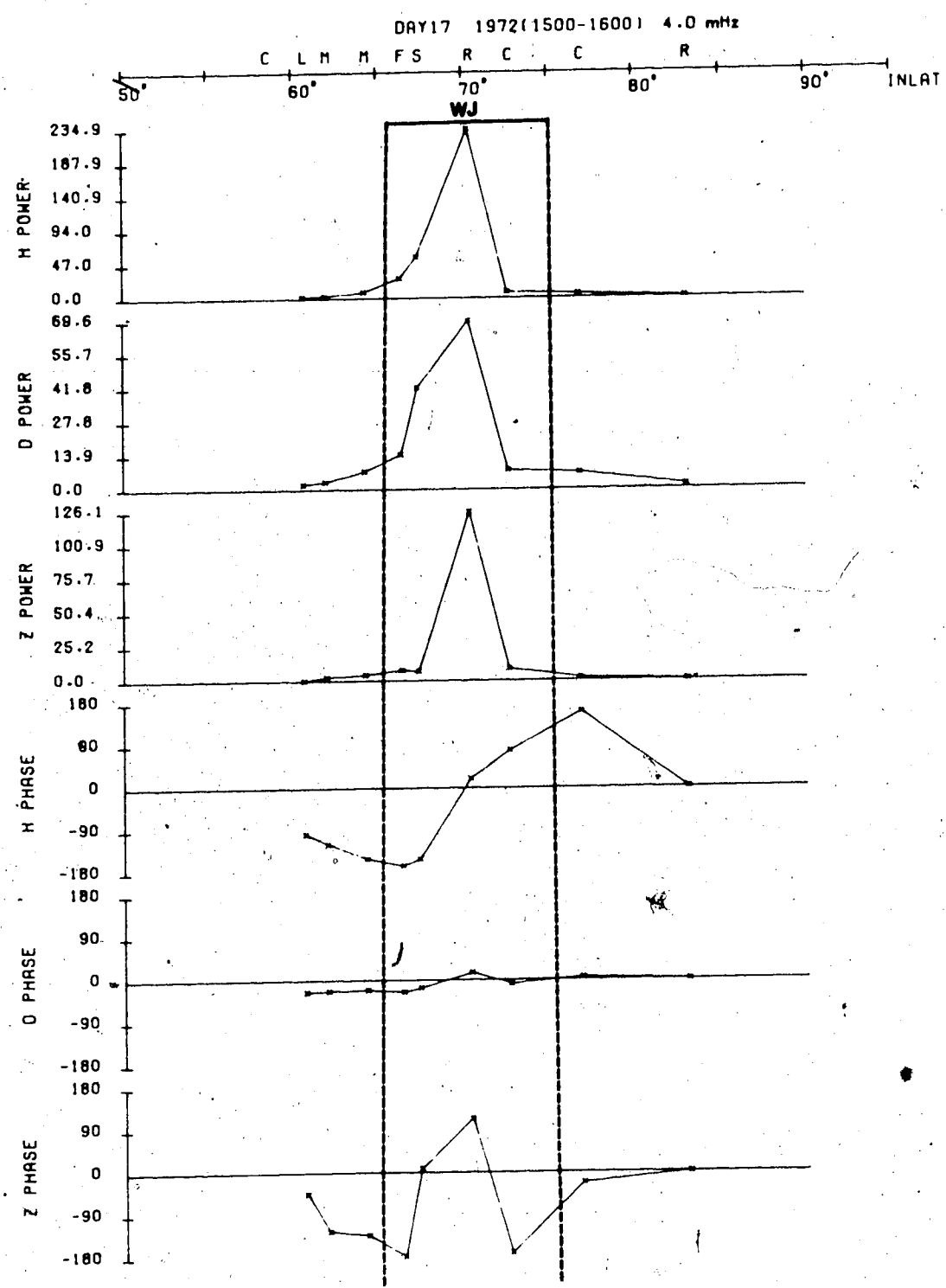


Figure 48

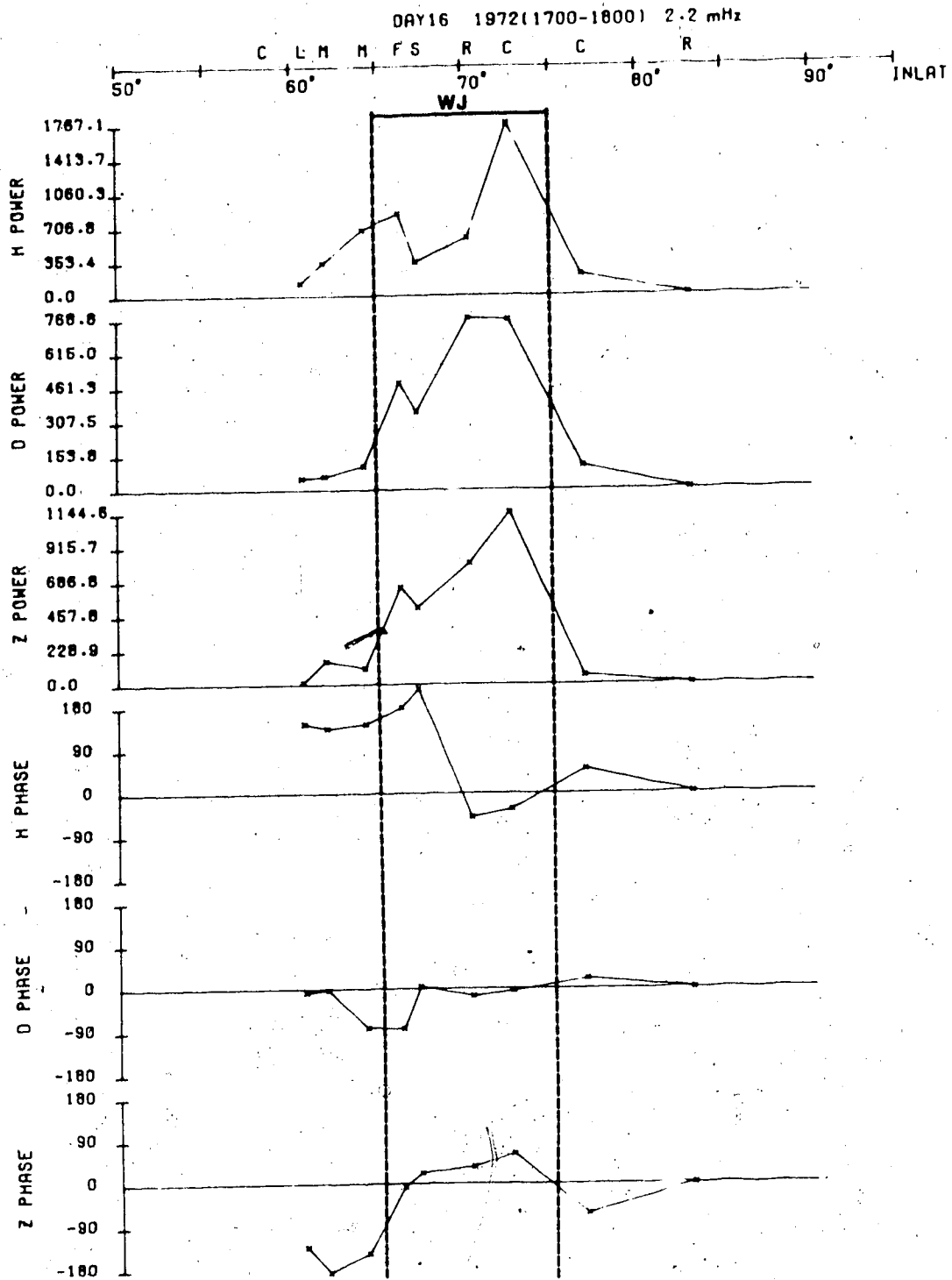


Figure 49

plane can be attributed to the change in phase of H and the two reversals in the D-Z plane can readily be understood as due to phase changes in Z. The sense of polarization in the H-Z plane can be understood using information regarding the phase difference between H and Z at the stations in conjunction with the relative phase changes across the stations.

We have shown earlier in this section from the intensity contour plots that the intensity maximum follows the electrojet. The results of the polarization analysis also indicate that the demarcation line follows the electrojet. It would therefore be of interest to see how the line of peak intensity is related to the demarcation line particularly in the horizontal plane. The results of superimposing the line of peak intensity and the demarcation line in H-D plane on the background electrojet for the three events are shown in Figures 50, 51 and 52. It is apparent from these plots that, while both lines follow each other, they do not coincide with each other, which implies that linear polarization does not occur in the region of peak intensity. We feel that our stations were sufficiently close enough to render the above statement valid.

We conclude this section by showing how pulsations respond to electrojet motion. We have compiled in Table 5 the hourly averages of interplanetary magnetic field parameters and the Kp values. It can be seen from Table 5 and the

DAY 16 1972

1.3 - 2.5 mHz

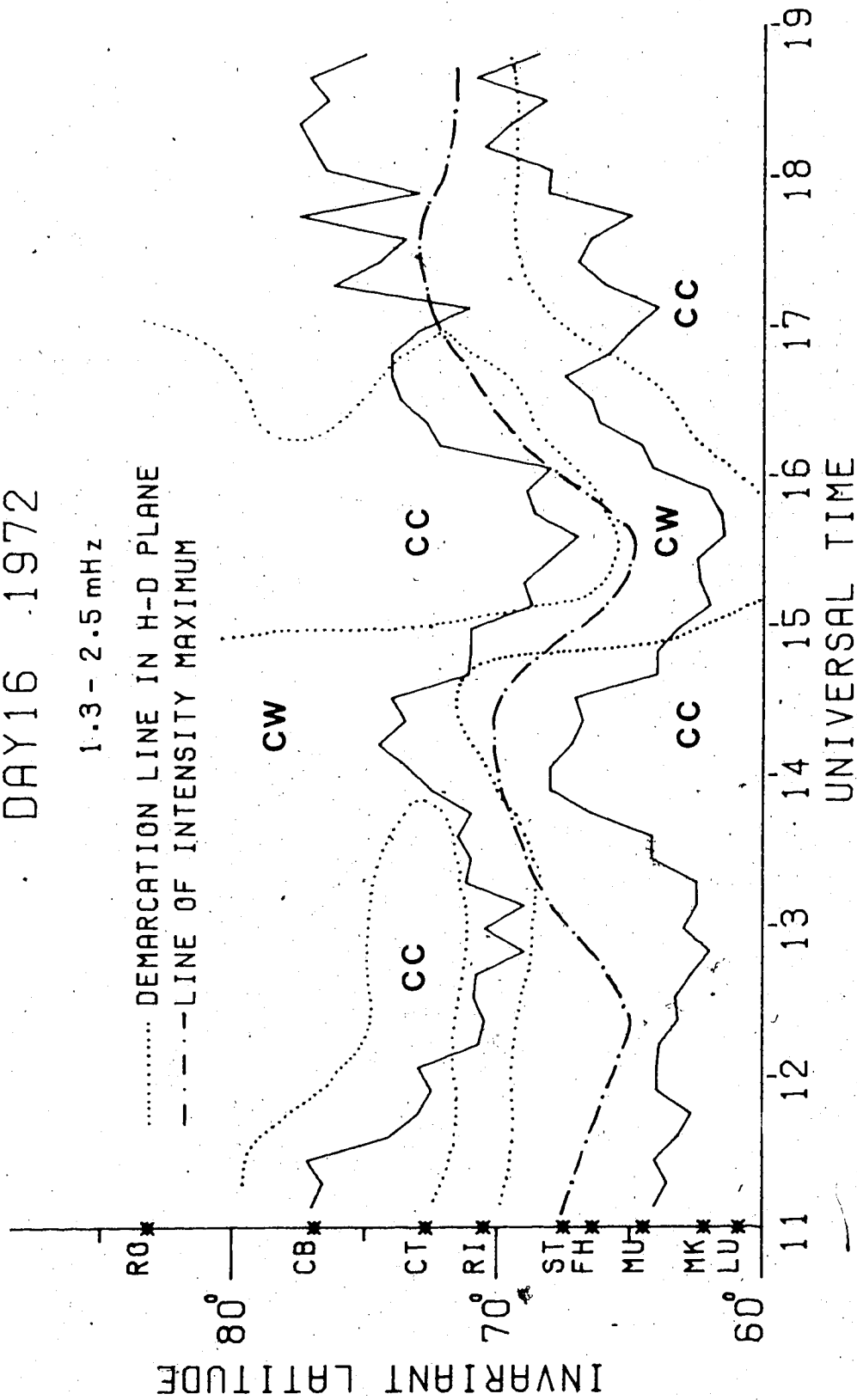


Figure 50

DAY 235 1972

2.0 - 3.0 MHz

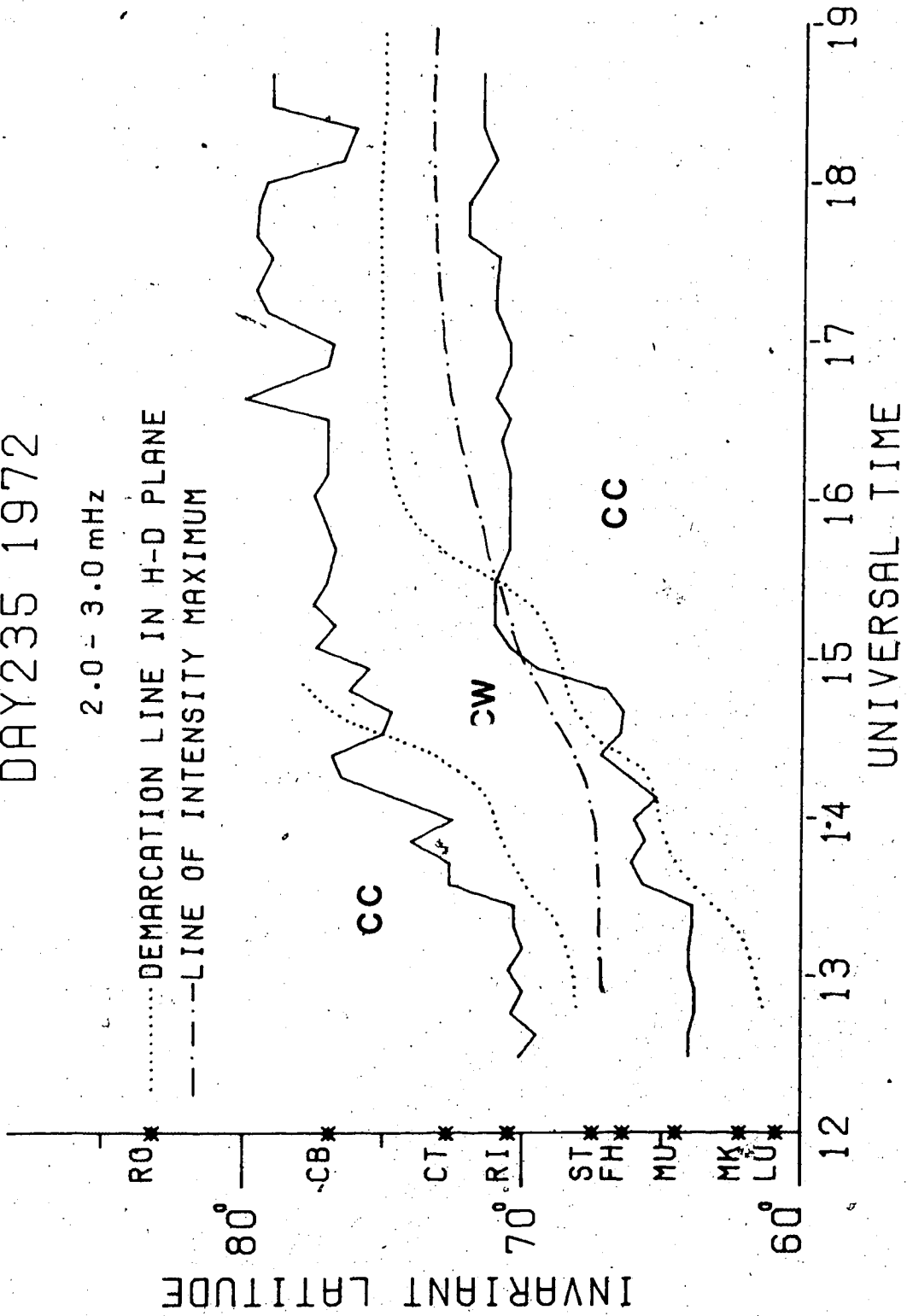


Figure 51

DAY 17 1972

3.3 - 5.1 mHz

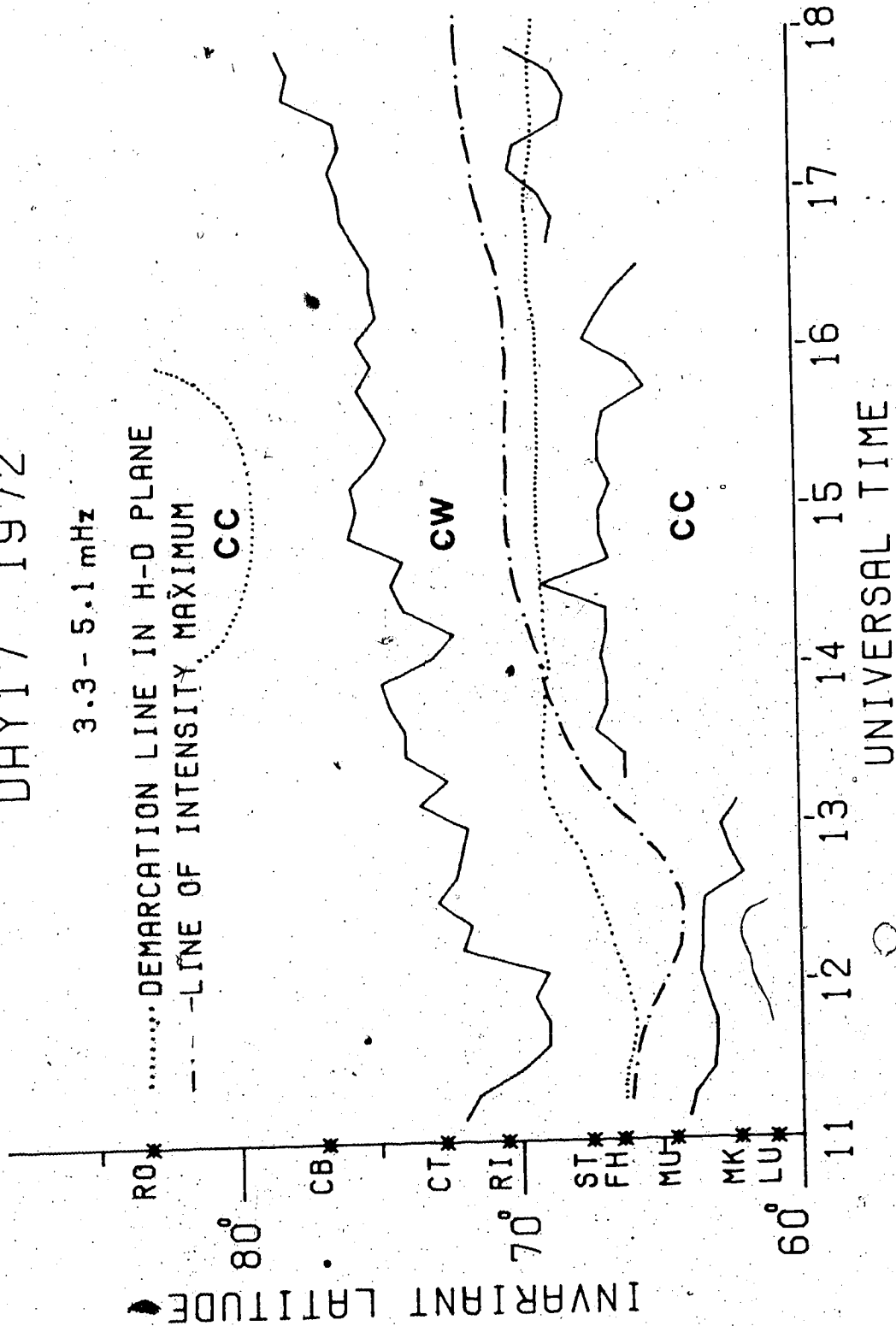


Figure 52

TABLE 5 Hourly averages of interplanetary magnetic field parameters ( $\theta$  is the angle between the field vector and the solar ecliptic plane in degree and  $B_z$  is the north-south component of the field in  $\gamma$ ) and Kp values

Day 235, 1971

UT	12	13	14	15	16	17	18
$\theta$	-40	-52	-46	38	27	-24	-27
$B_z$	-2.3	-4.9	-2.4	3.1	2.2	-1.0	-1.5
Kp	2+		2+				

Day 16, 1972

UT	11	12	13	14	15	16	17	18
$\theta$	11	-16	14	6	-35	-57	-5	21
$B_z$	2.5	-3.6	2.8	1.3	-6.8	-9.2	-1.2	3.8
Kp	5+			4-				

Day 17, 1972

UT	11	12	13	14	15	16	17
$\theta$	-6	1	15	-32	-73	-41	0
$B_z$	-0.6	0.1	1.2	-2.2	-5.1	-2.9	0.0
Kp	2+			3+			



plots containing the positions of the electrojet that the electrojet moved in response to the changes in the interplanetary magnetic field reflecting the changing level of magnetospheric convection. The Kp values indicate that the magnetic conditions for our events were moderate.

Figure 53 shows that the pulsational activity in the 2-3 mHz band jumped from low signal levels to peak intensity when the electrojet was in a transient state moving from low latitudes to higher latitudes. A second maximum, though not as intense as the first one, occurs after the electrojet reached its northern positions. The interplanetary data indicates that there were changes in the interplanetary magnetic field in the time interval for the second maximum (viz., the normal component of the IMF turned southward in the interval 16-17 UT). Thus, although the spatial condition of the electrojet was stable, the change in level of magnetospheric convection due to changes in the interplanetary magnetic field might produce changes in the intensity of the current system associated with the electrojet resulting in the burst of activity.

Figures 54 and 55 again show the enhancement of signal strength in the low frequency band and higher frequency band of the Pc 5 spectrum associated with changes in electrojet configuration. The higher frequency band appears to respond earlier to motions of the electrojet than the lower frequency band.

DAY 235 1971

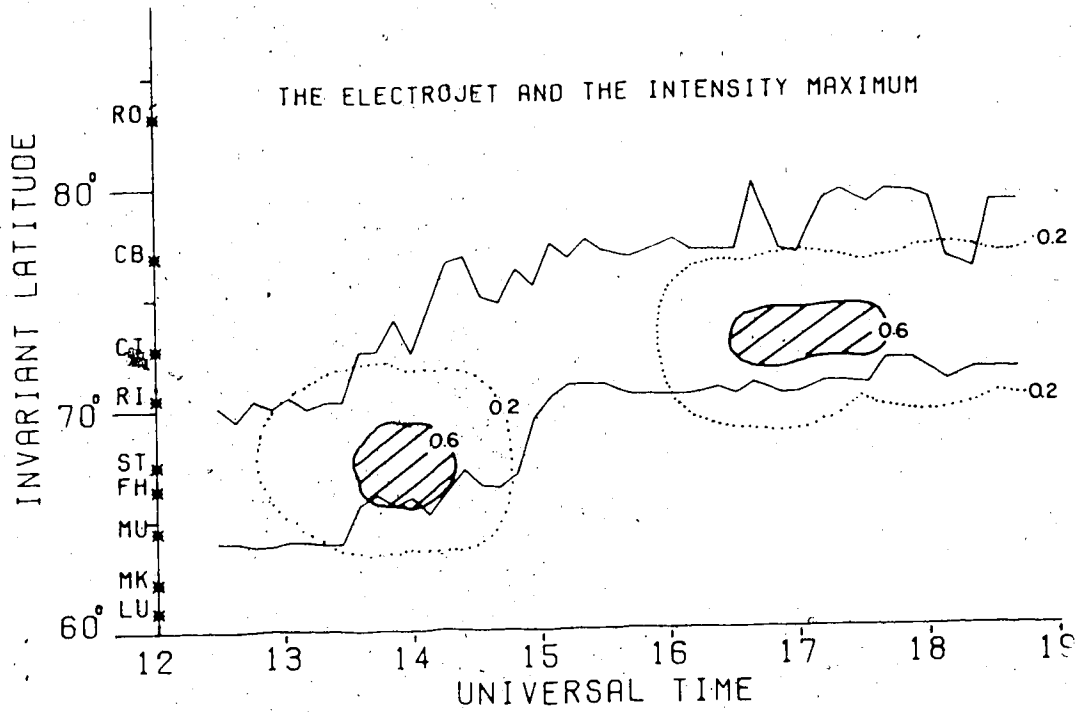
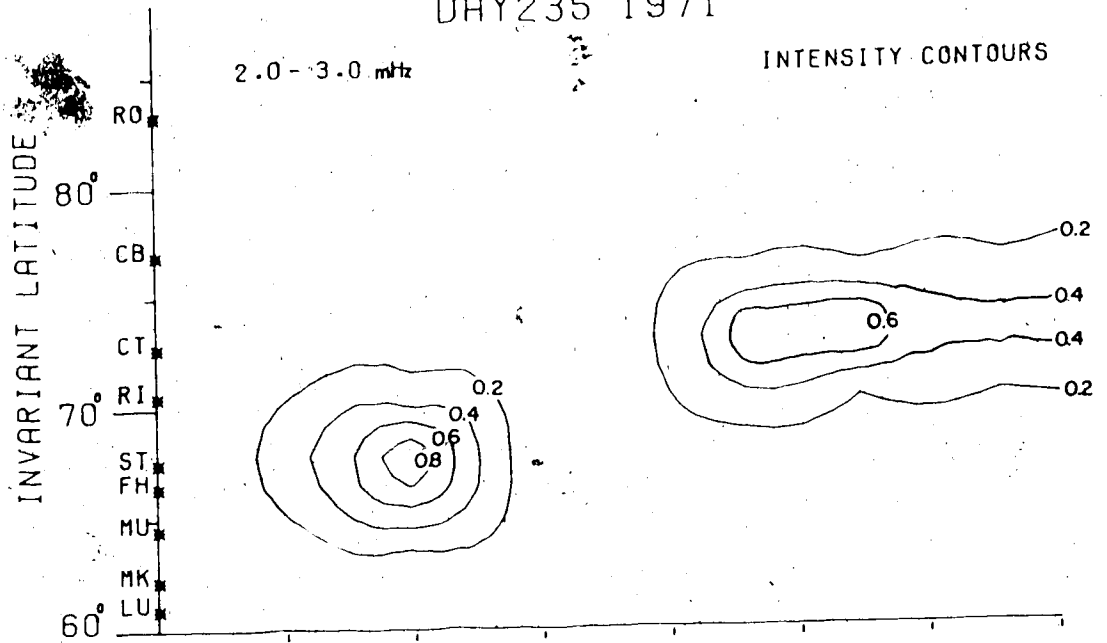


Figure 53



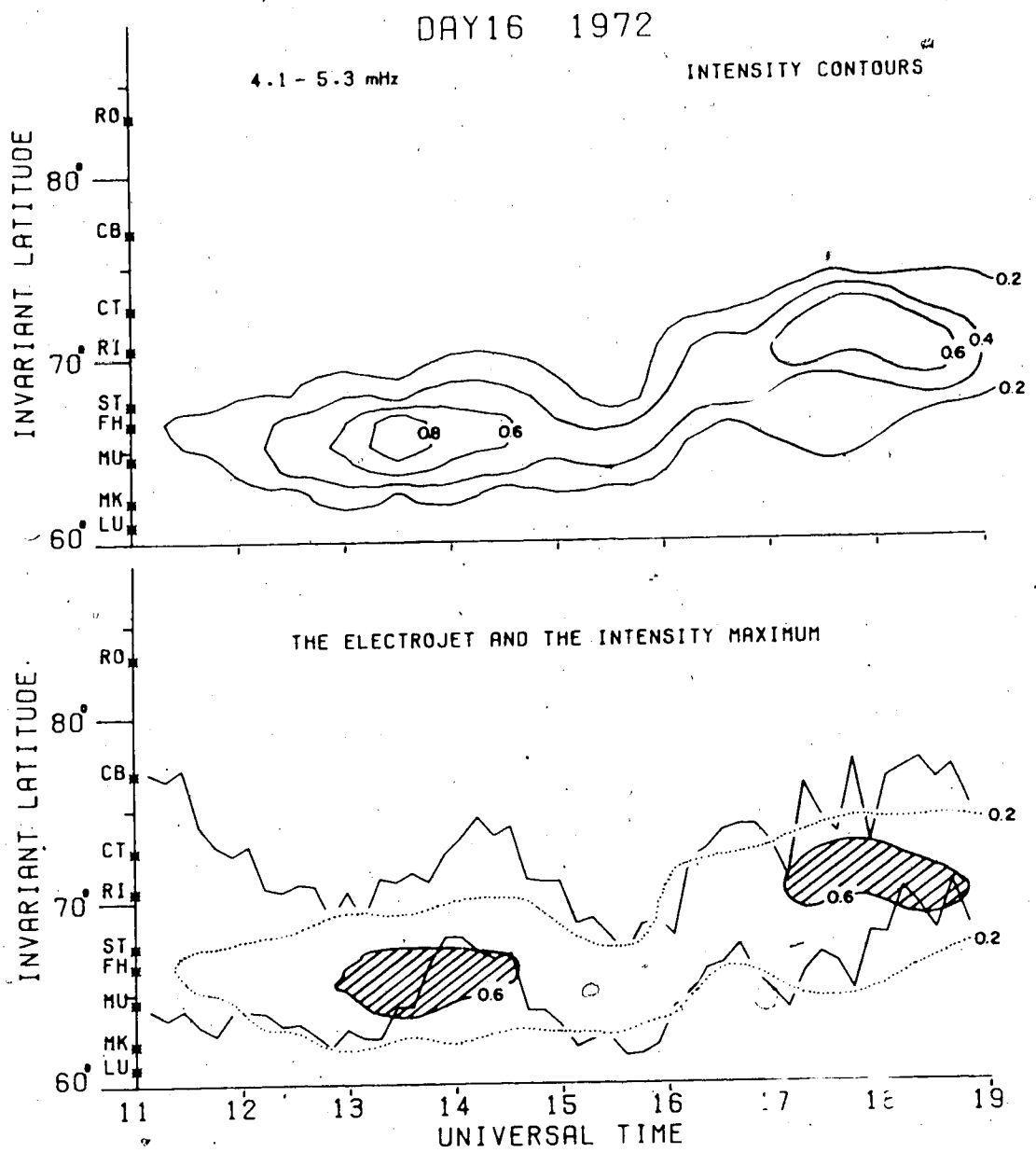


Figure 55

Figures 56 and 57 illustrate that both the low frequency band and high frequency band of the activity on Day 17, 1972 jumped to 20% of their peak intensities as the equatorward border moved northward rapidly. The signal level then remained relatively unchanged over the next three hours until the time when there was another rapid motion of the equatorward border northward. The pulsational activity reaches its peak power at that time.

#### 4.2 Evidence for the Spatial Oscillations of the Electrojet

In the previous section we have presented the characteristics of pulsations with the electrojet superimposed on the background. The locations of the electrojet boundaries were inferred from a series of successive latitude profiles at about 10 minute intervals. The result of plotting the locations of the borders as a function of time would therefore only indicate the trend of the electrojet giving only a macroscopic picture of the locations of the electrojet. We now present in this section the locations of the electrojet which were inferred from a series of successive latitude profiles only 23 seconds apart. Thus, the result of plotting the borders of the electrojet as a function of time would provide a microscopic picture of the spatial behaviour of the electrojet. It will be shown in the following diagrams that the borders of the electrojet behaved in an oscillatory fashion and that the oscillations of the

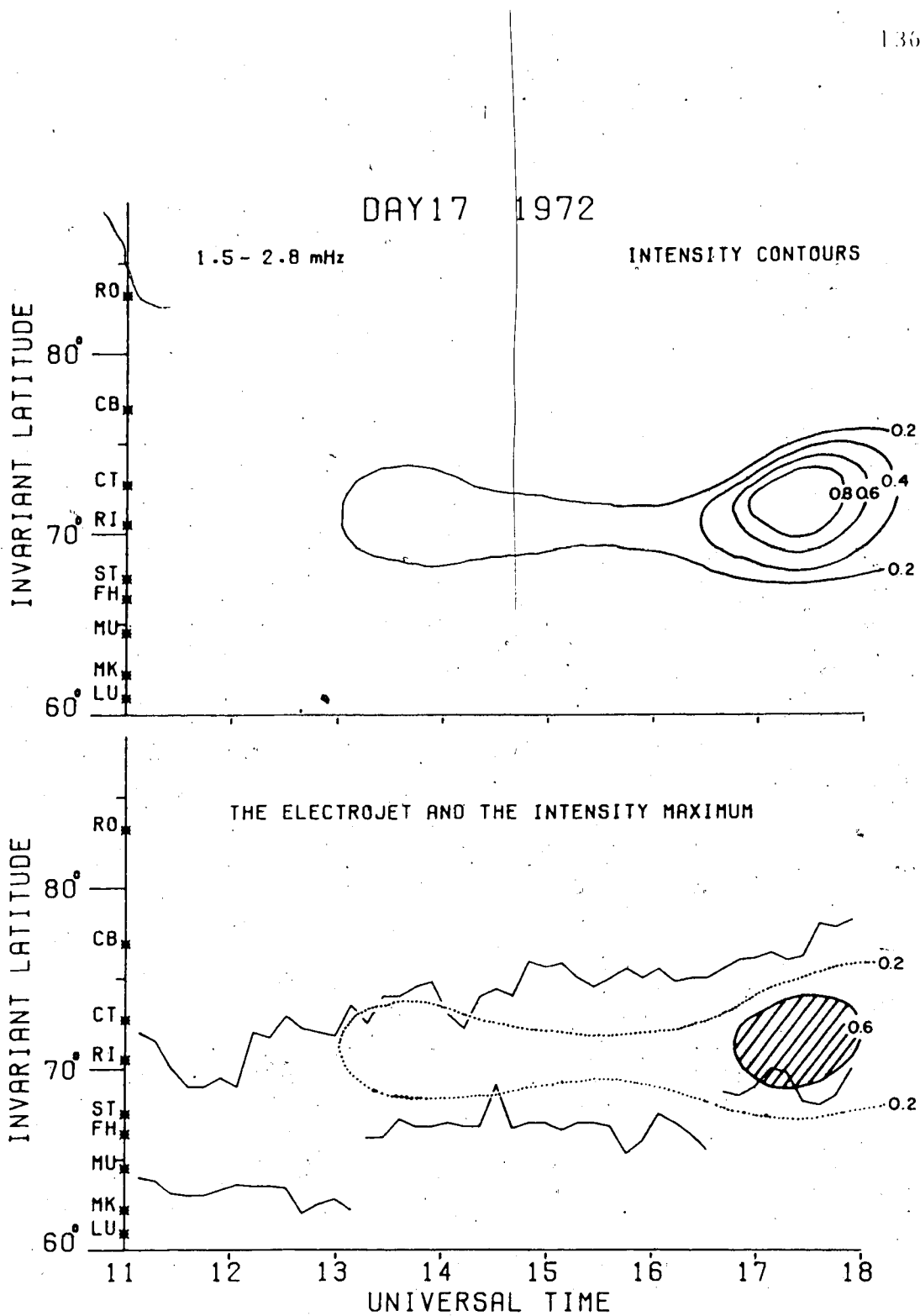


Figure 56

DAY 17 1972

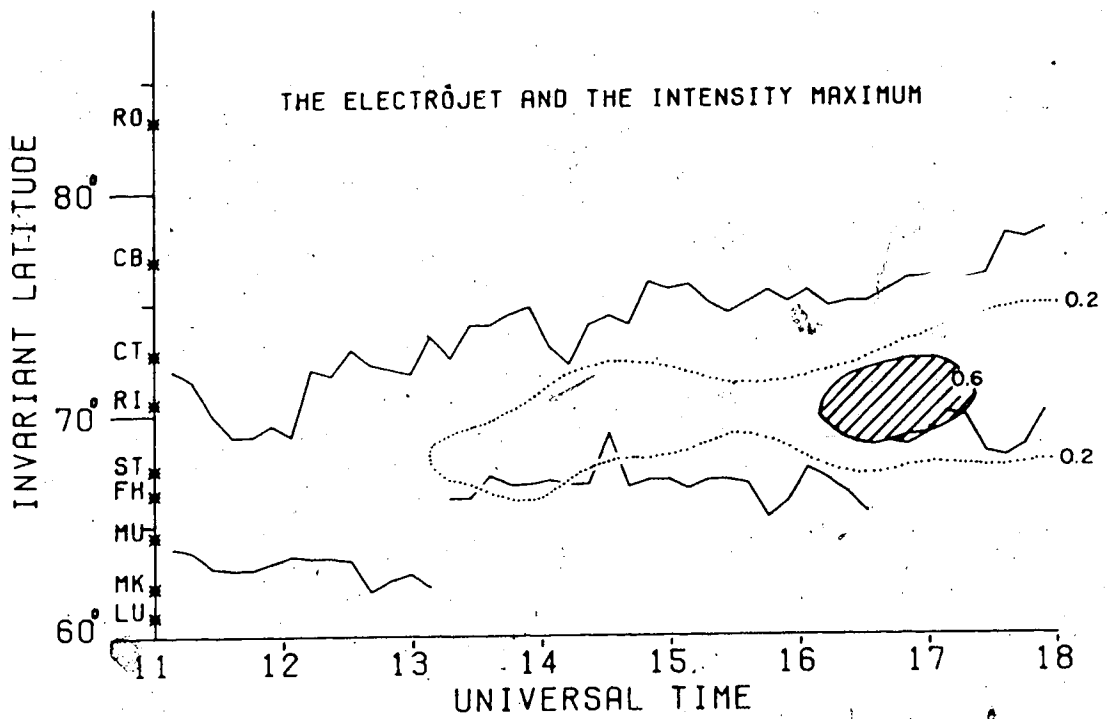
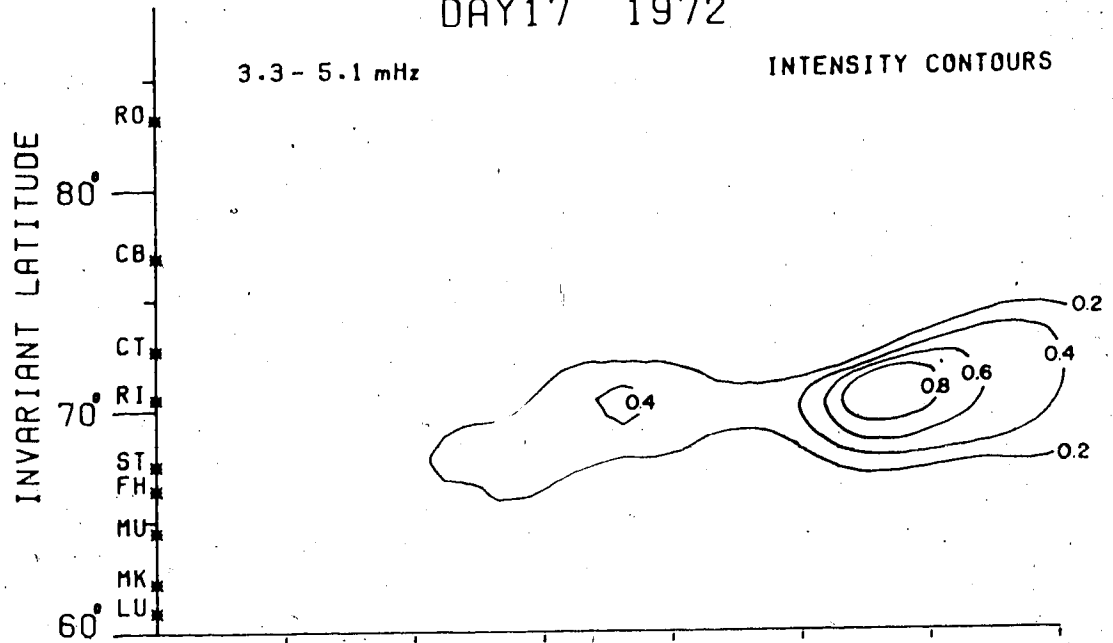


Figure 57

borders seem to occur in unison with the micropulsations.

The magnetogram shown in Figure 23 for Day 17, 1972 event shows that in the interval of 1300 and 1400 UT, the pulsations at high latitude notably at CONT are of lower frequency than the pulsations at lower latitudes. This is due to the fact that the poleward border of the electrojet oscillates more slowly than the equatorward border of the electrojet as illustrated in Figure 58. In Figure 58, we have plotted the poleward border and the equatorward border (inferred from latitude profiles 23 seconds apart) as a function of Universal Time. We have also superposed the pulsations in the Z component recorded at CONT (which is close to the poleward border) and at FTCH (which is near the equatorward border). It can be seen that there is a remarkable resemblance between the border oscillations and magnetic oscillations. As mentioned earlier, the timing for CONT might be off by as much as 1 minute. However, this error on the very long period wave trains shown in the diagram would produce effects which are hardly visible to the eye.

Figure 59 shows the correspondence between the motion of the equatorward border and the pulsations recorded at MCMU and MENK just slightly south of that border. Note the higher frequency oscillations recorded at  $\sim$  1220 UT seem to correspond to the higher frequency oscillation of the equatorward border of the electrojet.

Figure 60 illustrates that both the poleward and



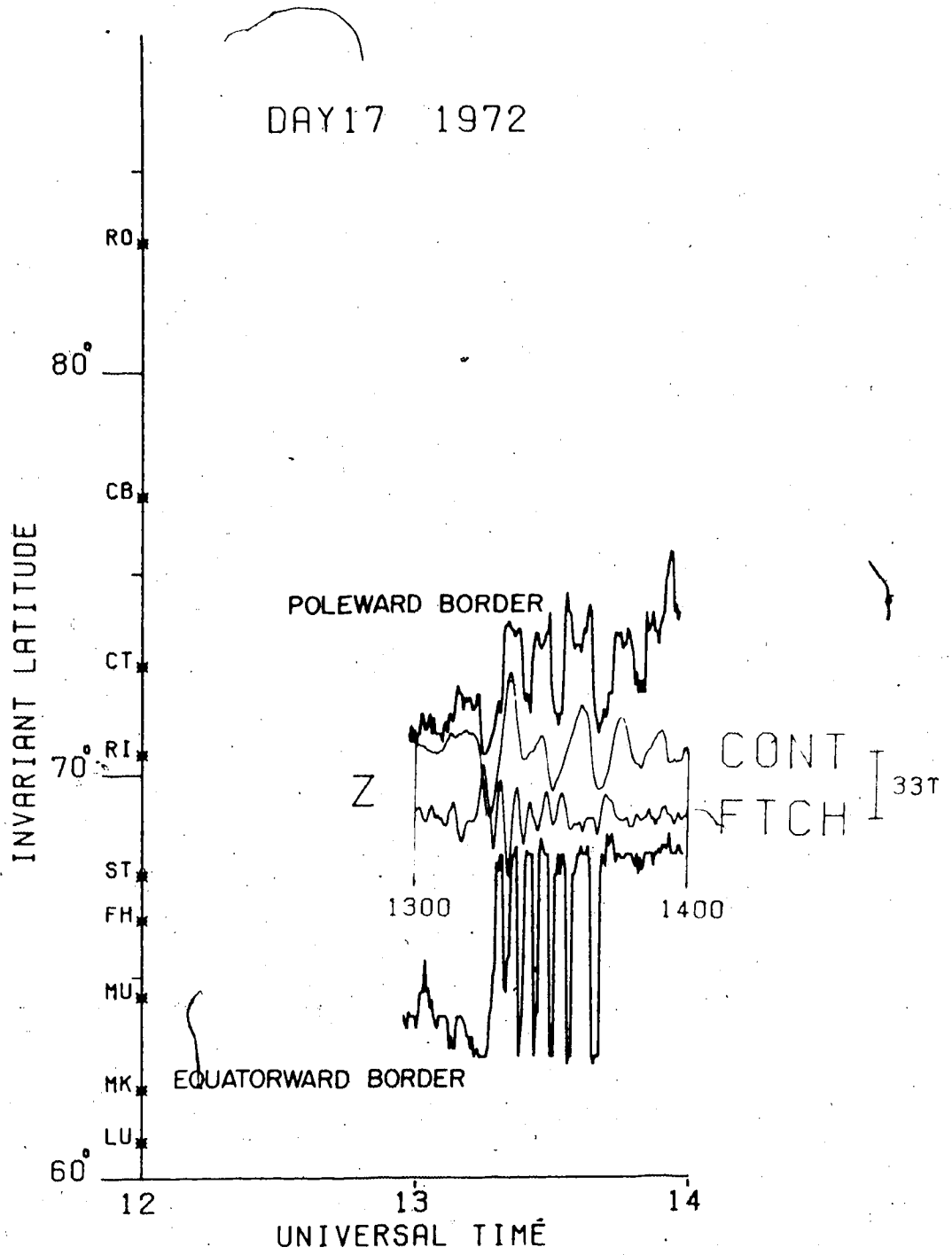


Figure 58

DAY 17 1972

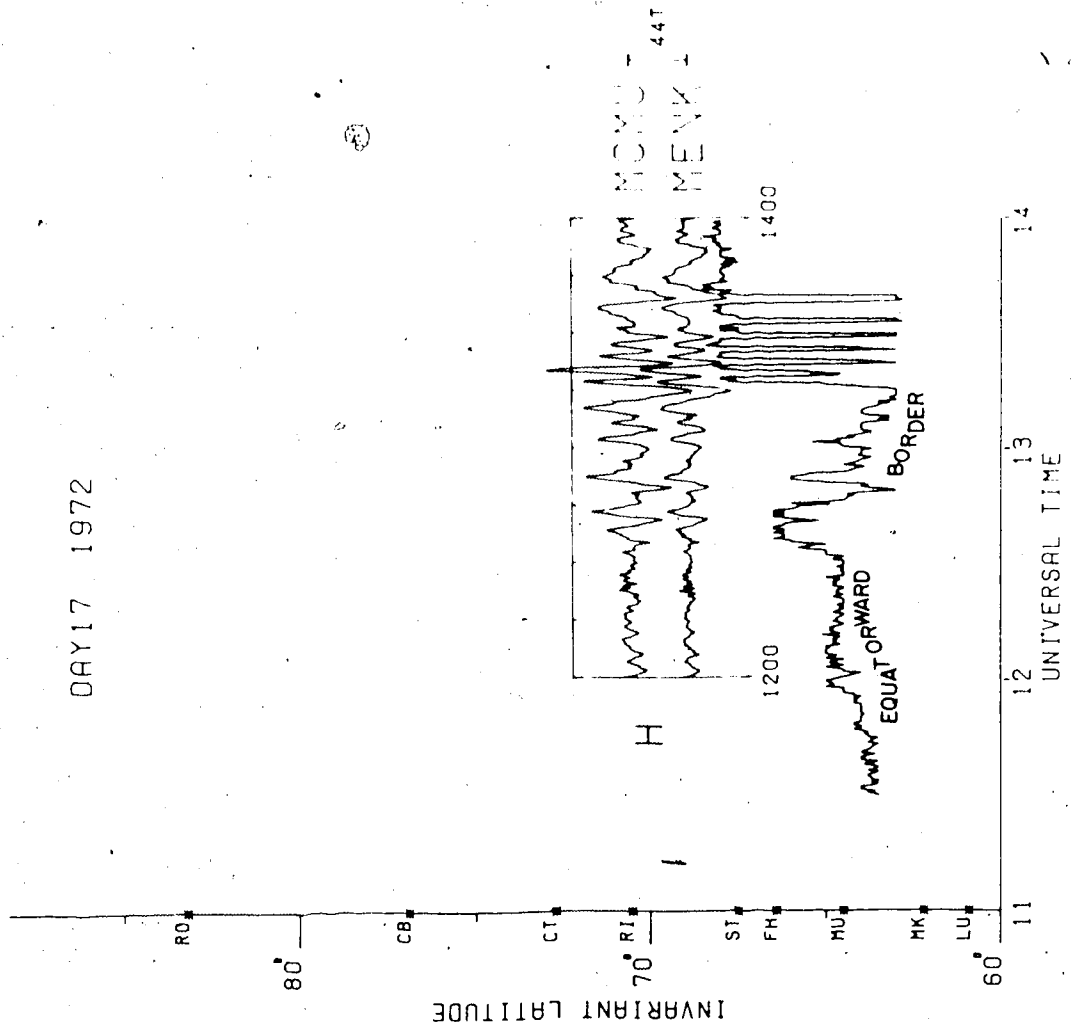


Figure 59

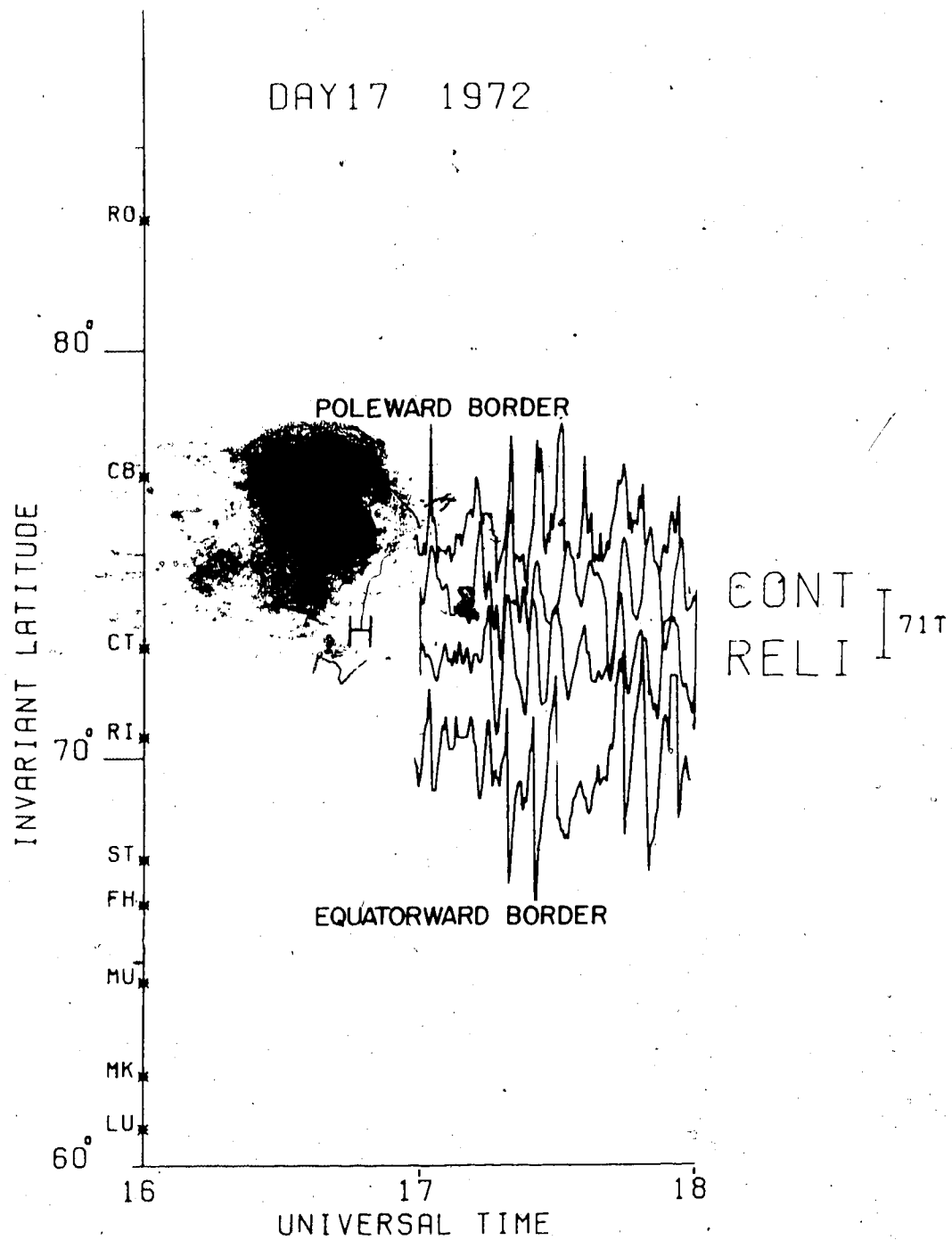


Figure 60

equatorward borders oscillate in a similar manner for the interval 1700-1800 UT in contrast to the interval 1300-1400 UT. As a result, the station close to the poleward border (i.e., CONT) and the station close to the equatorward border (i.e., RELI) oscillate with the same frequency in contrast to the oscillations recorded at CONT and FTCH between 1300 and 1400 UT which are quite different.

The border of the electrojet which is determined from the  $\Delta Z$  extremum from the latitude profile seems to oscillate in phase with the magnetic pulsations in the Z component and slightly out of phase with the horizontal components particularly with the D component. This is illustrated in Figure 61 where the magnetic pulsations in 3 components recorded at SMIT are presented together with the variations in the position of the equatorward border of the electrojet.

A plot of the magnitude of the negative  $\Delta X$  extremum (denoted by HMAX) of the latitude profile as a function of Universal Time is shown at the bottom of Figure 61. It indicates that the three dimensional current system producing the H perturbation also fluctuates in its intensity. Thus it would appear that the Pc 5 micropulsations contain contributions from both the spatial oscillations of the westward electrojet and temporal oscillations in the intensity of the electrojet. In the following section we shall explore the implications of this suggestion.

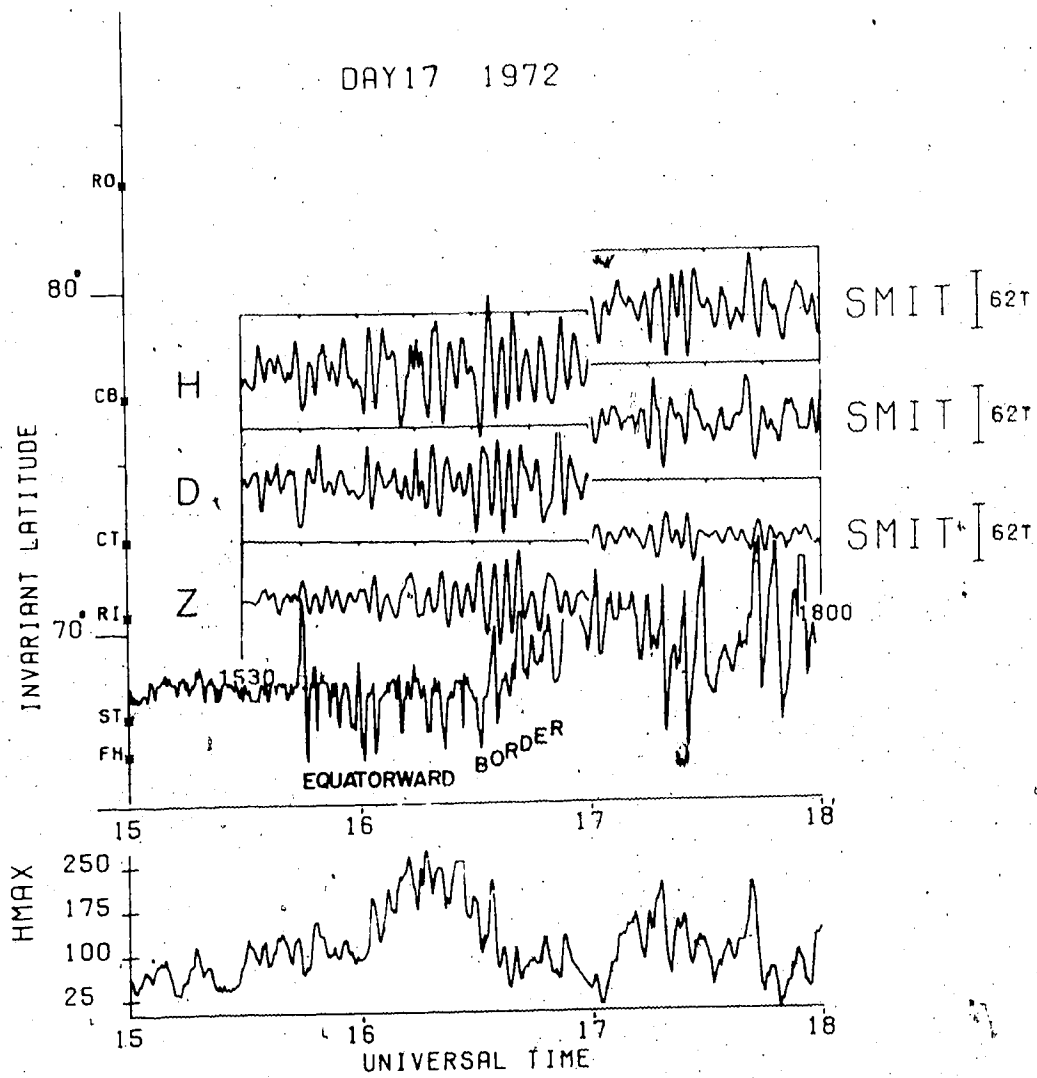


Figure 61

### 4.3 Generation Mechanism of Pc 5 Micropulsations

Our study of the latitudinal variations of the spectral components of the Pc 5 micropulsations indicates that all spectral components peak at the same latitudinal range and that the low frequency component maximizes both at low latitude and high latitude (see Figures 33, 34 and 35). It is evident that these observations do not readily support the field line resonance model which predicts a latitudinal dependence of the spectral components. Furthermore, it has also been shown that the demarcation line in the horizontal plane does not coincide with the line of intensity maximum as predicted by the field line resonance model (see Figures 14, 50, 51 and 52). Besides, there has been no conclusive experimental proof for the existence of Kelvin Helmholtz instability which has long been regarded as a source for the excitation of field line resonance. We are therefore compelled to consider other alternatives for the generation of Pc 5 micropulsations although it must be emphasized that the field line resonance model might be operative in some specific occasions as will be shown in the next chapter.

In the previous sections, we have presented the pulsation data against the background of the convection westward electrojet. It is obvious that the intensity maximum and the polarization follow the electrojet (see for

example, Figures 26 and 47) and that the signal strength of the pulsations is markedly enhanced in conjunction with sudden changes in the position of the equatorward border of the electrojet (see for example, Figure 57). We have further demonstrated that during and after the sudden shifts in position, the equatorward border of the electrojet oscillates spatially at a frequency which is a dominant component of the Pc 5 spectrum (see for example, Figure 59). These facts, coupled with the observation that there is always a large perturbation in  $Z$ , point to the convection westward electrojet and its associated three dimensional current system as a possible source for Pc 5 pulsations.

To obtain a rough picture of the physics of the current system we may regard it as an electric circuit with lumped impedances as shown in Figure 62. Boström [1972] has used a similar equivalent circuit for the substorm current system and found that the circuit rings in the Pi 2 frequency range in response to variations in current flow through the ionosphere. The ringing mentioned above represents LC-oscillations of the equivalent circuit, and we shall follow Boström's technique by attempting to construct an equivalent circuit whose ringing will constitute Pc 5 micropulsations. Holzer and Reid [1975] and Reid and Holzer [1975] have also used a similar circuit analogy to study the response of the coupled magnetosphere-ionosphere system to changes in dayside field line reconnection rate. The construction of our equivalent circuit is based on the following reasoning.

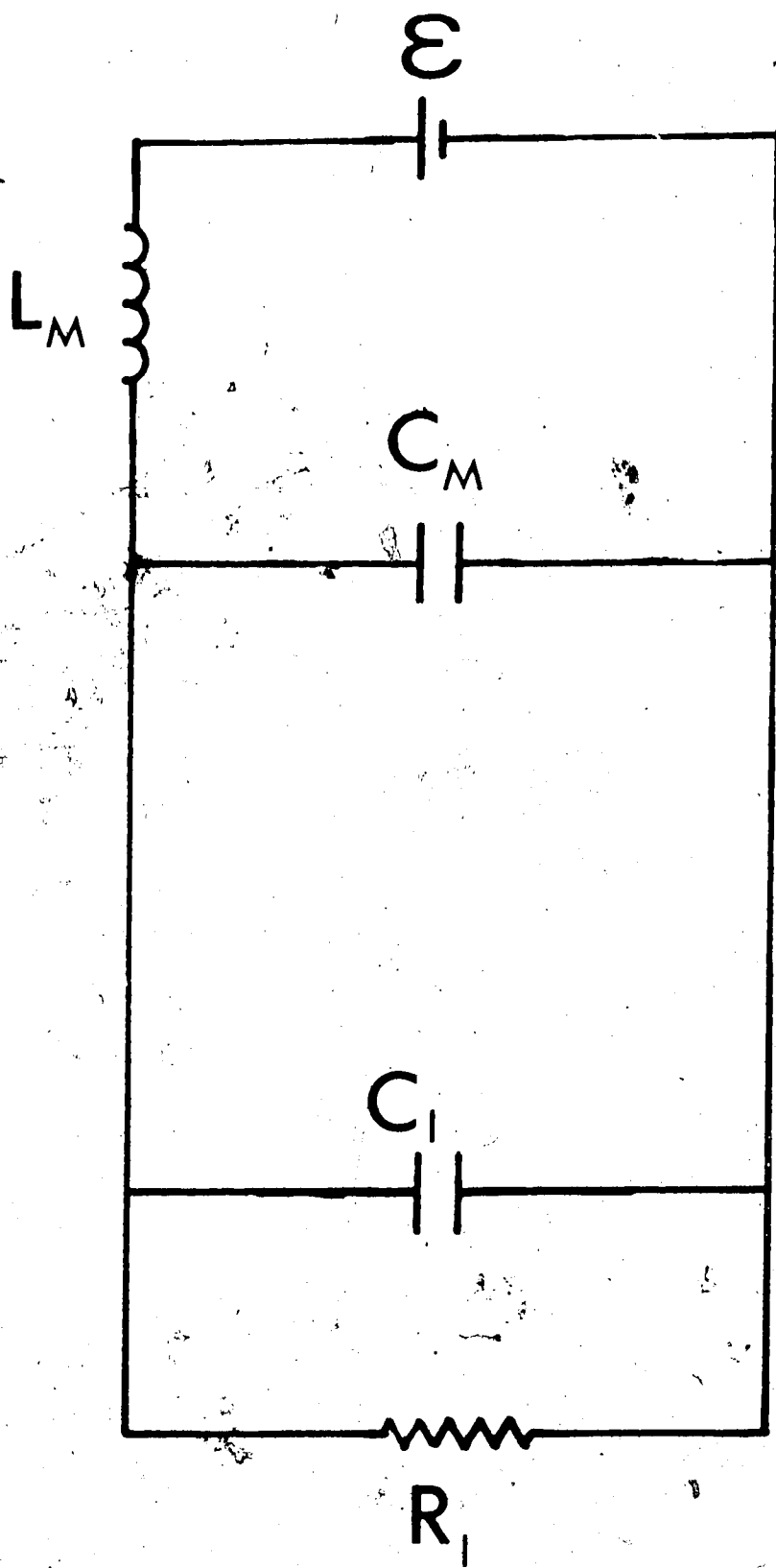


Figure 62



In Figure 5 we have shown the configuration of the auroral electrojets and field aligned currents associated with convective processes in the magnetosphere. From this figure it would appear that the westward electrojet stretches from near noon to midnight. The huge scale size of this system makes it possible that Pc 5 micropulsations could be explained by LC-oscillations of any electrical circuit associated with the volume of space occupied by the three dimensional current system. For example, Rostoker and Boström [1975] calculated values of  $L \approx 35$  H and  $C \approx 9 \times 10^4$  F for a smaller circuit associated with the eastward electrojet in the evening sector and found the frequency of LC-oscillations to be  $\sim 0.1$  MHz which would be well outside the Pc 5 frequency range. However, Hughes and Rostoker [1976] have pointed out that the ionospheric conductivity discontinuity at the dawn meridian must be associated with the divergence of westward current in the ionosphere into field aligned current flowing up the field lines into the magnetosphere. Thus there is, confined to the pre-noon quadrant, a three dimensional current system involving downward field-aligned current near noon diverging into westward ionospheric Hall current with subsequent divergence into upward field aligned current flow at the dawn meridian. It is oscillations of this current system which we shall use to attempt to explain the origin of Pc 5 micropulsations.

Consider the dawn and dusk meridian and the convecting plasma drifting through it. Rostoker and Boström [1976] have proposed a mechanism by which the Birkeland currents are driven through the extraction of kinetic energy from the magnetotail plasma by braking the motion of the plasma as it drifts towards the flanks of the magnetosphere. Mozer and Lucht [1974] have found that the equatorward directed electric field decreases in magnitude as one moves from pre-dawn to post-noon (see Figure 63). Hence, as the plasma moves from a tail like to a dipole like magnetic field configuration as shown in Figure 64, it is slowed down as indicated by the decrease in the equatorward directed electric field. One may then consider that the energy extracted from the drifting plasma may provide the electrical energy to drive current systems in the pre-noon quadrant. Hence, the voltage source in Figure 62 is associated with the extraction of energy from the convecting plasma. Consider a region of space bounded by field lines poleward and equatorward of the auroral oval and confined within three time zones. Then, the current carrying volume can be represented by a rectangular box of length  $l$  (length of field lines in the generator region)  $\sim 15 R_E$ , width  $W$  (azimuthal extent of 3 time zones in the equatorial plane)  $\sim 15 R_E$  and thickness  $b$  (the separation between the field lines from the poleward borders and equatorward borders of the auroral oval mapped to the equatorial plane)  $\sim 5 R_E$ . Then the magnetic energy associated with the current flow in the volume gives

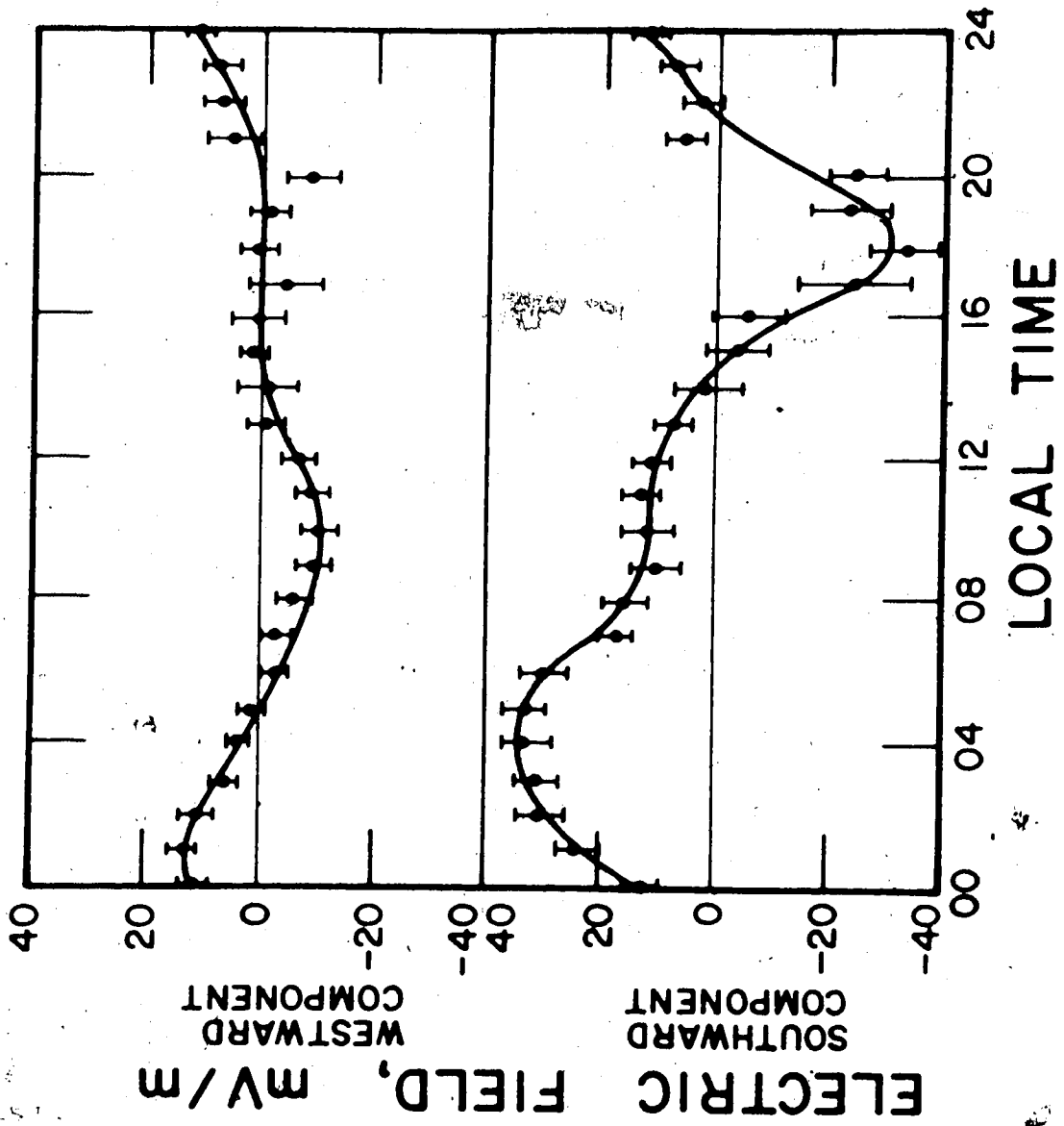


Figure 63

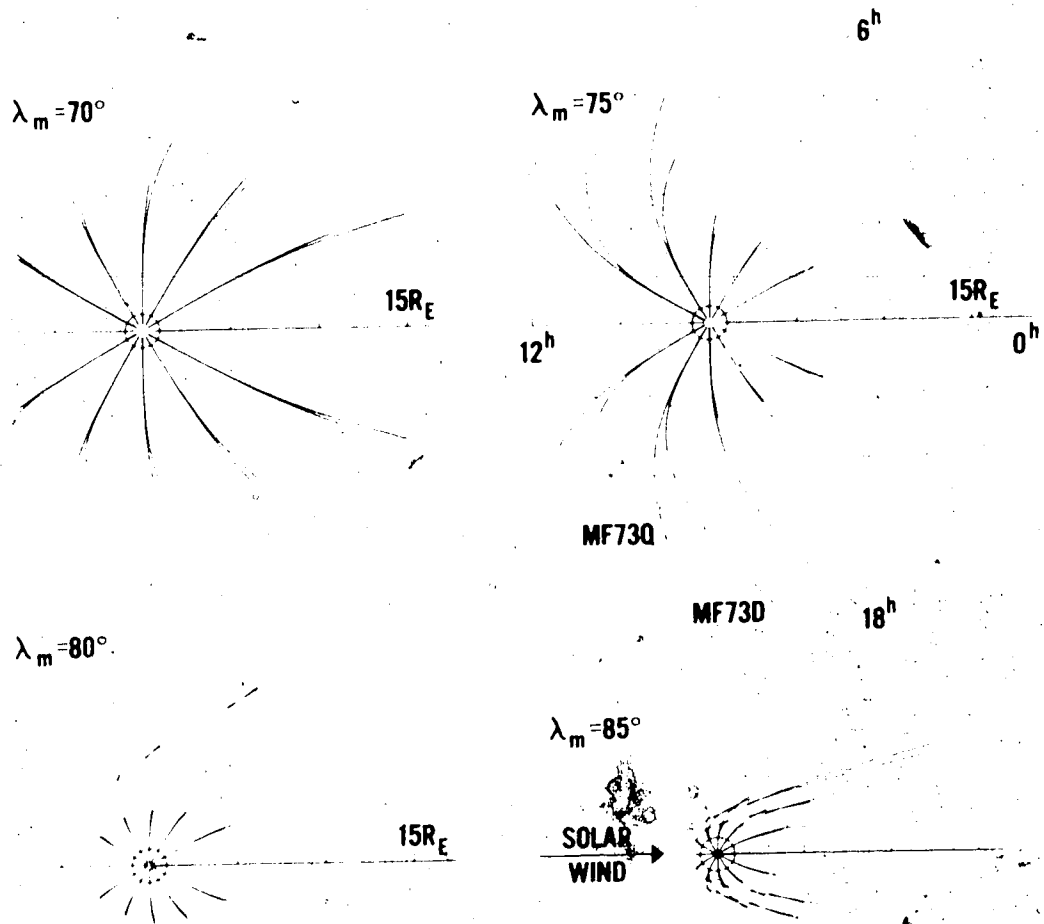


Figure 64

rise to the inductance  $L_M$  in Figure 62 and the kinetic energy associated with the convecting plasma within the volume is represented by the capacitance  $C_M$ . The dissipative Pedersen currents flowing in the ionosphere are equivalent to the dissipative current flowing through the ionospheric resistance  $R_I$ . The high number densities of  $O^+$  in the F layer and the changing electric field due to the transient response of the circuit gives rise to the displacement current through the capacitor  $C_I$ . Thus, the equivalent LCR circuit is based on the geometry of the current flow.

Using the expressions developed by Rostoker and Boström [1976], we can determine the values for  $L$ ,  $C$  and  $R$  and compute the resonant frequency of the circuit to appraise the viability of LCR circuit in representing the magnetospheric circuit. The inductance  $L_M$  can be evaluated by estimating the magnetic energy associated with a current uniformly distributed in the volume of length  $l \sim 15 R_E$ , with  $W \sim 15 R_E$  and thickness  $b \sim 5 R_E$ . By equating this to the energy stored in an inductance carrying the same total current, viz.,

$$W_m = \iiint \frac{B^2}{2\mu_0} d\tau = \frac{\mu_0 b l I^2}{12 W} = \frac{1}{2} L I^2$$

we find that  $L_M$  is  $\sim 7$  H.

The capacitance represents the kinetic energy of the convecting plasma. Assuming a uniform plasma velocity  $v \sim 1.7 \times 10^4$  m/sec ( $v = \frac{E}{B}$  where  $E \sim 0.33$  mV/m and  $B \sim 20\gamma$  in the equatorial plane) in the same volume as used in the

case of the inductance and, equating the kinetic energy in the region to the energy stored in a capacitor, viz.,

$$W_k = \iiint \frac{\rho v^2}{2} d\tau = \frac{\rho v^2}{2} \frac{W b l}{2} = \frac{1}{2} C_M V^2$$

we find that  $C_M \sim 3 \times 10^3$  F where we have used  $\rho \sim 8 \times 10^{-21}$  kg/m<sup>3</sup> (for  $n \sim 5$  cm<sup>-3</sup>) and  $V \sim 10^4$  volts.

For an F-region of thickness 100 km centered on  $\sim 300$  km altitude, the ionosphere can (neglecting end effects) be represented by a parallel plate capacitor with capacitance

$$C_I = \frac{\epsilon A}{d}$$

where the dielectric constant of the plasma is

$$\epsilon = \frac{\rho}{B^2} = \frac{n m_i}{B^2}$$

$\rho$  being the mass density of the ions,  $n$  the number density,  $m_i$  the molecular weight of  $O^+$  times amu and  $B$  the ambient magnetic field. Hence,  $\epsilon \sim 3 \times 10^{-5}$  F/m for  $n \sim 3 \times 10^{12}$  m<sup>-3</sup>. For  $A \sim 500$  km  $\times$  3 time zones and  $d \sim 100$  km,  $C_I \sim 9$  F.

Assuming an ionospheric resistivity of  $\eta \sim 5 \times 10^4$   $\Omega$ m averaged over the region of the ionosphere from  $\sim 110$  km to 160 km, the ionospheric resistance below the F-region is estimated to be

$$R_I = \frac{\eta d}{A} \sim 0.3 \Omega$$

From these values, it can be seen that the circuit shown in Figure 62 can further be simplified to a circuit shown in Figure 65. The values for the circuit parameters are summarized in Table 6.

As mentioned earlier, the energy source is the kinetic energy of the plasma drifting through the dawn sector. The kinetic energy flux of drifting plasma through a surface in the dawn meridian of area of length  $l \sim 15 R_E$  and width  $b \sim 5 R_E$  perpendicular to the flow is

$$P_{\text{mech}} = \left(\frac{\rho v^2}{2}\right) \cdot v l b$$

The electric power dissipated in the auroral electric region is

$$P_{\text{elec}} = IV = IE_I d$$

For  $E_I \sim 20$  mV/m [Mozer and Lucht, 1974] and  $d \sim 500$  km and  $I \sim 10^4$  A, we obtained

$$P_{\text{elec}} \sim 10^8 \text{ W}$$

The requirement of  $P_{\text{mech}} > P_{\text{elec}}$  yields  $v > 20$  km/sec. Such velocities are consistent with the velocity in the equatorial plane near  $L \sim 10$ . Near  $L \sim 10$ ,  $B \sim 20\gamma$ ,  $E \sim 0.33$  mV/m and  $v = \frac{E}{B} \sim 17$  km/sec. Thus, the kinetic energy available in the plasma drifting past the dawn meridian is adequate to supply the energy requirements

TABLE 6  
Equivalent Circuit Parameters for Model Current System

---

Inductance of generator region	$L_M$	7 H
Capacitance of generator	$C_M$	$3 \times 10^{-3}$ F
Capacitance of F-region	$C_I$	9 F
Resistance of Ionosphere	$R_I$	0.3 $\Omega$

---



associated with the ionospheric electrojet system. The equivalent circuit of Figure 65 is therefore valid.

The model current system presented in Figure 65 is effectively a steady state system. The results of our analysis of Pc 5 pulsations suggest that these micropulsations are excited in conjunction with changes in the size and intensity of the electrojet system. We therefore wish to study what occurs if we perturb the current in equivalent circuit shown in Figure 62. A sudden change of  $i$  in the circuit will cause a sudden change in the current flow. This will set up an oscillation in the circuit whose frequency is that for the  $L_M C_M$  portion of the circuit, viz.

$$\omega = (L_M C_M)^{-\frac{1}{2}}$$

For the equivalent circuit parameters shown in Table 6, this frequency is in the Pc 5 frequency range, viz., for  $L_M = 7$  H and  $C_M = 3 \times 10^3$  F we obtain

$$f \sim 1 \text{ mHz}$$

which is at the long period end of the Pc 5 spectrum.

(Higher frequencies may be excited by exciting oscillations over a lesser latitude range or within a narrower electrojet.)

The oscillations we have been discussing above, generated through a sudden change in the driving force, will

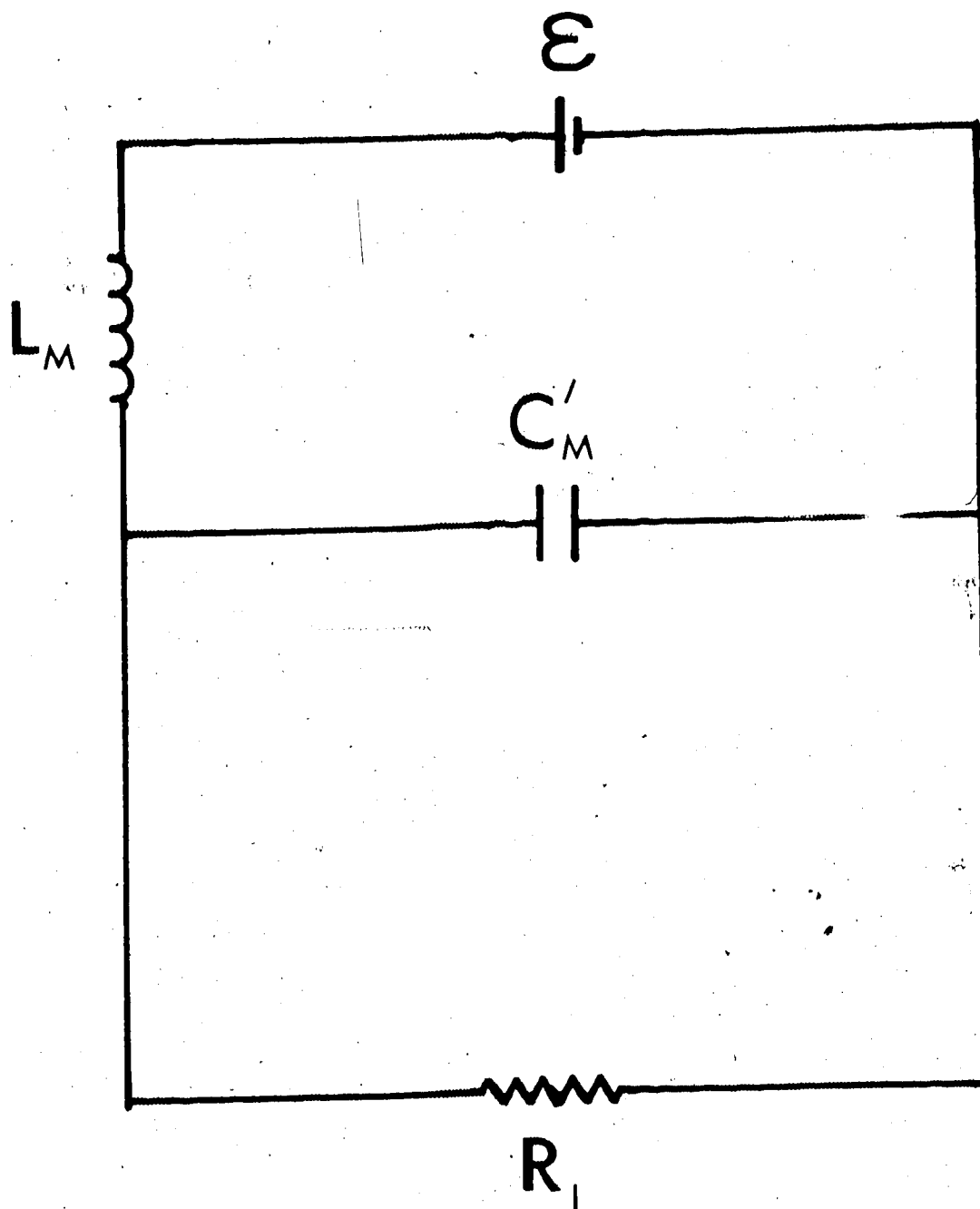


Figure 65

be imposed on the ionospheric portion of the circuit which consists of a resistance ( $R_I$ ) and capacitance ( $C_I$ ) in parallel with one another. Of course, the current through  $C_I$  will lead the current through  $R_I$  by  $90^\circ$  which provides the out-of-phase component of the perturbation magnetic field necessary to create a polarization ellipse for the pulsation in the horizontal plane. Were it not for the F region displacement current, an oscillating current system could only lead to linear polarization for the pulsation.

The model we have discussed above presents Pc 5 as an impulsive wave train, which belies the term "continuous" given to this class of pulsation. However, as we have pointed out earlier, the Pc 5's we have observed appear to be a series of impulsive wave trains which often blend together to give the impression that they are continuous in nature. The precise behaviour of the pulsations is controlled primarily by  $C_M$  and  $R_I$ . Clearly, the more energy there is in the generator region, the larger will be the effective capacitance of the equivalent circuit and thus the lower will be the lowest frequency in the Pc 5 spectrum. In addition the RC-time constant of the circuit will determine whether or not the Pc 5 pulsations appear as a quasi-continuous chain of oscillations or as a series of separated damped wave trains. Again it is clear that the more energy there is in the generator region (i.e., the more energy there

is stored in the magnetosphere) the longer will be the RC-time constant for the circuit. This effect is reflected by the fact that while one might expect  $C_M$  to increase with increased energy storage in the magnetosphere, the conductivity is controlled primarily by solar UV in the morning sector so that  $R_I$  will be relatively unchanged unless electron precipitation becomes extraordinarily high. The overall effect of the changes in  $L$ ,  $C$  and  $R$  with changing levels of energy storage in the magnetosphere is that for lower energy levels the low frequency component of the Pc 5 spectrum will be higher and the oscillations will appear as impulsive damped wavetrains while for higher energy levels the low frequency component of the Pc 5 spectrum will be lower and the wave trains will tend to merge with one another.

From the above considerations, we would like to present the following model for the Pc 5 pulsations.

A change in IMF (interplanetary magnetic field) and/or solar wind velocity produces changes in the convective velocity of the drifting plasma inside the magnetosphere. As a result, the energy available to drive the current system is changed. The adjustment in the size of the electrojet leads to spatial oscillations and the change in current intensity leads to intensity variations. The spatial and temporal oscillations of the electrojet combine to

generate the magnetic pulsations observed on the ground (see Figure 61).

The actual currents responsible for the generation of Pc 5 micropulsations form a three-dimensional system with currents flowing downward into the electrojet in the pre-noon quadrant, westward through the ionosphere as part of the westward electrojet (Hall current), and back into the magnetosphere at dawn (because of the conductivity discontinuity near dawn due to enhanced photo-ionization in the day time). The entire system is enclosed by the Birkeland current sheet pairs closed in the ionosphere through southward flowing Pedersen current (see Figure 5). Because of the relatively short longitudinal extent of a portion of the westward electrojet associated with the pulsations, ground based magnetometers should be able to detect perturbations from both components of the three-dimensional current system. The contribution from both components of the current system is well illustrated by a series of latitude profiles shown in Figure 66. Figure 66 consists of six latitude profiles, each about 2 minutes apart. The borders of the convection westward electrojet are indicated by arrowheads at the bottom of each frame. It can be seen in Figure 66 that  $\Delta Y$  steps of the latitude profiles on the left column (i.e., profiles A, C and D) were located at lower latitudes than the  $\Delta Y$  steps of the latitude profiles on the right column (i.e., profiles B, D and F). The  $\Delta Y$  profiles of

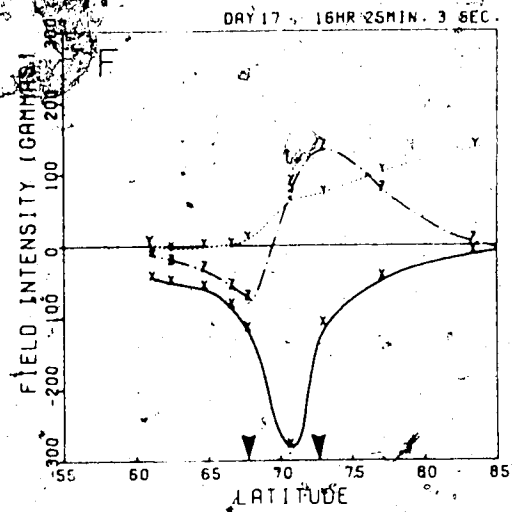
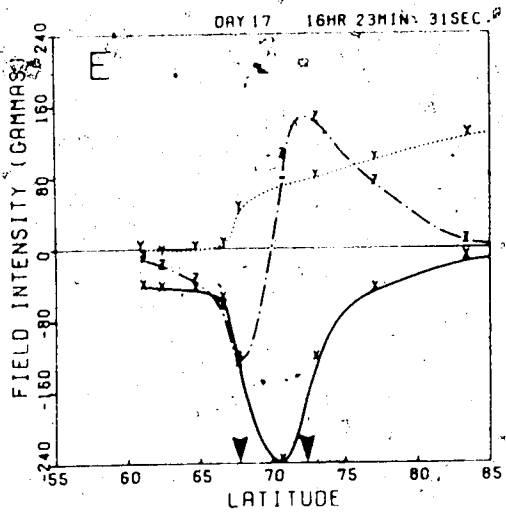
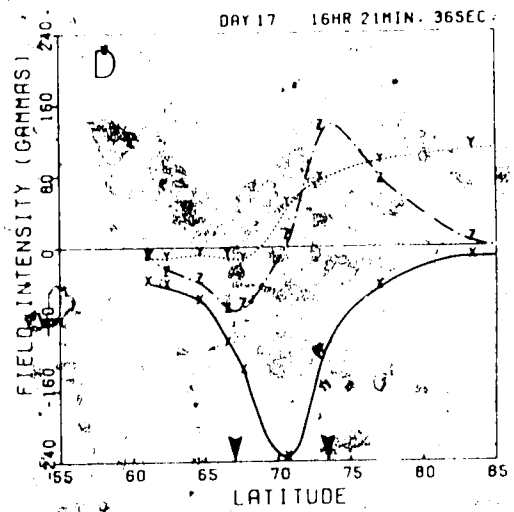
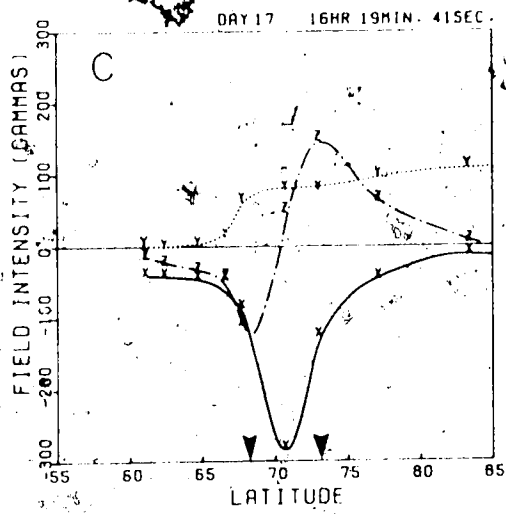
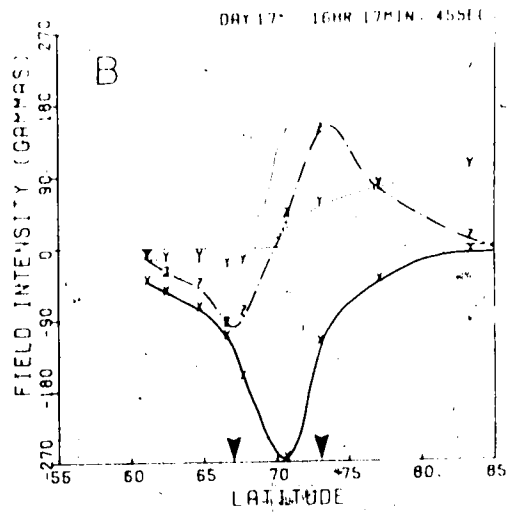
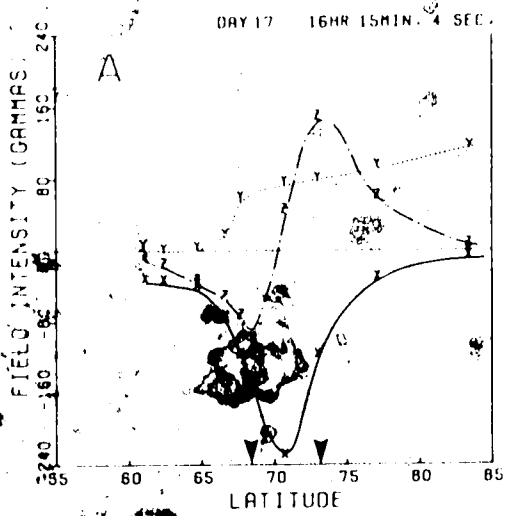
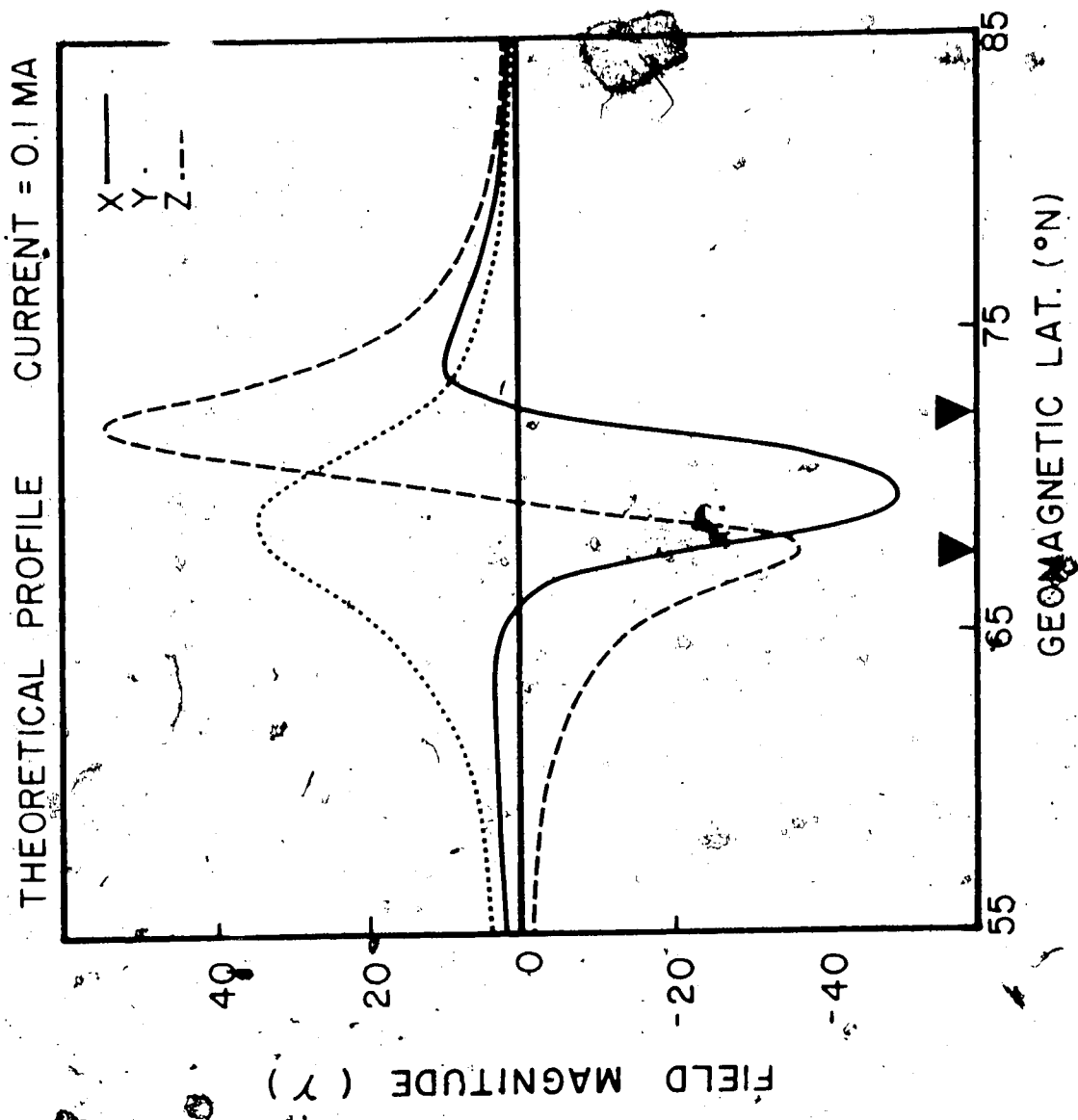


Figure 66

latitude profiles B, D and F indicate the net downward field-aligned current flow across the electrojet while the  $\Delta Y$  profiles of latitude profiles A, C and E shows the net downward field-aligned current flow and the 'end effect' of the westward electrojet portion of which is diverted up the field lines near dawn. Note also in Figure 66 the periodic spatial movement of the equatorward border of the electrojet. In order to gain a better insight to the changes produced by such a current system, we employed the techniques of Kisabeth [1972] to construct a model three-dimensional current system utilizing both the Hall current circuit and the direct current circuit involving the Birkeland current sheets. In the model a current system with  $4^\circ$  of latitudinal extent and  $16^\circ$  of longitudinal extent was utilized where the Hall and Pedersen currents were distributed uniformly within the ionospheric electrojet region. A current of  $10^5$  A was employed and the total Hall current flow was set equal to the total Pedersen current flow for demonstration purposes.

We show in Figure 67 the latitude profile taken along a meridian  $4^\circ$  to the west of the central meridian (which bisects the electrojet). The arrow heads on the Figure mark the borders of the electrojet. Note that the  $\Delta Y$  profile does not have a positive step going from south to north as is evident in the observed latitude profiles





because net downward field-aligned current flow was not accounted for in the theoretical profile.

The electrojet borders were allowed to oscillate spatially with an amplitude of  $1^\circ$  of latitude and the current was permitted to oscillate in strength with an amplitude equal to 3% of the total current flow. Figure 68 shows the differential profile for one quarter cycle of the oscillation. The similarity of this profile with the observed differential profiles shown in Figure 69 is striking. The data used to construct the profiles in Figure 69 were 4-100 mHz bandpass filtered to show the magnetic perturbations of micropulsations at  $\sim 5$  mHz. The two profiles are about one quarter of a cycle apart. The polarity pattern can be seen to relate to the relative phase changes of each component across our line of stations as shown earlier in Figures 48 and 49 which indicate that the D<sub>z</sub> component normally does not experience a pronounced change in phase across the electrojet while the H-component experiences a  $180^\circ$  phase change across the electrojet and the Z-component suffers pronounced phase changes at the borders of the electrojet. An additional phase change in the H-component is seen at  $\sim 74^\circ$  in Figure 68. This is not a statistical feature of the data but is seen on some occasions (viz. the early hours of Day 16, 1972 shown in Figure 36). Of course our choice of Hall current and

### DIFFERENTIAL PROFILE

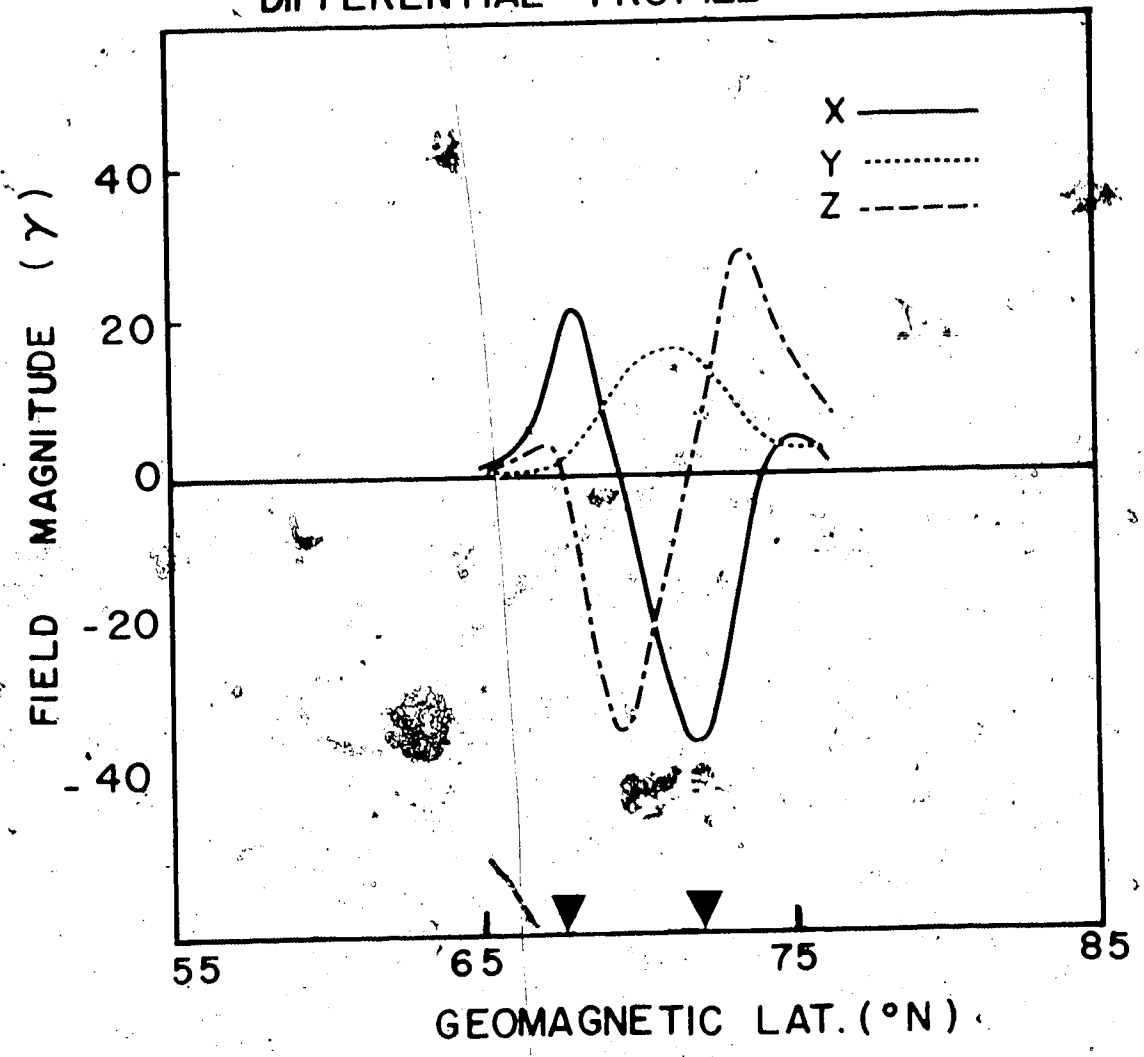


Figure 68

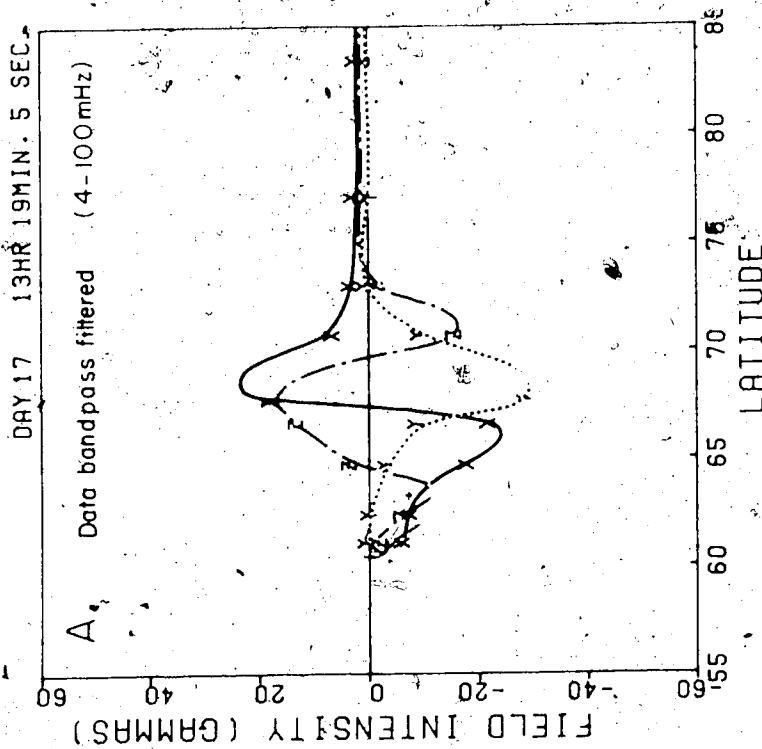
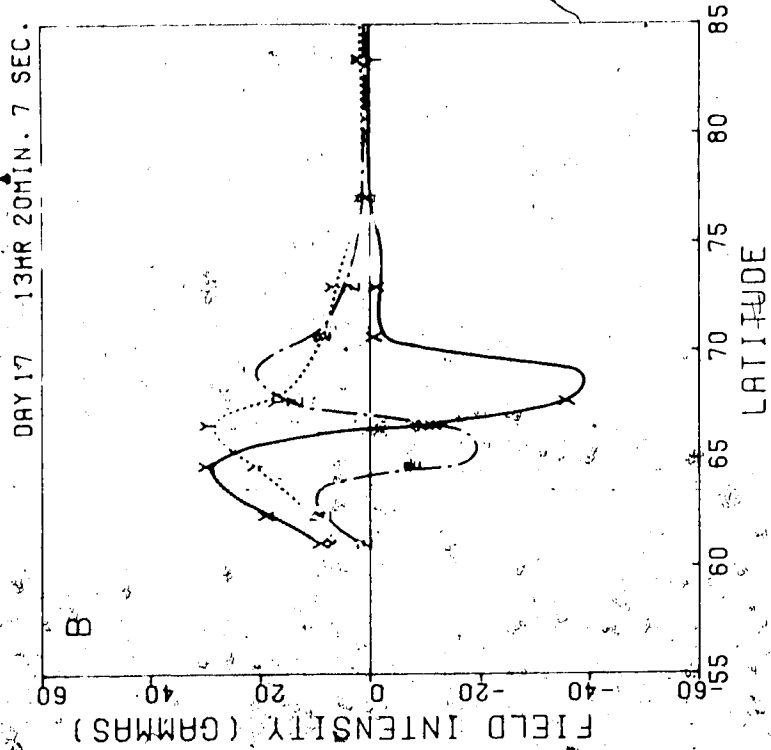


Figure 69

Pedersen current intensities is somewhat arbitrary (although the chosen values are quite reasonable). Variations in the current densities coupled with changes in the positions of the points of observation with respect to the current system will cause different relative phase patterns to appear.

However, it can be seen that our model provides a plausible explanation of the relative phase changes of the components of the disturbance across the electrojet.

The above considerations explain the observed relative phase changes across our line of stations. However, if there is no phase difference between the components at a given location, one would only observe linear polarization with the "lines" tilted in the first quadrant (components in phase) or the second quadrant (components  $180^\circ$  out of phase). However the ellipses turn up and switch in the sense of polarization across the stations, implying that there exist phase differences between components at a given location. We shall seek to explain these effects as follows.

First, let us consider the polarization in the H-D plane. The contribution to D comes from the direct "ohmic" current and a displacement current flowing in and to some extent above the F-region. The displacement current provides the out-of-phase component to D, which results in the total D perturbation being out of phase with H. The displacement current arises from a separation of the positive

and negative charges by a changing electric field. It is defined as

$$j_D = \frac{\partial \vec{D}}{\partial t} = \epsilon \frac{\partial \vec{E}}{\partial t} + \frac{\rho}{B^2} \frac{\partial \vec{E}}{\partial t}$$

where  $\vec{D}$  is the displacement,  $\vec{E}$  the electric field,  $\epsilon$  the dielectric constant,  $\rho$  the mass density of the plasma ( $= Nm_j$ , where  $N$  is the number density and  $m_j$  = mean molecular weight  $\times$  amu) and  $B$  the magnetic field. Using nominal values near the peak of the F-layer (i.e., mean molecular weight of 17,  $N \sim 2 \times 10^6 \text{ cm}^{-3}$ ,  $B \sim 55,000 \gamma$ , and a conductivity of  $\sim 2 \times 10^{-5} \text{ Sm}^{-1}$ ) and considering a period of  $\sim 200$  sec ( $f \sim 5 \text{ MHz}$ ), we find that the displacement current is about 1/10 of the ohmic current:

$$\left| \frac{j_D}{j_\Omega} \right| = \left| \frac{\partial \vec{D}}{\partial t} \right| = \frac{\omega \epsilon}{\sigma} \approx 0.1$$

Thus, the displacement current has a small but significant contribution to the  $D$  perturbation.

Since current going through a capacitance leads the current going through a resistor in a parallel RC circuit by  $90^\circ$ , one can express the perturbation in  $D$  observed on the ground as

$$D = D_\Omega \cos \omega t + D_{D_0} \cos \left( \omega t + \frac{\pi}{2} \right) \quad (16)$$

where  $D_\Omega$  includes the contributions to the magnetic pertur-

bation due to the ohmic component of the ionospheric current flow and the field-aligned currents (and is in phase with H) and  $D_p$  is the contribution to the magnetic perturbation due to the displacement current. Equation (16) can be expressed as

$$D = D_0 \cos(\omega t + \theta)$$

$$\text{where } D_0 = \sqrt{D_{\Omega}^2 + D_D^2}$$

$$\theta = \tan^{-1} \frac{D_D}{D_{\Omega}}$$

$\theta$  is then the phase difference between the D component and the H component. It can be seen from Figures 68 and 69 that the H and D components vary in the same sense south of the  $\Delta X$  cross-over. Thus D leads H south of the  $\Delta X$  cross-over producing counter-clockwise (CC) polarization in the H-D plane. North of the  $\Delta X$  cross-over, H and D vary in the opposite sense. Hence, the phase difference due to the displacement current causes H to lead D in phase, producing the observed clockwise (CW) polarization (see Figure 45).

The earth has a finite conductivity that causes the induced fields to be phase-shifted with respect to the inducing or source field. The phase shifting of the internal field contribution results in complex total (i.e., inducing plus induced) field components at the surface. Nopper and Hermance [1974] have shown that the induction effect of the earth causes phase changes in H and Z with H leading Z. Again, from Figures 68 and 69, one can see that

as one moves from south to north,  $\Delta Z$  and  $\Delta X$  vary in the same sense (i.e., H leads Z resulting in CW polarization in the H-Z plane), and then in the opposite sense in a rather limited latitudinal range (i.e., Z leads H resulting in CC polarization), and then in the same sense again (CW polarization) and finally in the opposite sense again (CC polarization). This agrees well with the observed senses of polarization in the H-Z plane (see Figures 37, 40 and 43) although over some intervals the CC regime in the middle of the CW regions was not observed possibly because its limited extent made it difficult to detect using our stations.

At a given station, D leads H due to the effect of the displacement current and H leads Z due to the effect of induction. It therefore follows that D leads Z. Again referring to Figures 68 and 69, moving from south to north, one can see that  $\Delta Z$  and  $\Delta Y$  vary in the same sense (i.e., D leads Z resulting in CW polarization in the D-Z plane), and then in the opposite sense (i.e., Z leads D resulting in CC polarization) and finally in the same sense again (i.e., CW polarization). This agrees with the observed senses of polarization (see Figure 47).

The above considerations explain the observed sense of polarization in three orthogonal planes. The orientation of the major axis of the ellipse is due to the relative magnitudes of the components and to the size of the phase

difference between the components. A more detailed study on the polarization characteristics would undoubtedly yield additional information on the subject of induction.



## CHAPTER V

### 'Pc 4' ACTIVITY IN THE MORNING SECTOR

#### 5.1 Observations

As mentioned earlier in the first chapter, the occurrence of 'Pc 4' giant pulsations is rare. We have only noted four events from almost five years of data recorded at our stations. They occurred on Day 347, 1971, Day 253, 254 and 255, 1974. The events all occurred in the morning sector.

The magnetograms both unfiltered and filtered (with a 1-20 MHz digital bandpass filter) for the events are shown in Figures 70, 71 (Day 347, 1971), 72, 73 (Day 253, 1974), 74, 75 (Day 254, 1974), 76 and 77 (Day 255, 1974).

It can be seen from Figures 70 and 71 that the 'Pc 4' pulsations for Day 347, 1971 are highly localized in latitude maximizing at MCMU and MENK and their highly sinusoidal wave forms are barely detectable at the northern stations like CAMB and CONT. The event of Day 347, 1971 lasted for about half an hour and appears as a single 'beat' or amplitude modulated signal.

The events recorded in 1974 recur for successive days at intervals of about 24 hours; such a periodicity has been observed in the past by Sucksdorff [1939]. The

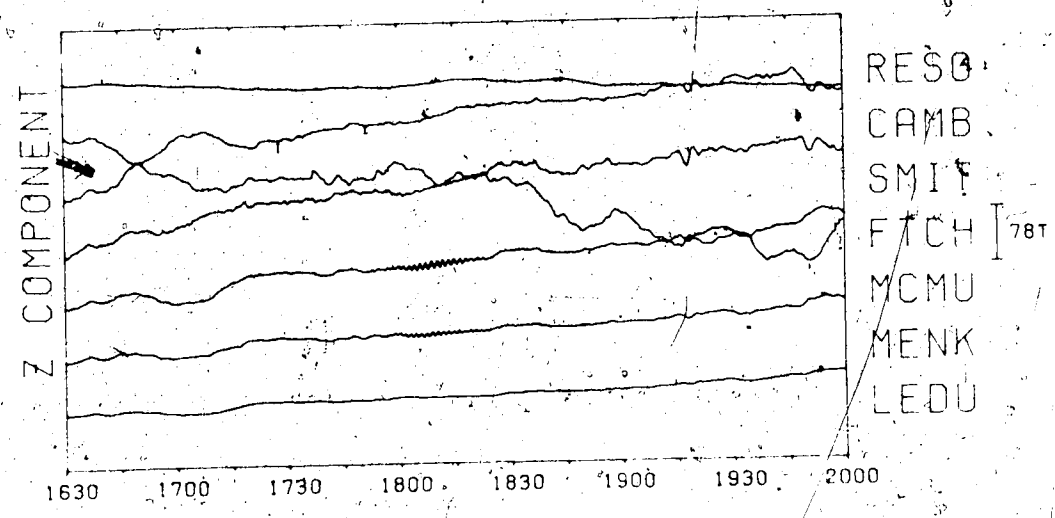
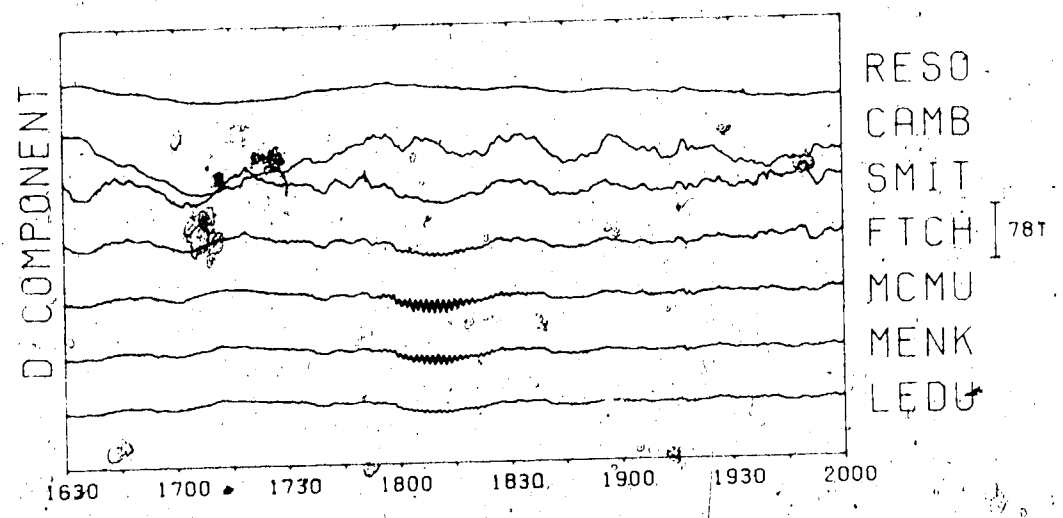
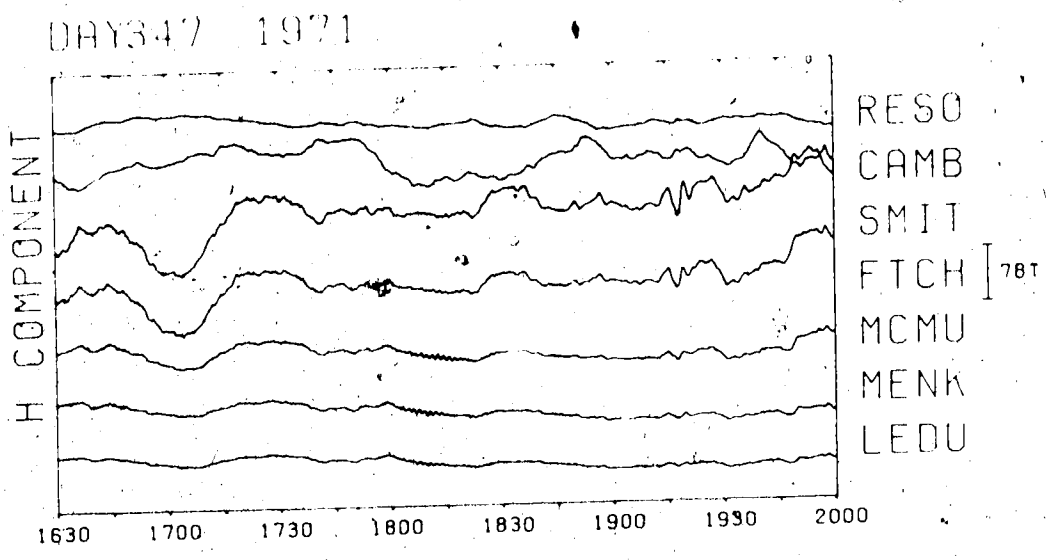


Figure 70.

DAY347 1971

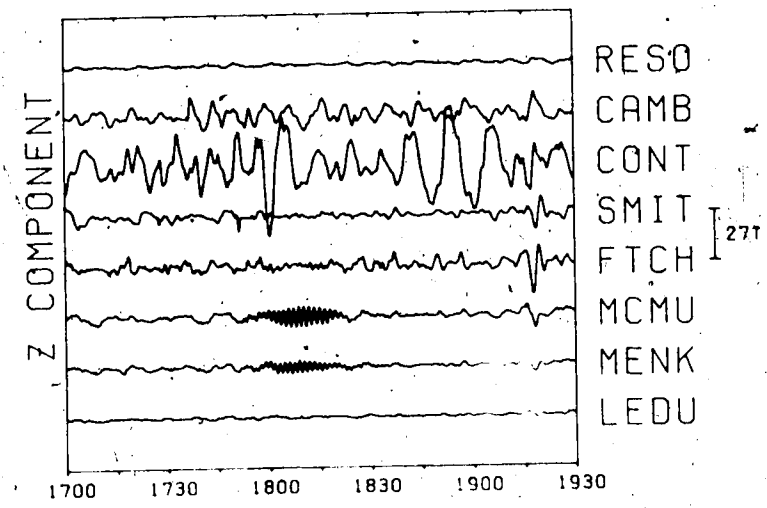
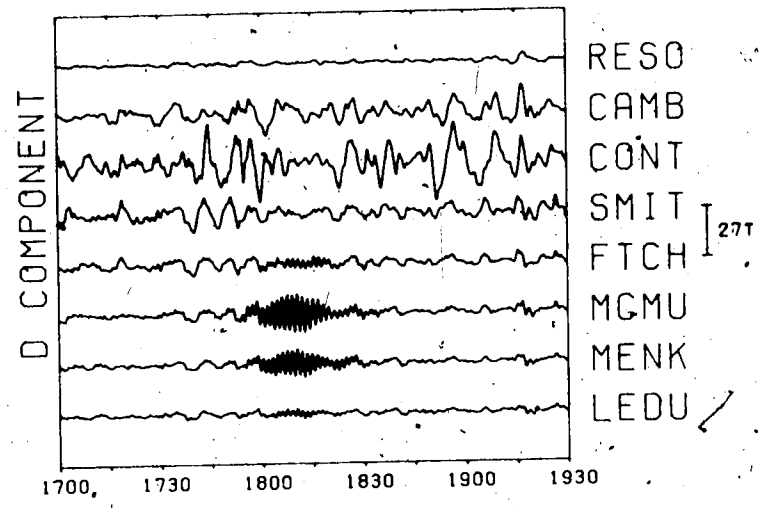
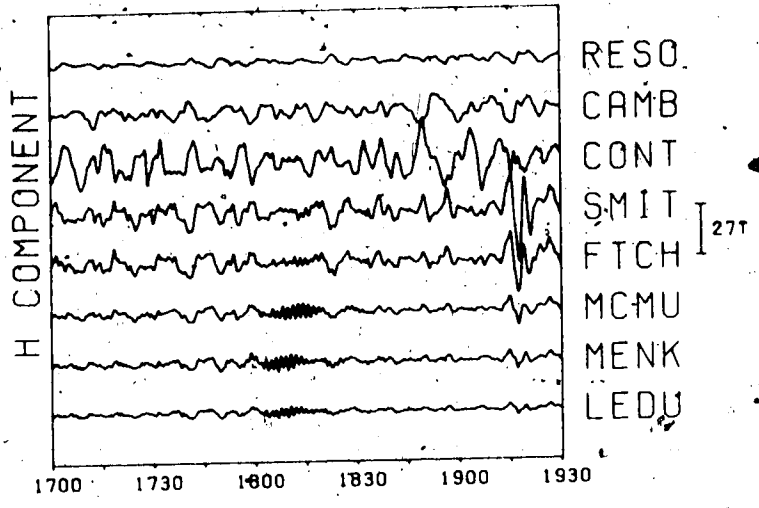
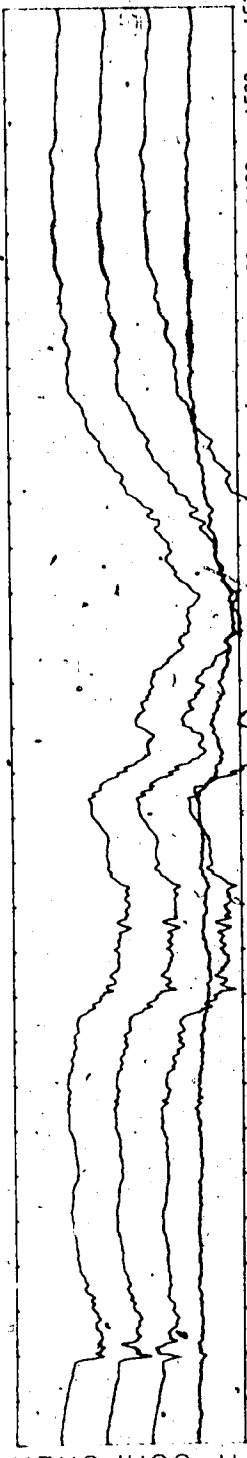


Figure 71

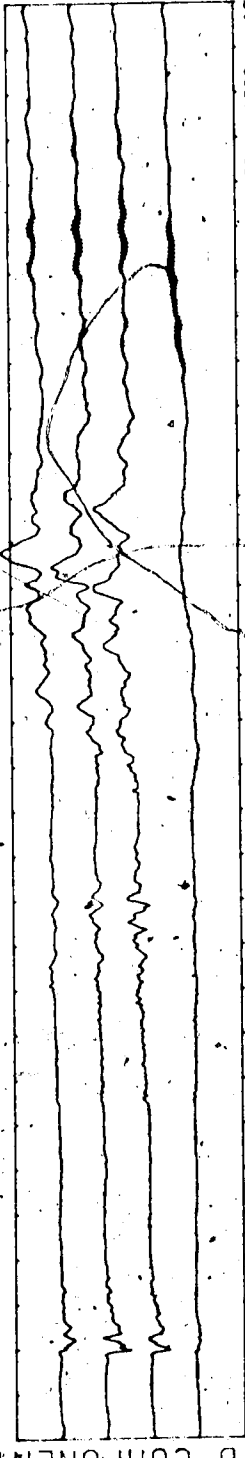
DAY 253 1974

H COMPONENT



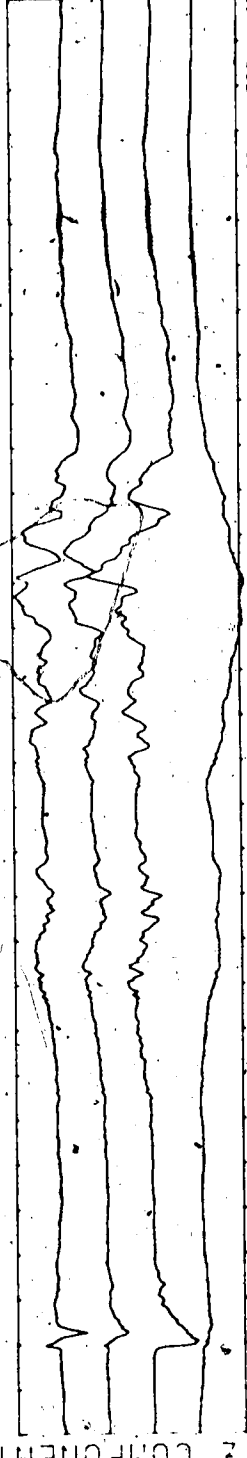
URAN  
SMIT  
HAYR  
MCMU

D COMPONENT



URAN  
SMIT  
HAYR  
MCMU

COMPONENT



URAN  
SMIT  
HAYR  
MCMU

Figure 72

DAY253 1974

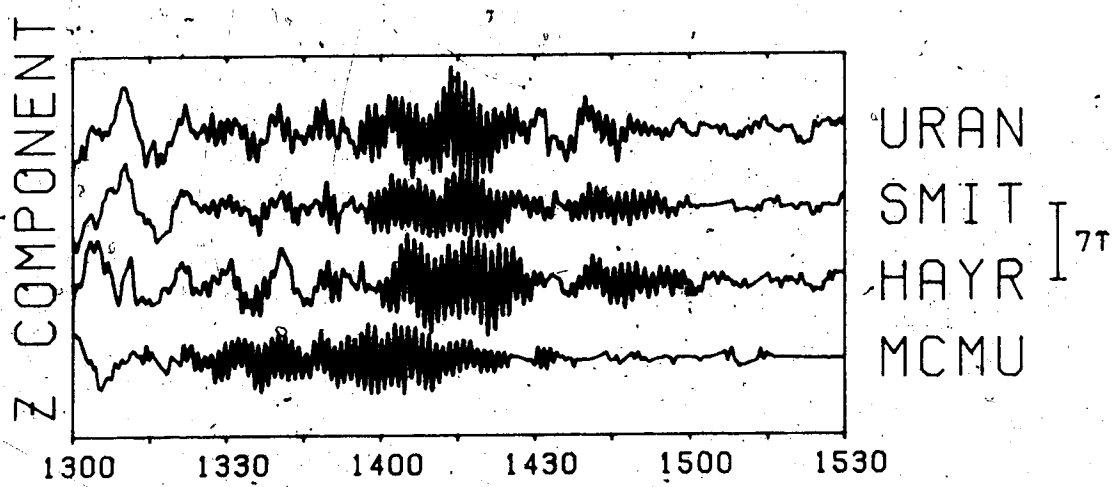
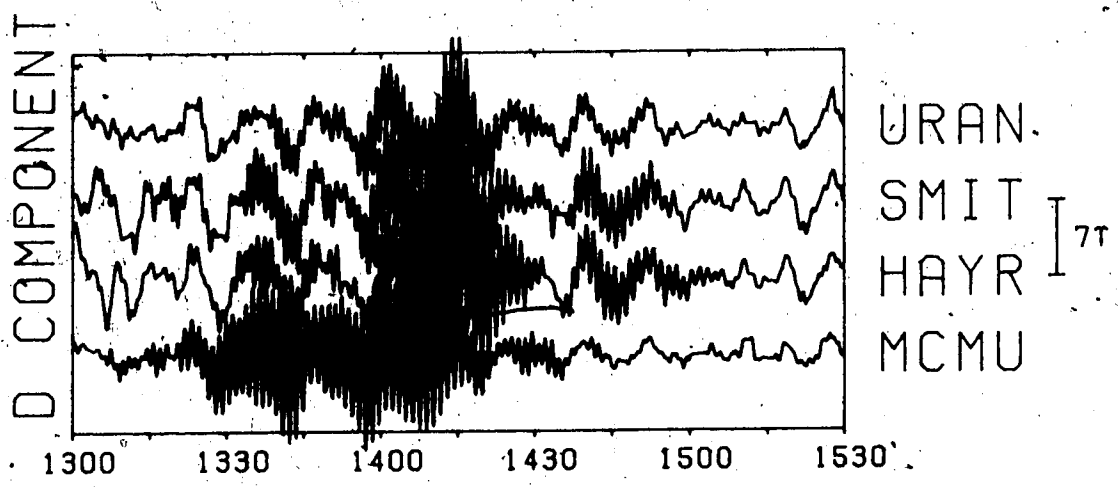
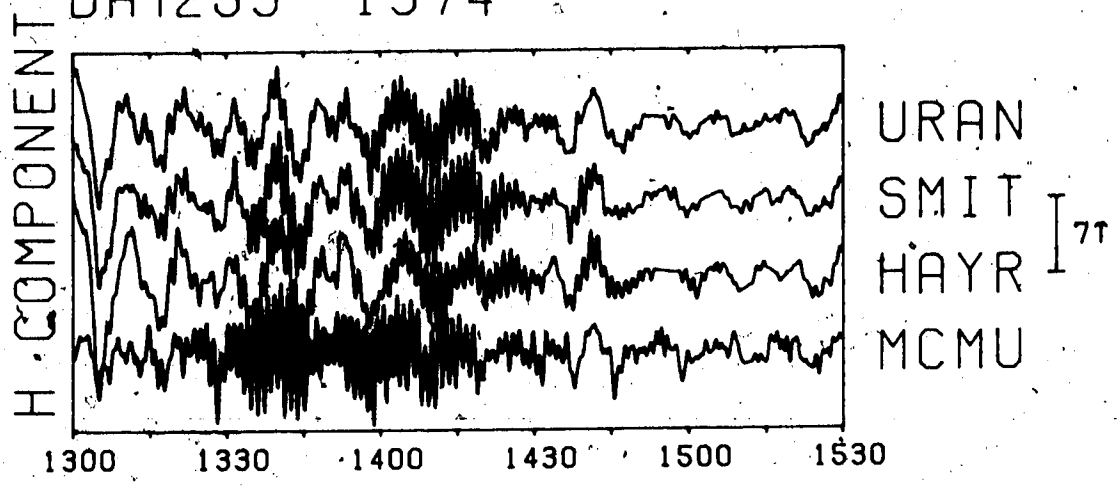


Figure 73

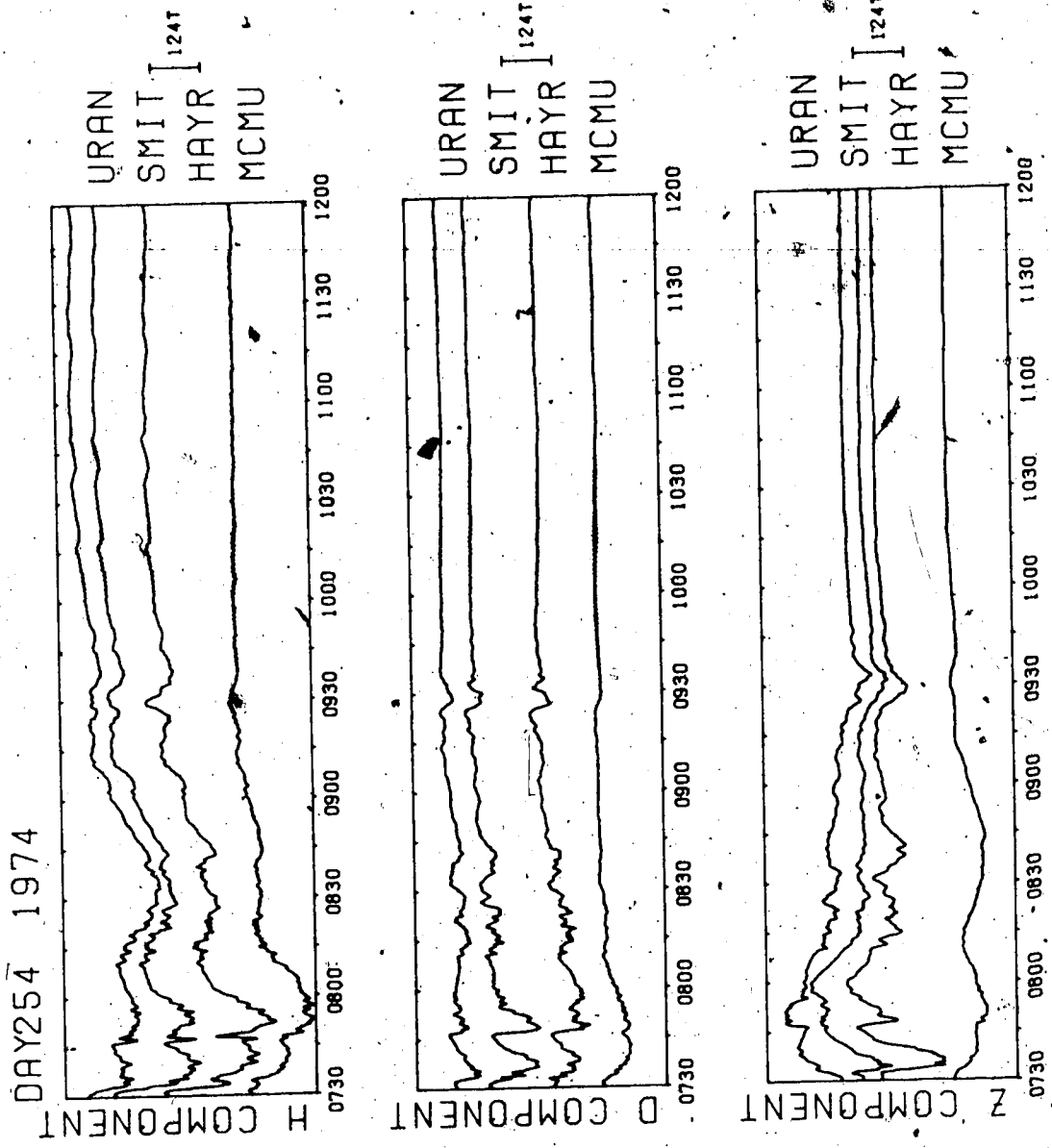


Figure 74

DAY 254 1974

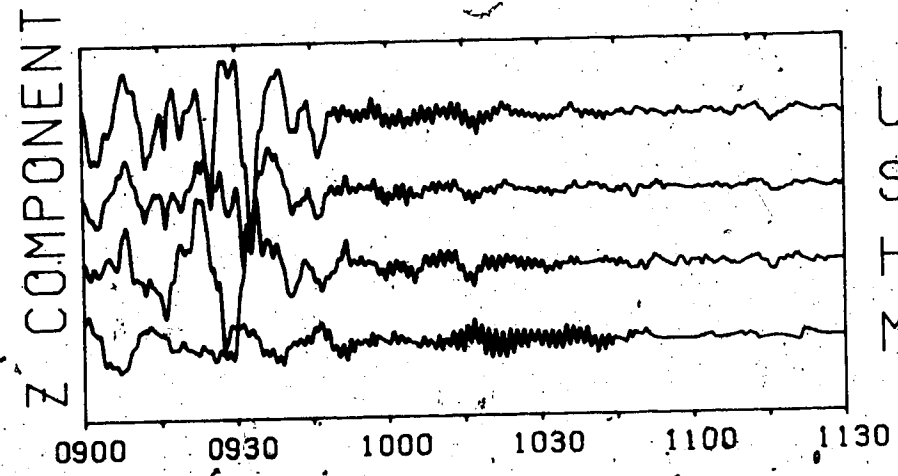
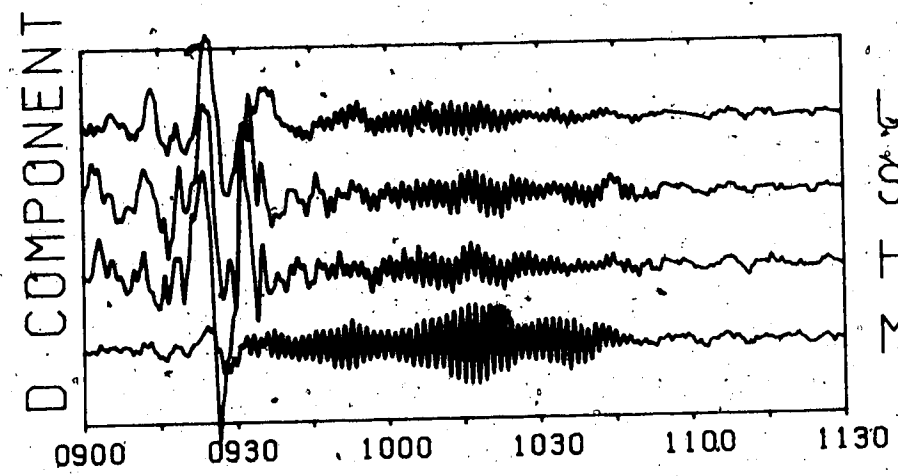
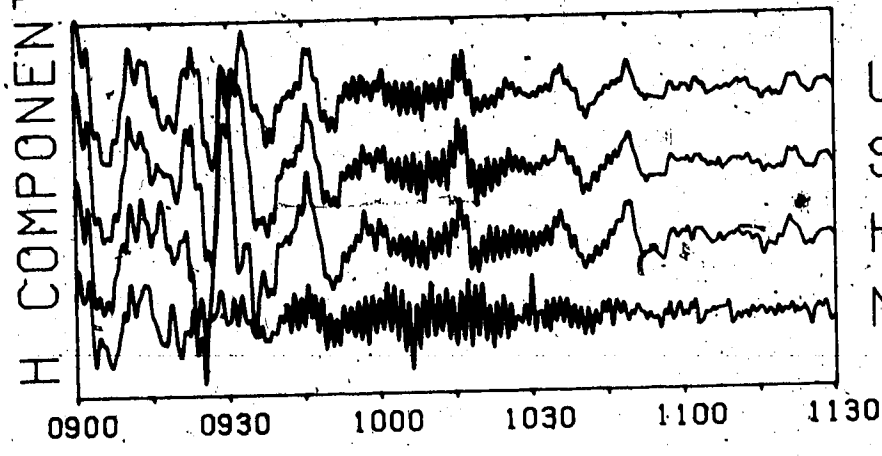


Figure 75

DAY255, 1974

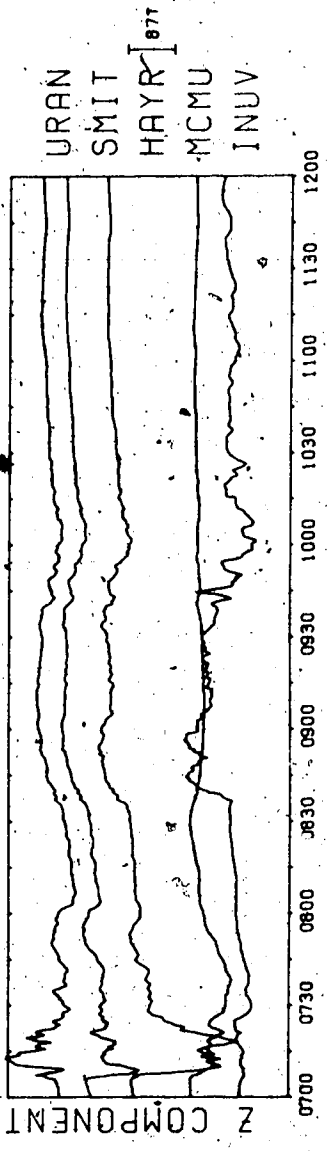
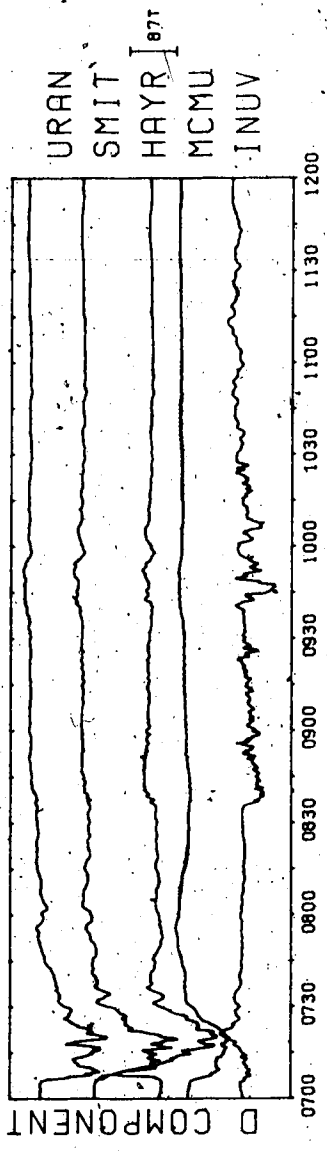
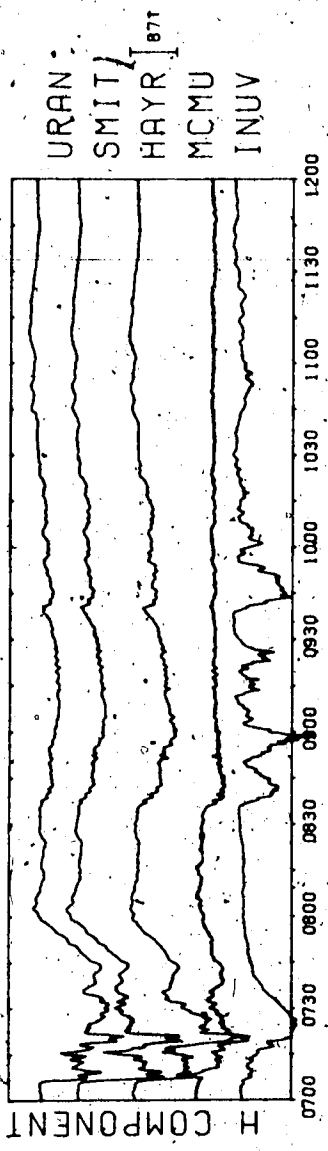


Figure 76



DAY255 1974

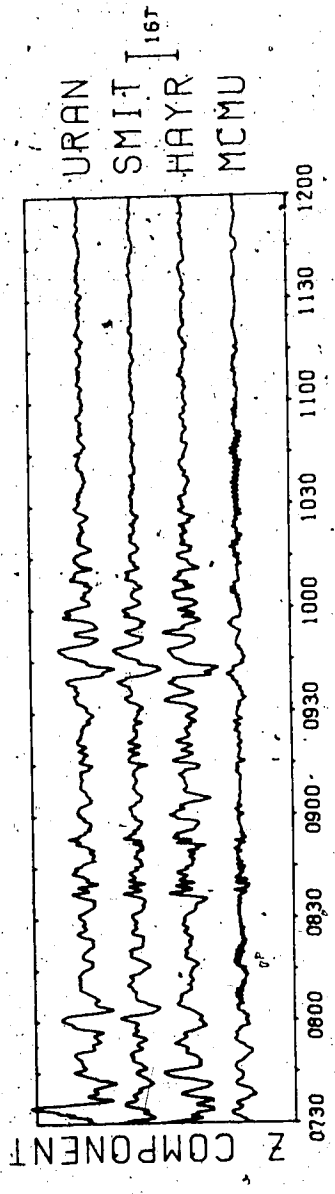
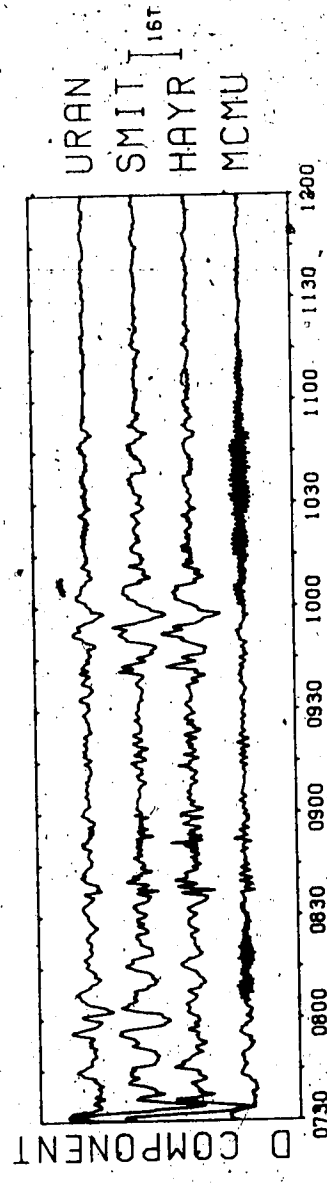
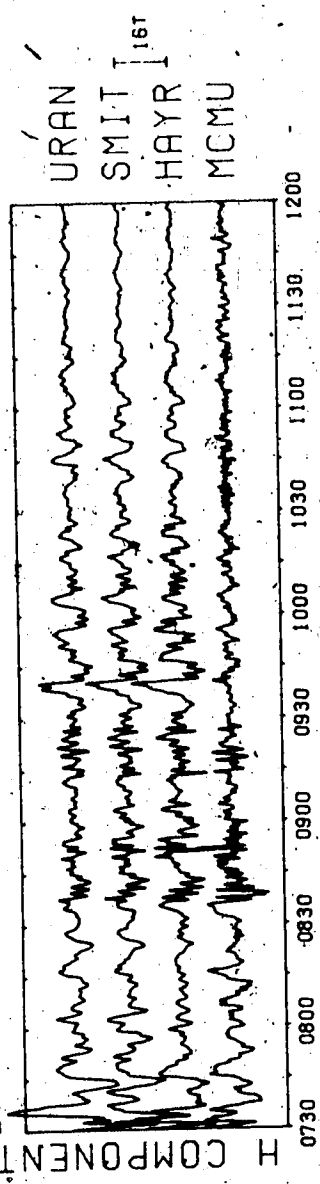


Figure 77

unfiltered magnetograms for these events indicate that the magnetosphere was in a quiet state. The substorms that occurred around midnight were of small magnitude which hardly exceeded  $150\gamma$ . The filtered magnetograms show that the wave trains appear in 'beats' and that MCMU appeared to register the 'Pc 4' wave train before the other stations. The 'beat' feature of the pulsation was most pronounced in the D-component at MCMU for the Day 254, 1974 event. The 'Pc 4' pulsation was obvious only at MCMU for the Day 255, 1974 event. This event seems to occur in two separate bursts, the first one beginning at 0800 UT lasting for about half an hour and the second one beginning at 1000 UT lasting for about an hour. It is interesting to note, from Figure 76, that the onset of substorm activity as seen in the midnight sector at the station of Inuvik ( $71.5^{\circ}\text{N}$  geographic) coincides with the termination of the 'Pc 4' wave trains which were initiated at  $\sim 0805$  UT. The substorm activity persisted until  $\sim 1000$  UT at which time the 'Pc 4' activity reappeared. The Pi 2 activity at low latitude stations were also evident during the interval. This behaviour of the micropulsations is extremely interesting in that it suggests that conditions of low activity must prevail in order that the source mechanism for 'Pc 4' giant pulsations can function. It should be pointed out that Rostoker and Fälthammer [1967] noted that Pc 5 events tended

to occur in the decay phase of magnetic storm activity and that any Pc 5 activity in progress seemed to be terminated at the onset of a magnetic storm. Thus, there is an apparent tendency for both Pc 5 and 'Pc 4' giant pulsations to be associated with decaying or low level activity in the magnetosphere, while the source mechanisms appear to be less effective during periods of increasing magnetospheric activity.

To study the frequency content of the 'Pc 4', raw power spectra were computed and are presented in the next few diagrams.

Figure 78 shows the raw power spectra for Day 347, 1971 in the interval of 1745 and 1845 UT. The erratic appearance of the spectrum is due to the fact that the spectra were unsmoothed (see Figure B2 in Appendix B for the appearance of the peaks resulting from smoothing). The frequency of 'Pc 4' is revealed by the spectra to be in the 10-12 mHz band. The peaks in the 10-12 mHz band seem to shift from high frequency to low frequency going from south to north. The double peak structure is evident at SMIT, FTCH, MCMU and MENK. The double peak feature might be due to statistical fluctuations of the estimates (see again Figure B2 in Appendix B for the variations of the confidence interval and the bandwidth) and might not be real. However, if it is real, then the 'beating' appearance of the 'Pc 4'

DAY 347 1971 (1745-1845)

H

D

Z



$12 / \mu\text{Hz}$

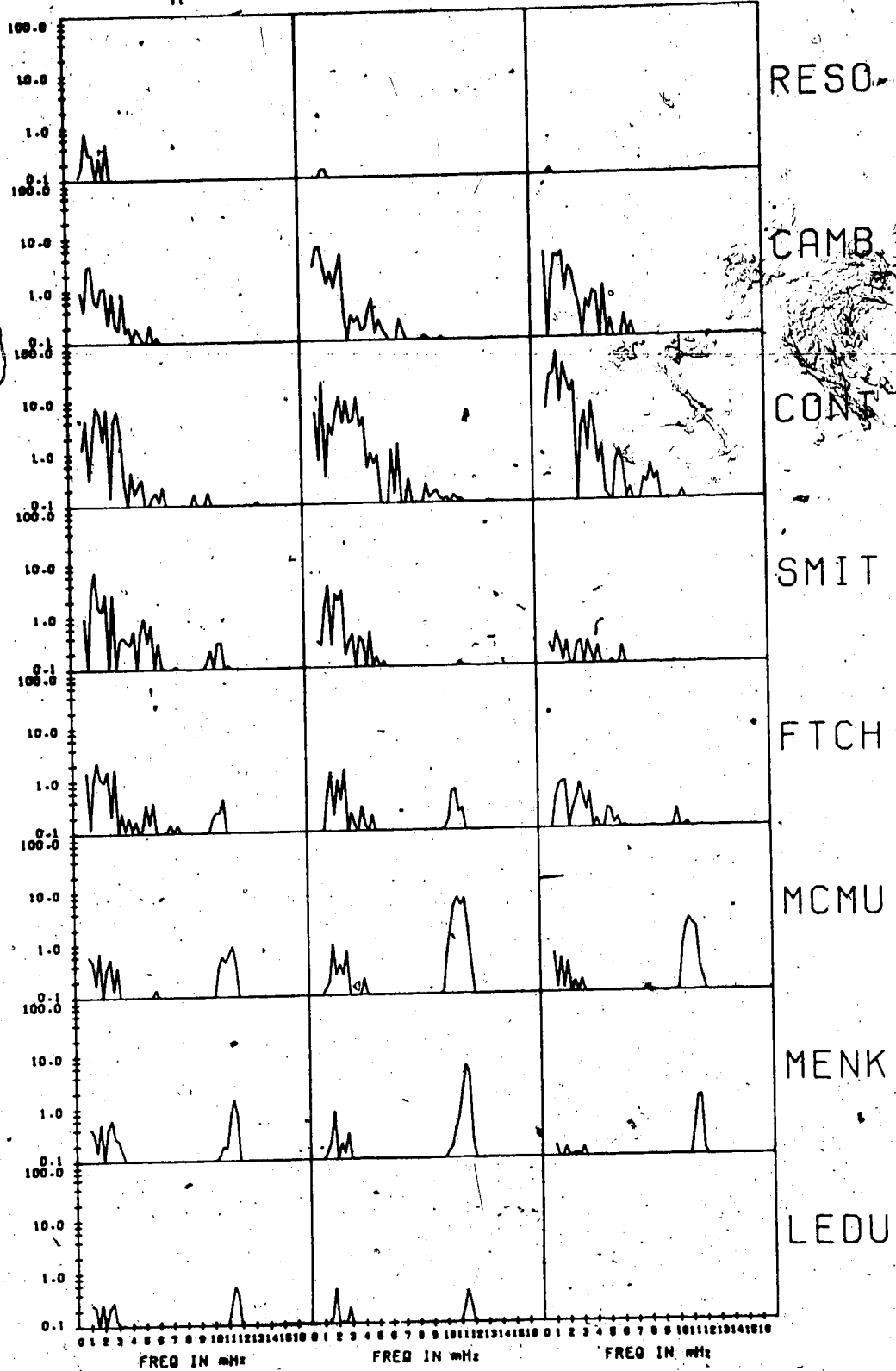


Figure 78

pulsations on the magnetograms can readily be explained as due to the addition of two waves with nearly the same frequency. The northern stations such as CONT show large powers in the low frequency band of the spectrum and some high frequency peaks across the Pc 4 band. This is associated with the convection westward electrojet noted at the northern stations of CAMB and CONT for this time interval as shown in Figure 79. The 'Pc 4' peak in the spectra which is evident at the southern stations well away from the electrojet is evidently not related to the convection westward electrojet which has been shown in the previous chapter to be the source of Pc 5 pulsations.

The spectra for Day 253, 1974 in the interval between 1300 and 1430 shown in Figure 80 indicates that the 'Pc 4' pulsations have frequency in the 11.5-13.5 mHz band. The double peak features are evident at all the stations except MCMU which shows multiple peak structure. The most dominant peak is centered at 12-12.5 mHz.

Figure 81 shows the spectra for Day 254, 1974 in the interval between 0945 UT and 1045 UT. The 'Pc 4' peaks are clustered in the 11-12.5 mHz band. The double peak feature is evident at most stations, the 11.5 mHz peak being the most dominant one. The most remarkable feature of these spectra is the complete absence of powers in any other frequency except the 'Pc 4' frequency in the D compo-

DAY 347 1971

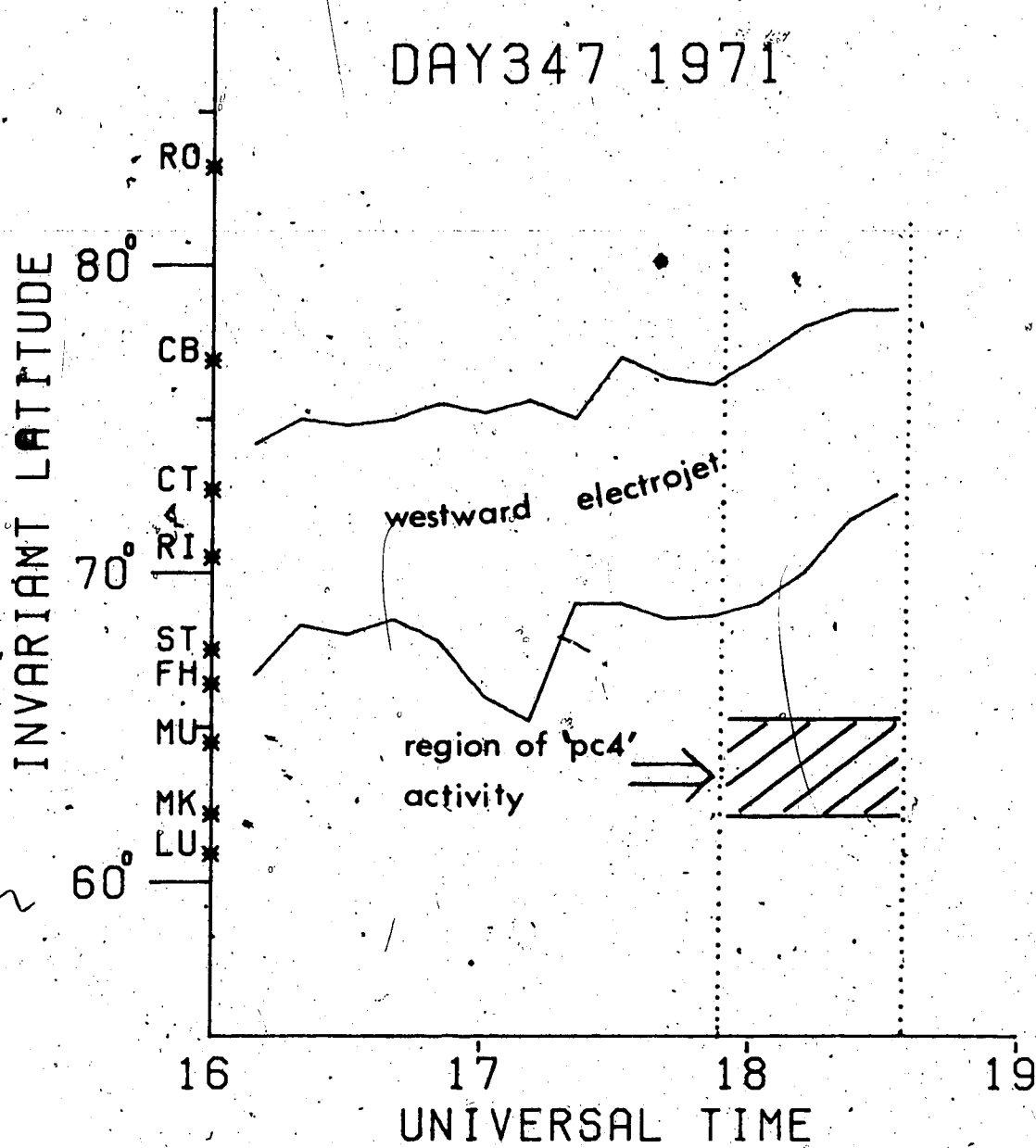


Figure 79

DAY 253 1974 (1330-1430)

H

0

Z

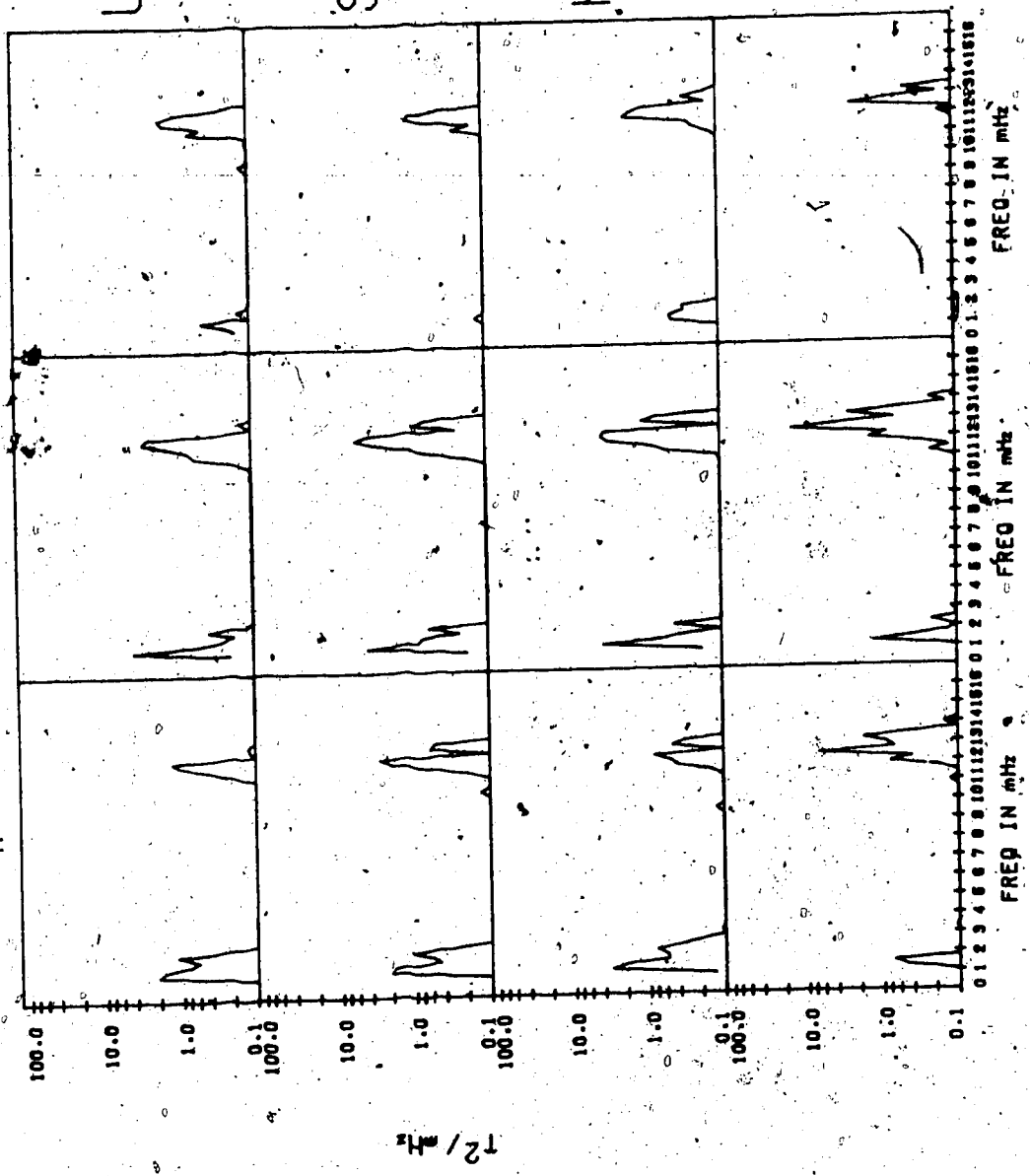
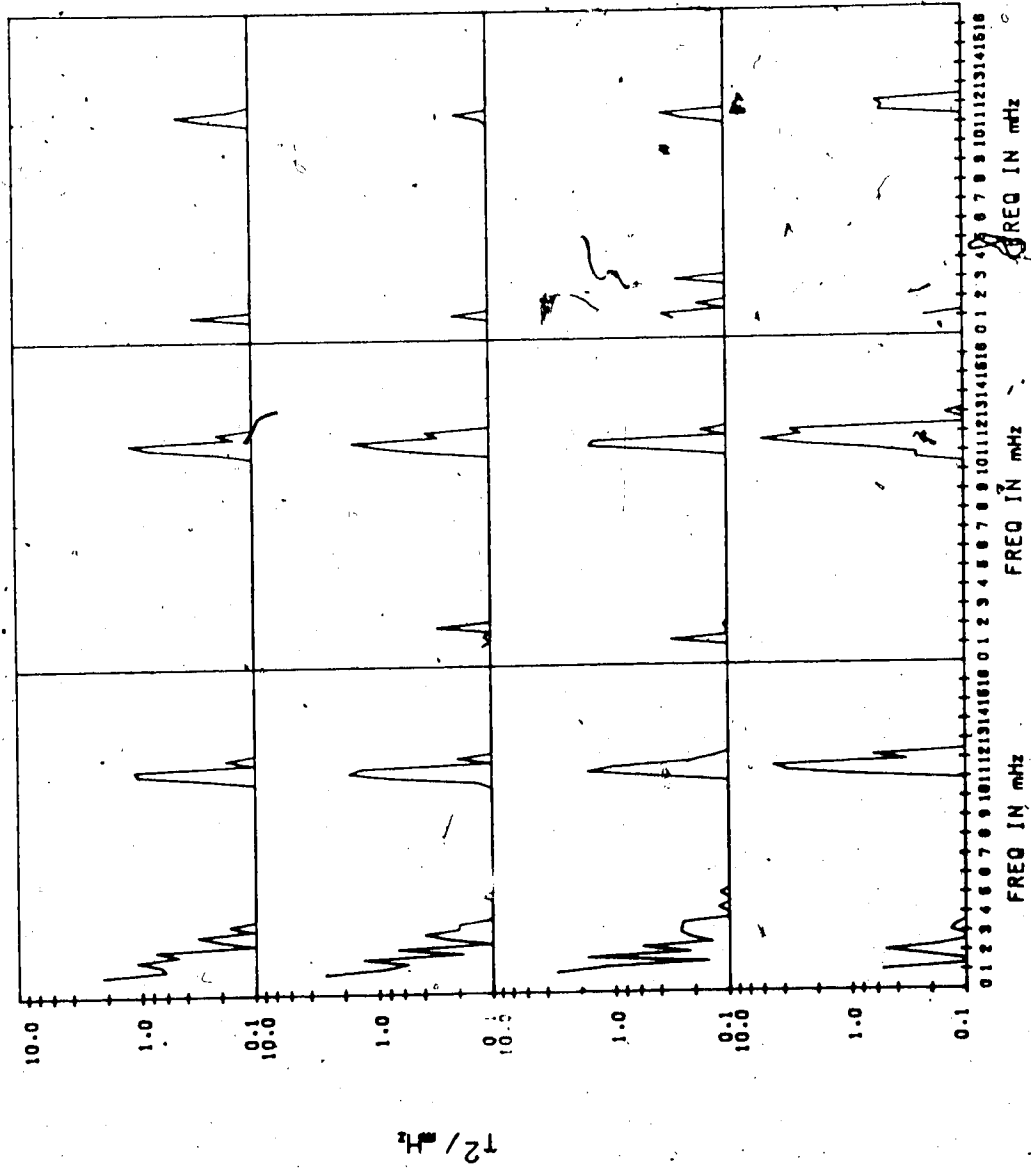


Figure 80

DAY 254 1974 (1945 - 1045)

H D Z





ment at URAN and MCMU. This implies that the signal is virtually noise-free reflecting the quiet state of the magnetosphere and that the signal is highly monochromatic.

The spectra for Day 255, 1974 in the interval between 1000 UT and 1100 UT are shown in Figure 82. The 'Pc 4' peak centered at  $\sim 11.7$  MHz is only pronounced at MCMU. The double peak feature is evident in the D-component at MCMU. Note also the complete absence of powers in any other frequency except the 'Pc 4' band in D at MCMU.

To study the characteristics of the 'Pc 4' pulsations, polarizations and phases were determined using the smoothed spectral estimates. The powers in three components, the relative phases across the stations and the polarization ellipses were plotted as a function of invariant latitude or dipole longitude for the 'Pc 4' spectral component for each event. The results are shown in the next few diagrams.

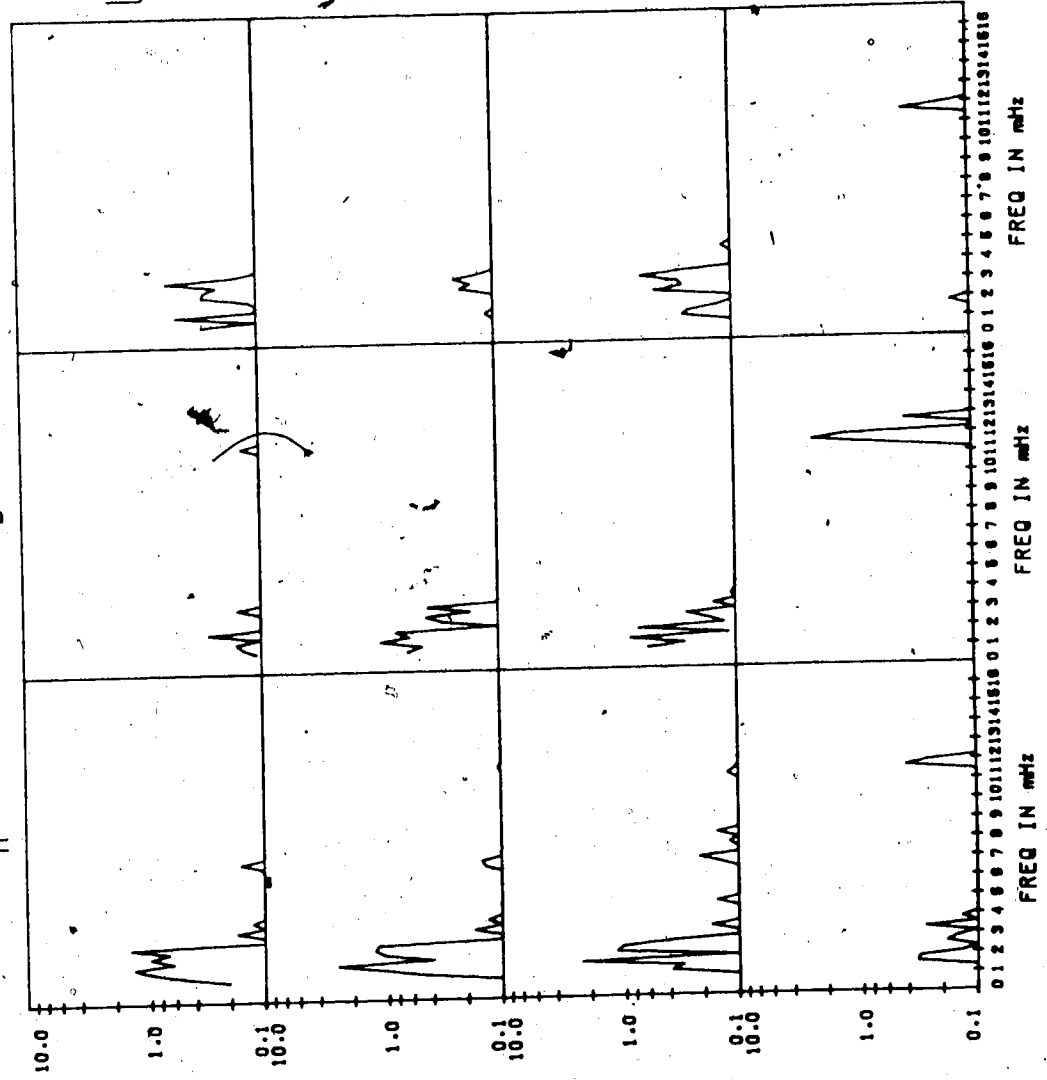
Figure 83 is the latitude profile for the pulsation characteristics at 11.2 MHz for Day 347, 1971 in the interval between 1745 and 1845. The latitude profile of the power indicates that the event is highly localized in latitude. The H power profile suggests that the peak power probably lies between MCMU and MENK. The power drops off rapidly to noise level in about  $4^\circ$  away from the peak. The relative phase plot shows that there is rapid phase change

DAY 255 1974 (1000-1100)

Z

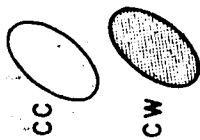
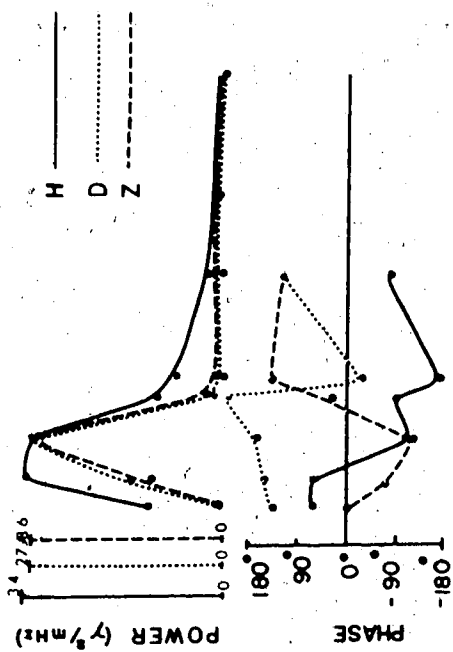
D

H



DAY 347, 1971 (1745-1845) 11.2 MHz

INLAT  
 L M F S C C R  
 60° 70° 80° 90°



between MCMU and MENK in H and between FTCH and SMIT in D. The phases at higher latitude stations were not plotted because of their low powers. The polarization ellipses projected in the H-D plane indicate that there is a switch in the sense of polarization between MCMU and MENK from CW sense of polarization to CC sense of polarization. In going from SMIT to LEDU, the ellipses in H-D plane are tilted towards the first quadrant except at MCMU where it is tilted towards the second quadrant and inclined towards the D direction indicating the large power in D. In going from SMIT to LEDU, the ellipses in the H-Z plane are aligned predominantly in the H direction with the exception of MCMU where the ellipse is tilted towards Z. The sense of polarization switches from CW to CC between MCMU and MENK. The sense of polarization in the H-Z plane for the stations where the effect of 'Pc 4' pulsations is felt is the same as the sense of polarization in the H-D plane. This behaviour is contrast to that of Pc 5 discussed in the last chapter. For the Pc 5 pulsations whose origin lies in the electrojet, the sense of polarization in the H-Z plane is opposite to the sense of polarization in the H-D plane.

Figures 84, 85 and 86 show longitude profiles of the characteristics of the 'Pc 4' giant pulsations recorded on Day 253, 254 and 255, 1974. The data from MCMU are

DAY 253,74 (1330 - 1430) at 12.5 MHz  
 DIPOLE LONG.

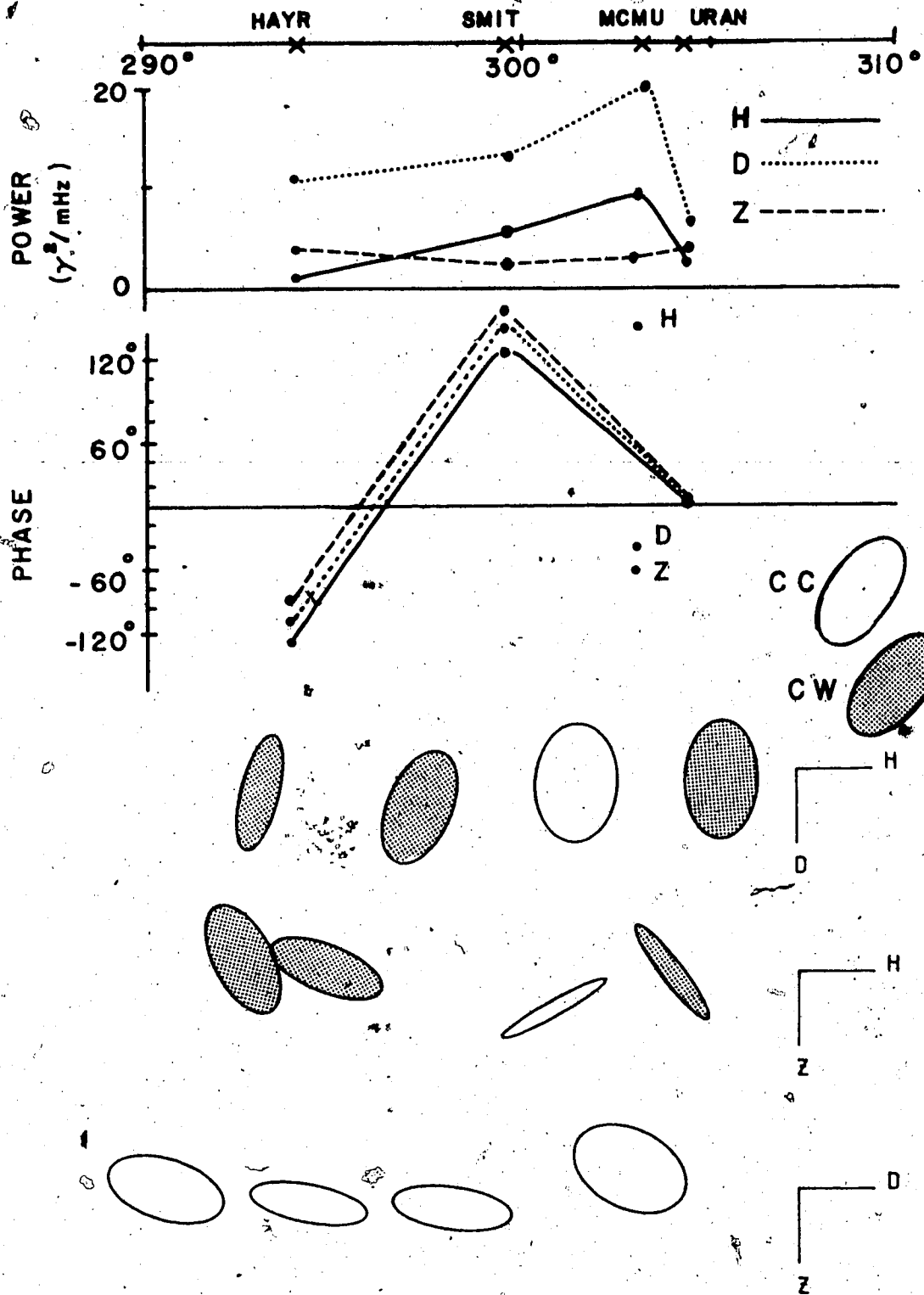


Figure 84

DAY 254, 74 (0945 - 1045) at 11.7 MHz

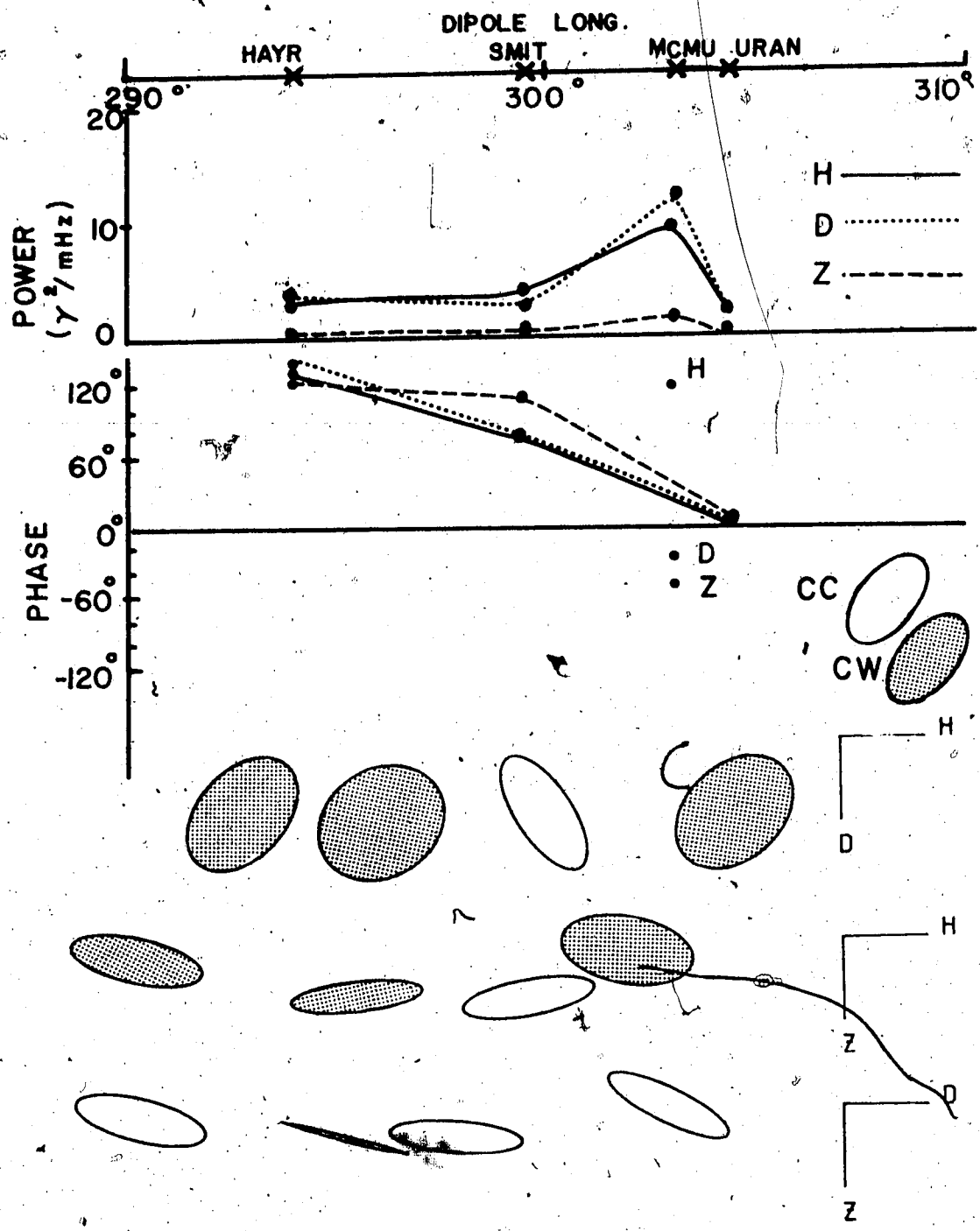


Figure 5

DAY 255,74 (1000 - 1100) at 11.7 MHz

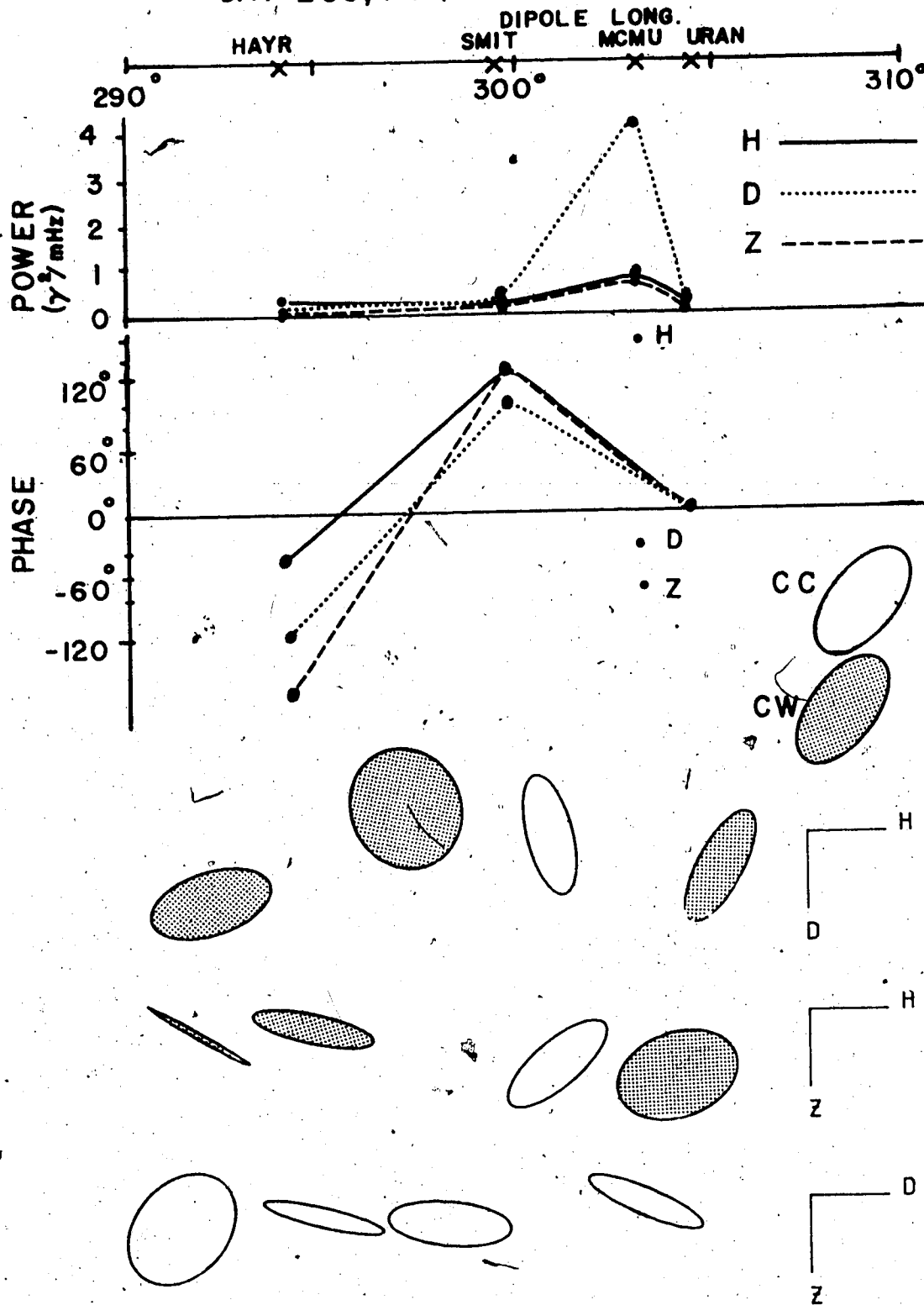


Figure 86

included on these profiles to allow comparisons to be made, although it must be remembered that MCMU is  $\sim 3^\circ$  equatorward of the other three stations and is nearly due south of URAN.

On Day 253 we see the power at 12.5 MHz over the Universal Time interval 1330-1430. The power is largest at MCMU, but tends to vary little in longitude over the  $\sim 15^\circ$  span of the coverage. The change in sense of polarization in the H-D and H-Z planes between MCMU and URAN is consistent with the source region being centered between these two stations. It is interesting to note that the senses of polarization in the H-D, H-Z and D-Z planes do not change across the longitudinal span of the array. However, there are outstanding phase reversals between URAN and SMIT and between SMIT and HAYR in all three components. We shall discuss the significance of these phase changes later in this chapter.

On Day 254 using the power at 11.7 MHz over the interval 0945-1045 UT we see behaviour of the micropulsation characteristics much the same as on Day 253, although the power levels are slightly lower. Again the peak power is at MCMU and there are phase changes in the H-D and H-Z planes between MCMU and URAN. Aside from a tendency for linear polarization in the D-Z plane at SMIT, the polarizations are unchanged over the longitude span of the array. Again the outstanding changes in relative phase in all three compo-



nents between URAN and SMIT are present but between SMIT and HAYR there is little relative phase change.

On Day 255, using the power at 11.7 MHz over the interval 1000-1100 UT, we again see behaviour of the micropulsation characteristics identical to those for Days 254 and 255. For this day the signal is highly localized in latitude, with MCMU being closest to the center of the source region. However, the power levels are considerably reduced from those on the previous two days. The relative phase changes in longitude precisely parallel those for Day 253.

For purposes of comparison with previous workers we draw attention to the detailed studies of Pc 4 giant pulsations which have been carried out by Eleman [1966] using data from eleven high latitude stations in Scandinavia. He claimed that these pulsations were distinguished by the fact that the vertical component of the perturbation is almost as large as the horizontal component near the center of the disturbed region. In agreement with Eleman we find that the vertical component may have magnitudes comparable to that of H near the source region although the power in the D-component usually exceeds that in the H-component. Although he found for most of the events that the pulsations were polarized in the CC sense in the horizontal plane, on some occasions he observed the polarization in the

horizontal plane to be polarized CW at the northern stations and CC at the southern stations. The latitudinal profile of the power and ellipses of the event we studied suggests that the stations north of the power peak had CW ellipses while stations to the south had CC ellipses in the horizontal plane. He also contended that the region of disturbance tended to remain fixed geographically during the lifetime of the 'Pc 4' pulsation event. He was unable, however, to settle on any theoretical explanation of the source of 'Pc 4' pulsations.

#### 5.2 Generation Mechanism for 'Pc 4'

Veldkamp [1960], after studying a 'Pc 4' event which had maximum amplitude at  $\sim 57^\circ$ N geomagnetic, contended that the observed period of 105 sec fits well with eigenoscillations of period  $\sim 100$  sec predicted by Obayashi and Jacobs [1958] for field lines penetrating  $57^\circ$  geomagnetic latitude. Annexstad and Wilson [1968], after studying 'Pc 4' events recorded at College and its conjugate, Macquarie Island, suggested that the 'Pc 4' is a result of the first even mode of transverse hydromagnetic wave propagating along field lines to conjugate points.

It would be of interest to estimate the eigenperiod of the toroidal and poloidal oscillations for field lines emanating from  $L=5.4$  which is the L value for MCMU where the amplitude of 'Pc 4' was maximized. We estimate the eigenperiod using the results of Orr and Matthew [1971].

Starting with the wave equation (4) for hydro-magnetic waves in a cold collisionless magnetized plasma derived earlier in Chapter II and assuming that the magnetospheric plasma is composed of protons and electrons with a number density distribution  $n = n_0 \left(\frac{r_0}{r}\right)^m$ , where  $n$  and  $n_0$  are the proton number densities at  $r$  and  $r_0$  respectively ( $r_0$  being the equatorial geocentric distance), Orr and Matthew derived an equation for axisymmetric toroidal oscillations and another equation for asymmetric guided poloidal oscillations. Both equations were integrated numerically for different plasma distribution defined by  $m = 2, 3$  and  $4$  and using the boundary condition that the electric field is zero at the earth's surface. The period for any particular field line with maximum equatorial geocentric distance  $r_0 = L$  is given by

$$T = 2\pi \left(\frac{r_0}{R_E}\right)^3 \frac{r_0}{B_E} \left[\frac{\mu_0 m_p n_0}{k c}\right]^{\frac{1}{2}} \quad (17)$$

where  $R_E = 6.37 \times 10^6$  m

$B_E = 3.12 \times 10^{-5}$  webers/m<sup>2</sup> (equatorial surface value of earth's magnetic field)

$\mu_0 = 4\pi \times 10^{-7}$  H/m

$m_p = 1.673 \times 10^{-27}$  kg

$k c = \omega^2 n_0$ , the eigenvalue for axisymmetric toroidal oscillations or asymmetric poloidal oscillations

Using equation (17) for  $L=5.4$  and the number densities of plasma in the plasma trough and inside the plasmapause in the equatorial plane (see Chappell, 1974), we obtain the following eigenperiods compiled in Table 7.

The eigenperiod  $T$  is in seconds and the frequency  $f$  is in mHz. It can be seen from the Table 7 that the first harmonic asymmetric guided poloidal oscillations for number densities of  $5 \text{ cm}^{-3}$ ,  $6 \text{ cm}^{-3}$  and  $10 \text{ cm}^{-3}$  have frequencies ranging from 8.9 mHz to 13.6 mHz depending on the number density and the power law of density distribution. The observed frequencies of our 'Pc 4' events lie in that range. The first harmonic axisymmetric toroidal oscillations for  $n_0 = 10 \text{ cm}^{-3}$  and the second harmonic axisymmetric toroidal oscillations for  $n_0 = 100 \text{ cm}^{-3}$  also have frequencies very close to the observed frequencies. Equation (4) is a very simplified representation of the much more complicated conditions in the magnetosphere. As mentioned earlier in Chapter II, toroidal and poloidal oscillations are generally coupled together. The shear mode is decoupled for resonance condition. The above calculation is to obtain a rough estimate of the range of frequencies within which the experimental observation should lie. The results are that the computed resonant frequencies seem to agree with the observed frequencies, thus giving some support to the contention that field line resonance might be the cause of the 'Pc 4' pulsations as it is definitely not related to the

Table 7 Eigenperiods for Axisymmetric Toroidal and Asymmetric Poloidal Oscillations

n <sub>0</sub>	1st Harmonic				2nd Harmonic					
	Toroidal		Poloidal		Toroidal					
1	T	24.3	24.9	25.9	32.8	33.9	35.4	9.9	10.6	11.5
	f	41.2	40.2	38.6	30.5	29.5	28.2	101.0	94.3	87.0
5	T	54.5	55.9	58.2	73.6	76.1	79.3	22.1	23.7	25.8
	f	18.3	17.9	17.2	13.6	13.1	12.6	45.2	42.2	38.8
6	T	59.6	61.1	63.7	80.4	83.2	86.7	24.2	25.9	28.2
	f	16.8	16.4	15.7	12.4	12.0	11.5	41.3	38.6	35.5
10	T	76.9	78.9	82.1	103.8	107.3	111.8	31.2	33.5	36.3
	f	13.0	12.7	12.2	9.6	9.3	8.9	32.1	29.9	27.5
100	T	243.4	249.6	259.9	328.3	339.5	353.9	98.8	105.9	115.0
	f	4.1	4.0	3.8	3.0	2.9	2.8	10.1	9.4	8.7
m		2	3	4	2	3	4	2	3	4

auroral westward electrojet which is the primary source for Pc 5 pulsations. Furthermore, the reversal of sense of polarization in latitudes across the intensity peak is predicted by the field line resonance model of Chen and Hasegawa [1974a] and Southwood [1974]. The monochromatic character of the 'Pc 4' events as demonstrated by the power spectra (see for example, the power spectra in D for MCMU and URAN in Figure 81) suggests that the driving force is composed of nearly monochromatic waves. This possibility was solved by Chen and Hasegawa [1974a] and Hasegawa and Chen [1974] as a steady state case. The solution exhibits surface wave away from the resonant field line and shear Alfvén waves near the resonant field line. The 'Pc 4' events presented here therefore strongly suggest the excitation of shear Alfvén waves by a monochromatic source. The tilt of the ellipses in the horizontal plane does not agree with that predicted by Chen and Hasegawa [1974] and Lanzerotti et al. [1974] who showed that the major axis direction does not switch across the resonant region and lies in the 2nd quadrant. Our observations indicate that there is some switch in the tilt of the ellipses across the resonant region. This might be due to the possible effects of the ionosphere on the rotation of the ellipse orientations [Hughes, 1974].

Finally, we would like to discuss several characteristics of this type of pulsations which are unique. An

examination of the standard magnetograms and an estimation of the wave number  $m$  using the relative phase change in longitude ( $m \approx 36$ ) indicate that the phenomenon is highly localized in longitude. 'Pc 4' pulsations might be a manifestation of the quiet state of the magnetosphere as exemplified by the event of Day 255, 1974 where the onset of substorm stops 'Pc 4' which reappears when the substorm activity terminates.

The daily recurrence tendency of the 1974 events suggests that the pulsations might be related to some structure within the magnetosphere (such as the plasmopause) which is maintained over a significant period of time. However, the plasmopause extends over all hours in local time, and hence one might ask why the oscillation region is so confined spatially. This leads one to look for some significant magnetospheric parameter which may suffer some transition in the local magnetic time regime occupied by the pulsations. It is interesting to note that the electric field observations of Mozer and Lucht [1974] (see Figure 63) indicate a transition from westward electric field to eastward electric field in the early morning hours and near noon. Such a transition would be associated with magnetic flux tubes drifting equatorward in the region of westward electric field and poleward in the region of eastward electric field. Thus field lines mapping to the plasmopause may suffer shear flows

at the region of electric field transition, and this may well prove to be a region which can be perturbed should the character of the convective flow be subjected to any change.



## CHAPTER VI

### SUMMARY OF RESULTS AND CONCLUSIONS

In this thesis we have studied in detail the characteristics of Pc 5 micropulsation activity in the morning sector and we have documented several cases of the rare 'Pc 4' giant pulsations. The following summarizes the major findings of this thesis.

#### 6.1 Pc 5 Micropulsations

One significant finding of this thesis is that there is no clear latitudinal dependence of the principal spectral components of the Pc 5 pulsations. The observation that all the spectral components peak within the same latitudinal range occupied by the convection westward electrojet rules out the possibility that Pc 5 pulsations are generated by the resonant oscillations of field lines for a reasonably normal density distribution of thermal plasma in the magnetosphere. This finding and the results of the analysis of the intensity contours and polarization parameters of the major spectral bands using the convection electrojet as a frame of reference point strongly to the three-dimensional current systems as a primary source for the Pc 5 micropulsations. In fact, we have shown that the spatial oscillations of the borders of the electrojet occur at frequencies which are clearly identifiable in the Pc 5 micropulsations.

We have emphasized that Pc 5 wave trains appear to be composed of a series of impulsive wave trains which merge together to present a picture of continuous activity. The response of the Pc 5 micropulsations to rapid changes in the configuration of the electrojet lends weight to the contention that Pc 5 pulsations should be thought of as a series of impulsive wave trains, each wave train being associated with a rapid change in magnetospheric parameters. In particular, the rapid poleward motion of the equatorward border of the electrojet are associated with marked enhancement of power in the Pc 5 spectrum. The Pc 5 oscillations therefore appear to represent the transient response of the three dimensional magnetosphere-ionosphere current system associated with large scale convection within the magnetosphere. The fact that the reconfiguration of the electrojet appears to occur in response to changes in the north-south component of the interplanetary magnetic field lends weight to our suggestion that sudden changes in the level of convection in the magnetosphere are responsible for the initiation of ringing of the current system (as proposed by Boström [1972] among others).

Based on our observational results, we have presented an equivalent circuit representing the magnetosphere-ionosphere current system. We have postulated that the current system is driven through the extraction of

kinetic energy from the plasma convecting sunward past the flanks of the magnetosphere, in manner discussed by Rostoker and Boström [1976]. A sudden change in the convective flow results in a sudden change of the convection electric field (which also drives the westward electrojet) resulting in a perturbation of the electric circuit. The perturbation will cause ringing at the frequency of the LC oscillations of the equivalent circuit. We have demonstrated that these oscillations would be in the Pc 5 frequency range for a circuit involving downward current flow near noon linked by the westward electrojet to upward flow at the dawn meridian.

Finally we have shown how a combination of spatial and temporal variations of the electrojet can give a plausible explanation of the relative phase change across our stations. Furthermore, by introducing the displacement current in the F-region and induction in the earth, we can explain the observed senses of polarization in the three orthogonal planes.

## 6.2 'Pc 4' Micropulsations

In contrast to the Pc 5 micropulsations, we have found evidence that the 'Pc 4' giant pulsations are not related to the westward electrojet although they appear to be influenced by the initiation of substorm activity. The latitude profile of the power in the principal spectral component reveals that this type of pulsation is highly

localized in latitude and the large azimuthal wave number deduced from the phase difference in longitude indicates that the activity is also highly localized in longitude. This feature might be related to the transition of the azimuthal electric field. The observed frequency of 'Pc 4' pulsations compares favourably with the eigenfrequency of the field lines penetrating the region of maximum amplitude for the asymmetric poloidal oscillations. The highly monochromatic nature of the event and the reversal in the sense of polarization across the region of peak intensity give support to the popular field line resonance model by Chen and Hasegawa [1974] and Southwood [1974].

### 6.3 Conclusions

There are undoubtedly different source mechanisms for different classes of ultra low frequency micropulsations. There might even be competing sources within the same class. From the detailed analysis of the Pc 5 micropulsation events, we contend that the three dimensional current system associated with magnetospheric convection dominates other sources in its contribution to the low frequency band of the micropulsation spectrum. However, we would expect that away from the influence of the electrojet during quiet conditions the field lines might be excited to resonate at their natural frequencies under certain conditions. The rare 'Pc 4' giant pulsations may well be due to field line resonances. Finally,

it should be pointed out that long period micropulsations, in addition to being a monitor of the solar-terrestrial interaction, might provide a useful tool for the study of induction in the earth.

## REFERENCES

- Alekseev, I.I., and V.P. Shabansky, A model of a magnetic field in the geomagnetosphere, *Planet. Space Sci.*, 20, 117, 1972.
- Alfvén, H., On the existence of electromagnetic-hydromagnetic waves, *Ark. Mat.* 29B, No. 2, 1942.
- Alfvén, H., and C.-G. Fälthammer, *Cosmical Electrodynamics*, Oxford University Press, 1963.
- Alpaslan, T., Spectral behaviour of short period body waves and the synthesis of crustal structure in Western Canada, M.Sc. Thesis, University of Alberta, Edmonton, Canada, 1968.
- Annexstad, J.O., and C.R. Wilson, Characteristics of Pg micropulsations at conjugate points, *J. Geophys. Res.*, 73, 1805, 1968.
- Arnoldy, R.L., Signature in the interplanetary medium for substorms, *J. Geophys. Res.*, 76, 5189, 1971.
- Atkinson, G., and T. Watanabe, Surface waves on the magnetospheric boundary as a possible origin of long period geomagnetic micropulsations, *Earth Planet. Sci. Lett.*, 1, 89, 1966.
- Barfield, J.N., R.L. McPherron, P.J. Coleman, Jr., and D.J. Southwood, Storm-associated Pc 5 micropulsation events observed at the synchronous equatorial orbit, *J. Geophys. Res.*, 77, 143, 1972.
- Barston, E.M., Electrostatic oscillations in inhomogeneous cold plasma, *Ann. Phys.*, 20, 282, 1964.
- Biermann, L., Kometenschwerfe and solare Korpuskularstrahlung, *Z. Astrophys.*, 29, 274-286, 1951.
- Birkeland, Kr., *The Norwegian Aurora Polaris Expedition 1902-03, Vol. 1, On the Cause of Magnetic Storms and the Origin of Terrestrial Magnetism, first section*, H. Aschehoug and Co., Christiania, 1908.

- Birkeland, Kr., The Norwegian Aurora Polaris Expedition 1902-03, Vol. 1, On the Cause of Magnetic Storms and the Origin of Terrestrial Magnetism, second section, H. Aschehoug and Co., Christiania, 1913.
- Boller, B.R., and H.L. Stolov, Kelvin-Helmholtz instability and semiannual variation of geomagnetic activity, J. Geophys. Res., 75, 6073, 1970.
- Bonnevier, B., R. Boström, and G. Rostoker, A three-dimensional model current system for polar magnetic substorms, J. Geophys. Res., 75, 107, 1970.
- Born, M., and E. Wolf, Principles of Optics, Pergamon Press, New York, 1959.
- Boström, R., Magnetosphere-ionosphere coupling, in: Critical Problems of Magnetospheric Physics, (ed. E.R. Dyer), IUCSTP Secretariat, c/o National Academy of Sciences, Washington, D.C., 139, 1972.
- Brown, W.L., L.J. Cahill, L.R. Davis, C.E. McIlwain, and C.S. Roberts, Acceleration of trapped particles during magnetic substorm on April 18, 1965, J. Geophys. Res., 73, 153, 1968.
- Campbell, W.H., Geomagnetic pulsations, in: Physics of Geomagnetic Phenomena, (ed. S. Matsushita and W.H. Campbell), Academic Press, New York, 821-909, 1967.
- Carovillano, R.L., H.R. Radoski, and J.F. McClay, Poloidal hydromagnetic plasmaspheric resonances, Phys. Fluids, 9, 1860, 1966.
- Chandrasekhar, S., A.N. Kaufman, and K.M. Watson, The stability of the pinch, Proc. Roy. Soc. (London), 245A, 435, 1958.
- Chapman, S., and V.C.A. Ferraro, A new theory of magnetic storms, Terrest. Magn. Atmosph. Elec., 36, 77-97, 1931.
- Chapman, S., Interplanetary space and the earth's outermost atmosphere, Proc. Roy. Soc. (London), 253A, 462, 1959.
- Chappell, C.R., Recent satellite measurement of the morphology and dynamics of the plasmasphere, Rev. Geophys. Space Phys., 10, 961, 1972.

- Chappell, C.R., Detached plasma regions in the magnetosphere, *J. Geophys. Res.*, 79, 1861, 1974.
- Chen, L., and A. Hasegawa, A theory of long-period magnetic pulsations, 1, Steady state excitation of field line resonance, *J. Geophys. Res.*, 79, 1024, 1974a.
- Chen, L., and A. Hasegawa, A theory of long-period magnetic pulsations, 2, Impulse excitation of surface eigenmode, *J. Geophys. Res.*, 79, 1033, 1974b.
- Cladis, J.B., Multiply coupled oscillations of field lines in the magnetosphere: modulation of trapped particles and ionospheric currents, *J. Geophys. Res.*, 76, 2345, 1971.
- Dessler, A.J., The stability of the interface between the solar wind and the geomagnetic field, *J. Geophys. Res.*, 66, 3587, 1961.
- Dessler, A.J., and J.A. Eejer, Interpretation of Kp index and M-region geomagnetic storms, *Planet. Space Sci.*, 11, 505, 1963.
- Dungey, J.W., Conditions for the occurrence of electrical discharges in astrophysical systems, *Phil. Mag.*, 44, 725, 1953.
- Dungey, J.W., Electrodynamics of the outer atmosphere, *Ionos. Res. Lab. Sci. Rep. 69*, Pennsylvania State University, 1954.
- Dungey, J.W., Interplanetary magnetic field and the auroral zones, *Phys. Rev. Letters*, 6, 47, 1961.
- Dungey, J.W., Effects of electromagnetic perturbations on particles trapped in the radiation belts, *Space Sci. Rev.*, 4, 199, 1965.
- Dungey, J.W., Hydromagnetic waves, in: *Physics of Geomagnetic Phenomena*, (ed. S. Matsushita and W.H. Campbell), Academic Press, New York, 913, 1967.
- Dungey, J.W., and D.J. Southwood, Ultra low frequency waves in the magnetosphere, *Space Sci. Rev.*, 10, 672, 1970.
- Egeland, A., Spectral density functions of hydromagnetic emissions at high latitude, *Nature*, 208, 539, 1965.
- Eleman, F., Studies of giant pulsations, continuous pulsations, and pulsation trains in the geomagnetic field, *Ark. För Geof.*, 5, 231, 1966.



- Ellis, G.R.A., Geomagnetic micropulsations, *Austr. J. Phys.*, 13, 625, 1960.
- Fairfield, D.H., and L.J. Cahill, Jr., Transition region magnetic field and polar magnetic disturbances, *J. Geophys. Res.*, 71, 155, 1966.
- Fejer, J.A., Hydromagnetic stability at a fluid velocity discontinuity between compressible fluids, *Phys. Fluids*, 7, 499, 1964.
- Ferraro, V.C.A., and C. Plumpton, *Magneto-fluid mechanics*, Oxford University Press, 1966.
- Fowler, R.A., B.J. Kotick, and R.D. Elliot, Polarization analysis of natural and artificially induced geomagnetic micropulsations, *J. Geophys. Res.*, 72, 2871, 1967.
- Frank, L.A., Plasma in the earth's polar magnetosphere, *J. Geophys. Res.*, 76, 5202, 1971.
- Fukunishi, H., L.J. Lanzerotti, and C.G. MacLennan, Three-dimensional polarization characteristics of magnetic variations in the Pc 5 frequency range at conjugate areas near L=4, *J. Geophys. Res.*, 80, 3973, 1975.
- Gentleman, W.M., and G. Sande, Fast Fourier transform for fun and profit, AFIPS proc., Fall Joint-Computer Conf., 29, 563, 1966.
- Green, C.A., The longitudinal phase variation of mid-latitude Pc 3-4 micropulsations, *Planet. Space Sci.*, 24, 79, 1976.
- Grossmann, W., and J. Tataronis, Decay of MHD waves by phase mixing, 2, The theta-pinch in cylindrical geometry, *Z. Phys.*, 261, 217, 1973.
- Gupta, J.C., Occurrence studies of geomagnetic micropulsations Pc 5 at high latitudes, *J. Atmos. Terr. Phys.*, 35, 2217, 1973.
- Gupta, J.C., Amplitude variation of Pc 5 pulsations at high latitude, *Radio Sci.*, 9, 757, 1974.
- Harang, L., Observations of micropulsations in the magnetic records at Tromso, *Terrest. Mag.*, 37, 57, 1932.

- Harang, L., Oscillations and vibrations in magnetic record at high latitude stations, *Terrest. Mag.*, 41, 329, 1936.
- Harang, L., Pulsations in an ionized region at height of 650-800 km during the appearance of giant pulsations in the geomagnetic records, *Terrest. Mag.*, 44, 17, 1939.
- Harang, L., Pulsations in the terrestrial magnetic records at high latitude stations, *Geophys. Publ.*, 13, 3, 1940-1944.
- Hasegawa, A., Drift mirror instability in the magnetosphere, *Phys. Fluids*, 12, 2642, 1969.
- Hasegawa, A., Plasma instabilities in the magnetosphere, *Rev. Geophys.*, 9, 703, 1971.
- Hasegawa, A., and L. Chen, Theory of magnetic pulsations, *Space Sci. Rev.*, 16, 347, 1974.
- Heikkila, W.J., Aurora, *EOS Trans. AGU*, 54, 764, 1973.
- Helmholtz, H., Ueber discontinuierliche Flüssigkeitsbewegungen, *Wissenschaftliche Abhandlungen*, 146, J.A. Barth, Leipzig, 1882, translation by Guthrie in *Phil. Mag.*, Ser. 4, 36, 337, 1868.
- Heppner, J.P., A study of relationships between the aurora borealis and the geomagnetic disturbances caused by electric currents in the ionosphere, Ph.D. Thesis, Calif. Inst. of Technol., Pasadena, Calif., 1954.
- Heppner, J.P., The Harang discontinuity in auroral belt ionospheric currents, *Geophys. Publ.*, 29, 105, 1972.
- Hirasawa, T., Long-period geomagnetic pulsations (Pc 5) with typical sinusoidal waveforms, *Rep. Ionos. Space Res. Japan*, 24, 66, 1970.
- Holzer, T.E., and G.C. Reid, The response of the day side magnetosphere-ionosphere system to time-varying field line reconnection at the magnetopause, 1, Theoretical Model, *J. Geophys. Res.*, 80, 2041, 1975.
- Hughes, T.J., and G. Rostoker, Current flow in the magnetosphere during periods of moderate activity, *J. Geophys. Res.*, submitted for publication, 1976.

- Hughes, W.J., The effect of the atmosphere and ionosphere on long period magnetospheric micropulsations, Planet. Space Sci., 22, 1157, 1974.
- Hultqvist, B., Plasma waves in the frequency range 0.0001-10 cps in the earth's magnetosphere and ionosphere, Space Sci. Rev., 5, 599, 1966.
- Jacobs, J.A., and K. Sinno, World-wide characteristics of geomagnetic micropulsations, Geophys. J., 3, 333, 1960.
- Jacobs, J.A., Y. Kato, S. Matsushita, and A. Troitskaya, Classification of geomagnetic micropulsations, J. Geophys. Res., 69, 180, 1964.
- Jacobs, J.A., and K.O. Westphal, Geomagnetic micropulsations in Physics and Chemistry of the Earth, 5, 157, 1964.
- Jacobs, J.A., and C.S. Wright, Geomagnetic micropulsation results from Byrd Station and Great Whale River, Can. J. Phys., 43, 2099, 1965.
- Jacobs, J.A., Geomagnetic Micropulsations, Springer-Verlag, New York, 1970.
- Jenkins, G.M., and D.G. Watts, Spectral Analysis and its Applications, Holden-Day, San Francisco, 1968.
- Kaneda, E., S. Kokubun, T. Oguti, and T. Nagata, Auroral radar echoes associated with Pc 5, Rep. Ionos. Space Res. Japan, 18, 165, 1964.
- Kato, Y., and S. Akasofu, Outer atmospheric oscillation and geomagnetic micropulsation, Sci. Rep. Tohoku Univ., Ser. 5, Geophys., 7, 103, 1955.
- Kato, Y., and T. Watanabe, Studies on geomagnetic pulsations, Pc., Sci. Rep. Tohoku Univ., Ser. 5, Geophys., 8, 111, 1957.
- Kato, Y., and T. Saito, Morphological study of geomagnetic pulsations, J. Phys. Soc. Japan, 17, Suppl. A-II, 34, 1962.
- Kato, Y., and T. Utsumi, Polarization of long period geomagnetic pulsation, Pc 5, Rep. Ionos. Space Rev. Japan, 18, 214, 1964.

- Kelvin, L., Influence of wind and capillarity on waves in water supposed frictionless, Hydrodynamics and General Dynamics, Cambridge, England, 1910.
- Kimura, I., and H. Matsumoto, Hydromagnetic wave instabilities in a nonneutral plasma-beam system, Radio Sci., 3, 333, 1968.
- Kisabeth, J.L., and G. Rostoker, Development of the polar electrojet during polar magnetic substorms, J. Geophys. Res., 76, 6815, 1971.
- Kisabeth, J.L., The dynamical development of the polar electrojets, Ph.D. Thesis, Univ. of Alberta, Edmonton, Canada, Fall, 1972.
- Kisabeth, J.L., Substorm fields in and near the auroral zone, Phys. Earth Planet. Int., 10, 241, 1975.
- Kokubun, S., and T. Nagata, Geomagnetic pulsation Pc 5 in and near the auroral zone, Rep. Ionos. Space Res. Japan, 19, 158, 1965.
- Korobkova, G., N. Nikitina, E. Zubareva, and V.A. Troitskaya, Giant pulsations in the Soviet Arctic (for the period 1935-1956), I.A.G.A. Symposium on Rapid Geomagnetic Variations, Utrecht, 1959.
- Lam, H., and G. Rostoker, The relationship of Pc 5 micro-pulsation activity in the morning sector to the auroral westward electrojet, EOS Trans. AGU, 56, 1043, 1975.
- Langel, R.A., Near-earth magnetic disturbance in total field at high latitudes, 2, Interpretation of data from Ogo 2, 4, and 6, J. Geophys. Res., 79, 2373, 1974.
- Lanzerotti, L.J., A. Hasegawa, and N.A. Tartaglia, Morphology and interpretation of magnetospheric plasma waves at conjugate points during December Solstice, J. Geophys. Res., 77, 6731, 1972.
- Lanzerotti, L.J., H. Fukunishi, A. Hasegawa, and L. Chen, Excitation of the plasmopause at ULF frequencies, Phys. Rev. Lett., 31, 624, 1973.
- Lanzerotti, L.J., and H. Fukunishi, Modes of magneto-hydrodynamic waves in the magnetosphere, Rev. Geophys., 12, 724, 1974.

- Lanzerotti, L.J., H. Fukunishi, and L. Chen, ULF pulsation evidence for the plasmopause, 3, Interpretation of polarization and spectral amplitude studies of Pc 3 and Pc 4 pulsations near L=4, J. Geophys. Res., 79, 4648, 1974.
- Lanzerotti, L.J., G.G. MacLennan, H. Fukunishi, J.K. Walker, and D.J. Williams, Latitude and longitude dependence of storm time Pc 5 type plasma wave, J. Geophys. Res., 80, 1014, 1975.
- Lassen, K., Relation of the plasma sheet to the nighttime auroral oval, J. Geophys. Res., 79, 3857, 1974.
- Lundquist, S., Studies in magneto-hydrodynamics, Ark. Fysik., 5, 297, 1952.
- McClay, J.F., On the resonant modes of a cavity and the dynamical properties of micropulsations, Planet. Space Sci., 18, 1673, 1970.
- McClay, J.F., On the asymmetric nature of micropulsations, I, The spectrum, Planet. Space Sci., 21, 2193, 1973.
- McDiarmid, I.B., J.R. Burrows, and M.D. Wilson, Solar particles and dayside limit of closed field lines, J. Geophys. Res., 77, 1103, 1972.
- Mead, G.D., and D.H. Fairfield, A quantitative magnetospheric model derived from spacecraft magnetometer data, J. Geophys. Res., 80, 523, 1975.
- Meng, C.I., B. Tsurutani, K. Kawasaki, and S.I. Akasofu, Cross-correlation analysis of the AE index and the interplanetary magnetic field  $B_z$  components, J. Geophys. Res., 78, 617, 1973.
- Mozer, F.S., and P. Lucht, The average auroral zone electric field, J. Geophys. Res., 79, 1001, 1974.
- Nagata, T., S. Kokubun, and T. Iijima, Geomagnetically conjugate relationships of giant pulsations at Syowa Base, Antarctica and Reykjavik, Iceland, J. Geophys. Res., 68, 4621, 1963.
- Nopper, Jr., R.W., and J.F. Hermance, Phase relations between polar magnetic substorm fields at the surface of a finitely conducting earth, J. Geophys. Res., 79, 4799, 1974.

- Obayashi, T., and J.A. Jacobs, Geomagnetic pulsation and the earth's outer atmosphere, *Geophys. J.*, 1, 53, 1958.
- Obertz, P., and O.M. Raspopov, Study of the spatial characteristics of type Pc 5 geomagnetic pulsations, *Geomag. Aeron.*, 8, 424, 1968.
- Ol', A.I., Long period gigantic geomagnetic field pulsations, *Geomag. Aeron.*, 3, 90, 1963.
- Orr, D., and J.A.D. Matthew, The variation of geomagnetic micropulsation period with latitude and the plasmopause, *Planet. Space Sci.*, 19, 897, 1971.
- Orr, D., Magnetic pulsations within the magnetosphere: A review, *J. Atmos. Terr. Phys.*, 35, 1, 1973.
- Parker, E.N., The hydrodynamic theory of solar corpuscular radiations and stellar winds, *Astrophys. J.*, 132, 821, 1960.
- Parker, E.N., *Interplanetary dynamical processes. Interscience Monographs in Physics and Astronomy, Vol. VIII*, Interscience Publ., 1963.
- Paulson, K.V., A. Egeland, and F. Eleman, A statistical method for quantitative analysis of geomagnetic giant pulsations, *J. Atmos. Terr. Phys.*, 27, 943, 1965.
- Pope, J.H., An explanation for the apparent polarization of some geomagnetic micropulsations, *J. Geophys. Res.*, 69, 399, 1964.
- Radoski, H.R., Magnetic toroidal resonances and vibrating field lines, *J. Geophys. Res.*, 71, 1891, 1966.
- Radoski, H.R., Highly asymmetric MHD resonances: the guided poloidal mode, *J. Geophys. Res.*, 72, 4026, 1967.
- Radoski, H.R., The effect of asymmetry on toroidal hydro-magnetic waves in a dipole field, *Planet. Space Sci.*, 20, 1015, 1972.
- Radoski, H.R., A theory of latitude dependent geomagnetic micropulsations: The asymptotic fields, *J. Geophys. Res.*, 79, 595, 1974.

- Rankin, D., and R. Kurtz, Statistical study of micropulsation polarizations, *J. Geophys. Res.*, 75, 5444, 1970.
- Reid, G.C., and T.E. Holzer, The response of the dayside magnetosphere-ionosphere system to time-varying field line reconnection at the magnetopause, 2, Erosion event of March 27, 1968, *J. Geophys. Res.*, 80, 2050, 1975.
- Rolf, B., Giant Micropulsations at Abisko, *Terrest. Mag.*, 36, 9, 1931.
- Rosenbauer, H., H. Grunwaldt, M.D. Montgomery, G. Paschmann, and N. Sckoppe, Heos 2 plasma observations in the distant polar magnetosphere: The plasma mantle, *J. Geophys. Res.*, 80, 2723, 1975.
- Rostoker, G., and C.G. Fälthammar, Relationship between changes in the interplanetary magnetic field and variations in the magnetic field at the earth's surface, *J. Geophys. Res.*, 72, 5583, 1967.
- Rostoker, G., H. Lam, and W.D. Hume, Response time of the magnetosphere to the interplanetary electric field, *Can. J. Phys.*, 50, 544, 1972.
- Rostoker, G., and J.C. Samson, Pc micropulsations with discrete latitude-dependent frequencies, *J. Geophys. Res.*, 77, 6249, 1972.
- Rostoker, G., and R. Boström, A mechanism for driving the gross Birkeland current configuration in the auroral oval, 81, 235, 1976.
- Rostoker, G., The entry of the solar wind plasma into the magnetosphere and the formation of the plasma sheet, *J. Geophys. Res.*, submitted for publication, 1976.
- Saito, T., Mechanisms of geomagnetic continuous pulsations and physical states of the exosphere, *J. Geomag. Geoelect.*, 16, 115, 1964.
- Saito, T., and S. Matsushita, Geomagnetic pulsations associated with sudden commencements and sudden impulses, *Planet. Space Sci.*, 15, 573, 1967.
- Saito, T., Geomagnetic pulsations, *Space Sci. Rev.*, 10, 319, 1969.

- Samson, J.C., J.A. Jacobs, and G. Rostoker, Latitude-dependent characteristics of long-period geomagnetic micropulsations, *J. Geophys. Res.*, 76, 3675, 1971.
- Samson, J.C., Spectral characteristics of Pc 4 and Pc 5 geomagnetic micropulsations, Ph.D. Thesis, University of Alberta, Edmonton, Alberta, Canada, 1971.
- Samson, J.C., and G. Rostoker, Latitude-dependent characteristics of high-latitude Pc 4 and Pc 5 micropulsations, *J. Geophys. Res.*, 77, 6133, 1972.
- Samson, J.C., Three-dimensional polarization characteristics of high-latitude Pc 5 geomagnetic micropulsations, *J. Geophys. Res.*, 77, 6145, 1972.
- Sedláček, Z., Electrostatic oscillations in cold inhomogeneous plasma, 1, Differential equation approach, *J. Plasma Phys.*, 5, 239, 1971a.
- Sedláček, Z., Electrostatic oscillations in cold inhomogeneous plasma, 2, Integral equation approach, *J. Plasma Phys.*, 6, 187, 1971b.
- Sen, A.K., Stability of the magnetospheric boundary, *Planet. Space Sci.*, 13, 131, 1965.
- Sersen, P.H., An electrical recording magnetometer, *Can. J. Phys.*, 35, 1387, 1957.
- Siebert, M., Geomagnetic pulsations with latitude dependent periods and their relation to the structure of the magnetosphere, *Planet. Space Sci.*, 12, 137, 1964.
- Southwood, D.J., The hydromagnetic stability of the magnetospheric boundary, *Planet. Space Sci.*, 16, 587, 1968.
- Southwood, D.J., J.W. Dungey, and R.J. Etherington, Bounce resonant interaction between pulsations and trapped particles, *Planet. Space Sci.*, 17, 349, 1969.
- Southwood, D.J., Some features of field line resonances in magnetosphere, *Planet. Space Sci.*, 22, 483, 1974a.
- Southwood, D.J., Recent studies in micropulsation theory, *Space Sci. Rev.*, 16, 413, 1974b.



- Southwood, D.J., Micropulsations and the plasmopause, *Ann. Géophys.*, t.31, 101, 1975.
- Stewart, B., On the great magnetic disturbance which extended from August 28 to September 7, 1859, as recorded by photography at the Kew Observatory, *Phil. Trans. Roy. Soc. London*, 423, 1861.
- Störmer, C., Sur les trajectoires périodiques des corpuscles électriques dans l'espace sous l'influence du magnétisme terrestre, avec application aux perturbations magnétiques, *Comptes Rendus*, 143, 1906.
- Sucksdorff, E., Giant pulsations recorded at Sodankyla during 1914-1938, *Terrest. Mag.*, 44, 157, 1939.
- Swift, D.W., A new interpretation of long period micropulsations, *J. Geophys. Res.*, 72, 4885, 1967.
- Trigg, D.F., P.H. Sersen, and P.A. Camfield, A solid-state electrical recording magnetometer, Preprint, Earth Physics Branch, Dept. Energy, Mines and Resources, Ottawa, Canada, 1970.
- Troitskaya, V.A., Micropulsations and the state of the magnetosphere, in: *Solar-Terrestrial Physics*, edited by J.W. King and W.S. Newman, Academic Press, 213, 1967.
- Uberoi, C., Alfvén waves in inhomogeneous magnetic fields, *Phys. Fluids*, 15, 1673, 1972.
- Veldkamp, J., A giant geomagnetic pulsation, *J. Atmospheric Terrest. Phys.*, 17, 320, 1960.
- Voelker, H., Observations of geomagnetic pulsations: Pc 3, 4, and Pi 2 at different latitudes, *Ann. Géophys.*, 24, 245, 1968.
- Walker, J.K., Space-time association of the aurora and magnetic disturbances, *J. Atmos. Terr. Phys.*, 26, 951, 1964.
- Watanabe, T., Hydromagnetic oscillation of the outer ionosphere and geomagnetic pulsation, *J. Geomag. Geoelec.*, 10, 195, 1959.

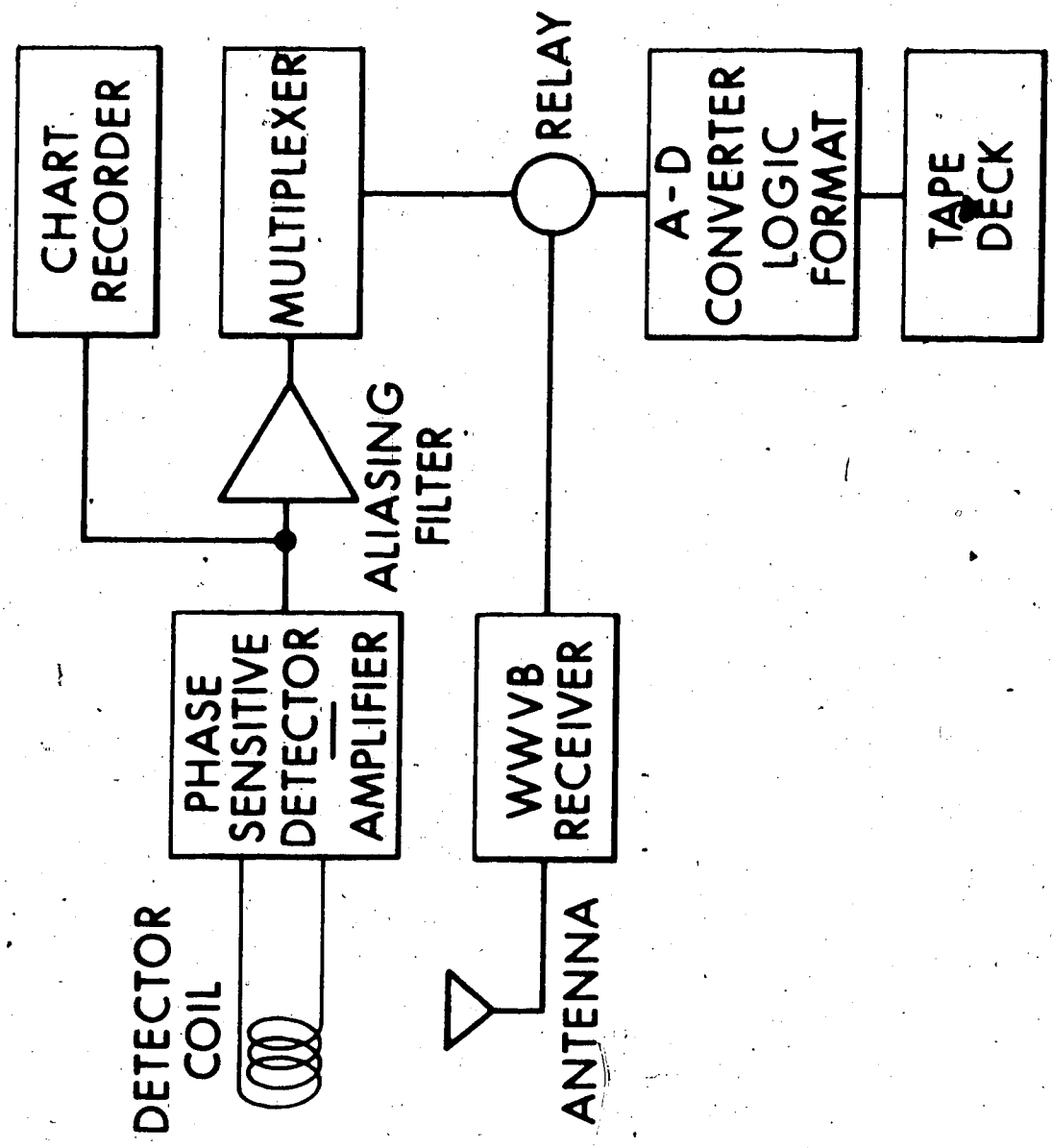
- Westphal, K.O., and J.A. Jacobs, Oscillations of the earth's outer atmosphere and micropulsations, *Geophys. J.*, 6, 360, 1962.
- Wilson, C.R., Conjugate three-dimensional polarization of high-latitude micropulsations from a hydromagnetic wave-ionosphere current model, *J. Geophys. Res.*, 71, 3233, 1966.
- Yasuhara, F., Y. Kamide, and S.-I. Akasofu, Field aligned and ionospheric currents, *Planet. Space Sci.*, 23, 1355, 1975.
- Zmuda, A.J., and J.C. Armstrong, The diurnal flow pattern of field-aligned currents, *J. Geophys. Res.*, 79, 4611, 1974.

## APPENDIX A

### INSTRUMENTATION

The equipment used to measure and record the fluctuations of the earth's magnetic field is basically a three component fluxgate magnetometer, whose output (in the form of DC voltage levels) is recorded on magnetic tape using an analog-to-digital recording system. The recording of data in digital form enables maximum efficiency for data handling through the ability to directly process the data using a computer. The basic components of the recording system are shown in Figure A1. Each system includes a three-component fluxgate magnetometer, analog-to-digital converter, digital tape recorder, WWVB time code receiver and the necessary external power supplies and regulators. Data were recorded on seven-track magnetic tapes at a rate of 1.56 samples/second (corresponding to a sample interval of 1.92 second/component). The records were timed by recording a WWVB time code signal for 2 minutes directly on tape at 7.5 hours intervals.

All magnetometers, except the one at Leduc (where a Sharpe MF0-3 was used), were three-component fluxgate magnetometers of the type designed by Dr. P. H. Serson of the Geomagnetic Division of the Department of Energy, Mines



and Resources and manufactured by E.D.A. Electronics Ltd. The theory behind the fluxgate system has been discussed by Serson [1957] and the design specifications and results of tests performed on the magnetometer under normal field conditions have been presented in detail by Trigg et al. [1970]. The Sharpe MF0-3 magnetometer has similar specifications except for better long term stability ( $\pm 1\gamma/24$  hrs at constant temperature), a smaller temperature coefficient ( $\pm 0.5\gamma/^\circ\text{C}$ ) and a broader frequency response (D.C. to 55 Hz, -3db).

The sensing head of the magnetometer was mounted on an aluminum pole set in concrete at the bottom of a plastic container. The head was located where it was not likely to be disturbed by moving magnetic objects. The container was buried in the ground to reduce diurnal temperature variations, the top being  $\sim 6$  to 10 inches below the surface. The outputs from the X, Y and Z amplifiers are linear over the dynamic range ( $\pm 10\text{V}$ ) as shown in Figure A2. The phase and gain curves are essentially flat from DC to 0.1 Hz as shown in Figure A3. The sensitivity, resolution and dynamic range of the magnetometer are 1 volt/100 $\gamma$ ,  $\pm 1\gamma$ , and  $\pm 1000\gamma$  (from baseline) respectively.

The major problem with the fluxgate magnetometer is its sensitivity to temperature variation. The value of the temperature coefficient given by the manufacturer of the

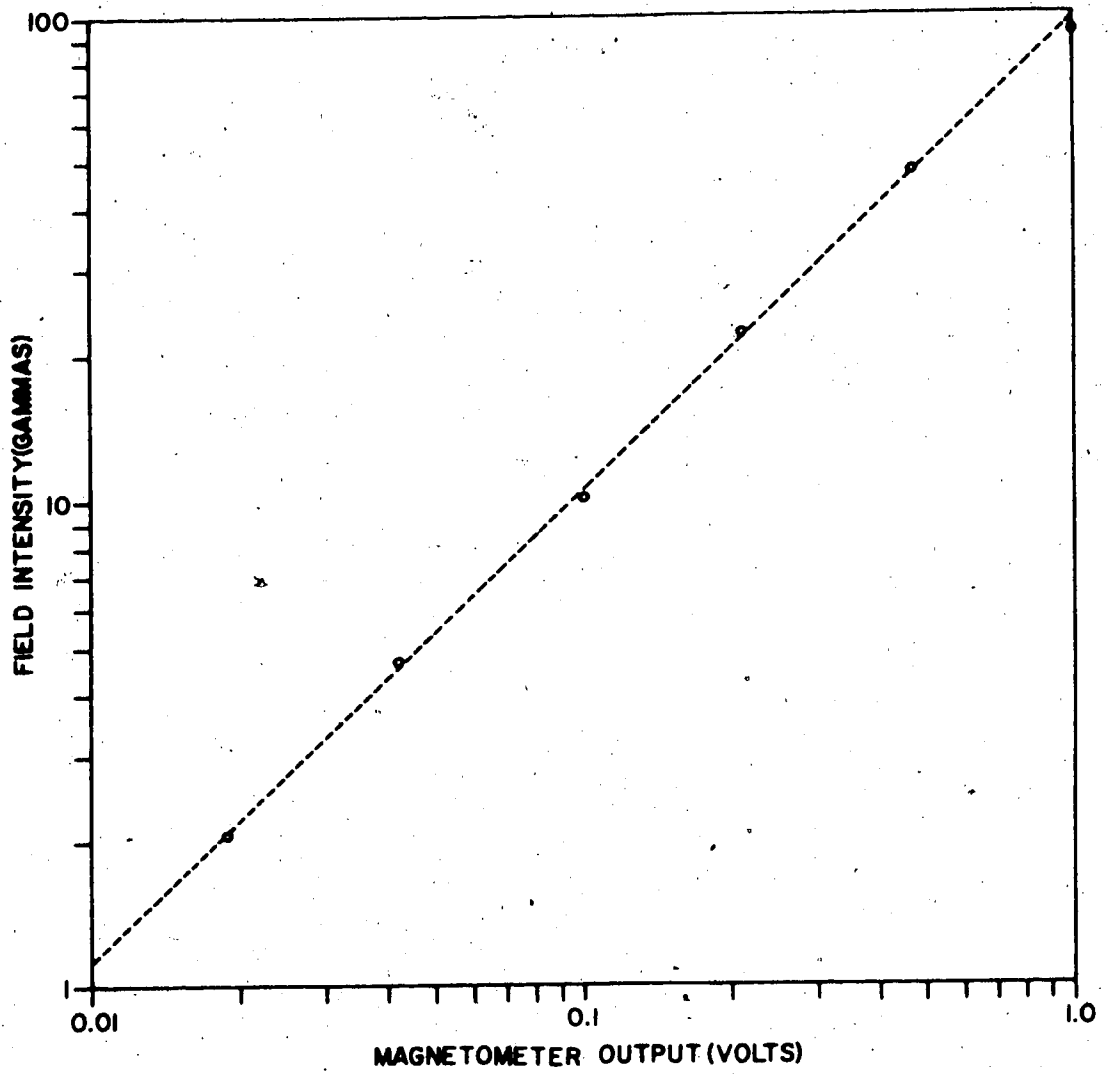


Figure A2

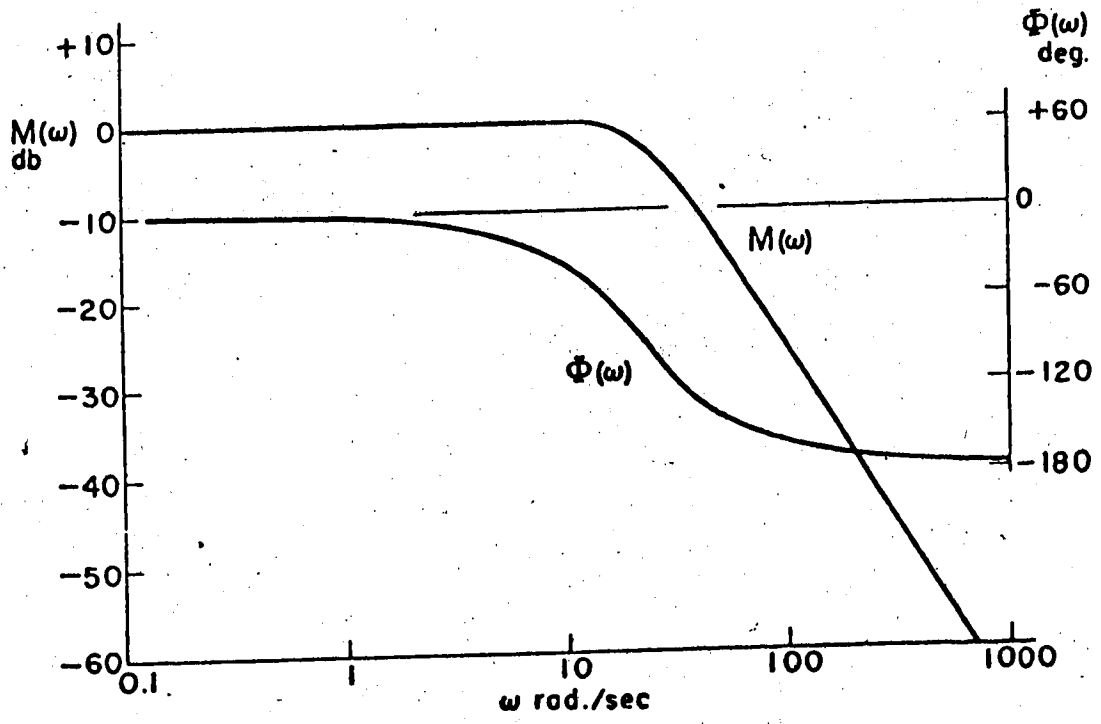


Figure A3

magnetometer is less than  $1\gamma/^\circ\text{C}$ . However, the stability and drift tests completed by Trigg et al. [1970] showed that the fluctuations of the Y baseline (up to  $20\gamma$ ) were much larger than expected and could not be explained by temperature drifts. Also a temperature coefficient of  $10\gamma/^\circ\text{C}$  was necessary to explain the variation of the Z-component baseline.

The analog-to-digital system is based on the Redcor 720 A-D converter, with multiplexer bypass line for WWVB, WWVB-to-data relay, and a variable stepping rate system coupled to a crystal oscillator as shown in Figure A4. The multiplexer is effectively three switches, one for each of the three component channels, controlled by the sequencer. The sequencer controls the sampling order (HDZHDZ...), initiation of sampling of the multiplexer and the conversion of input voltage in the analog-to-digital converter. Before the signal from the multiplexer is fed to the analog-to-digital converter it is buffered. The input of the buffer can be coupled to the output of the multiplexer or the output of the WWVB receiver. This selection is controlled by a 400 Hz crystal oscillator (with a maximum deviation from nominal frequency of  $\pm 0.005$  per cent) and the associated divider circuit. The stepping rate was changed from 1.56/sec (sample interval of 1.92 sec/component) to 50.0/sec while the WWVB time signal was being recorded. The relay switches from data to WWVB time signal on every eighth block.



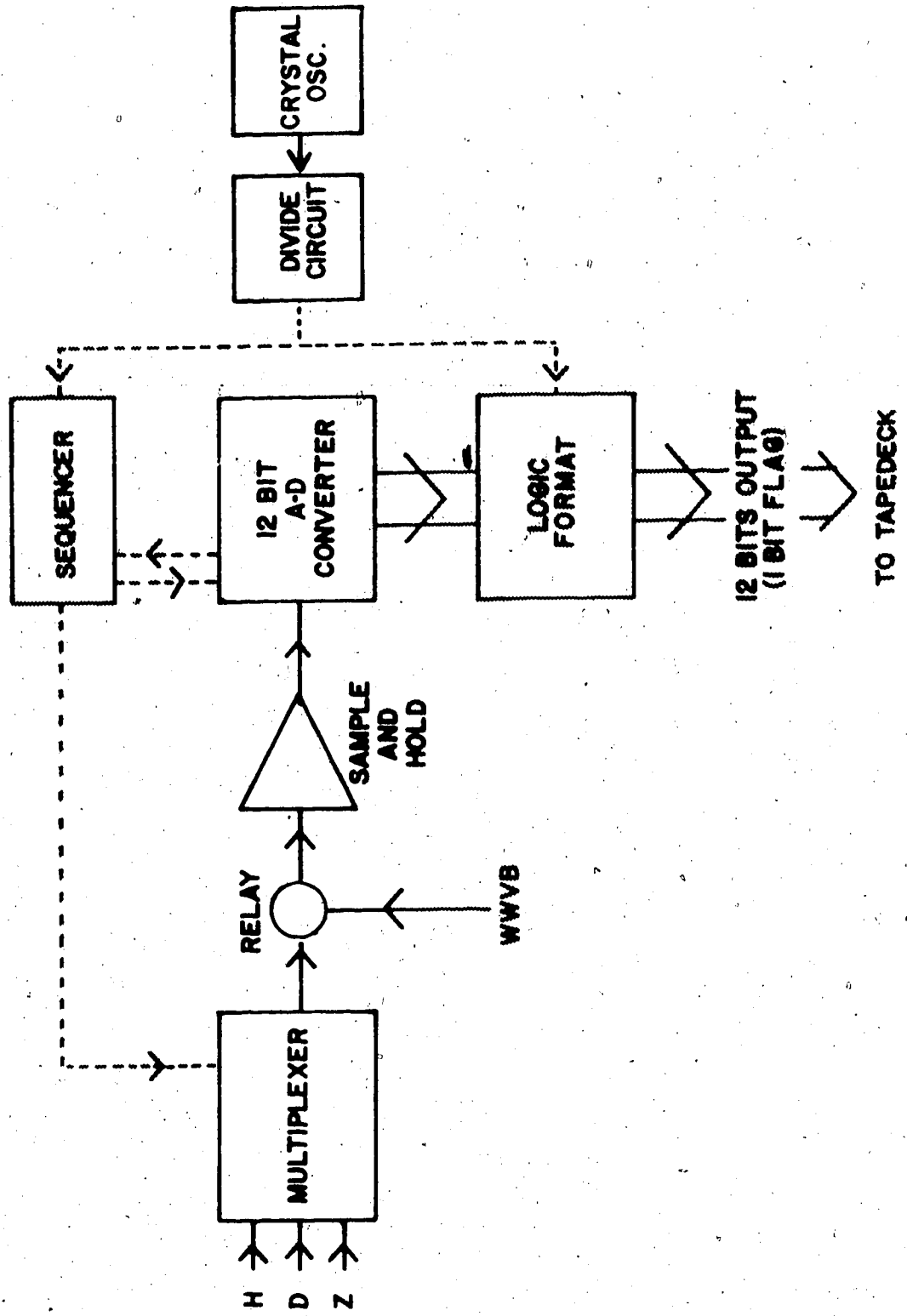


Figure A4

The 12-bit A-D converter (the least significant bit was used as a flag to identify errors in the sampling order) output was formatted into 2 byte samples (each byte being 6 bits long) and recorded on a 7-track Peripheral Equipment incremental write tape deck. Each block contained 6144 samples and represented 65 min 32.2 sec of magnetic data or 122.8 sec of WWVB time signal. Since the dynamic range was  $\pm 1000\gamma$  and there were 11 digital bits, the quantizing interval (amplitude sample interval) is  $0.976\gamma$  ( $2000\gamma/2^{11}$ ) which is approximately the same as the resolution of the magnetometer ( $\pm 1\gamma$ ).

The component outputs from the magnetometer were passed through two stage low-pass filters to remove frequency components above the Nyquist frequency (0.26 Hz) to avoid aliasing. The filters also served as buffers to isolate the multiplexer from the magnetometer by limiting the voltage input to less than  $\pm 12$  volts.

Because of the critical sequence of events that must take place to properly arm the unit for recording, an automatic restart unit was used to turn the system back on after a power failure. The auto restart has built-in logic to initiate control pulses to the logic board and tape transport in proper sequence to ensure the unit starts up properly. The WWVB time signal was also recorded immediately following the power failure to increase the timing reliability.

## APPENDIX B

### DETERMINATION OF POLARIZATION PARAMETERS AND PHASES FROM 3-DIMENSIONAL VECTOR TIME SERIES

Previous methods for estimating the characteristics of micropulsations such as mean-periods, mean-amplitudes and polarization hodograms directly from the raw data (i.e., amplitude-time recordings of the perturbations) are often cumbersome and restrictive and the results are sometimes misleading [e.g. Pope, 1964; Egeland, 1965]. Recently, researchers in the field of micropulsations have adopted the cross-spectral formalism to determine the polarization characteristics of micropulsations. The approach is based on the quasi-monochromatic wave theory of physical optics as outlined in Born and Wolf [1959]. This technique has been applied by Fowler et al. [1967], Rankin and Kurtz [1970], Samson et al. [1971] and Fukunishi et al. [1975] among others.

From an analysis presented by Born and Wolf [1959], the polarization parameters for a quasi-monochromatic wave field at a given field point can be obtained in terms of the elements of the following 3-dimensional covariance matrix

$$J = \begin{vmatrix} \langle B_x(t)B_x^*(t) \rangle & \langle B_x(t)B_y^*(t) \rangle & \langle B_x(t)B_z^*(t) \rangle \\ \langle B_y(t)B_x^*(t) \rangle & \langle B_y(t)B_y^*(t) \rangle & \langle B_y(t)B_z^*(t) \rangle \\ \langle B_z(t)B_x^*(t) \rangle & \langle B_z(t)B_y^*(t) \rangle & \langle B_z(t)B_z^*(t) \rangle \end{vmatrix}$$

where the B's are the orthogonal magnetic field components, the brackets indicate a time average and the asterisks denote the complex conjugate. In general, the time-averaged elements can be expressed as

$$\langle B_i B_j^* \rangle = \frac{1}{T} \int_t^{t+T} B_i(t) B_j^*(t) dt$$

for each  $J_{ij}$  element. This integral is evaluated, in practice, by using the relationships among the covariance functions and the associated cross-spectral functions. This is expressed as

$$\begin{aligned} \phi_{ij}(\tau) &= \frac{1}{T} \int_0^T B_i(t+\tau) B_j^*(t) dt \\ &= \int_{\Delta f} \phi_{ij}(f) e^{i2\pi f\tau} df \end{aligned}$$

where  $\phi_{ij}$  is the covariance function,  $\tau$  is the time lag, and  $\Delta f$  is the effective bandwidth of the signal. When  $i = j$ ,  $\phi_{ij}$  is the auto power spectral density. When  $i \neq j$ ,  $\phi_{ij}$  is the cross power spectral density. When  $\tau = 0$ , we have

$$\langle B_i B_j^* \rangle = \phi_{ij}(0) = \int_{-\infty}^{\infty} \phi_{ij}(f) df = J_{ij}$$

Hence, the polarization parameters can be formulated in terms of the auto power and cross power spectral estimates.

The property that the real symmetric part of the cross spectral matrix is diagonal in the principal axis system is utilized to determine the apparent plane of polarization. The real part of the cross spectral matrix is diagonalized as follows:

$$R[\text{Re } J]R^{-1} = \begin{vmatrix} J'_{11} & 0 & 0 \\ 0 & J'_{22} & 0 \\ 0 & 0 & J'_{33} \end{vmatrix}$$

where  $R$  is the rotation matrix and we have chosen  $J'_{11} > J'_{22} > J'_{33}$ . The transform of the total matrix is then

$$RJR^{-1} = \begin{vmatrix} J'_{11} & iJ'_{12} & iJ'_{13} \\ -iJ'_{12} & J'_{22} & iJ'_{23} \\ -iJ'_{13} & -iJ'_{23} & J'_{33} \end{vmatrix}$$

If the eigenvector associated with the minimum eigenvalue (i.e.,  $J'_{33}$ ) is used as the wave normal direction and the full matrix is rotated so that one of the new orthogonal axes corresponds to the wave normal direction assuming that the non-plane polarized vector series is random, the

cross spectral matrix of the plane polarized signal is given by

$$\begin{vmatrix} (J'_{11} - J'_{33}) & iJ'_{12} & 0 \\ -iJ'_{12} & (J'_{22} - J'_{33}) & 0 \\ 0 & 0 & 0 \end{vmatrix} \quad (A1)$$

Hence, the degree of polarization can be expressed as the ratio of the apparent plane polarized signal intensity to the total signal intensity as follows:

$$R1 = \frac{(J'_{11} - J'_{33}) + (J'_{22} - J'_{33})}{J'_{11} + J'_{22} + J'_{33}}$$

where we have used the fact that the trace of the matrix is equal to the intensity.

At this point, the 2-dimensional analysis of Fowler et al. [1967] and Rankin and Kurtz [1970] can be applied to the matrix representing the plane polarized signal. The plane polarized signal is composed of a vector moving randomly in the plane in which the signal is polarized and another vector whose two orthogonal components are completely correlated. Hence, the matrix (A1) can be expanded in the form

$$\begin{vmatrix} (J'_{11} - J'_{33}) & iJ'_{12} \\ -iJ'_{12} & (J'_{22} - J'_{33}) \end{vmatrix} = \begin{vmatrix} P_{11} & iP_{12} \\ -iP_{12} & P_{22} \end{vmatrix} + \begin{vmatrix} u & 0 \\ 0 & u \end{vmatrix}$$

where  $P$  is the matrix of the completely correlated vector series with  $\det[P] = 0$  and  $U$  is the matrix of the random plane polarized component. Solving for  $U$  (the eigenvalue or characteristic root of the matrix  $J$ ), we get

$$U = \frac{1}{2}[J'_{11} + J'_{22} - 2J'_{33}] \pm \frac{1}{2}[(J'_{11} + J'_{22} - 2J'_{33})^2 - 4 \det[J']]^{1/2}$$

The root with the positive sign is rejected since it gives negative values for the auto-powers of the polarized signal  $P_{11}$  and  $P_{22}$ .

Hence, the matrix of the completely correlated vector series can be expressed in terms of the original plane polarized matrix  $J'$  and the ratio of the completely coherent signal intensity to the plane polarized signal intensity given by the expression

$$R_2 = \frac{(J'_{11} - J'_{33} - U) + (J'_{22} - J'_{33} - U)}{(J'_{11} - J'_{33}) + (J'_{22} - J'_{33})}$$

can be determined.

To interpret the matrix  $P$  in terms of the quantitative polarization parameters, consider the following mathematical illustration

$$[y \quad x] \begin{vmatrix} P_{11} & iP_{12} \\ -iP_{12} & P_{22} \end{vmatrix} \begin{vmatrix} y \\ x \end{vmatrix} = P_{11} P_{22}$$

Expanding the above equation gives

$$\frac{x^2}{P_{11}} + \frac{2 \operatorname{Re} P_{12}}{P_{11} P_{22}} xy + \frac{y^2}{P_{22}} = 1 \quad (\text{A2})$$

Equation A2 is the equation of an ellipse in the coordinate system  $(x, y)$ . The ellipse can then be projected on to the 3 orthogonal planes and the ellipticities, polarization angles and sense of polarization on each plane can be determined.

Thus far we have discussed the cross-spectral matrices  $J_{ij}$  at a given station for the determination of the polarization parameters. Station-to-station cross-spectral estimates  $J_{ij}(r_m, r_n, f)$  (where  $J_{ij}$  is the cross-spectral estimate at frequency  $f$  of component  $i$  at station  $r_m$  and component  $j$  at station  $r_n$ ) can be calculated. These estimates can then be used to determine the coherency and phases between pairs of stations according to the following expressions. The coherency estimator is given by [see Jenkins and Watts, 1968]

$$K_{ij}(r_m, r_n, f) = \left[ \frac{L_{ij}^2(r_m, r_n, f) + Q_{ij}^2(r_m, r_n, f)}{J_{ij}(r_m, r_m, f) J_{ij}(r_n, r_n, f)} \right]^{1/2}$$

where  $J_{ij} = L_{ij} + i Q_{ij}$  is the station-to-station cross-spectral estimate. The coherency  $K_{ij}$  is a measure of the correlation of component  $i$  at station  $r_m$  with component  $j$  at station  $r_n$ . The phase estimator is given by



$$F_{ij}(r_m, r_n, f) = \text{arc tan} \left[ \frac{-Q_{ij}(r_m, r_n, f)}{L_{ij}(r_m, r_n, f)} \right]$$

The phase estimator  $F_{ij}$  is a measure of the phase difference between component  $i$  at station  $r_m$  and component  $j$  at station  $r_n$ .

The raw auto-power and cross-power spectral estimates are calculated by means of the Fast Fourier Transform algorithm [Gentleman and Sande, 1966] and are subsequently smoothed for the determination of the polarization parameters and phase estimators. The necessary conditioning of the raw data, such as removal of the mean, detrending by passing through a digital bandpass filter, cosine-tapering the initial and final 10% of the data and addition of zeroes, is first carried out before applying the Fast Fourier Transform.

Let  $X_N$  be the time series consisting of the original time series  $X_m$  and added zeroes to give  $N$  points. The discrete Fourier transform of the time series  $X_N$  is

$$A(n) = \frac{1}{N} \sum_{j=0}^{N-1} X_N(j) e^{-i2\pi jn/N} \quad n=0,1,2,\dots,\frac{N}{2}$$

where  $n$  is a sample at point  $n\Delta f$  ( $\Delta f = \frac{1}{N\Delta t}$  and  $\Delta t$  is the sample interval). The periodogram is given by

$$I(n) = \frac{N^2}{m} |A(n)|^2$$

The periodogram can be smoothed by taking a simple moving average

$$\bar{P}(n\Delta f) = \frac{1}{N} \sum_{p=-k}^k I(n\Delta f - p\Delta f)$$

Such smoothing yields a resultant spectral window which has roughly a rectangular shape. The shape of such a spectral window corresponding to simple moving average smoothing of the periodogram for  $k=7$  and  $m/N = 0.9$  is shown in Figure B1. The variance of the spectral estimate  $\bar{P}$  depends on the bandwidth of the spectral window. An example of the variation of the variance with bandwidth is shown in Figure B2. It can be seen that one trades variance with resolution and vice versa. The spectral estimates used for the computation of polarization parameters and phase estimators were smoothed using a wide spectral window with 14 degrees of freedom.

The raw cross-power spectral estimates of two time series  $X(t)$  and  $Y(t)$  are given by

$$\frac{N^2}{m} A(n) B^*(n)$$

where  $A(n)$  and  $B(n)$  are the discrete Fourier transform of  $X(t)$  and  $Y(t)$  respectively. To obtain the smoothed cross-power spectral estimates, the real and imaginary parts of the spectrum are averaged separately. The spectral window in each case is identical to that for the auto-power case.

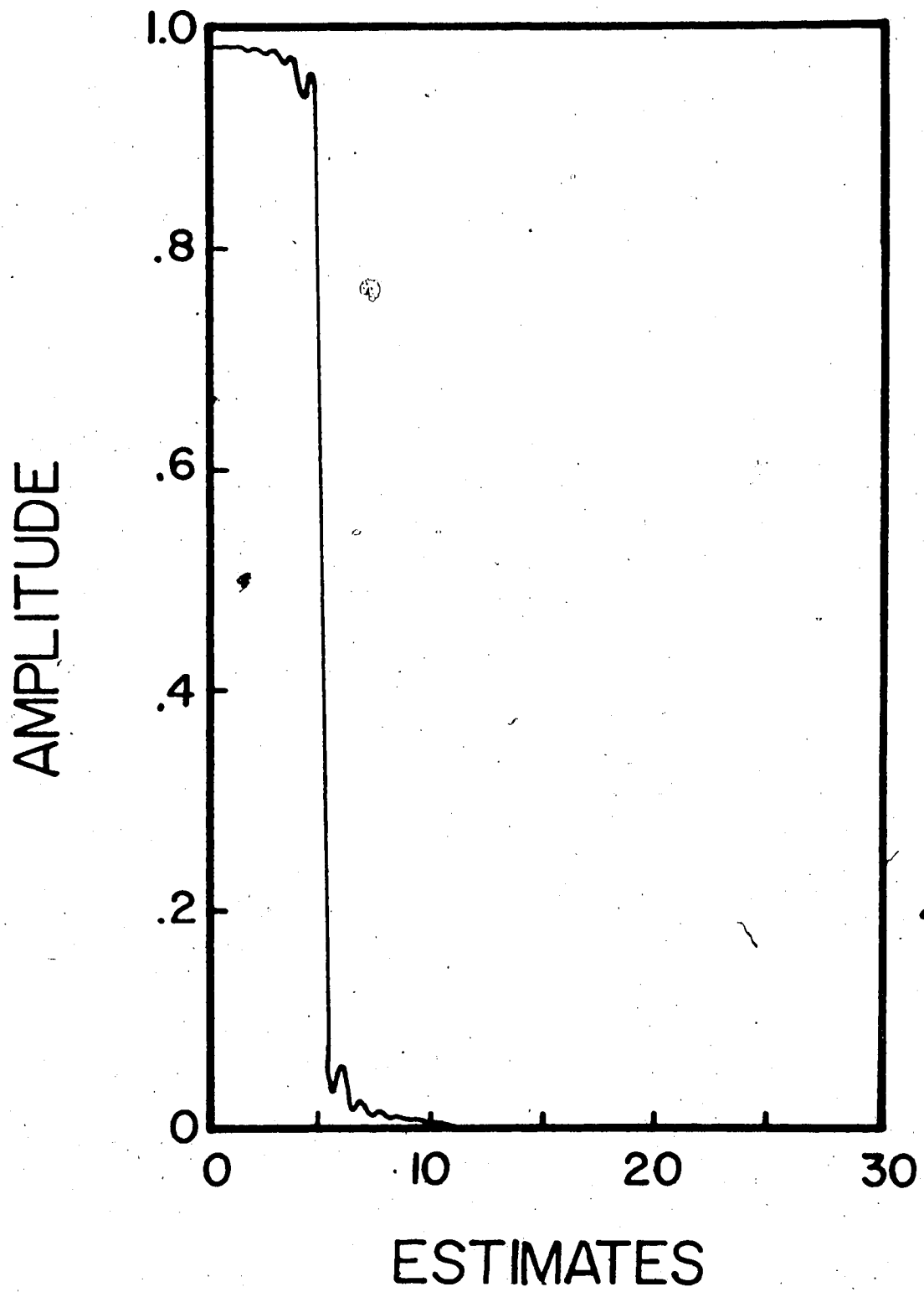
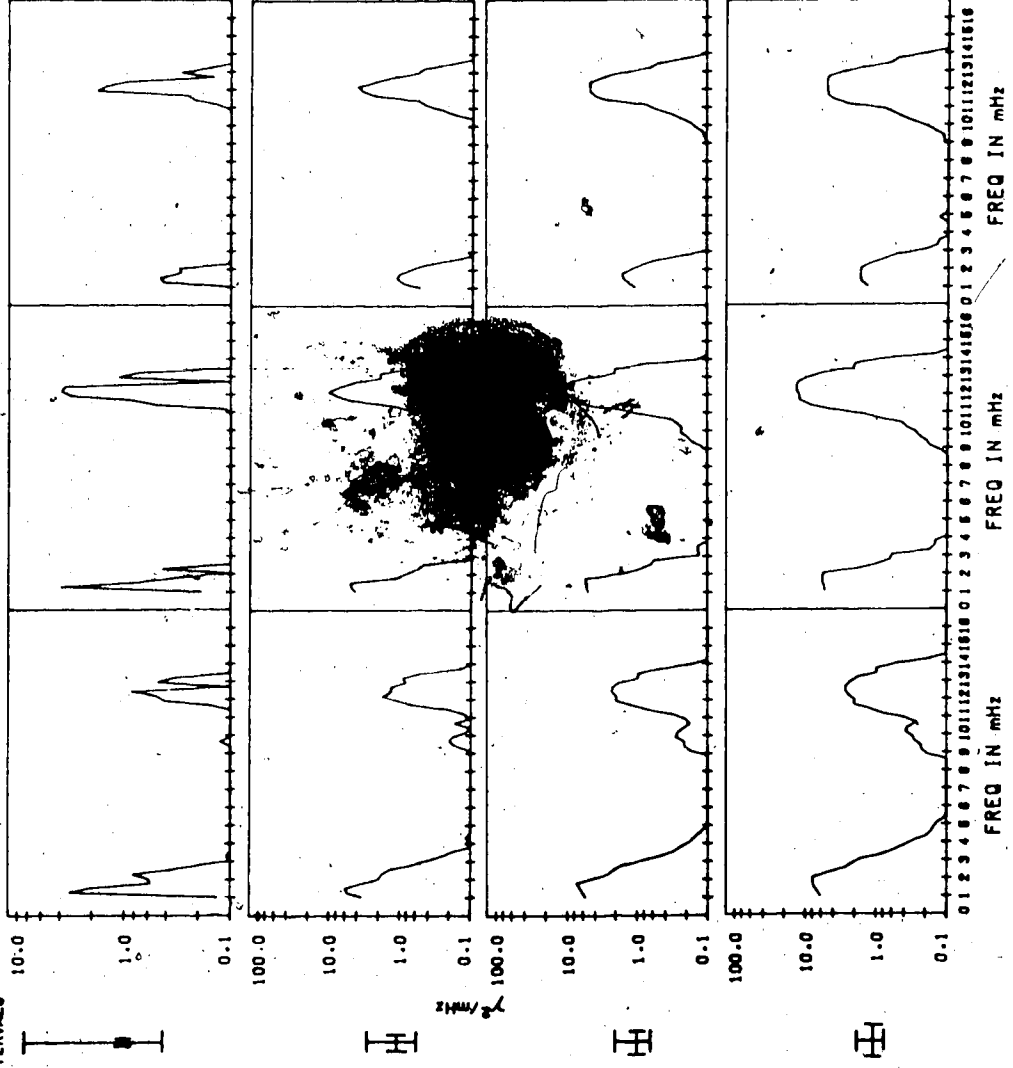


Figure B1

DAY 253 1974 (1330-1430)

H . . . . . D . . . . . Z

BANDWIDTH  
90%  
CONFIDENCE  
INTERVALS



## APPENDIX C

### INFERENCE OF ELECTRIC CURRENTS FROM GROUND MAGNETIC DATA

Ground-based magnetometers measure the integrated effect of all magnetospheric and ionospheric current systems. A useful technique to infer the flow of currents from ground magnetic data is to portray the magnetic perturbations in the form of a latitude profile. In the latitude profile, the magnitudes of three components (H, D, Z) are plotted as a function of the latitude of the observing stations at a given instant of time assuming all the stations lie on a common magnetic meridian. Then, by comparing the observed latitude profile to theoretically calculated latitude profiles based on certain model current systems, one can comment on the strength of the current system, the borders of the current, etc. This technique has been used by Walker [1964], Bonnevier et al. [1970] and Kisabeth and Rostoker [1971]. Since our line of stations was positioned approximately along a common geomagnetic meridian, displaying the magnetic data in the form of latitude profile rendered the comparisons between observed profiles and theoretical profiles particularly meaningful.

Kisabeth [1972, 1975] has used 3-dimensional equivalent current systems to model the polar electrojet.

He formulated Biot-Savart's law in spherical coordinates for an arbitrary current loop external to the earth's surface. The result of his computations is an expression for a component of the magnetic perturbation (at a point in the surface of the earth due to a current loop) in the form of an integral of a simple third order matrix which may be evaluated numerically for an arbitrary three-dimensional current system in the magnetosphere.

A few samples of theoretical latitude profiles computed by Kisabeth [1972] are presented here to illustrate how different profiles look for different current systems.

Consider an ionospheric current system  $20^\circ$  long and  $5^\circ$  wide flowing westward with field-aligned Birkeland currents flowing down the field lines to the eastern edge and flowing up the field lines at the western edge of the ionospheric westward electrojet. Figure C1 shows the latitude profile which would be observed on a meridian  $6^\circ$  west of the center of the current system. The shaded rectangle in Figure C1 represents an ionospheric current of one million amperes distributed uniformly across the electrojet. It can be seen that the borders of the electrojet are delineated by the extrema in  $\Delta Z$ . The central portion of the electrojet is characterized by  $\Delta Z = 0$  and the  $\Delta H$  maximum. The D profile represents the difference between two large contributions from Birkeland currents at the edges of the electrojet. The

# THEORETICAL PROFILE

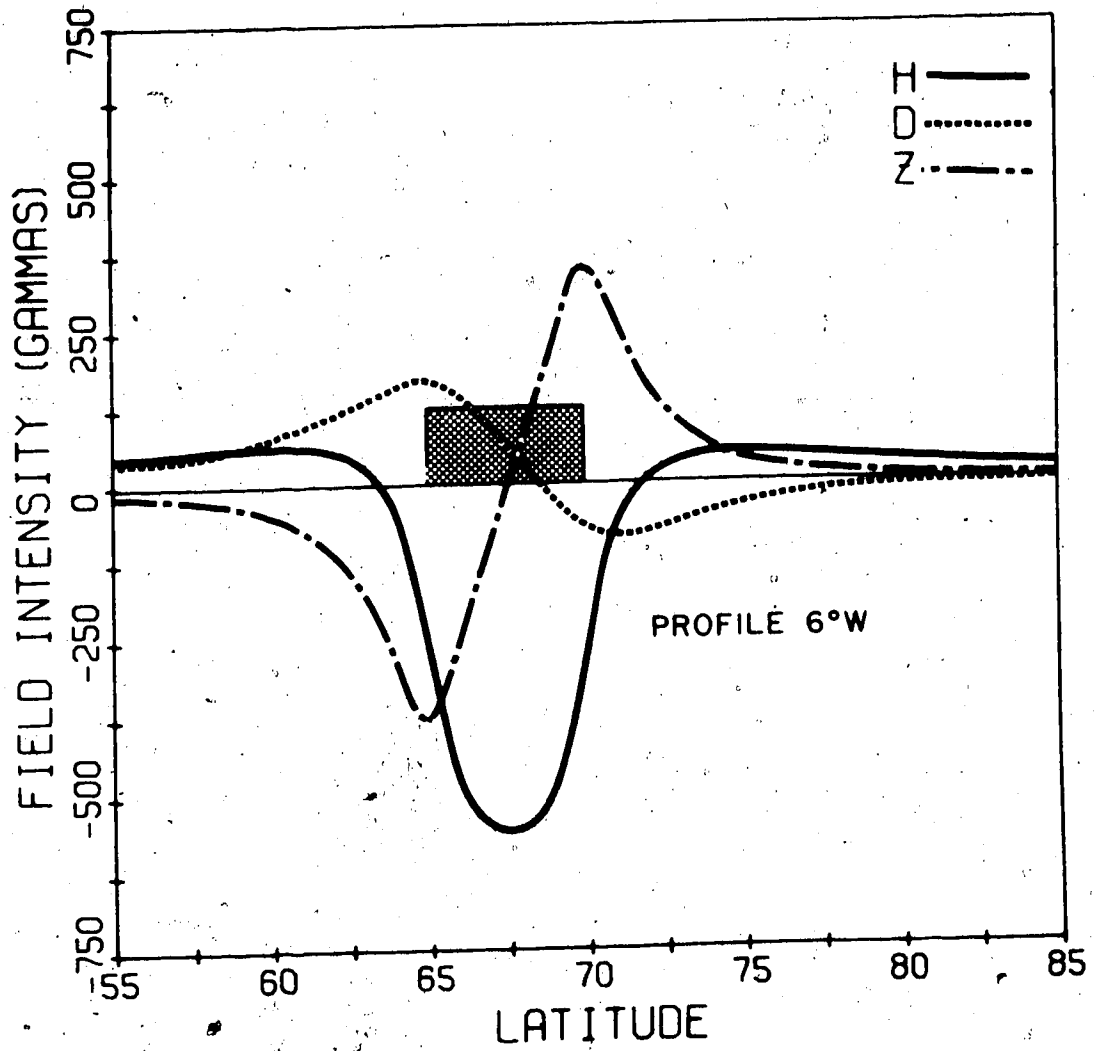


Figure C1

positive H bay regime and the D-component perturbation pattern would be absent had the perturbation been generated by a purely westward ionospheric electrojet.

Figure C2 shows latitude profiles associated with current systems having various latitudinal current distributions. Figure C2A shows a latitude profile which would be observed on a meridian  $5^\circ$  east of the center of the ionospheric electrojet having the same width and length as the current for Figure C1. The current density has a normal distribution across the electrojet. It can be seen that each border of the electrojet lies approximately midway between the extremum in  $\Delta Z$  and  $\Delta H = 0$ . Since this profile represents observations east of the center of the electrojet, the D profile has signs opposite to that of the D profile in Figure C1 which represents observation west of the center of the electrojet. Figure C2B shows a profile  $10^\circ$  east of the center of an ionospheric westward electrojet of length  $40^\circ$  and width  $10^\circ$  with Birkeland currents at the eastern and western edges. The current distribution is enhanced at the northern border. The asymmetries in the latitudinal current distribution can be observed from the latitude profiles. The effect of the enhanced northern border is exhibited clearly in the H and Z profiles. Figure C2C shows the magnetic effect associated with coexisting eastward and westward electrojets, each having different central meridians. Note the enhanced



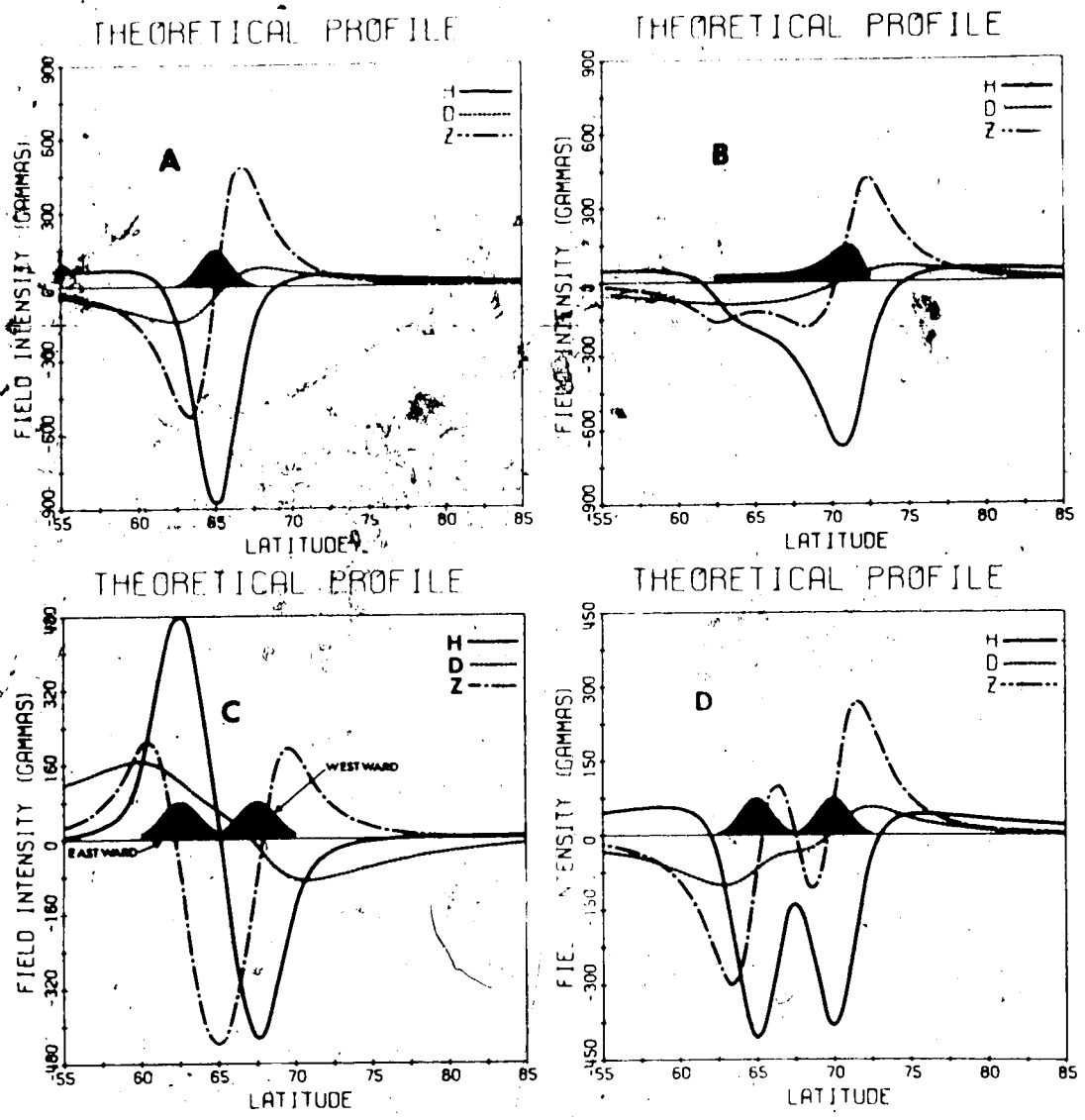


Figure C2

-Z regime between the two electrojets due to the same sense of the Z components of the two electrojets in that region. The eastward electrojet produces a positive H profile opposite to that produced by a westward electrojet. Figure C2D shows a profile due to a double westward electrojet, each having the same parameters as those for the system in Figure C2A. Note the partial cancellation of the component in the region between the two electrojets.

If a profile is obtained for a simple three-dimensional E-W current system far to the east or west of the line of stations, the component profiles are considerably broadened and the separation of the peaks in  $\Delta Z$  will be greater than the width of the actual current system.

Having shown the theoretical latitude profiles due to E-W ionospheric currents with Birkeland currents at the eastern and western edges, we now present two theoretical profiles computed by Kisabeth [1972] for a N-S three-dimensional current system. In this model system the Birkeland currents flow from the magnetosphere to the northern edge of the southward directed ionospheric sheet current and out at the southern edge back to the magnetosphere. The N-S current is  $4^\circ$  long and  $4^\circ$  wide. Figure C3 shows a latitude profile  $2^\circ$  east of the central meridian and Figure C4 shows a latitude profile  $2^\circ$  west of the central meridian. It can be seen that the Z and H profiles are reversed for both cases while the D profiles remain the same.

# THEORETICAL PROFILE

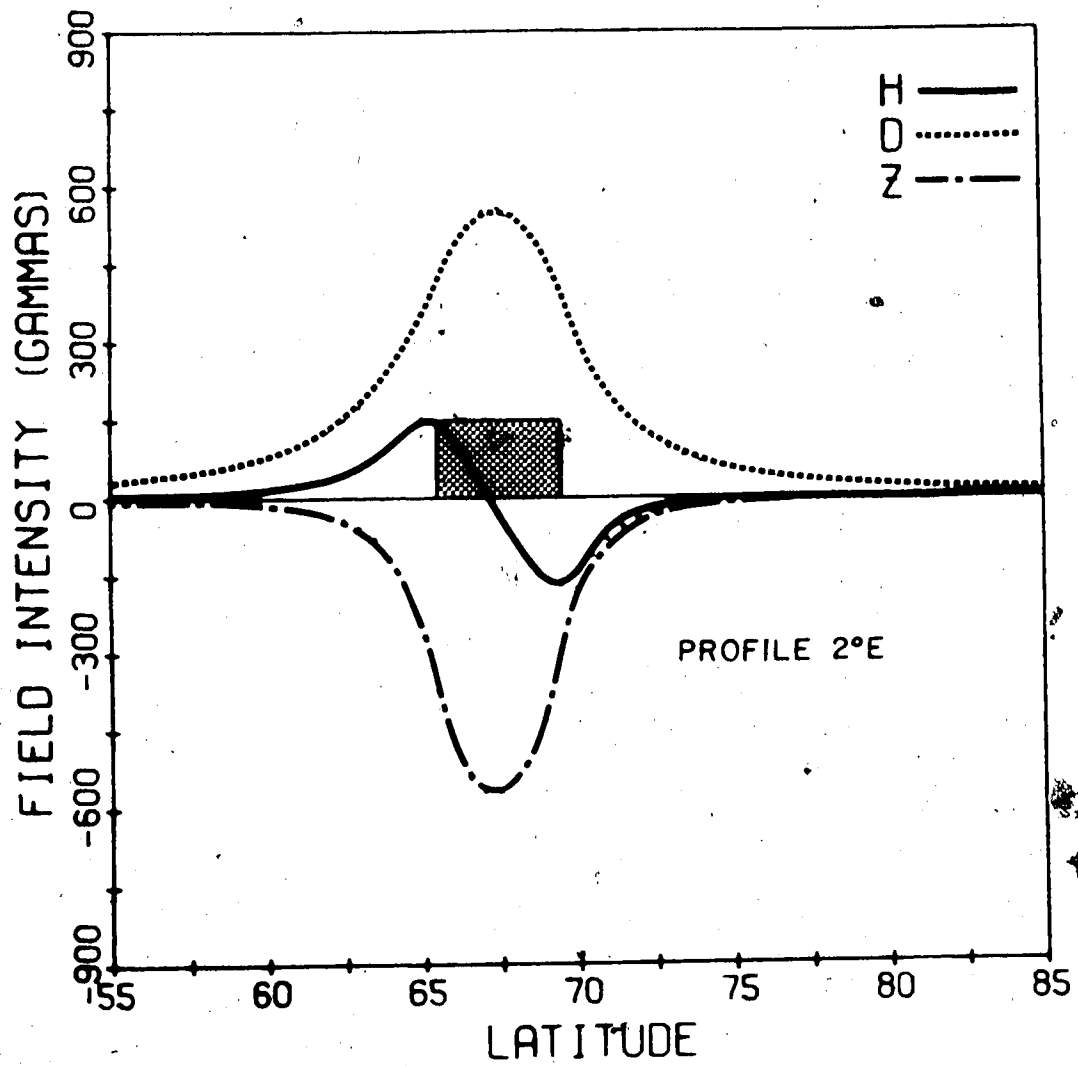


Figure C3

## THEORETICAL PROFILE

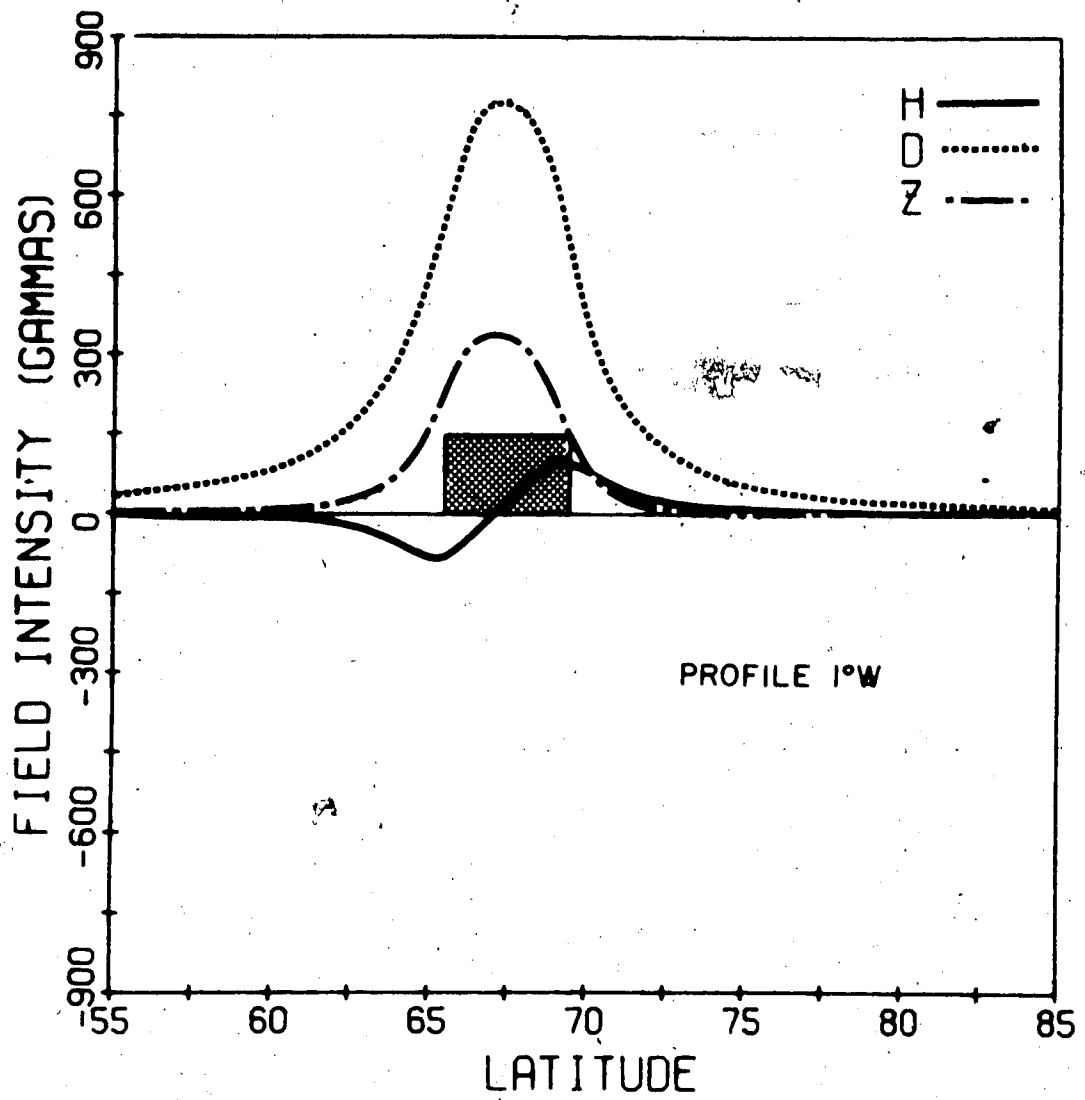


Figure C4

There is distinct similarity between the model latitude profiles of the three-dimensional E-W current systems and observed latitude profiles in the morning sector in the H and Z component. Although the exact locations of the borders of the electrojet cannot be determined because of lack of knowledge of the exact latitudinal current distribution, we can, nevertheless, use the Z component extrema to delimit the latitudinal range over which significant electrojet current flows. If we define the electrojet borders by the extrema in  $\Delta Z$  (for uniform latitudinal current density distribution) or one degree poleward/equatorward of extrema in  $\Delta Z$  (for normal current density distribution across the electrojet), we can estimate the equatorward border of the electrojet to within  $\pm 1^\circ$  and the poleward border to within  $\pm 1.5^\circ$  (the larger probable error for the poleward border estimate stemming from the sparser station coverage at higher latitudes).

The model three-dimensional E-W current systems used in computing the theoretical profiles described in this Appendix restrict the Birkeland current to flow at each end of the ionospheric electrojet. In fact Birkeland current flow is probably distributed along the entire length of the westward (or eastward) electrojet (see Figure 5). Therefore, the observed D component profile does not correspond to the computed D profile. The observed D profile also provides

information regarding the degree of tilt of the current system with respect to the line of observing stations. In most cases, the observed D-component profile shows a positive step-like function across the electrojet in the morning sector [Hughes and Rostoker, 1976]. This is an indication of the presence of net downward field-aligned currents noted by Yasuhara et al. [1975] using polar orbiter data from the TRIAD satellite.

